Controlling Architecture in Molecular Bottlebrushes

Joanna Burdyńska

Carnegie Mellon University

Department of Chemistry

Spring 2015

In partial fulfillment of the requirements for the Ph.D. degree in Chemistry

ABSTRACT

This work explores the synthesis of molecular bottlebrushes with complex architectures and their applications in various areas of material science. The first chapter reviews current progress in the bottlebrush field, focusing on recent advances in the areas of synthesis, physical properties and potential applications of bottlebrushes. Chapters II to IV discuss the relationship between structural details of homocomponent brushes and their physical properties. Chapter II summarizes the synthesis of graft copolymers with varying grafting densities, and lengths of the side chains and backbones, followed by the correlation of the graft structure with a thermal diffusion behavior. Chapter III describes the effect of the graft length on viscoelasticity of brushes with a constant backbone size. The work in Chapter IV introduces a new class of cylindrical brushes with bimodal length of side chains, and discusses their behavior on surfaces. The following Chapters (V and VI) cover the use of functional ATRP multiinitiators as a method of tuning the structure of bottlebrushes. Chapter V describes several examples of diinitiators incorporated into the brush core to either embed a labelled tag or to incorporate a mechanosensitive group. Chapter VI focuses on the use of more complex ATRP multiinitiator with a molecular spoked wheel core that allows for the formation of mechanosensitve molecular stars. The final Chapter VII discusses ABA triblock brushes inspired by the structure of a lubrication protein, and discusses their applications as lubricants in aqueous and organic media.

ACKNOWLEDGEMENTS

There are a lot of people I need to thank for being a part of my life over the past five years. Without them this Ph.D. would not only be much more difficult but simply impossible. First, I would like to thank Prof. Krzysztof Matyjaszewski for accepting me to his group and believing that I could fit in to the team of excellent scientists that surround him. Kris has always provided me with a great degree of freedom allowing me to incorporate new ideas into projects and, most importantly, to lead them at my own pace. He thought me how to be highly independent but also how to work with other people via collaborations and teaching.

I would like to acknowledge Dr. Jim Spanswick for always having a nice word to say to cheer me up, and for being there to help me with my papers and thesis writing. I also want to thank Prof. Sergei S. Sheiko for being an absolutely wonderful collaborator. Without him and his students the research I did would not be possible. Sergei was always very welcoming during mu visits at UNC; I always enjoyed my trips there, and even more, our scientific discussions that every time left me even more inspired and excited about the research we were doing together.

All of people I have met in the Matyjaszewski group made my time in Pittsburgh absolutely amazing. We had struggled together and we had laughed together, which left me with a lot of different memories. In particular, I would like to thank Dr. Nick Tsarevsky for always having some great advice and for his hilarious, sometimes

unbelievable, stories. Hong Cho and Sangwoo Park for being the sweetest group members always concerned about other people, even when they had their own problems.

This journey has been very special because of the numerous friends I met here. Wojtek and Laura Jakubowscy were the first people I met in USA and also became first friends I made in here. They took me to their house and helped me out during my first weeks in Pittsburgh. Soon after, the circle of friends was expanded by Annie Elsen and Nick Wahrer. The five of us together had a lot of great moments, spending out free time grilling, playing games and having awesome pizza nights at PHI. Over the year the group has expanded when my Polish fellows Paweł and Paulina Kryś, and Maciek and Gosia Kopeć had joined us. They have brought a lot of laugh into my life, but also reminded me of my home country, Poland, which I miss a lot every day. Gino, who has been a great support during the months of my Ph.D. He has brought a lot of happiness into my life and made me believe in myself again. I want to say the most special thanks to Dr. Annie Elsen, my true best friend. She has been there for me all the time, laughing when I laughed and crying when I cried. The most dedicated and special friend anyone can dream of, my missing twin that I found all the way across the Ocean.

Tę pracę dedykuję mojej Kochanej Rodzinie, przede wszystkim Rodzicom, Bratu, Bratowej oraz Babciom. Bez ich bezwzględnego wsparcia i miłości nie byłoby mnie tutaj. To co mam zawdzięczam moim Rodzicom, to oni nauczyli mnie szcunku do siebie I do innych, to dzięki nim jestem tym kim jestem. This work is dedicated to my wonderful Family who shaped me into the person I am today.

TABLE OF CONTENTS

LIST OF ABBREVIATIONS

ABA	ABA – triblock copolymer
AIBN	2,2′-azobisisobutyronitrile
AFM	Atomic Force Microscopy
Ant	Anthracene and maleic anhydride Diels – Alder adduct
ARGET	activator regenerated by electron transfer
ATRP	atom transfer radical polymerization
BB	Backbone
BA	butyl acrylate
bpy	2,2'-bipyridine
CDTB	cumyl dithiobenzoate
CRP	controlled radical polymerization
CTA	chain transfer agent
DMAP	4-(*N*,*N*-dimethylamino)pyridine
DMA	Dynamic Mechanical Analysis
dNbpy	4,4′-di-(5-nonyl)-2,2′-bipyridine
DP	degree of polymerization
DTBP	2,4-di-*tert*-butylphenol
EBiB	ethyl 2-bromoisobutyrate
eq.	equivalent
et al.	*et alii, et alia*

GPC	Gel permeation chromatography
HEMA-TMS	2-(trimethylsiloxyethyl)ethyl methacrylate
HMW	high molecular weight
i.e.	*id est*
MALLS	multiangle laser light scattering
Me_6TREN	tris[2-(dimethylamino)ethyl]amine
MI	macroinitiator
MMA	methyl methacrylate
MPC	2-Methacryloyloxyethyl phosphorylcholine
MSW	Molecular
MW	molecular weight
MWD	molecular weight distribution
NMP	nitroxide mediated polymerization
NMR	nuclear magnetic resonance
Pa	Pascal
PDI	polydispersity index
PMDETA	*N,N,N′,N″,N″*-pentamethyldiethylenetriamine
ppm	parts per million
P*n*BA	poly(*n*-butyl acrylate)
PBiBEM	poly[(2-bromoisobutyryloxy)ethyl methacrylate]
PSt	polystyrene
RAFT	reversible addition-fragmentation chain transfer

rt	room temperature
SCs	side chains
SEC	size exclusion chromatography
SFA	Surface Force Apparatus
Sp	spiropyrane
St	styrene
***t*BA**	*tert*-butyl acrylate
TEA	triethylamine
TEMPO	(2,2,6,6-Tetramethylpiperidin-1-yl)oxy
THF	Tetrahydrofuran
ThFFF	Thermal Field Flow Fractionaction
TPMA	tris[(2-pyridyl)methyl]amine
Tri	1,2,3-triazole

LIST OF FIGURES

Figure VI.2 DLS measurements of two samples of **$MSW_{6\text{-}OtBDMS}$** (6 mg/mL in toluene and chloroform) (a) CONTIN-analysis, recorded 765 min and 945 min after dissolving the sample, respectively. In toluene, 85 % of the scattered light is attributed to the monomer whereas in $CHCl_3$ it is 95 %. (b) Cumulant-analysis of the autocorrelation curves at 30°. The evolution of the first cumulant over time is displayed: for the toluene solution a very slight increase of the first cumulant can be observed, while it is constant for the $CHCl_3$ solution. (p.191)

Figure VI.3 GPC traces of (a) $[P(HEMA\text{-}TMS_{450})]_6$ **$((450\text{-}TMS)_6$**, black), $(PBiBEM_{450})_6$ **$((450\text{-}Br)_6$**, red), $(PBiBEM_{450}\text{-}g\text{-}(PnBA_{20})_6$ (**$(450\text{-}g\text{-}20)_6$**, blue) and $(PBiBEM_{450}\text{-}g\text{-}(PnBA_{40})_6$ (**$(450\text{-}g\text{-}40)_6$**, green), (b) $[P(HEMA\text{-}TMS_{300})]_6$ (**$(300\text{-}TMS)_6$**, black), $(PBiBEM_{300})_6$ (**$(300\text{-}Br)_6$**, red), $(PBiBEM_{300}\text{-}g\text{-}(PnBA_{60})_6$ (**$(300\text{-}g\text{-}60)_6$**, blue) and (PBiBEM300-*g*-$(PnBA_{150})_6$ (**$(300\text{-}g\text{-}150)_6$**, green). (p.196)

Figure VI.4 GPC traces (a) of $[P(HEMA\text{-}TMS\neg450)]_6$ (**$(450\text{-}TMS)_6$**, black), $(PBiBEM_{450})_6$ **$((450\text{-}Br)_6$**,) after drying (blue-dashed), sonication in THF for 5 min. (magenta line) and 1 h (red line). DLS analysis of b) $(PBiBEM_{450})_6$ sonicated in THF for 1 h (**$(450\text{-}Br)_6$**, pale red) and dry (**$(450\text{-}Br)_6$**, blue and red) performed in THF solutions at C = 10 mg/mL. (p.198)

Figure VI.5 AFM height micrographs of thin films prepared by spin-casting of (450-Br)6 solutions in a) chloroform and b) THF and **$(450\text{-}TMS)_6$** solutions in c) chloroform and d) THF using mica as the substrates. The concentration of the solutions used for spin casting was ~ 0.001 mg/ml. (p.201)

LIST OF TABLES

LIST OF SCHEMES

SECTION I

INTRODUCTION

CHAPTER I

RECENT PROGRESS IN THE FIELD OF MOLECULAR BOTTLEBRUSHES

Preface

The following chapter will discuss the recent progress in the area of molecular bottlebrushes, focusing on research conducted over the past five years. There are few excellent reviews that provide detailed information on the synthesis, characterization and diverse applications of molecular bottlebrushes.[1-3] Therefore, to avoid unnecessary repetition, this section will cover only the most recent advances in the field.

I.1 Introduction

Molecular bottlebrushes have attracted a great deal of attention as building blocks for the fabrication of nanomaterials. Bottlebrushes, (cylindrical macromolecular brushes, molecular brushes, bottlebrush copolymers, (BBCs)) are a class of graft copolymers with polymeric branches densely grafted from a polymeric backbone. Due to the steric

overcrowding caused by the side chains, bottlebrushes are forced to stretch and adopt an extended, cylindrical conformation.[4-6] The rigid nature of BBCs is the primary contributor to the development of their unusual physical properties, which are often dramatically different from their linear counterparts with similar average composition. Therefore, there has been a growing interest in improving the synthetic tools that can be applied to expanding the range of composition, architecture and topology of BBCs, which would additionally facilitate access to more complex bottlebrushes with new properties.

I.2 Synthesis of Bottlebrush Copolymers

The first molecular bottlebrushes, referred to as 'poly(macromonomers)', were synthesized by Tsukahara by conventional free radical polymerization (FRP) of macromonomers.[7-9] The nature of the polymerization did not allow for control over the brush length, leading to macromolecules with broad molecular weight distributions. The discovery of controlled/living polymerizations (CRP/LRP) has revolutionized the field of densely grafted copolymers by enabling access to variety of brushes with tunable compositions, molecular size and topologies.[10]

Bottlebrush polymers are typically synthesized via one of three basic approaches: 'grafting onto', 'grafting from' or 'grafting through', Figure I.1.[2] 'Grafting onto' relies on pre-made, well-defined backbones and side chains, which are connected together via coupling reactions. While this should lead to well-defined BBCs the process often suffers from steric issues and poor linking efficiencies, thus causing formation of bottlebrushes

with fairly low graft densities. The developments of new synthetic techniques, such as 'click' and nucleophilic substitution reactions,[11-14] have significantly improved the efficiency of graft attachment, thus giving access to more dense bottlebrushes. However, to push the coupling to high conversions it is often required the use an excess of chains to be grafted. As a consequence, laborious purification techniques need to be employed to remove unreacted side chains from the final product.[2] An additional limitation of the 'grafting to' procedure is a limited number of attachable grafts, which severely restricts the number of brush compositions accessible through that approach.[14-18]

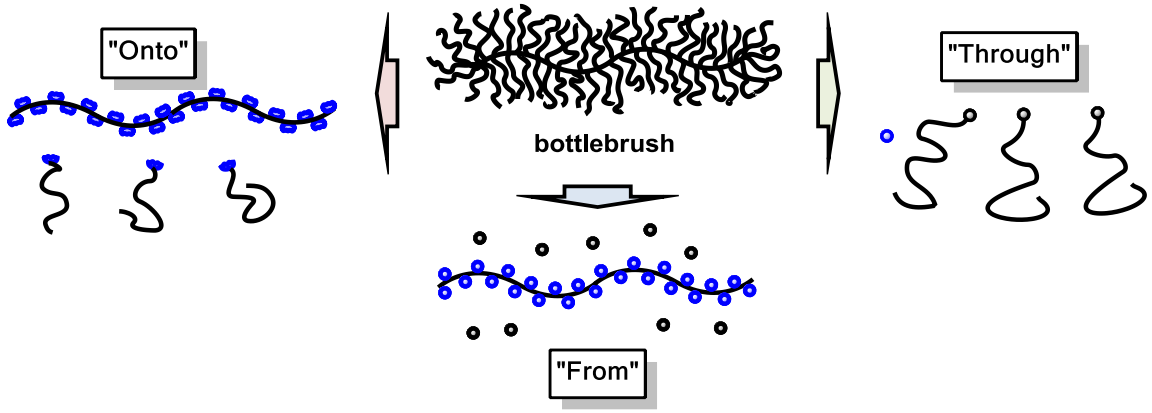

Figure I.1 Synthetic approaches for the formation of molecular bottlebrushes.

The 'grafting through' approach utilizes well-defined macromonomers that produce brush copolymers with a side chain at every repeat unit, i. e. bottlebrushes with 100% grafting densities, Figure I.1. Initially, this technique was mainly exploited by FRP, thus giving poor control over the length, or degree of polymerization (DP), of formed macromolecules. On the other hand, most attempts of employing CRP in the 'grafting through' of macromonomers have failed due to issues related to large steric

hindrance between grafts, low concentration and poor accessibility of the terminal functional groups. A relatively small number of reports detail successful grafting through reactions, which shows that very few macromonomers can be polymerized via CRP and reach high conversions or high DP. The presence of residual macromonomers still remains a purification issue.[19,20] The advent of ruthenium-catalyzed ring opening metathesis polymerization (ROMP), in particular the modified 2nd generation Grubbs' catalyst, was a milestone in reviving 'grafting through'.[21-23] ROMP has opened access to a wide number of macromonomers that can be polymerized to very high conversions, hence resolving the hassle of laborious purification. In addition, ROMP enables good control over the brush length producing BBCs with narrow molecular weight distributions (*Đ*).[23] Steric issues affect the 'grafting through' of macromonomers prepared by both CRP and ROMP; however, it is crucial to stress the significant difference in the size of the monomeric units obtained in each method. In a fully stretched chain, the norbornene unit length is 0.62 nm, whereas that of vinyl monomers is 0.25 nm. Therefore, the steric congestion in BBCs generated by ROMP of norbornene macromonomers is significantly reduced when compared to brushes prepared from vinyl-containing monomers. Therefore ROMP provided brushes with approximately 40% grafting density of what is attained by the 'grafting from' of vinyl macromonomers polymerized by CRP. Ping et al. have recently showed that copolymerization of an alternating macromonomer and small molecule monomers can be used to reduce the steric congestion in brushes formed by the 'grafting through' via ATRP.[24] In this case, maleimide macromonomers were copolymerized with styrene under ATRP conditions,

since those two comonomers copolymerize in a nearly alternating fashion. The results showed the formation of grafts copolymers with DPs ~ 100; however the molecular weight distributions of the brushes were quite broad. Even though, these findings indicate CRP might have a future in preparing densely grafted copolymers via the 'grafting through' approach.[24]

The third, most common route is the 'grafting from' procedure. 'Grafting from' relies of the use of a well-defined multifunctional macroinitiator, which is used to simultaneously polymerize branches from the distributed initiator functionalities. In comparison to other synthetic methods, the purification in the 'grafting from' is much more straightforward and often only requires precipitation of the BBC into a non-solvent to remove small molecule monomers. 'Grafting from' is mainly performed via CRP methods, in particular ATRP, reversible addition fragmentation chain transfer (RAFT) and nitroxide mediated (NMP) polymerizations, in order to attain control over the DP of the grafted chains. ATRP is still the predominant process for generation of bottlebrushes via the 'grafting from' procedure. ATPR is known to facilitate access to a vast number of complex architectures through control over composition, dimensions and topologies. One of the drawbacks of normal ATRP is the high concentrations of copper catalyst (>1000 ppm) employed in polymerization. The residual copper might be an issue, particularly in materials considered for metal-free applications, such as electronics or biomaterials. Recently, our group has reported the successful synthesis of bottlebrushes prepared via ATRP with low ppm of copper catalyst.[25] ICAR (initiators for continuous activator regeneration) and SARA (supplemental activator and reducing agent) ATRP methods

were successfully applied to the formation of BBCs, while requiring only 50 ppm of copper. Even though the control over the polymerizations was fairly good, the dispersity of bottlebrushes prepared with low ppm catalyst were broader (1.6-1.7) and initiation efficiencies were lower (~50%), than values attained via normal ATRP (~1.2 and ~90%).[25-27]

Amongst all CRP techniques, ATRP is the superior method of generating bottlebrushes via 'grafting from'. Reversible addition–fragmentation chain transfer (RAFT) polymerization, on the other hand, is much less commonly utilized due to issues related to the attachment of RAFT chain transfer agent (CTA) to the backbone.[28] A RAFT CTA consists of two main parts, the stabilizing group, the Z-group, and the reinitiating group, the R-group, both of which can be used as an anchor to attach to the poly-initiator backbones.[29,30] There are significant complications related to either approach. In the tethered Z-group method the propagating radicals leave the backbone, consequently causing problems with reattachment to the brush, as with the grafting to method (Scheme I.1A). On the other hand, in the R-group method, the transfer reaction can occur between adjacent CTAs on the same brush, or between neighboring brushes (Scheme I.1B). Indeed, the R-group approach was proven to be a poor synthetic method generating bottlebrushes with broad, often bimodal, distributions. The poor control in the R-group route is related to the large size and multifunctional nature of BBCs, which considerably limits the efficiency of transfer of radicals between growing bottlebrushes.

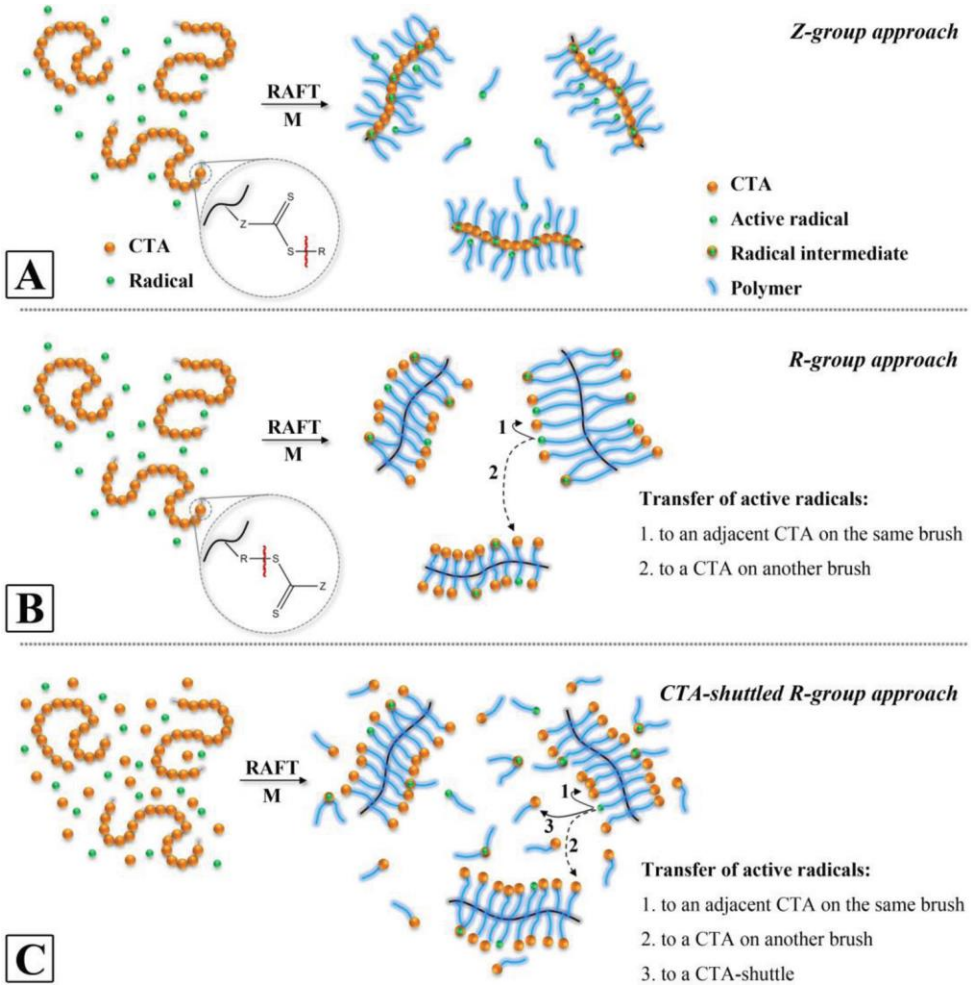

Scheme I.1 Proposed mechanisms of the Z-group approach (A), the R-group approach (B) and the "CTA-shuttled" R-group approach (C) to synthesize CPBs. The red wavy line indicates where monomer will be inserted.[28]

Müller et al. proposed a way of improving the R-group approach by developing the so called the 'CTA-shuttled' grafting from procedure (Scheme I.1C).[28] The concept of the 'CTA-shuttled' methods relies on adding a low molecular weight CTA to the reaction mixture, to enable a more efficient transfer of radicals. The 'CTA-shuttled' grafting from procedure has proved to be a successful way of facilitating intermolecular transfer of

radicals. It allowed the synthesis of monomodal brush copolymers with narrow *Đ* values, as opposed to traditional the R-group 'grafting from' approach. Nevertheless, it is worth noting that addition of an external CTA results in the formation of an additional set of linear polymers that still need to be removed from the final brush product.[28]

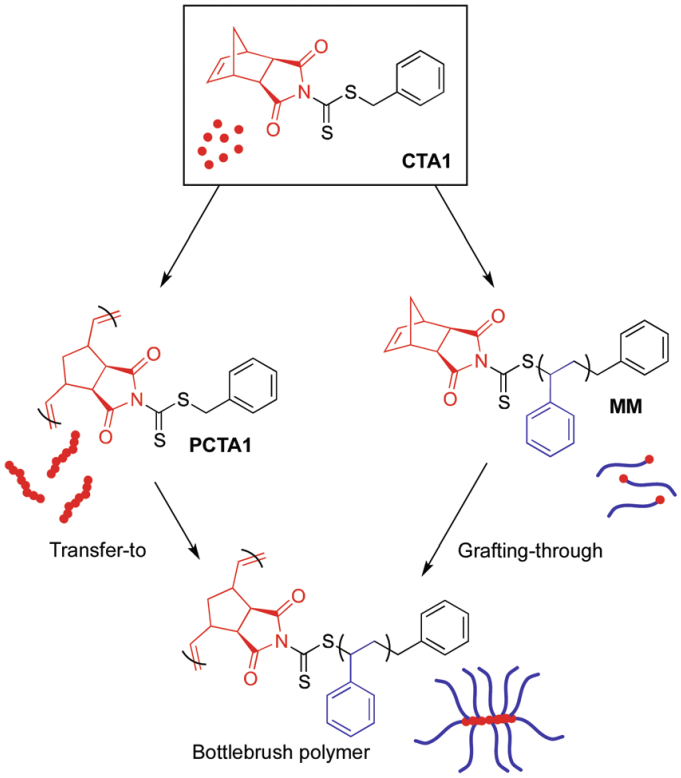

Scheme I.2 Preparation of bottlebrush polymers from polymerizable CTA by transfer to or grafting-through.[31]

Brush copolymers prepared by the 'grafting from' exploit multifunctional macroinitiators with functional groups located along the backbone. The number of steps involved in the macroinitiator preparation is often determined by the types of polymerizations employed in the total synthesis of bottlebrushes. Typically, when only

one polymerization procedure is applied, multiple synthetic steps are required to generate the backbone. For instance, a commonly used ATRP macroinitiator (poly[2-(2-bromoisobutyryloxy)ethyl methacrylate] (PBiBEM)), is generally prepared in two stages. First, 2-trimethylsiloxyethyl methacrylate is polymerized via ATRP, followed by a chemical modification of the polymer with ATRP-active, 2-bromoisobutyryloxy-moieties. However, the same macroinitiator can also be synthesized via direct polymerization of 2-(bromoisobutyryloxy)ethyl methacrylate when RAFT is employed for the synthesis of the backbone. This is facilitated by the use of a functional monomer containing an ATRP initiating group that does not interfere with a RAFT polymerization.

Recently, Matson et al. reported the concept of using a directly polymerizable CTA agent, consisting of a monomer capable of undergoing ROMP, a norbornenes with RAFT- active dithiocarbamate groups as a substituant, at respective Z- and R-positions (Scheme 1.2).[31] The ROMP polymerization of such CTA yielded a polyCTA with RAFT units attached to the backbone through R-groups. The polyCTA was then employed in the preparation of bottlebrushes via the RAFT polymerization of styrene (Scheme 1.2). The applied synthetic methodology is known as the 'transfer to' process and it shares the characteristics of both the 'grafting from', and 'grafting to' approaches. The 'transfer to' procedure relies on formation of a reactive backbone, as in the 'grafting from' procedure, however, similar to the 'grafting to' approach, the side chains reattach to the backbone, which occurs during growth the grafts. As a result, the branches are connected to the brush core via dithiocarbamate linkages, thus enabling the cleavage of grafts via aminolysis, and providing a way of generating degradable bottlebrushes.[31]

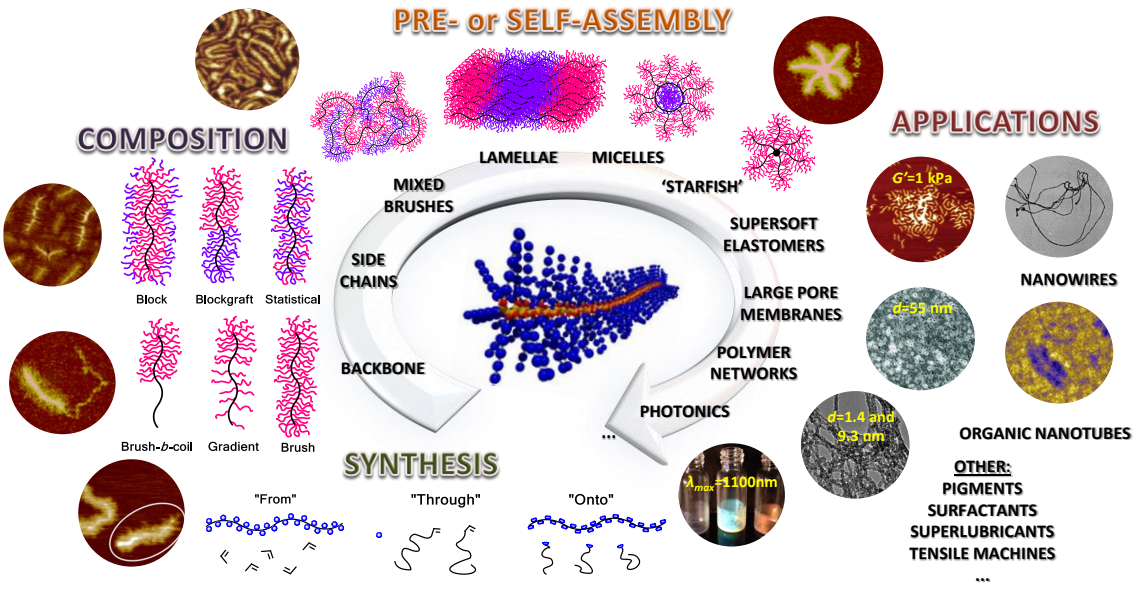

Figure I.2 Molecular bottlebrushes with various compositions and architectures, their properties and potential applications.[74]

The ability to combine CRP techniques with each other or/and with other polymerization methods, such as ring opening polymerization (ROP), provides access more advanced architectures and expands the range of monomers that can be incorporated into the brush. A careful design of backbones and side chains enables the synthesis of branched copolymers with divers topologies, including core-shell,[32-35] di-[36-40] and tri-blocks,[41] gradient,[42,43] brush-tail,[44] and star-shaped[45] brushes (Figure I.2). Such unique macromolecules have also been extensively investigated in areas of molecular tensile machines,[46-48] supersoft elastomers,[49,50] photonics,[37,51-57] organic nanotubes,[32,58-61] bio-inspired materials,[62-70] networks and porous materials,[39,71] and lithography (Figure 1.2).[72,73]

I.3 Physical Properties of Molecular Bottlebrushes

Molecular bottlebrushes are a unique class of dense graft copolymers, whose physical properties are primarily dictated by high steric congestion between the side chains. The shape persistent nature of brush copolymers has a strong influence on their properties, which are often drastically different from that of their linear counterparts.[1-3] This topological difference affects the behavior of BBCs at surfaces, in solution as well as in bulk.

The shape-persistent nature of bottlebrushes strongly affects their physical properties.[7,75,76] Molecular bottlebrushes are naturally disentangled polymers, meaning the stretched conformation of BBCs in bulk, in most cases, prevents them from forming intermolecular entanglements. Consequently, brush copolymers display behavior of materials with Rouse-like relaxation dynamics with no rubbery plateau.[49,77-80] Hillmyer and Bates et al. performed detailed studies of the zero-shear viscosities (η_0) of BBCs prepared via ROMP of polypropylene macromonomers. This approach provided a series of molecular brushes with a fixed branch size and consistently increasing length of the backbone (DP = 11-732). The results of zero shear viscosity measurements were plotted against molecular weight (M_w) showing power law fits of $\eta_0 \sim M_w^{\alpha}$, with two distinct regimes. At low molecular weights, the dependence ($\alpha < 0.5$) was weak, which was attributed to a progressively increasing compactness of short brush copolymers, which are star-like brushes. However, at higher molecular weights (HMW), the scaling changed

to Rouse Rouse-like dynamics, α = 1.2, which was related to the sphere-to-cylinder conformational transition seen as the DP of BBCs increase.[81] The results show the oscillatory shear measurements have great potential as a tool to verify the shape of various graft copolymers systems. It could be employed to establish a more distinct border between star-like vs brush-like and less densely grafted copolymers vs molecular bottlebrushes, hence reducing the instances of overuse of term 'molecular bottlebrush' to encompass a range of structures.

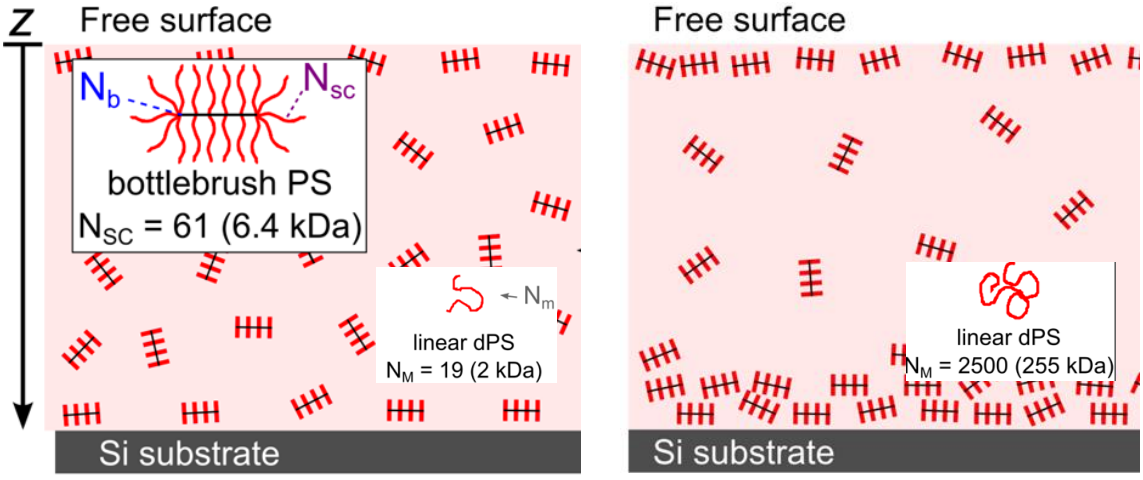

Figure I.3 Cartoon illustrating the segregation profiles at different N_M ratios.[82]

Bottlebrush copolymers have attracted a significant level of attention from scientists interested in developing rheology modifiers and surface coatings.[57,79,81,83,84] However, currently these specialty materials are not readily available on large scale; hence focus has been directed towards utilizing them as additives for cheaper commercially available materials. Stein and Verduzco et al. examined the phase behavior of brush copolymers mixed with deuterated linear polystyrene (PS).[82] The main goal was

to determine the wetting and dewetting transition of the mixture, or in other words, the transition between dispersion and aggregation of the bottlebrush additives. They found that the transition is controlled by the relative ratio of the degree of polymerizations (DP_L) of the linear polymer to that of the side chains (DP_{SC}). When the ratio is fairly low ($\leq$1.6) the brushes are dispersed throughout the film, Figure I.3. However, at sufficiently high ratio (N_M~8) the bottlebrushes begin to aggregate at interfaces, Figure I.4. This behavior is related to an entropic depletion attraction effect,[85] which causes larger branched molecules to adsorb to the interfaces. The data shows that sufficiently long BBCs can be employed as potential additives to modify various surfaces.[82]

Recent work published by Sheiko et al. highlighted an unusual behavior of incompatible brush copolymers at air-water interfaces.[86] Sheiko studied the surface behavior of immiscible materials under compression, based on the difference in their topologies. When two immiscible linear polymers, hydrophobic and hydrophilic, were blended together a clear phase-separation was observed (Figure I.4A). However, when the same tests were performed using incompatible bottlebrushes, a clear transition from a phase-segregation to a perfect-intercalation was identified, Figure I.4B. When BBCs were subjected to compression, the intermolecular distance gradually decreased, thus forcing the grafts on the hydrophilic brush to reach toward the water sub-phase. At sufficiently high compression intercalation occurred, thus inducing an increment of the brush and hence the relaxation of hydrophobic grafts, Figure I.4C. The induced mixing at the interfaces enabled the formation of long-range arrays of chemically immiscible

materials, which can be potentially applied in photovoltaic films, multifunctional coatings, and enzymatically active surfaces.[86]

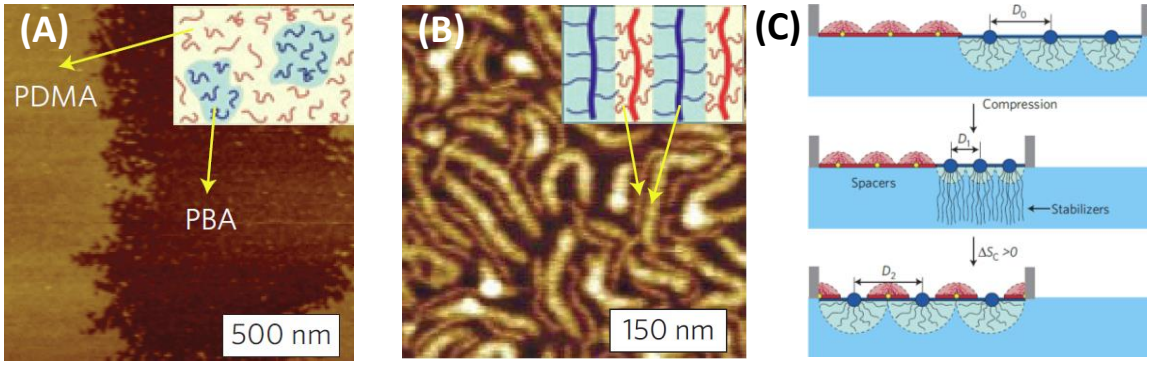

Figure I.4 AFM height images of 50/50 mixture of P*n*BA and PDMA with: (A) linear and (B) bottlebrush topologies. (C) Mixing of incompatible P*n*BA and PDMA brushes under compression. Hydrophobic (P*n*BA) brushes act as spacers whereas hydrophilic (PDMA) ones behave like stabilizes.[86]

I.4 Self-assembly of Block Bottlebrushes in Bulk and on Surfaces

The above section highlights the pronounced differences between physical properties of homo-component polymers with linear and bottlebrush architectures. Similar differences in properties can be extended to more complex, multicomponent brush copolymers. Diblock bottlebrushes have attracted significant attention due to their bulk and solution properties, and their ability to phase separate into interesting morphologies.

Linear block copolymers with sufficiently incompatible blocks can phase separate and the two phases can self-assemble into various morphologies including spheres, cylinders, gyroid and lamellae. Microphase separation relies on the segregation strength (χN), which results from the interaction parameter (χB) of the blocks and the overall degree of polymerization (N). The type of phase domain is based on the volume fraction monomers, while the domain spacing (D) depends on the molecular weight of the block polymer. The self-assembly of linear block copolymers has been utilized in the formation of periodic materials, such as photonics; however, the methodology suffers from the limitation in domain spacing arising from the high entanglement density of long block copolymers.

The use of BBCs can be employed to circumvent some issues associated with the linear blocks. The dense grafting of side chains as well as extended conformation of molecular bottlebrushes results in a significant drop in the entanglement density. Therefore, bottlebrushes are capable of overcoming the kinetic barrier for self-assembly of HMW species, which is not attainable with linear copolymers.[57] Early results showed that block brushes can phase separate into well-defined lamellae morphologies with domain spacing ~100 nm, much higher than that attained by linear blocks.[36,37,87,88] As noted above, recent advances in ROMP technique have had a significant influence on the synthesis of molecular bottlebrushes, particularly block brush copolymers (BBBCs). Grubbs et al. conducted seminal work when performing systematic studies on synthesis of symmetrical block brushes for photonic applications.[51,53-57] All of his reported block

brushes were synthesized via the 'grafting through' approach, by utilizing sequential ROMP of norbornene-functionalized macromonomers.

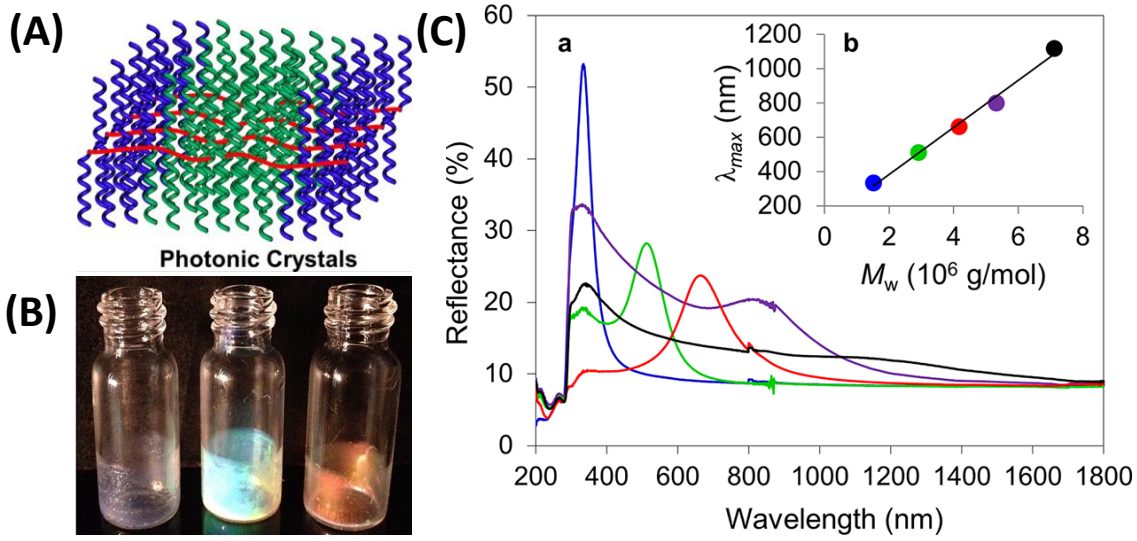

Figure I.5 A) Cartoon visualization of lamellae morphology formed by head-to-head self-assembly of block brushes. B) Visual images of block brushes reflecting different wavelengths. C) The reflectance plotted against wavelengths for block brushes with different MWs, and linear dependence of reflected wavelength vs. MW of the brush.[55]

The initial studies by Grubbs and co-workers focused on determining the effect of BBBCs molecular weight on their phase separation ability. For that purpose, a series of symmetrical block brushes with varying molar masses (1512 – 7119 kDa) was prepared, and then self-assembled into solid thin-films via controlled solvent evaporation methods. The rigid nature of brushes facilitated a rapid, head-to-head assembly of all BBBCs, except for the highest MW sample, thus forming photonic materials ranging from ultra-violet to near-infrared, Figure I.5 A,B. Most importantly, the observed maximum

reflected wavelengths scaled linearly with increasing molecular weights of the block brushes, Figure I.VC. These findings are crucial for the design of tunable photonic materials with predictable band gap size.[55]

The preliminary discoveries on self-assembly of BBBCs have directed the studies towards mixtures of symmetrical bottlebrushes with different molecular weights. Surprisingly, the blends of low and high MW block brushes formed highly uniform lamellar morphologies, showing a similar behavior to that of a single block brush. In addition, the size gap progressively increased with increasing weight fraction of HMW brush component. The outcome of this research shows that BBBCs blends can be applied to the preparation of a wide range of photonic materials with a band gap size controlled by the relative ratio of BBBCs components.

Addition of linear homopolymers (HPs) is a common way of adjusting the band gap in periodic materials generated from linear block copolymers. A HP dopant acts as a plasticizer, thus allowing for swelling of a domain in a predictable manner.[89,90] Grubbs and co-workers tested the same technique by swelling block brushes with linear homopolymers.[53] It results in a high degree of swelling of the lamellae morphology, reaching up to 180% of the initial domain size. The reflected maximum wavelengths of obtained arrays were as high as ~1410nm; much higher than those attainable by previous methods of assembling of BBBCs. Doping with HPs resulted in a good control over long distance assembling of block brushes, providing reflective thin films with periodicities between 100 and 500 nm. Grubbs et al. also showed that this method can be further

advanced by employing functional HPs. The concept is based on the modification of the swollen block by an addition of linear homopolymers with pendant functionalities. The functional groups might be used to tune the properties of the swollen block, such as reflectivity, higher stability via cross-linking, or stimuli-responsiveness.[53]

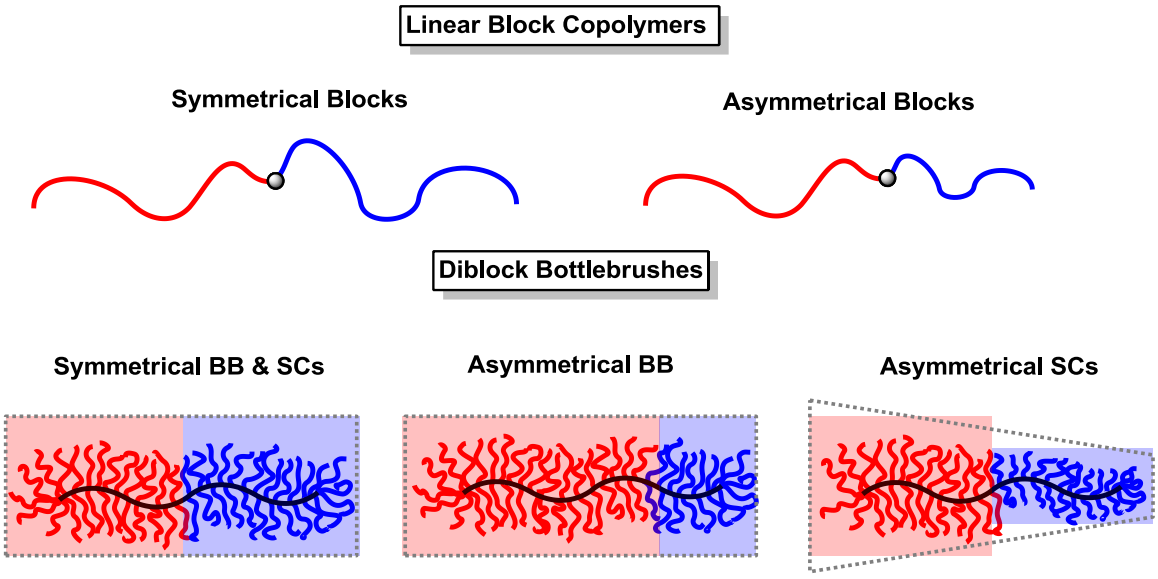

Figure I.6 Schematic representation of linear clock copolymers and diblock brushes with different block symmetries.

Self-assembly of block bottlebrushes is a powerful tool for generation of photonic materials with tunable band gaps. The size of the domain is controlled by the MW of the block bottlebrushes, and can be further adjusted by doping with either different BBBC or linear HP. Those methodologies enable access to well-ordered lamellar nanostructures that reflect IR light and can be applied as thin-film coatings in urban areas.

It is well known that diblock copolymers phase segregate into different morphologies predicted by the phase diagram. In linear BCs, the nature of a formed nanostructure relies mainly of the volume (*f*) ratio of the constituent blocks (Figure I.6). BCs with similar block volumes self-assembly into lamellae morphologies, transitioning to curved morphologies with an increasing volume ratio of blocks.

Work on self-assembly of BBBCs by Grubbs focused explicitly on symmetrical block brushes (Figure 1.6). As expected, the results showed exclusively a phase separation into lamellae microstructures. In Rzayev's early studies on self-assembly of block brushes, more emphasis was put on understanding the effect of topology on their phase separation. The results proved that the rigid nature of bottlebrushes plays an equal, if not more important, role in the assemby process to that of the volume ratio of blocks. Rzayev noted that introducing a fairly high level of asymmetry (f = 0.3) into bottlebrushes does not affect their lamellae morphology, which is consistent with the rigid nature of bottlebrush macromolecules (Figure I.6). However, highly asymmetric BBBCs did not assemble into any ordered structures, which was ascribed to insufficient flexibility of bottlebrushes preventing them from packing into assemblies with curved interfaces.[36] These results suggested that the morphology in block brushes is not necessarily governed by the volume fractions of blocks, but by their structural design.[36,87,88]

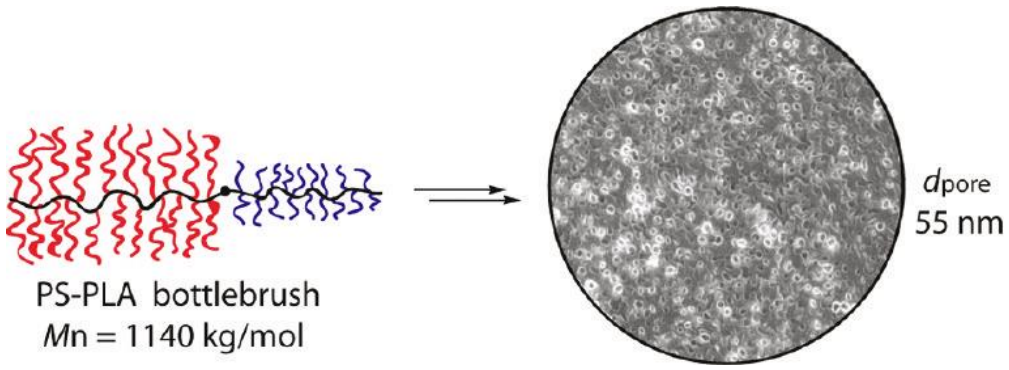

Figure I.7 Formation of nanoporous materials from assymetric PS-PLA block brush.[39]

The shape-persistent nature of brush copolymers facilitates their self-assembly into lamellae nanostructure with large domain spacing. On contrary, the same property significantly hampers their ability to form curved morphologies. Rzayev and co-workers proved that this issue can be circumvented by introducing a large discrepancy between the lengths of grafts in each block of BBBCs (Figure I.6). [39] For that purpose, a block brush with polystyrene (PS) and polylactide (PLA) grafts was synthesized so that PS side chains were three times the size of PLA (Figure I.7). SAXS analysis of the BBBC indicated on the presence of domains with spacing of 70 nm, without detecting any clear morphology. A presence of a degradable component (PLA) enabled a selective removal of one block from aligned polymer monoliths. SEM imaging of the material provided clear evidence on the formation of porous structure. The pore size distribution was fairly narrow, but more importantly the pore diameter was 55 ± 16 nm (Figure I.7), which is notably larger than what is attainable by templating with linear diblock copolymers. Templating with block brushes provides an access to a larger number of nanoporous

materials with a broader pore size range, which might be useful in applications such as ultrafiltration and templating.[39]

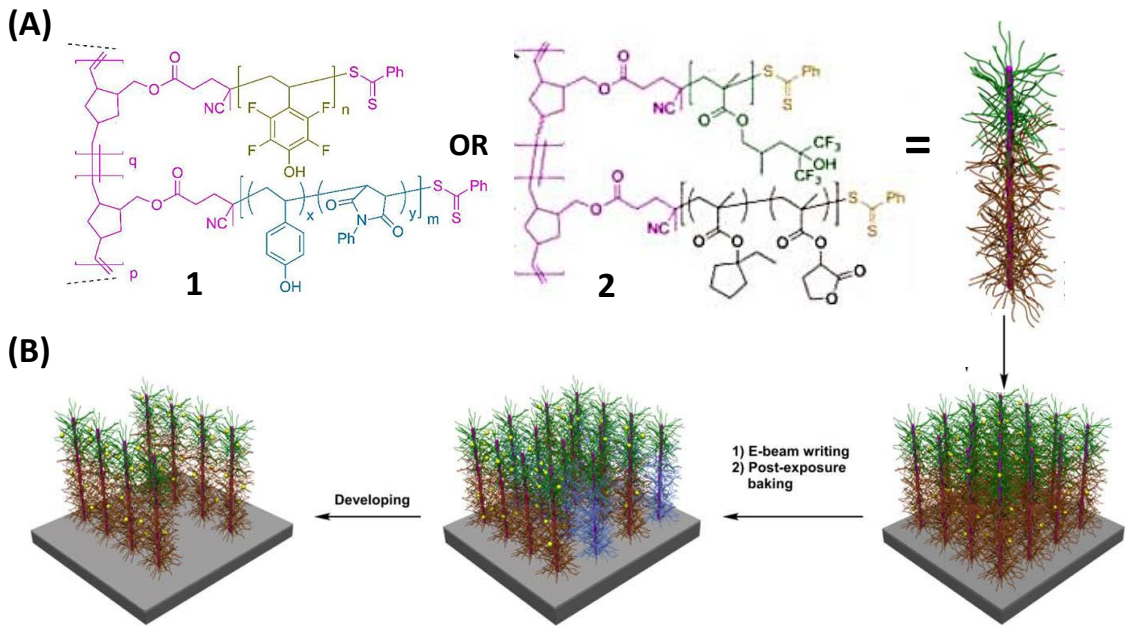

Scheme I.3 (A) Structures (**1** and **2**) of diblock brushes with short (top) fluorinated and long cross-linkable (bottom) blocks. (B) Schematic representation of lithographic process performed by using a monolayer thin film comprised of ideally vertically aligned block brushes and physically blended phot-acid generator.[73,91]

Wooley et al. has presented a very interesting application of using block brushes may as templates for nanopaterns.[73,91] For that purpose, brushes were composed of two segments, the shorter block comprised of fluorinated monomers and the longer one containing cross-linkable functionalities (Scheme 1.3A). The presence of fluorinated block facilitated a vertical alignment of brushes on silica wafers, and the acid-sensitive block enabled a selective photo-crosslinking of brushes (Scheme 1.3B). This is a high-

resolution, high-sensitivity negative/positive-tone photoresist technique that allows for top-down single-molecule line-width (~30nm) imaging. The concept may have applications in photolithography as well as chemically-amplified resists for microelectronic devices.[73,91]

I.5 Self-assembly of Block Bottlebrushes in Solution

Besides ongoing studies on self-assembly of BBBCs in melt, there has been an increasing interest in investigating of their solution behavior. Wooley et al. studied the aqueous self-assembly of symmetrical, amphiphilic block brush. The results showed the formation of spherical aggregates, but with a broad size distribution.[92] A few other studies on BBBCs amphiphiles have also shown the formation of spherical aggregates; however, the data was provided for dry samples, with no insight into initial shape and composition of micelles.[92-94]

Morphologies generated by linear amphiphiles rely on their interfacial curvature, which is governed by the volume and length of the hydrophobic block, known as a molecular packing parameter.[95] Generally, an increasing curvature (increasing length of one block) induces the transition from bilayers to networks, cylinders and eventually spheres. Rzayev et al. have performed detailed studies on aqueous self-assembly of block brush amphiphiles, and used the packing parameter to explain obtained morphologies.[96] It was suggested that the interfacial curvature in brush amphiphiles increases with increasing asymmetry in grafts lengths (Figure I.8A); however, due to the rigid nature of

brushes such changes in curvature are not as evident when the size discrepancy occurs within the brush backbone (Figure 1.8B).[96]

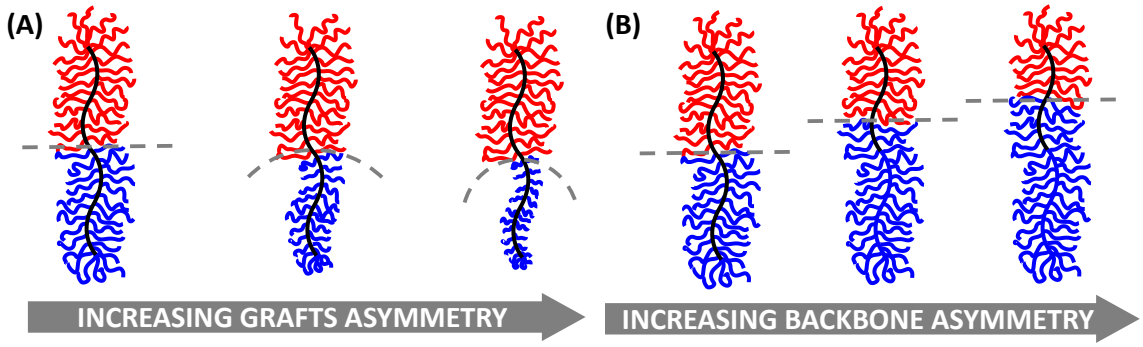

Figure I.8 Interfacial curvatures in block brushes with asymmetry in (A) side chains and (B) backbone.

The studies were performed on a series of amphiphilic brushes with varying side chains discrepancies i.e. packing parameters. The use of cryo-TEM enabled testing of formed ensembles in their native state. The results of visualization proved the formation of various morphologies from spheres and cylindrical micelles to bilayers, which were governed by the asymmetry in the grafts lengths. These materials were described as 'giant surfactants' that can be employed in the rational fabrication of a range of micellar structures in narrow morphological window.[96]

I.6 Templating with Molecular Bottlebrushes

The cylindrical shape and controllable dimensions of molecular bottlebrushes are one of their most appealing characteristics of the macromoleculaes. Recently, attention

has been directed towards their application as single-molecule templates for generation of organic and hybrid nanoobjects. Bottlebrushes can be viewed as covalently bonded cylindrical micelles, a physically self-assembled system, which commonly used to generate nanoobjects. When brush is employed as a template, the size of the resulting object is determined by the dimensions of the initial template. In addition, BBCs templating does not require pre-assembly and provides access to a wide variety of tunable dimensions and compositions.

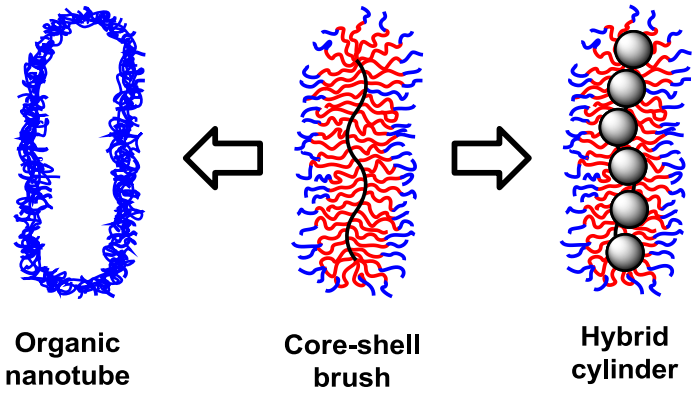

Figure I.9 Core-shell brushes as templates for hybrid materials and organic nanotubes.

Core-shell bottlebrushes have attracted particular interest as templates for hybrid materials and organic nanotubes. Hybrid materials synthesized by that method rely on the utilizing the core as the pre-cursor of the inorganic component. This is realized by employing a functional monomer in the core, which acts either as an inorganic precursor itself or as a binder for the inorganic salts (Figure I.9). On the contrary, the shell of the brush acts as a protecting layer, which prevents intermolecular fusion of hybrid cylinders and leakage of the precursor, but also provides solubility of the template in the reaction

medium. The dimensions of the hybrid cylinder are controlled by the size of the initial core-shell brush.

In early studies, Schmidt et al. showed that the 'grafting through' of macromonomers can be employed to prepare brush templates for synthesis of gold nanowire. Even though the wires were formed, the method did not provide any control over their length.[97] In contrast, the core-shell templates prepared by the 'grafting from', approach proved to be superior to the initial approach, enabling excellent control over the size of the formed nano-cylinders. Additionally, by introducing poly(acrylic acid) core into brushes, it could be loaded with inorganic salts, which upon oxidation form inorganic hybrids, such as magnetite, CdSe nanoparticles and cylinders.[98]

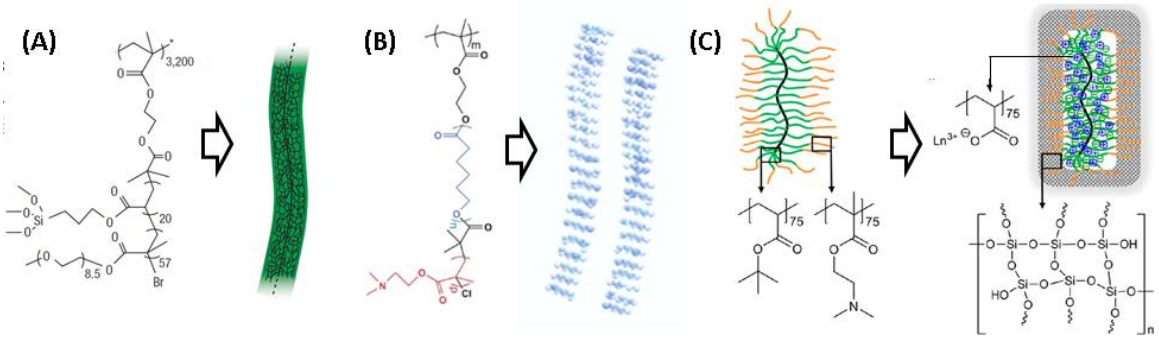

Figure I.10 Hybrid materials prepared via core-shell bottlebrush templating. Silica (A) wire, (B) nanotube and (C) nanocylinder with a rare-metal core.[99-101]

Müller et al. have prepared a series of core-shell brushes, with core composed of trimethoxysilyl-containing monomer, a precursor of silica (Figure 1.10A). The data showed that the design of core-shell brushes could be employed to control the dimensions of the obtained silica wires. In this case, the lengths and widths of the wires were

governed by the corresponding degrees of polymerization of the core and backbone.[100] Müller et al. has utilized the concept of a core-shell triblock brush in the formation of silica nanotubes (Figure 1.10B). In this case, the core was composed of two blocks serving different purposes.

The first block was composed of degradable component, allowing for the core removal and the formation of the hollow interior. The second block consisted of amino-based monomers capable of binding to silica precursor. This technique enables a straightforward way of preparing hollow silica wires (Figure 1.10B) with gap size determined by the fraction of degradable block incorporated in the template.[101] The same concept was used by Müller et al. to generate TiO_2 hybrid nanotubes.[102,103] The group has also expanded the idea of core-shell bottlebrushes templates to rare metal complex silica hybrids. In this case, acidic core was loaded with rare metal salts and then the amino-functionalized shell was transformed into silica shell (Figure 1.10C). Depending on the nature of the rare metal complex, the silica hybrids showed interesting luminescence and paramagnetic properties. They were even tested as potential MRI contrast agents, showing higher brightness than those available commercially.[99]

Over the past few years, Rzayev et al. have performed thorough studies on studying core-shell brush templates for the preparation of organic nanotubes (Figure I.9). Rzayev has shown that core-shell templating is an excellent technique to form organic nanotubes.

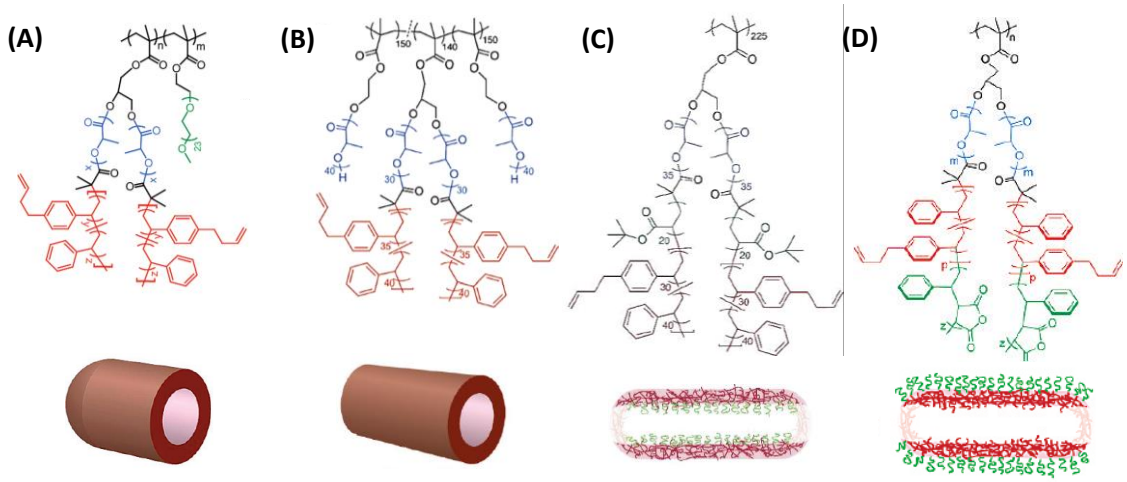

Figure I.11 Chemical compositions of core-shell bottlebrushes used in the formation of nanostructures with topologies: (A) one opened end, (B) both ends opened, (C) functional interior and (D) functional exterior nanotubes.[32,58-60]

The backbone of the brush controls the final length of the nanotube; however it can also be used to tune the entire topology of the organic hybrid. For instance, by modifying ends of the backbones, enabling access to fully sealed nanocontainers or tubes with open wither one or both ends (Figure I.11 C and D, A, and B respectively).[32,58]

The core-shell structure of the brush is governed by the size and composition of its core, which can be modified in numerous ways, thus controlling the topology of the final nanotube. The first block of the core is composed of a degradable component, such as polylactide, which is removed to form a hollow nanotube (Figure I.11). The second block consists of a monomer with cross-linkable units, a precursor of the shell, which can be stabilized via chemical or photocrosslinking (Figure I.11).[60,61] It not only provides a method to stabilize of the final tube shape, but it can also be used to introduce a

degradability into the nanotube, for instance by using dithio-crosslinkers.[60] In addition, the design of the external block can be employed to adjust the solubility or to modify the surface properties of the organic nanotubes (Figure I.11D). For example, an incorporation of the hydrophilic shell enabled water solubility, whereas the presence of a hydrophobic monomer enabled internalization of nanotubes into cells (Figure I.11D).[59] It was also shown that the interior of the nanotube can be functionalized to provide the ability to fine-tune the organic nanotubes for size and charge selective molecular transportation (Figure I.11C).[104] The work presented here proves that core-shell bottlebrushes have a great potentials as templates for the preparation of organic and hybrid nanotubes with controllable dimensions.

I.7 Thesis Organization

Selected chapters presented in this thesis are based on previously published manuscripts. A list of all publications which I coauthored during my PhD is listed below:

1) **Burdyńska, J.**; Li, Y.; Aggarwal, A. V.; Höger, S.; Sheiko, S. S.; Matyjaszewski, K. "Synthesis and Arm Dissociation in Molecular Stars with a Spoked Wheel Core and Bottlebrush Arms" *J. Am. Chem. Soc.* **2014**, *136*, 12762-12770.
2) Franczyk, A.; He, H.; **Burdyńska, J.**; Hui, C. M.; Matyjaszewski, K.; Marciniec, B. "Synthesis of high molecular weight polymethacrylates with POSS moieties by ATRP" *ACS Macro Letters*, **2014**, *3*, 799-802.

3) Li, Y.; Nese, A.; Hu, X.; Lebedeva, N. V.; LaJoie, T. W.; **Burdyńska, J.**; Stefan, M. C.; You, W.; Yang, W.; Matyjaszewski, K.; Sheiko, S. S. "Shifting Electronic Structure by Inherent Tension in Molecular Bottlebrushes with Polythiophene Backbones" *ACS Macro Letters* **2014**, *3*, 738−742.

4) Banquy, X.; **Burdyńska, J.**; Lee, D.-W.; Matyjaszewski, K. and Israelachvili, J. "Bio-inspired bottle brush polymer exhibits low friction and Amontons-like behavior" *J. Am. Chem. Soc.* **2014**, *136*, 6199–6202.

5) Elsen, A. M.; **Burdyńska, J.**; Park, S.; Matyjaszewski, K. "Activators Regenerated by Electron Transfer Atom Transfer Radical Polymerization in Miniemulsion with 50 ppm of Copper Catalyst" *ACS Macro Lett.* **2013**, *2*, 822-825.

6) Park, S.; Cho, H. Y.; Wegner, K. B.; **Burdyńska, J.**; Magenau, A. J. D.; Paik, H.-j.; Jurga, S., and Matyjaszewski, K. "Star Synthesis Using Macroinitiators via Electrochemically Mediated Atom Transfer Radical Polymerization" *Macromolecules* **2013**, *46*, 5856–5860.

7) Stals, P. J. M.;* Li, Y.;* **Burdyńska, J.**;* Nicolay, R.; Nese, A.; Palmas, A. R. A.; Matyjaszewski, K.; Meijer, E. W. and Sheiko, S. S. "How Far Can We Push Polymer Architectures?" *J. Am. Chem. Soc.* **2013**, *135*, 11421–11424.

8) Elsen, A. M.; **Burdyńska, J.**; Park, S.; Matyjaszewski, K. "Active Ligand for Low PPM Miniemulsion Atom Transfer Radical Polymerization" *Macromolecules* **2012**, *45*, 7356–7363.

9) **Burdyńska, J.**; Cho, H. Y.; Mueller, L.; Matyjaszewski, K. "Synthesis of star polymers using ARGET ATRP" *Macromolecules* **2010**, *435*, 9227–9229.

I.8 Thesis Mission

The goal of this thesis is to show how ATRP can be combined with synthetic techniques to form advanced bottlebrush architectures with interesting, and diverse, properties. The research described in this thesis was divided into four sections.

Section I is an introduction to molecular bottlebrushes, their synthetic methods, physical properties and applications. The summary focuses on the current progress that was made in the brush field over the past five years.

Section II focuses on the structure-property relationship of bottlebrushes with the same composition, but varying structural factors. Chapter 2 describes the synthesis of brushes with different grafting densities and with varying lengths of grafts and backbone, and the effect of the topology on thermal diffusion is presented. In chapter 3 synthesis of bottlebrushes with constant length of the backbone and varying side chains is discussed and the effect of the structural details on the viscoelastic behavior is presented. Chapter IV describes brushes with monomodal and bimodal grafts lengths, their synthesis and characterization via AFM.

Section III represents the use of functional ATRP multiinitiators for the formation of bottlebrushes. Chapter 5 describes the use of diinitiators for the preparation of new machanosensors, as well as the way of incorporating small tags into the brush center. Chapter 6 provides the summary of the use of hexainitiator for the preparation of molecular stars with machanosensitive properties.

Section IV is a description of synthetic molecular bottlebrushes inspired by biological molecules. It discusses the use of synthetic brushes as lubricants for human joint and oil engines.

I.9 References

(1) Lee, H.-i.; Pietrasik, J.; Sheiko, S. S.; Matyjaszewski, K. *Prog. Polym. Sci.* **2010**, *35*, 24-44.

(2) Sheiko, S. S.; Sumerlin, B. S.; Matyjaszewski, K. *Prog. Polym. Sci.* **2008**, *33*, 759-785.

(3) Zhang, M.; Mueller, A. H. E. *J. Polym. Sci., Part A: Polym. Chem.* **2005**, *43*, 3461-3481.

(4) Lecommandoux, S.; Chécot, F.; Borsali, R.; Schappacher, M.; Deffieux, A.; Brulet, A.; Cotton, J. P. *Macromolecules* **2002**, *35*, 8878-8881.

(5) Zhang, B.; Grohn, F.; Pedersen, J. S.; Fischer, K.; Schmidt, M. *Macromolecules* **2006**, *39*, 8440-8450.

(6) Rathgeber, S.; Pakula, T.; Wilk, A.; Matyjaszewski, K.; Beers, K. L. *J. Chem. Phys.* **2005**, *122*, 124904-124913.

(7) Wintermantel, M.; Schmidt, M.; Tsukahara, Y.; Kajiwara, K.; Kohjiya, S. *Macromolecular Rapid Communications* **1994**, *15*, 279-284.

(8) Tsukahara, Y.; Mizuno, K.; Segawa, A.; Yamashita, Y. *Macromolecules* **1989**, *22*, 1546-1552.

(9) Tsukahara, Y.; Tsutsumi, K.; Yamashita, Y.; Shimada, S. *Macromolecules* **1990**, *23*, 5201-5208.

(10) Beers, K. L.; Gaynor, S. G.; Matyjaszewski, K.; Sheiko, S. S.; Moeller, M. *Macromolecules* **1998**, *31*, 9413-9415.

(11) Mynar, J. L.; Choi, T.-L.; Yoshida, M.; Kim, V.; Hawker, C. J.; Frechet, J. M. J. *Chem. Commun.* **2005**, *41*, 5169-5171.

(12) Kolb, H. C.; Finn, M. G.; Sharpless, K. B. *Angew. Chem. Int. Ed.* **2001**, *40*, 2004-2021.

(13) Schappacher, M.; Billaud, C.; Paulo, C.; Deffieux, A. *Macromol. Chem. Phys.* **1999**, *200*, 2377-2386.

(14) Gadwal, I.; Rao, J.; Baettig, J.; Khan, A. *Macromolecules* **2014**, *47*, 35-40.

(15) Gao, H.; Matyjaszewski, K. *J. Am. Chem. Soc.* **2007**, *129* 6633-6639.

(16) Lahasky, S. H.; Serem, W. K.; Guo, L.; Garno, J. C.; Zhang, D. *Macromolecules* **2011**, *44*, 9063-9074.

(17) Johnson, J. A.; Lu, Y. Y.; Burts, A. O.; Lim, Y. H.; Finn, M. G.; Koberstein, J. T.; Turro, N. J.; Tirrell, D. A.; Grubbs, R. H. *J. Am. Chem. Soc.* **2011**, *133*, 559-566.

(18) Sun, J.; Hu, J.; Liu, G.; Xiao, D.; He, G.; Lu, R. *J. Polym. Sci., Part A: Polym. Chem.* **2011**, *49*, 1282-1288.

(19) Neugebauer, D.; Zhang, Y.; Pakula, T.; Matyjaszewski, K. *Macromolecules* **2005**, *38*, 8687-8693.

(20) Neugebauer, D.; Zhang, Y.; Pakula, T.; Sheiko, S. S.; Matyjaszewski, K. *Macromolecules* **2003**, *36*, 6746-6755.

(21) Li, Z.; Zhang, K.; Ma, J.; Cheng, C.; Wooley, K. L. *J. Polym. Sci. A Polym. Chem.* **2009**, *47*, 5557-5563.

(22) Jha, S.; Dutta, S.; Bowden, N. B. *Macromolecules* **2004**, *37*, 4365-4374.

(23) Xia, Y.; Kornfield, J. A.; Grubbs, R. H. *Macromolecules* **2009**, *42*, 3761-3766.

(24) Ping, J.; Qiao, Y.; Tian, H.; Shen, Z.; Fan, X.-H. *Macromolecules* **2015**, 10.1021/ma502414m.

(25) Nese, A.; Li, Y.; Sheiko, S. S.; Matyjaszewski, K. *ACS Macro Letters* **2012**, *1*, 991-994.

(26) Sumerlin, B. S.; Neugebauer, D.; Matyjaszewski, K. *Macromolecules* **2005**, *38*, 702-708.

(27) Neugebauer, D.; Sumerlin, B. S.; Matyjaszewski, K.; Goodhart, B.; Sheiko, S. S. *Polymer* **2004**, *45*, 8173−8179.

(28) Zheng, Z.; Ling, J.; Müller, A. H. E. *Macromolecular Rapid Communications* **2014**, *35*, 234-241.

(29) Gregory, A.; Stenzel, M. H. *Prog. Polym. Sci.* **2012** *37*, 38-105.

(30) Barner, L.; Davis, T. P.; Stenzel, M. H.; Barner-Kowollik, C. *Macromolecular Rapid Communications* **2007** *28*, 1539-1600.

(31) Radzinski, S. C.; Foster, J. C.; Matson, J. B. *Polym. Chem.* **2015**, 10.1039/c4py01567c.

(32) Huang, K.; Rzayev, J. *J. Am. Chem. Soc.* **2009**, *131*, 6880-6885.

(33) Lee, H.-i.; Jakubowski, W.; Matyjaszewski, K.; Yu, S.; Sheiko, S. S. *Macromolecules* **2006**, *39*, 4983-4989.

(34) Yu-Su, S. Y.; Sheiko, S. S.; Lee, H.-i.; Jakubowski, W.; Nese, A.; Matyjaszewski, K.; Anokhin, D.; Ivanov, D. A. *Macromolecules* **2009**, *42* 9008-9017.

(35) Cheng, G.; Boeker, A.; Zhang, M.; Krausch, G.; Mueller, A. H. E. *Macromolecules* **2001**, *34*, 6883-6888.

(36) Rzayev, J. *Macromolecules* **2009**, *42*, 2135-2141.

(37) Lee, H.-i.; Matyjaszewski, K.; Yu-Su, S.; Sheiko, S. S. *Macromolecules* **2008**, *41*, 6073-6080.

(38) Zehm, D.; Laschewsky, A.; Liang, H.; Rabe, J. P. *Macromolecules* **2011**, *44*, 9635-9641.

(39) Bolton, J.; Bailey, T. S.; Rzayev, J. *Nano Lett.* **2011**, *11*, 998-1001.

(40) Zehm, D.; Laschewsky, A.; Heunemann, P.; Gradzielski, M.; Prévost, S.; Liang, H.; Rabe, J. P.; Lutz, J.-F. *Polym. Chem.* **2011**, *2*, 137-147.

(41) Bolton, J.; Rzayev, J. *Macromolecules* **2014**, *47*, 2864-2874.

(42) Elsen, A. M.; Li, Y.; Li, Q.; Sheiko, S. S.; Matyjaszewski, K. *Macromolecular Rapid Communications* **2014**, *35*, 133-140.

(43) Lee, H.-i.; Matyjaszewski, K.; Yu, S.; Sheiko, S. S. *Macromolecules* **2005**, *38*, 8264-8271.

(44) Stals, P. J. M.; Li, Y.; Burdyńska, J.; Nicolaÿ, R.; Nese, A.; A., A. R.; Palmans; Meijer, E. W.; Matyjaszewski, K.; Sheiko, S. S. *J. Am. Chem. Soc.* **2013**, *135*, 11421-11424.

(45) Matyjaszewski, K.; Qin, S.; Boyce, J. R.; Shirvanyants, D.; Sheiko, S. S. *Macromolecules* **2003**, *36*, 1843-1849.

(46) Lebedeva, N. V.; Nese, A.; Sun, F. C.; Matyjaszewski, K.; Sheiko, S. S. *Proc. Natl. Acad. Sci* **2012**, *109*, 9276-9280.

(47) Li, Y.; Nese, A.; Lebedeva, N. V.; Davis, T.; Matyjaszewski, K.; Sheiko, S. S. *J. Am. Chem. Soc.* **2011**, *133*, 17479-17484.

(48) Li, Y.; Nese, A.; Matyjaszewski, K.; Sheiko, S. S. *Macromolecules* **2013**, *46*, 7196-7201.

(49) Pakula, T.; Zhang, Y.; Matyjaszewski, K.; Lee, H.-i.; Boerner, H.; Qin, S.; Berry, G. C. *Polymer* **2006**, *47*, 7198-7206.

(50) Zhang, Y.; Constantini, N.; Mierzwa, M.; Pakula, T.; Neugebauer, D.; Matyjaszewski, K. *Polymer* **2004**, *45*, 6333-6339.

(51) Gu, W.; Huh, J.; Hong, S. W.; Sveinbjornsson, B. R.; Park, C.; Grubbs, R. H.; Russell, T. P. *ACS Nano* **2013**, *7*, 2551-2558.

(52) Hong, S. W.; Gu, W.; Huh, J.; Sveinbjornsson, B. R.; Jeong, G.; Grubbs, R. H.; Russell, T. P. *ACS Nano* **2013**, *7*, 9684–9692.

(53) Macfarlane, R. J.; Kim, B.; Lee, B.; Weitekamp, R. A.; Bates, C. M.; Lee, S. F.; Chang, A. B.; Delaney, K. T.; Fredrickson, G. H.; Atwater, H. A.; Grubbs, R. H. *J. Am. Chem. Soc.* **2014**, *136*, 17374-17377.

(54) Miyake, G. M.; Piunova, V. A.; Weitekamp, R. A.; Grubbs, R. H. *Angew. Chem. Int. Ed.* **2012**, *51*, 11246-11248.

(55) Miyake, G. M.; Weitekamp, R. A.; Piunova, V. A.; Grubbs, R. H. *J. Am. Chem. Soc.* **2012**, *134*, 14249-14254.

(56) Sveinbjörnsson, B. R.; Weitekamp, R. A.; Miyake, G. M.; Xia, Y.; Atwater, H. A.; Grubbs, R. H. *Proc. Natl. Acad. Sci* **2012**, *109*, 14332-14336.

(57) Xia, Y.; Olsen, B. D.; Kornfield, J. A.; Grubbs, R. H. *J. Am. Chem. Soc.* **2009**, *131*, 18525-18532.

(58) Huang, K.; Canterbury, D. P.; Rzayev, J. *Macromolecules* **2010**, *43*, 6632-6638.

(59) Huang, K.; Jacobs, A.; Rzayev, J. *Biomacromolecules* **2011**, *12*, 2327-2334.

(60) Huang, K.; Johnson, M.; Rzayev, J. *ACS Macro Lett.* **2012**, *1*, 892-895.

(61) Onbulak, S.; Rzayev, J. *Polym. Chem.* **2015**, *6*, 764-771.

(62) Ding, J.; Xiao, C.; Tang, Z.; Zhuang, X.; Chen, X. *Macromol. Biosci.* **2011**, *11*, 192-198.

(63) Ding, J.; Xiao, C.; Zhao, L.; Cheng, Y.; Ma, L.; Tang, Z.; Zhuang, X.; Chen, X. *J. Polym. Sci. A Polym. Chem.* **2012**, *49*, 2665-2676.

(64) Chen, P.; Li, C.; Liu, D.; Li, Z. *Macromolecules* **2012**, *45*, 9579-9584.

(65) Yao, K.; Chen, Y.; Zhang, J.; Bunyard, C.; Tang, C. *Macromolecular Rapid Communications* **2013**, *34*, 645−651.

(66) Liu, Y.; Chen, P.; Li, Z. *Macromolecular Rapid Communications* **2012**, *33*, 287-295.

(67) Johnson, J. A.; Lu, Y. Y.; Burts, A. O.; Xia, Y.; Durrell, A. C.; Tirrell, D. A.; Grubbs, R. H. *Macromolecules* **2010**, *43*, 10326-10335.

(68) Tang, H.; Li, Y.; Lahasky, S. H.; Sheiko, S. S.; Zhang, D. *Macromolecules* **2011**, *44*, 1491-1499.

(69) Johnson, J. A.; Lu, Y. Y.; Burts, A. O.; Lim, Y.-H.; Finn, M. G.; Koberstein, J. T.; Turro, N. J.; Tirrell, D. A.; Grubbs, R. H. *J. Am. Chem. Soc.* **2011**, *133*, 559-566.

(70) Sowers, M. A.; McCombs, J. R.; Wang, Y.; Paletta, J. T.; Morton, S. W.; Dreaden, E. C.; Boska, M. D.; Ottaviani, M. F.; Hammond, P. T.; Rajca, A.; Johnson, J. A. *Nat. Commun.* **2014**, doi: 10.1038/ncomms6460.

(71) Wu, D.; Nese, A.; Pietrasik, J.; Yeru Liang, M. K.; Huang, L.; Kowalewski, T.; Matyjaszewski, K. *ACS Nano* **2012**, *6*, 6208-6214.

(72) Sun, G.; Cho, S.; Clark, C.; Verkhoturov, S.; Eller, M. J.; Li, A.; Pavia-Jiménez, A.; Schweikert, E. A.; Thackeray, J. W.; Trefonas, P.; Wooley, K. L. *J. Am. Chem. Soc.* **2013**, *135*, 4203-4206.

(73) Sun, G.; Cho, S.; Yang, F.; He, X.; Pavia-Sanders, A.; Clark, C.; Raymond, J. E.; Verkhoturov, S. V.; Schweikert, E. A.; Thackeray, J. W.; Trefonas, P.; Wooley, K. L. *J. Polym. Sci. A Polym. Chem.* **2015**, *53*, 193-199.

(74) Matyjaszewski, K.; Tsarevsky, N. V. *J. Am. Chem. Soc.* **2014**, *136*, 6513-6533.

(75) Wintermantel, M.; Gerle, M.; Fischer, K.; Schmidt, M.; Wataoka, I.; Urakawa, H.; Kajiwara, K.; Tsukahara, Y. *Macromolecules* **1996**, *29*, 978-983.

(76) Iwawaki, H.; Urakawa, O.; Inoue, T.; Nakamura, Y. *Macromolecules* **2012**, *45*, 4801−4808.

(77) Namba, S.; Tsukahara, Y.; Kaeriyama, K.; Okamoto, K.; Takahashi, M. *Polymer* **2000**, *41*, 5165−5171.

(78) Vlassopoulos, D.; Fytas, G.; Loppinet, B.; Isel, F.; Lutz, P.; Benoit, H. *Macromolecules* **2000**, *33*, 5960−5969.

(79) Hu, M.; Xia, Y.; McKenna, G. B.; Kornfield, J. A.; Grubbs, R. H. *Macromolecules* **2011**, *44*, 6935.

(80) Iwawaki, H.; Inoue, T.; Nakamura, Y. *Macromolecules* **2011**, *44*, 5414-5419.

(81) Dalsin, S. J.; Hillmyer, M. A.; Bates, F. S. *ACS Macro Lett.* **2014**, *3*, 423-427.

(82) Mitra, I.; Li, X.; Pesek, S. L.; Makarenko, B.; Lokitz, B. S.; Uhrig, D.; Ankner, J. F.; Verduzco, R.; Stein, G. E. *Macromolecules* **2014**, *47*, 5269-5276.

(83) Li, X.; Prukop, S. L.; Biswal, S. L.; Verduzco, R. *Macromolecules* **2012**, *45*, 7118-7127.

(84) Liu, B.; Narayanan, S.; Wu, D. T.; Foster, M. D. *Macromolecules* **2013**, *46*, 3190-3197.

(85) Rudhardt, D.; Bechinger, C.; Leiderer, P. *Phys. Rev. Lett.* **1998**, *81*, 1330-1333.

(86) Sheiko, S. S.; Zhou, J.; Arnold, J.; Neugebauer, D.; Matyjaszewski, K.; Tsitsilianis, C.; Tsukruk, V. V.; Carrillo, J.-M. Y.; Dobrynin, A. V.; Rubinstein, M. *Nat. Mater.* **2013**, *12*, 735-740.

(87) Runge, M. B.; Bowden, N. B. *J. Am. Chem. Soc.* **2007**, *129*, 10551-10560.

(88) Runge, M. B.; Lipscomb, C. E.; Ditzler, L. R.; Mahanthappa, M. K.; Tivanski, A. V.; Bowden, N. B. *Macromolecules* **2008**, *41*, 7687-7694.

(89) Winey, K. I.; Thomas, E. L.; Fetters, L. J. *Macromolecules* **1991**, *24*, 6182-6188.

(90) Kang, Y.; Walish, J. J.; Gorishnyy, T.; Thomas, E. L. *Nat. Mater.* **2007**, *6*.

(91) Sun, G.; Cho, S.; Clark, C.; Verkhoturov, S. V.; Eller, M. J.; Li, A.; Pavía-Jiménez, A.; Schweikert, E. A.; Thackeray, J. W.; Trefonas, P.; Wooley, K. L. *J. Am. Chem. Soc.* **2013**, *135*, 4203–4206.

(92) Li, Z.; Ma, J.; Cheng, C.; Zhang, K.; Wooley, K. L. *Macromolecules* **2010**, *43*, 1182-1184.

(93) Wu, D.; Zhao, C.; Tian, J.; Zhao, H. *Polym. Int.* **2009**, *58*, 1335-1340.

(94) Yang, Y. Q.; Guo, X. D.; Lin, W. J.; Zhang, L. J.; Zhang, C. Y.; Qian, Y. *Soft Matter* **2012**, *8*, 454-460.

(95) Israelachvili, J. N.; Mitchell, D. J.; Ninham, B. W. *J. Chem. Soc., Faraday Trans. 2* **1976**, *72*, 1525-1568.

(96) Fenyves, R.; Schmutz, M.; Horner, I. J.; Bright, F. V.; Rzayev, J. *J. Am. Chem. Soc.* **2014**, *136*, 7762-7770.

(97) Djalali, R.; Li, S. Y.; Schmidt, M. *Macromolecules* **2002**, *35*, 4282-4288.

(98) Xu, Y.; Yuan, J.; Fang, B.; Drechsler, M.; Muellner, M.; Bolisetty, S.; Ballauff, M.; Mueller, A. H. E. *Adv. Funct. Mater* **2010**, *20*.

(99) Zheng, Z.; Daniel, A.; Yu, W.; Weber, B.; Ling, J.; Müller, A. H. E. *Chem. Mater.* **2013**, *25*, 4585-4594.

(100) Yuan, J. Y.; Xu, Y. Y.; Walther, A.; Bolisetty, S.; Schumacher, M.; Schmalz, H.; Ballauff, M.; Müller, A. H. E. *Nat. Mater.* **2008**, *7*, 718-722.

(101) Müllner, M.; Lunkenbein, T.; Breu, J.; Caruso, F.; Müller, A. H. E. *Chem. Mater.* **2012**, *24*, 1802−1810.

(102) Müllner, M.; Lunkenbein, T.; Miyajima, N.; Breu, J.; Müller, A. H. E. *Small* **2012**, *8*, 2636-2640.

(103) Müllner, M.; Lunkenbein, T.; Schieder, M.; Gröschel, A. H.; Miyajima, N.; Förtsch, M.; Breu, J.; Caruso, F.; Müller, A. H. E. *Macromolecules* **2012**, *45*, 6981-6988.

(104) Huang, K.; Rzayev, J. *J. Am. Chem. Soc.* **2011**, *133*, 16726-16729.

SECTION II

STRUCTURE-PROPERTY RELATIONSHIPS IN MOLECULAR BOTTLEBRUSHES

CHAPTER II

PREPARATION OF A LIBRARY OF GRAFT COPOLYMERS FOR THERMAL FIELD-FLOW FRACTIONACTION (THFFF) STUDIES

Preface

The research described in the following chapter discusses the synthesis of a library of twelve graft copolymers with poly(*n*-butyl acrylate) side chains and varying topological features. Three architectural factors, including grafting density, and length of side chains and the backbone, were tuned to obtain this series of grafts copolymers. All polymers were prepared using the 'grafting from' method under normal ATRP conditions. The library of grafts was characterized via ThFFF, MALS and DLS techniques to determine the effect of topology on the thermal diffusion properties of branched polymers.

This was my first bottlebrush-related project and provided an excellent introduction to the field of molecular bottlebrushes. The time spent on synthesizing the series allowed me to gain a better understanding of how to adjust ATRP reaction conditions to tune various structural factors of bottlebrush molecules. In addition, I learnt important purification techniques for bottlebrushes, which were crucial in succeeding in more advanced projects examined during my PhD.

I synthesized all graft copolymers and characterized them by GPC and ^{1}H NMR. The graft copolymers were then sent for further analysis by Prof. Kim Williams at the Colorado School of Mines. Charles Ponyik, a graduate student in Williams' group, performed all analyses and correlations related to the study of thermal diffusion properties of graft copolymers, including DLS, MALS and ThFFF.

II.1 Introduction

Molecular bottlebrushes have attracted a great deal of attention due to their unique physical properties.[1-4] Bottlebrushes consist of a flexible backbone with grafted chains densely attached to it. The steric repulsion created between the grafts strongly affects the conformation of bottlebrush molecules, forcing them to adopt an entropically unfavored state, with highly extended backbone and side chains.[1-4] This greatly affects the properties of the brush macromolecules in the melt, as solids and in solution. For instance, the hydrodynamic radius of the brush-like structure in the solution is much smaller when compared to its linear analogue. In addition, the hydrodynamic radius is highly dependent on the ratio of the length of the side chains to the backbone, as well as the density of the grafts packed along the backbone.[3,4]

There are several different ways to synthesize molecular bottlebrushes, however the 'grafting from'[1,5-8] approach remains one of the most common and versatile techniques amongst them all. 'Grafting from' is predominately conducted through ATRP, which enables access to a great variety of branched copolymers with tunable grafting densities, as well as lengths of both the backbone and side chains. In contrast, when other approaches are considered, the control over such structural factors is often limited by steric hindrance issues. For instance, the 'grafting onto'[9] approach suffers from low grafting densities and only allows for linking short grafts to the backbone, whereas the 'grafting through'[10] approach generally results in preparation of brushes with relatively short backbones and in further limited to grafts with medium lengths.

The growing interest in molecular bottlebrushes has created a demand for the development of new characterization tools, which would provide a better understanding of the relationship between structure and properties in such macromolecules. Field-flow Fractionation (FFF) is a group of analytical techniques used specifically for characterization and separation of macromolecules. In this method an external field is applied perpendicularly to a stream of a fluid solution pumped through a channel, therefore causing separation of molecules[11] based on a polymer's size. FFF techniques are characterized by the type of field that is used to achieve separation. Multiple fields, such as electrical, centrifugal, or gravitational have been successfully applied in FFF systems. On the other hand, thermal Field-flow Fractionation (ThFFF) applies a temperature gradient to induce separation. In this process, a temperature difference is generated by heating the top wall of the channel, while cooling the bottom one (Figure II.1).[12-14] ThFFF is a separation method complementary to GPC, which enables separation based on a polymer's size and the interactions occurring at the polymer-solvent interface.

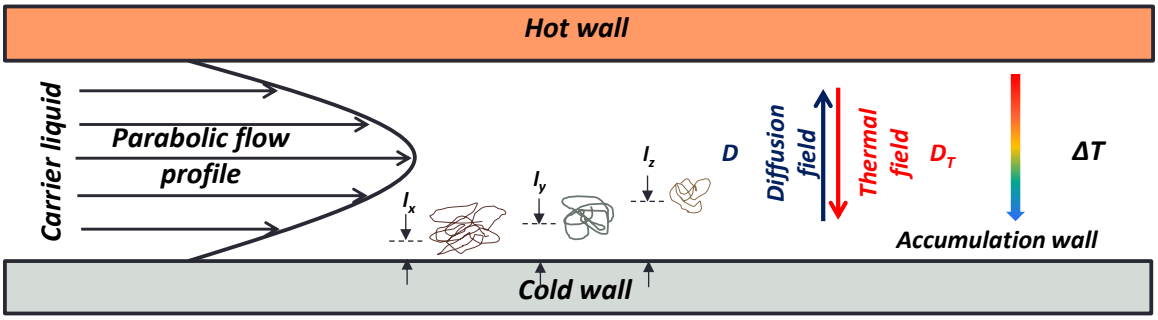

Figure II.1 Separation by Thermal Field-flow Fractionation (ThFFF).

ThFFF was successfully applied in the separation and characterization of macromolecules, such as polymers, nanogels or nanoparticles. Moreover, it allows for obtaining additional information about the chemistry of polymers by utilizing various organic solvents as the carrier liquid (Scheme II.1).[15] Therefore, polymeric materials can be separated by their molecular weight (MW) as well as by chemical composition. In other words, polymers with the same molecular weights but different compositions can be differentiated and separated from each other.[15]

In this research Thermal Field-Flow Fractionation (ThFFF) was employed for the development of a better way to characterize branched polymers. In addition to the separation based on a molecular weight and composition, ThFFF can be used to determine the architecture of the polymer by obtaining the Soret coefficient (S_T), which is the ratio of the polymer size to its interactions with surrounding solvent. ThFFF thereby enables the characterization of the degree of branching, and the type of architecture. Noteworthy, this method does not rely on the need for polymer standards that is often required in analytical methods such as GPC.

II.2 Experimental

Materials. *n*-Butyl acrylate (*n*BA, 99%, Acros), (2-trimetylsiloxy)ethyl methacrylate (HEMA-TMS, Scientific Polymer Products), methyl methacrylate (MMA, 99%, Aldrich) were purified by passing the monomer through a column filled with basic alumina to remove the inhibitor. 2,2′-Azobis(2-methylpropionitrile) (AIBN, 98%, Aldrich) was

recrystallized from methanol before use. 2-(2-bromoisobutyryloxy)ethyl methacrylate (BiBEM) was synthesized following previously reported procedures.[16,17] All other reagents: ethyl *α*-bromoisobutyrate (EBiB, 98%), *p*-toluenesulfonyl chloride (TsCl, >99%), 4-cyanobenzodithioate (CN-CDTB, 98%), copper(I) bromide ($Cu^{I}Br$, 99.999%), copper(II) bromide ($Cu^{II}Br_2$, 99.999%), copper(I) chloride ($Cu^{I}Cl$, 99.995%), copper(II) chloride ($Cu^{II}Cl_2$, 99.999%), 4,4′-dinonyl-2,2′-dipyridyl (dNbpy, 97%) *N,N,N',N'',N''*-pentamethyldiethylenetriamine (PMDETA, 99%), potassium fluoride (KF, 99%), tetrabutylammonium fluoride (TBAF, 1.0 M in THF), *α*-bromoisobutyryl bromide (98%), 2,5-di-*tert*-butylphenol (DTBP, 99%) and solvents were purchased from Aldrich and used as received without further purification.

Characterization. The conversion of *n*BA was determined from ^{1}H NMR spectra recorded in $CDCl_3$ as a solvent using Brüker 300 MHz spectrometer. Molecular weight distributions of the polymers were characterized by gel permeation chromatography (GPC) using Polymer Standards Services (PSS) columns (guard, 10^5, 10^3, and 10^2 Å), with THF eluent at 35 °C, flow rate 1.00 mL/min, and differential refractive index (RI) detector (Waters, 2410). The apparent number-average molecular weights (M_n) and molecular weight dispersities ($Đ$) were determined with a calibration based on linear poly(methyl methacrylate) (PMMA) standards and diphenyl ether as an internal standard, using WinGPC 6.0 software from PSS.

Synthesis of $PBiBEM_{20}$ (MI_{20}). CN-CDTB (0.0920 g, 0.3734 mmol), BiBEM (2.0 mL, 9.34 mmol), AIBN (0.0061 g, 0.0373 mmol) and toluene (0.2 mL) were added to a 10 mL

Schelenk flask. The flask was sealed and the solution was purged with nitrogen for 10 min. Afterwards the flask was immersed in an oil bath thermostated at 65 ˚C. The polymerization was stopped after 24 h when conversion had reached 99.5% as determined by ^{1}H ^{1}H NMR. The polymer was purified via two precipitations into hexanes, and dried under vacuum overnight. Number average molecular weight was determined by THF GPC using PMMA standards: $M_{n,GPC}$ = 6,140 and $Đ$ = 1.25. The DP_{BB} of the polymer based on M_n was determined as 20 and confirmed by ^{1}H NMR spectroscopy by comparison of the polymer to initiator signals.

Synthesis of P(HEMA-TMS)$_{100}$. A 25 ml Schlenk flask was charged with TsCl (0.0701 g, 0.3675 mmol), HEMA-TMS (20.0 mL, 91.9 mmol), dNbpy (0.150 g, 0.368 mmol), $Cu^{II}Br_2$ (4.1 mg, 0.0184 mmol), and anisole (5.0 mL). The solution was degassed by three freeze-pump-thaw cycles. During the final cycle, the flask was filled with nitrogen and $Cu^{I}Br$ (23.7 mg, 0.1654 mmol) was quickly added to the frozen reaction mixture. The flask was sealed, evacuated and back-filled with nitrogen five times and then immersed in an oil bath thermostated at 70 °C. Polymerization was stopped after 42 h reaching 40.9 % conversion as determined by ^{1}H NMR, which corresponded to a DP of 100. Number average molecular weight determined by THF GPC: $M_n = 1.82 \cdot 10^4$, and $Đ$ = 1.13. The reaction mixture was diluted with chloroform, passed through neutral alumina to remove the catalyst, then concentrated and used for the next step without further purification.

Synthesis of P(HEMA-TMS)$_{400}$. The reaction was performed, characterized and the product was purified in the same way as **P(HEMA-TMS)$_{100}$.** A 25 ml Schlenk flask was

charged with TsCl (0.0175 g, 0.0919 mmol), HEMA-TMS (20.0 mL, 91.9 mmol), dNbpy (0.150 g, 0.368 mmol), $Cu^{II}Br_2$ (6.1 mg, 0.0276 mmol), and anisole (2.2 mL). Polymerization was stopped after 66 h 45 min. reaching 41.0 % conversion, corresponding to a DP of ~400. THF GPC analysis: $M_n = 7.05 \cdot 10^4$, and $Đ = 1.20$.

Synthesis of P(HEMA-TMS)$_{120}$-*co*-PMMA$_{280}$. A 25 ml Schlenk flask was charged with EBiB (22.5 μL, 0.1531 mmol), HEMA-TMS (10.0 mL, 45.9 mmol), MMA (11.5 mL, 107 mmol), dNbpy (0.251 g, 0.613 mmol), $Cu^{II}Cl_2$ (6.2 mg, 0.0459 mmol), anisole (2.0 mL) and DMF (0.5 mL). The solution was degassed by three freeze-pump-thaw cycles. During the final cycle, the flask was filled with nitrogen and $Cu^{I}Cl$ (25.8 mg, 0.2603 mmol) was quickly added to the frozen reaction mixture. The flask was sealed, evacuated and back-filled with nitrogen five times and then immersed in an oil bath thermostated at 70 °C. Polymerization was stopped after 26.5 h reaching 39.6 % conversion as determined by ^{1}H NMR, which corresponded to a total DP of 400. The polymer was purified by two precipitations from methanol and one from hexanes, and then dried under vacuum. THF GPC analysis: $M_n = 4.86 \cdot 10^4$, and $Đ = 1.10$.

Synthesis of PBiBEM$_{100}$ (MI$_{100}$). A 100mL round-bottom flask was charged with **P(HEMA-TMS)$_{100}$** (10.0 g, 49.5 mmol), KF (3.51 g, 59.4 mmol) and then dry THF (50 mL) was added under nitrogen. The reaction mixture was cooled down in an ice bath, followed by the injection of tetrabutylammonium fluoride (0.50 mL, 1.0 M in THF, 0.50 mmol) and subsequent dropwise addition of α-bromoisobutyryl bromide (9.2 mL, 74.3 mmol) over the course of 30 min. After addition was completed, the reaction mixture was

allowed to reach room temperature and was stirred for another 16 h. Afterwards solids were filtered of and the mixture was added to methanol/water (70/30) to precipitate the polymer which was then re-dissolved in chloroform (100 mL) and passed through a column filled with basic alumina. The product **MI$_{100}$** was re-precipitated three times in hexanes and dried overnight under vacuum. THF GPC analysis gave: $M_n = 1.95 \cdot 10^4$, and $Đ = 1.12$.

Synthesis of PBiBEM$_{400}$ (MI$_{400}$). The functionalization of **P(HEMA-TMS)$_{400}$** and was performed following the same procedure as for **MI$_{100}$**. THF GPC analysis gave: $M_n = 7.50 \cdot 10^4$, and $Đ = 1.37$ for **MI$_{400}$**.

Synthesis of PBiBEM$_{120}$-*co*-PMMA$_{280}$ (MI$_{120\text{-}co\text{-}280}$). The functionalization of **P(HEMA-TMS)$_{120}$-*co*-PMMA$_{280}$** was performed following the same procedure as for **MI$_{100}$**, assuming 30 mol. % of HEMA-TMS. THF GPC analysis gave: $M_n = 5.00 \cdot 10^4$, and $Đ = 1.09$ for the formed **MI$_{120\text{-}co\text{-}280}$**. The dried and purified macroinitiator was also analyzed using ^{1}H NMR spectroscopy to determine to composition of the polymer. Integrations of –OCH_3 (MMA) and –CH_2– (BiBEM) 30.5 mol. % of PBiBEM, which corresponded to DP=120, and hence DP=280 of PMMA in the polymer of total DP=400.

Typical procedure used for grafting of P*n*BA side chains from the MIs

All grafts copolymers were synthesized in an analogous way to that reported below for preparation of **100-*g*-45**, using the macroinitiator and reagents ratios summarized in Table II.3.

Synthesis of PBiBEM$_{100}$-*g*-P*n*BA$_{45}$ (100-*g*-45). A 25 mL Schlenk flask equipped with a stir bar was charged with **MI$_{100}$** (0.0979 g, 0.3508 mmol), *n*BA (20.0 mL, 140.3 mmol), dNbpy (0.144 g, 0.351 mmol), $Cu^{II}Br_2$ (2.0 mg, 0.0088 mmol), and anisole (2.2 mL). The solution was degassed by three freeze-pump-thaw cycles. During the final cycle $Cu^{I}Br$ (23.8 mg, 0.1666 mmol) was quickly added to the frozen reaction mixture under a nitrogen atmosphere. The flask was sealed, evacuated, back-filled with nitrogen five times, and then immersed in an oil bath thermostated at 70 °C. The polymerization was stopped after 31 h, and the monomer conversion was determined by ^{1}H NMR, resulting in confirming that the brush polymer **100-*g*-45** had side chains with a DP~45. The polymer was purified by three precipitations from cold methanol, and dried under vacuum at room temperature, to a constant mass. Apparent molecular weight was determined using THF GPC: $M_n = 1.29 \cdot 10^5$ and $Đ = 1.30$.

Conditions of ThFFF analysis. The channel was set at a ΔT of 80 ˚C and the temperature of the cold wall was maintained at 37 ˚C. The carrier liquid (MEK) was pumped at a rate of 0.4 mL/min. The ThFFF channel was 127 μm thick and 2 cm breadth. The injection loop volume was 20 μL.

DLS settings. DLS was performed using a Wyatt Heleos II system with an external Wyatt QELS attachment. The fiber optic cable to the DLS was connected to the MALS detector 4 which had an incident light angle of 38.0˚.

Sample preparation. All polymers were dissolved in MEK. Results are not reported for **100-*g*-20** because of the insufficient amount of the material.

II.3 Results and Discussion

Thermal Field-Flow Fractionation (ThFFF) analysis was exploited as a method of determining the effect of a polymers topology on its thermal diffusion behavior. For that purpose, a series of graft copolymers was synthesized via the 'grafting from' method utilizing a combination of normal atom transfer radical (ATRP) and reversible addition-fragmentation chain transfer (RAFT) polymerizations. Figure II.2 illustrates a schematic representation of the library of prepared polymers. The series of twelve graft copolymers was designed to allow for a systematic study of three structural factors: i) the length of the side chains (DP_{SC} ~ 20, 50, 100), ii) the length of the backbone (DP_{SC} ~ 20, 100, 400), and iii) the grafting density (30% and 100%) (Figure II.2).

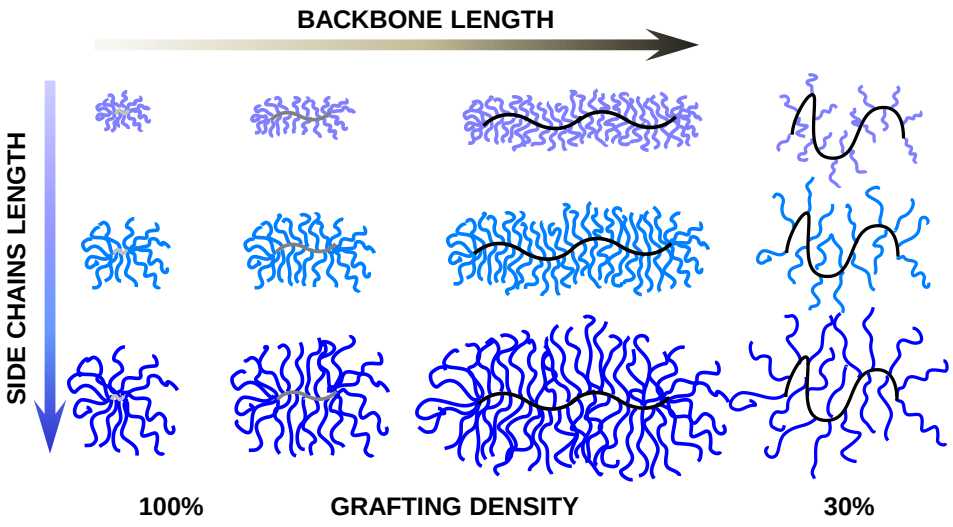

Figure II.2 The library of graft copolymers with varying grafting densities and lengths of both the backbone and side chains.

II.3.1 Synthesis of Graft Copolymers Library

The general synthetic approach that was applied in the synthesis of the polymer library is given in scheme II.1. The first step of the synthesis involved a preparation of ATRP macroinitiators with different backbone lengths, DP_{BB}: 20, 100 and 400. Afterwards, poly(*n*-butyl acrylate) (P*n*BA) side chains were grafted from the corresponding multifunctional macroinitiators to form graft copolymers, with varying grafts lengths, DP_{SC}: 20, 50 and 100. In addition, a macroinitiator with DP~400 consisting of only 30% of ATRP initiating groups was prepared to form analogous graft copolymers with a lower grafting density.

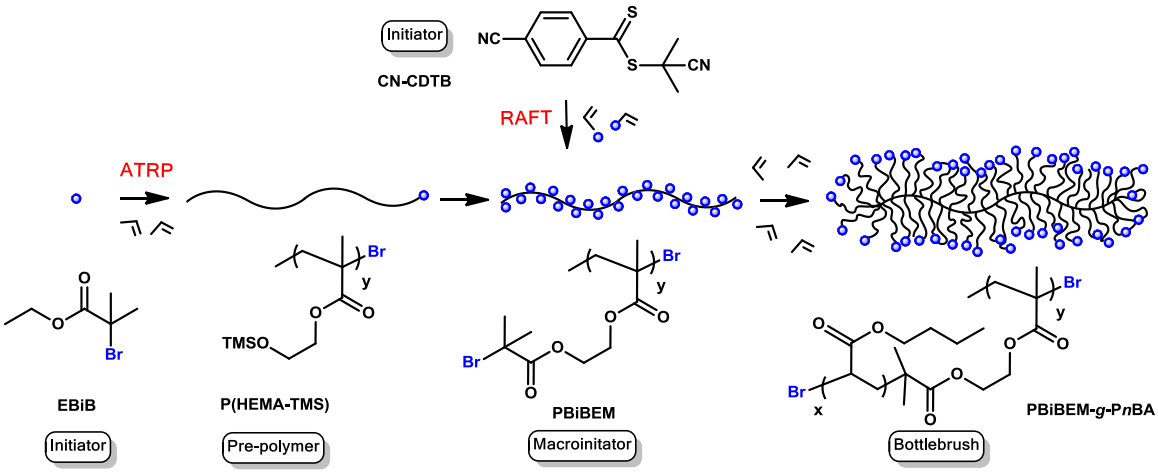

Scheme II.1 Synthetic approach used in the preparation of the library of graft copolymers.

RAFT polymerization of (BiBEM) 2-(2-bromoisobutyryloxy)ethyl methacrylate inimer allows for a direct formation of poly(2-(2-bromoisobutyryloxy)ethyl methacrylate) (PBiBEM) ATRP macroinitiator. On the other hand, the same polymers can be formed by

ATRP via a two-step process. First, the protected monomer, 2-(trimethysiloxy)ethyl methacrylate (HEMA-TMS) is polymerized, followed by removal of silyl groups and incorporation of ATRP initiating sites into P(HEMA-TMS) (Scheme II.1).

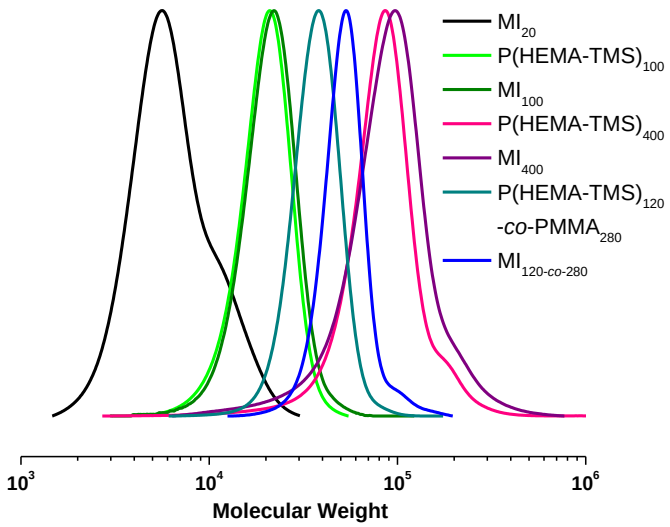

Figure II.3 GPC traces of **MI_{20}** (black), $P(HEMA\text{-}TMS)_{100}$ (light green), **MI_{100}** (green), $P(HEMA\text{-}TMS)_{400}$ (pink), **MI_{400}** (purple), $PMMA_{280}$-*co*-$P(HEMA\text{-}TMS)_{120}$ (light blue) and **$MI_{280\text{-}co\text{-}120}$** (blue).

First, three backbones with 100% grafting density at different degrees of polymerization (DP) 20, 100, 400 were prepared. RAFT polymerization was applied in the formation of PBIBEM macroinitiator with DP_{BB}=20 (**MI_{20}**). The ratio of reagents were: [CN-CDTB]:[BIBEM]:[AIBIN] = [1.0]:[25]:[0.1], 10 vol. % anisole, T = 65 ˚C. The reaction was stopped after 24 h after reaching 99.5% conversion. The GPC analysis of **MI_{20}** showed a polymer with M_n = 6,140 and $Đ$ = 1.25 (Table II.1). The DP_{BB} of **MI_{20}** was determined from M_n, as $DP_{BB} = M_n/MW_{BiBEM}$ = 6,140/279 = 20. GPC trace of **MI_{20}**

showed the presence of a significant high molecular weight shoulder attributed to intermolecular termination reaction via a chain coupling process (Figure II.3, black curve).

The RAFT polymerization of BIBEM was also tested for the synthesis of longer ATRP macroinitiators, i. e. with DPs > 20; however, all attempts failed due to the transfer

Table II.1 Characterization of PBiBEM macroinitiators with DPs: 20, 100 and 400.

Name	Method	x_M / % [a]	$M_n \cdot 10^{-3}$, [b]	$Đ$ [b]	DP_{BB} [c]
MI_{20}	RAFT	~99.5	6.14	1.25	20
P(HEMA-TMS)$_{100}$/MI_{100}	ATRP	40.9	18.2/19.5	1.13/1.12	100
P(HEMA-TMS)$_{400}$/MI_{400}	ATRP	41.0	70.5/75.0	1.20/1.37	400
P(HEMA-TMS)$_{120}$-*co*-PMMA$_{280}$/MI_{120}-*co*-280	ATRP	40.0	48.6/50.0	1.10/1.09	400

[a] Monomer conversion calculate from ^{1}H NMR, $x_M = \left(\frac{A_M \times A_{anisole,0}}{A_{M,0} \times A_{M\ anisole}}\right) \times 100\%$, A_M and $A_{anisole}$ are respective integrations for monomer and internal standard at the end of the reactions, and $A_{M,0}$ and $A_{ansiole,0}$ are the same signals at the beginning of the reaction. [b] Values obtained from THF GPC using linear PMMA standards. [c] Degree of the polymerization of the backbone calculated as $DP_{BB} = \frac{x_M \times DP_{target}}{100\%}$, where DP_{target} is a targeted DP.

reactions to ATRP sites leading to broadening of molecular weight distributions, and eventually to the gelation of the reaction mixture. Therefore, the traditional two-step ATRP approach was used for the synthesis of the macroinitiators. As shown in scheme II.1, the second method involves a polymerization of 2-(trimethylsiloxy)ethyl methacrylate (HEMA-TMS) via ATRP, followed by a subsequent esterification with ATRP-active moieties.

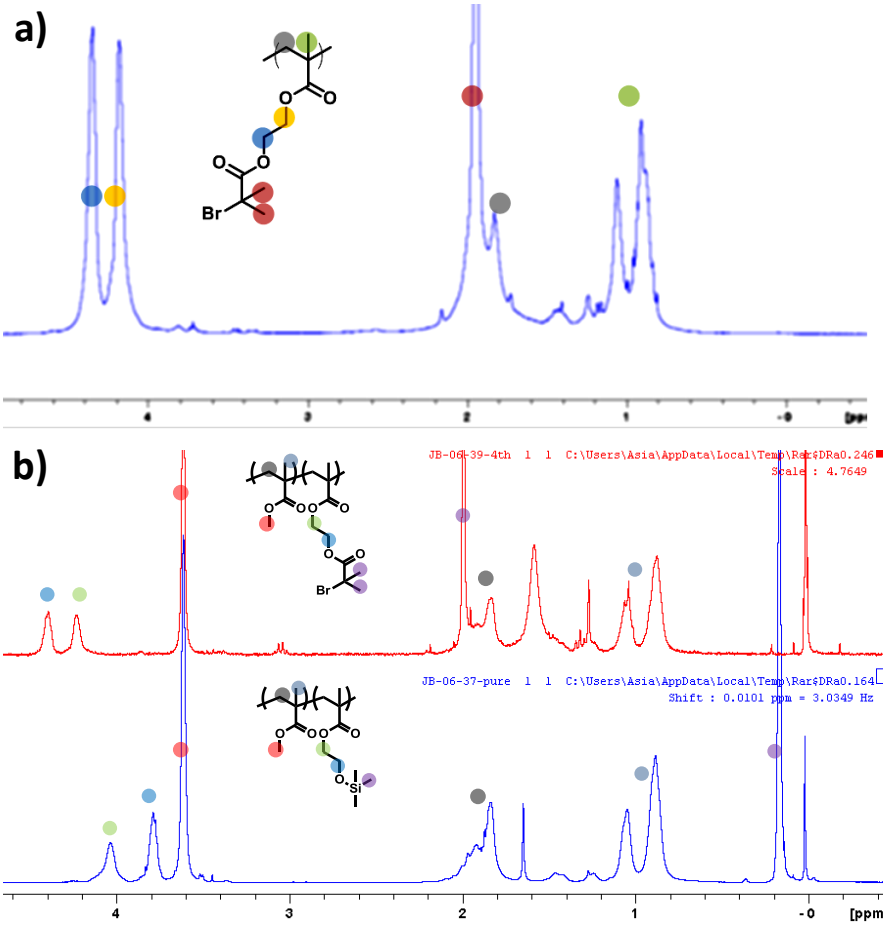

Figure II.4 ^{1}H NMR spectra of a) **MI$_{400}$** and b) **MI$_{280\text{-}co\text{-}120}$** with color-coded protons marked on each spectrum.

Two poly[2-(trimethylsiloxy)ethyl methacrylate] polymers were synthesized under normal ATRP conditions targeting the molar ratios of [HEMA-TMS]:[I] = 250 and 1000. Both polymerizations were performed with *p*-toluenesulfonyl chloride (TsCl) as an initiator (I) and CuBr/$CuBr_2$/dNbpy as a catalytic system, in 10 vol. % anisole at T = 70 ˚C. Polymerizations were stopped at ~40 % monomer conversions, resulting in the isolation of polymers with respective DPs of 100 (**P(HEMA-TMS)$_{100}$**) and 400 (**P(HEMA-TMS)$_{400}$**). **P(HEMA-TMS)$_{100}$** and **P(HEMA-TMS)$_{400}$** were characterized by GPC showing the formation of polymers with narrow MWDs, $Đ$ = 1.13 and 1.20, and $M_n = 1.82 \cdot 10^4$ and $7.05 \cdot 10^4$ respectively (Table II.1).

In order to prepare a backbone with only 30 mol. % of ATRP active initiating groups, HEMA-TMS was copolymerized with methyl methacrylate (MMA) using the ratio of [MMA]:[HEMA-TMS]:[I]]=[700]:[300]:[1]. The reaction was performed with ethyl α-bromoisobutyrate (EBiB) initiator (I) and CuCl/$CuCl_2$/dNbpy complexes, at T = 70 ˚C. The polymerization was stopped at 40 % monomers conversion obtaining a copolymer with the total DP of 400. The composition of the polymer was determined to be **P(HEMA-TMS)$_{120}$-*co*-PMMA$_{280}$**, assuming an equal reactivity ratio for both MMA and HEMA-TMS. The GPC characterization of **P(HEMA-TMS)$_{120}$-*co*-PMMA$_{280}$** gave $Đ$ = 1.10 and $M_n = 4.86 \cdot 10^4$ (Table II.1), providing a monomodal peak with narrow distribution (Figure II.3, light blue).

Table II.2 ATRP reaction conditions used for the preparation of graft copolymers.

Name*	PBiBEM	$[n\text{-BA}]_0$	$[CuBr]_0$	$[CuBr_2]_0$	[dNbpy/ PMDETA]
20-*g*-20	MI_{20}	400	0.475	0.025	1.0/-
20-*g*-50		350	0.2375	0.0125	-/0.25
20-*g*-100		700	0.475	0.025	-/0.5
100-*g*-16	MI_{100}	400	0.475	0.025	1.0/-
100-*g*-45		400	0.475	0.025	1.0/-
100-*g*-120		700	0.45	0.05	-/0.5
400-*g*-20	MI_{400}	1000	0.322	0.036	-/0.358
400-*g*-40		1000	0.322	0.036	-/0.358
400-*g*-120		1400	0.45	0.05	-/0.5
(120-*g*-17)-*co*-280	$MI_{120\text{-}co\text{-}280}$	200	0.5	0.1	1.2/-
(120-*g*-50)- *co*-280		400	0.475	0.025	1.0/-
(120-*g*-95)- *co*-280		1400	0.475	0.025	-/0.5

*All polymerizations were conducted in 10% (v/v) anisole at 70 °C. In each case the ratios of $[BiBEM]_0$ to other reagents was set at 1.0.

Afterwards, all pre-polymers were functionalized with ATRP reactive groups via one pot, two-step process. The modification reactions were accomplished using the following ratios of reagents: [HEMA-TMS]:[KF]:[TBAF]:[BiBBr]:[2,6-DTBP] = 1.0/1.2/0.01/1.2/0.01 in dry THF and at 0 ºC to room temperature. The final products, **MI$_{100}$**, **MI$_{400}$** and **MI$_{120\text{-}co\text{-}280}$**, were characterized by ^{1}H NMR spectroscopy, to confirm a full functionalization of HEMA-TMS groups via incorporation of 2-bromoisobutyryloxy-moieties. Figure II.4a shows the spectrum of **MI$_{400}$** with a fully functionalized backbone, confirming a full deprotection of –OTMS and a quantitative incorporation of ATRP functionalities. This is indicated by the disappearance of TMS signals as well as the downfield shift of both adjacent CH_2 peaks of P(HEMA-TMS) related to the formation of PBiBEM.[18] The identical spectrum was obtained for **MI$_{100}$** and is not presented here. In the case of **MI$_{120\text{-}co\text{-}280}$**, ^{1}H NMR analysis was used to confirm the disappearance of -OTMS signal as well as to determine the final composition of the copolymer. Figure II.4b shows the spectrum of **MI$_{120\text{-}co\text{-}280}$**, which confirmed a full incorporation of ATRP initiating functionalities. The integrations of –OCH_3 and –CH_2–protons were used to determine the molar ratio of PMMA to PBiBEM. It resulted in determining 30.5 mol. % of PBiBEM in **MI$_{120\text{-}co\text{-}280}$**, which corresponded to DP~120 of PBiBEM and DP~280 of MMA in the copolymer. GPC characterization of **MI$_{100}$**, **MI$_{400}$** and **MI$_{120\text{-}co\text{-}280}$** gave respective $Đ$ = 1.12, 1.37 and 1.09 (Table II.1), and M_n = $1.95 \cdot 10^4$, $7.50 \cdot 10^4$ and $5.00 \cdot 10^4$. GPC traces of all macroinitiators maintained their monomodality with narrow peaks width, thus confirming a high purity of macroinitiators (Figure II.3, green, purple and blue).

Table II.3 Summary of the results of the synthesis of graft copolymers.

Name	x_M / % [a]	M_n [b]	$Đ$ [b]	DP_{SC} [c]
20-*g*-20	5.6	44,600	1.25	22
20-*g*-50	15.7	75,000	1.24	50
20-*g*-100	16.1	156,000	1.19	100
100-*g*-16	4.0	98,400	1.17	16
100-*g*-45	11.3	129,000	1.30	45
100-*g*-120	16.5	344,000	1.15	120
400-*g*-20	2.1	335,000	1.18	20
400-*g*-40	3.9	416,000	1.19	40
400-*g*-120	8.5	1,450,000	1.37	120
(120-*g*-17)-*co*-280	7.7	143,000	1.07	17
(120-*g*-50)- *co*-280	12.2	292,000	1.12	50
(120-*g*-95)- *co*-280	6.8	582,000	1.11	95

[a] Monomer conversion determined by ^{1}H NMR using: $x_M = \left(\frac{A_{[M]} \times A_{[Anisole]_0}}{A_{[M]_0} \times A_{[Anisole]}}\right) \times 100\%$, where $A_{[M]_0}$ and $A_{[M]}$ are integrations of the monomer vinyl signals of at the beginning

and end of the reaction, and corresponding internal standard values. [b] Determined by THF GPC with PMMA standards. [c] $DP_{SC} = DP_{targeted} \cdot x_M/100\%$.

The 'grafting from' approach was applied to polymerize P*n*BA grafts from prepared macroinitiators. Normal ATRP was utilized to graft side chains with DP_{SC}: 20, 50 and 100 from respective macroinitiators: **MI_{20}**, **MI_{100}**, **MI_{400}** and **$MI_{120\text{-}co\text{-}280}$**. The reaction conditions employed in the synthesis of twelve graft copolymers are summarized in Table II.2. In general, when targeting a lower DP of the side chain (DP=20), a higher concentration of ATRP catalyst (1250 ppm) and less active ligand (dNbpy) was used. In contrast, longer grafts (DP=50, 100) were synthesized with lower amounts of copper (350-700 ppm) and a more active ligand, (PMDETA (*N*,*N*,*N'*,*N'*,*N*-pentamethyldi-ethylenetriamine)). All reactions were stopped below 20% monomer conversion, thus avoiding any significant intermolecular cross-linking and subsequent gelation of the polymerization mixture.

GPC analysis was then performed to determine the apparent number average molecular weights (M_n) and molecular weight distributions ($Đ$) of the graft copolymers. Although GPC does not provide the actual M_n values of grafted copolymers, it allows for assessment of the quality of the material. Figure II.5 shows GPC traces of the set of graft copolymers prepared from each macroinitiator: a) **MI_{20}**, b) **MI_{100}**, c) **MI_{400}** and d) **$MI_{120\text{-}co\text{-}280}$**. GPC traces of the macroinitiators showed a clear shift of signal towards higher molecular weight values after the grafting of side chains. In addition, the shift towards lower elution volumes progressively increased with increasing length of incorporated grafts.

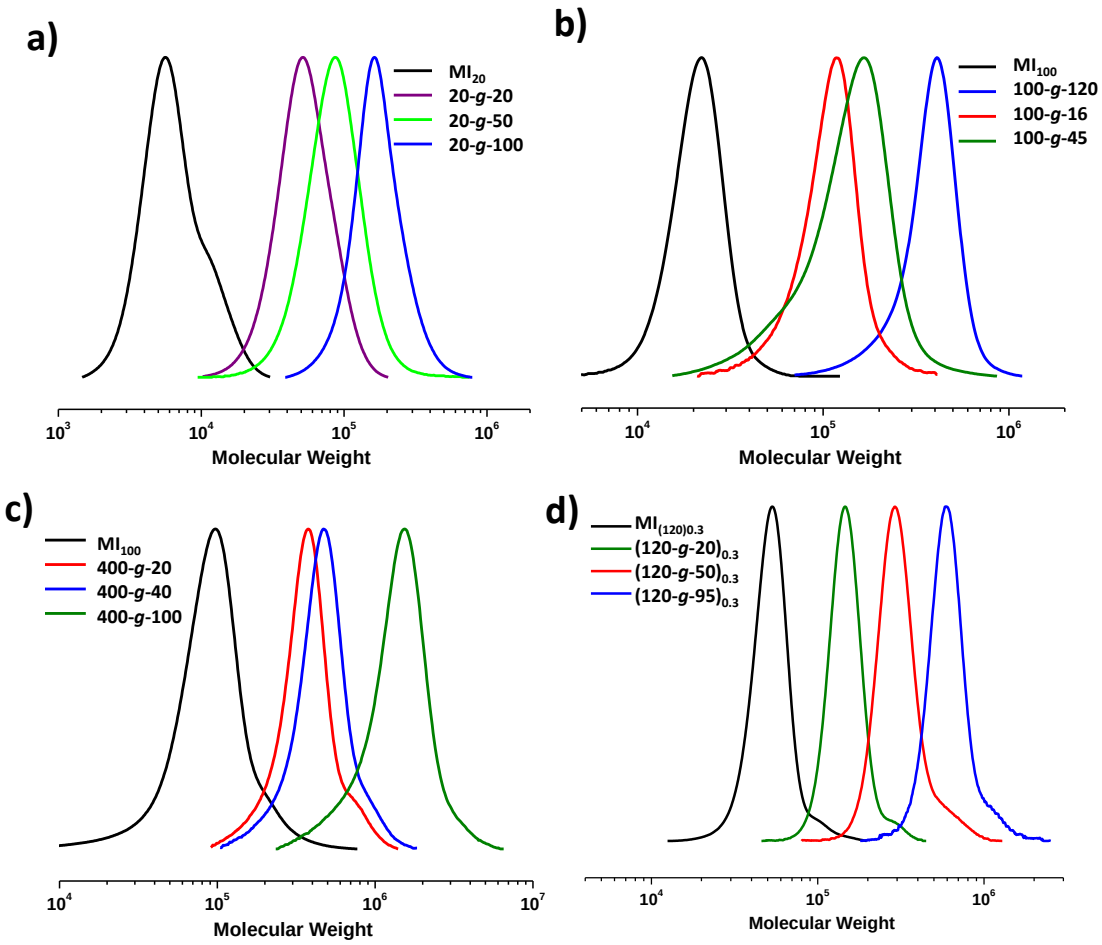

Figure II.5 GPC traces of graft copolymers prepared from macroinitiators a) **MI_{20}**, b) **MI_{100}**, c) **MI_{400}** and d) **$MI_{280\text{-}co\text{-}120}$**.

II.3.2 ThFFF Studies of Library of Graft Copolymers

Thermal Field-Flow Fractionation (ThFFF) was applied to characterize the library of nine polymers with 100% grafting density. As mentioned in the introduction, ThFFF can be utilized to obtain the Soret coefficient (S_T) by applying the equation II.1.

$$S_T = \frac{D_T}{D} \qquad \text{(II. 1)}$$

where, D_T and D, are a thermal diffusion and diffusion coefficients respectively. Diffusion coefficients (D), determined by batch mode DLS, were combined with retention times (λ), acquired from ThFFF, to calculate thermal diffusion coefficients (D_T) (equation II.2).

$$\boldsymbol{D_T = \frac{D}{\lambda \cdot \Delta T}} \qquad \text{(II.2)}$$

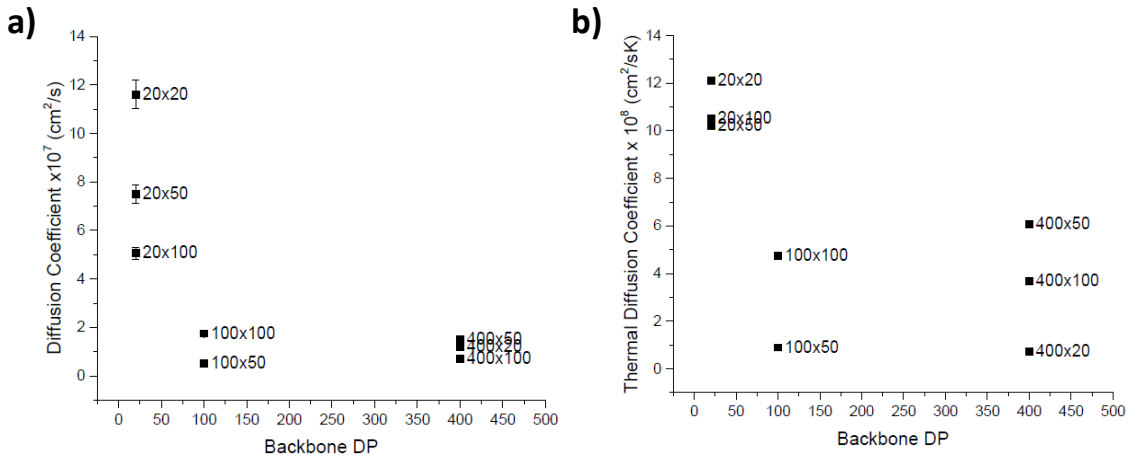

Figure II.6 Results obtained for graft copolymers with 100% grafting densities. a) Diffusion Coefficient (D) vs. Backbone DP_{BB} for different side chain lengths (DP_{SC}). b) Thermal Diffusion Coefficient vs. Backbone DP.

Figure II.6a shows the diffusion coefficient (D) plotted against the degree of polymerization of the backbone, DP_{BB}. For constant DP_{SC} and increasing DP_{BB} the

polymer size increases, and hence *D* is expected to decrease. Such a trend was observed for DP_{SC} ~ 100 series, i. e.: **20-*g*-100**, **100-*g*-120** and **400-*g*-120**. As expected, *D* values also decreased for the series of polymers with DP_{BB} = 20: **20-*g*-50**, **20-*g*-50** and **20-*g*-100**. However, anomalous *D* values were obtained for the series with DP_{BB} = 100 and 400. For example, *D* of **100-*g*-100** was expected to be lower than that of **100-*g*-45**. These results were reproducible and there is no clear explanation for such trends.

The *D* values (Figure II.6b) were then measured and the retention times (λ) were used to calculate corresponding thermal diffusion coefficients (equation II.2, D_T). D_T is known to be independent of molecular weight and remain constant for the same polymer-solvent combination. It was assumed that P*n*BA side chains of graft copolymers completely shield the backbone at 100% grafting density. Hence, it was expected that D_T values of densely grafted polymers should remain the same as that of a P*n*BA homopolymer. Therefore, the results in Figure II.6b are unexpected. The D_T values for DP_{BB} = 20 (**20-*g*-50**, **20-*g*-50** and **20-*g*-100**) agreed with that of the PnBA homopolymer. However, the series with longer $DP_{BB,}$ 100 and 400, showed significantly lower D_T values than that of the homopolymer. One proposed theory is that the dense grafting of P*n*BA side chains induces a colloid-like behavior instead of that of a linear chain. It is noted that the relative D_T within the DP_{BB} = 100 and 400 with varying grafts lengths series should not be compared because of the anomalous *D*'s that were observed in Figure II.6a.

The Soret coefficient (S_T) was obtained experimentally from the retention time (λ) measured by ThFFF, by applying the equation II.2. Figure II.7 shows experimental S_T plotted against theoretical S_T. The theoretical S_T was determined by calculating a D_T value using Mes theory, which relates D_T to solubility parameters, and a D value based on molecular mass relationships, where $D \alpha MM^{-0.5}$. A linear relationship was observed with a slope of 0.094. Other non-linear polymers have yielded different slopes, for instance star polymers showed the slope value of 0.47. These results suggest that different types of non-linear polymers may have a unique slope; however more studies are needed to confirm this proposal. The two outliers are the result of S_T anomalies that originate form initial anomalous D values. This might be related to the possibility of degradation of the brush brush samples.

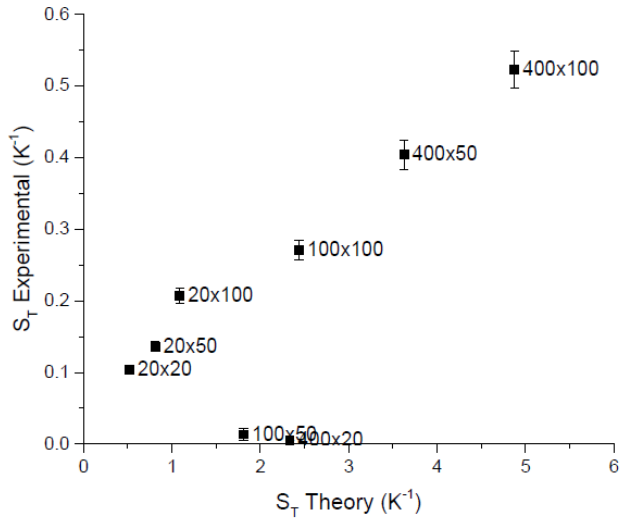

Figure II.7 Measured Soret Coefficient vs Predicted Soret Coefficient.

II.4 Summary

A set of twelve graft copolymers with varying structural factors was synthesized via the 'grafting from' approach under normal ATRP conditions. Three factors were taken into consideration during the synthesis: i) the backbone length (DP_{BB}=20, 100, and 400), ii) the length of the P*n*BA side chains (DP_{SC}=20, 50, and 100), and iii) the grafting density (30% and 100%). All polymers were characterized via GPC and ^{1}H NMR analyses, confirming the formation of well-defined polymers with narrow molecular weight distributions. In addition, the nine graft copolymers with 100% grafting density were further analyzed using DLS and ThFFF methods. A typical thermal diffusion behavior, similar to that of a linear polymer, was only observed for the series with the shortest backbone (DP_{BB}=20). In contrast, the polymer with longer backbones, 100 and 400, did not follow the expected trend and displayed a more colloidal-like behavior. In addition, DLS and ThFFF data was used to correlate the theoretical Soret coefficient with the experimental one, obtaining the slope value of 0.094.

The 'grafting from' approach proved to be an excellent method to access a variety of graft copolymers with controllable lengths of the backbone and side chains and tunable grafting density. ThFFF with an aid of DLS was successfully applied to characterize such polymers, showing potential as a tool to determine the topology of branched polymers.

II.5 References

(1) Sheiko, S. S.; Sumerlin, B. S.; Matyjaszewski, K. *Prog. Polym. Sci.* **2008**, *33*, 759-785.

(2) Lee, H.-I.; Pietrasik, J.; Sheiko, S. S.; Matyjaszewski, K. *Prog. Polym. Sci.*, **2010**, *35*, 24-44

(3) Lienkamp, K.; Ruthard, C.; Lieser, G.; Berger, R.; Groehn, F.; Wegner, G. *Macromol. Chem. Phys.* **2006**, *207*, 2050-2065.

(4) Lienkamp, K.; Noé, L.; Breniaux, M.-H.; Lieberwirth, I.; Groehn, F.; Wegner, G. *Macromolecules* **2007**, *40*, 2486-2502.

(5) Beers, K. L.; Gaynor, S. G.; Matyjaszewski, K.; Sheiko, S. S.; Moeller, M. *Macromolecules* **1998**, *31*, 9413-9415.

(6) Sumerlin, B. S.; Neugebauer, D.; Matyjaszewski, K. *Macromolecules* **2005**, *38*, 702-708.

(7) Cheng, G.; Boeker, A.; Zhang, M.; Krausch, G.; Mueller, A. H. E. *Macromolecules* **2001**, *34*, 6883-6888.

(8) Boerner, H. G.; Beers, K.; Matyjaszewski, K.; Sheiko, S. S.; Moeller, M. *Macromolecules* **2001**, *34*, 4375-4383.

(9) Gao, H.; Matyjaszewski, K. *J. Am. Chem. Soc.* **2007**, *129* 6633-6639.

(10) Neugebauer, D.; Zhang, Y.; Pakula, T.; Matyjaszewski, K. *Macromolecules* **2005**, *38*, 8687-8693.

(11) Thompson, G. H.; Myers, M. N.; C., G. J. *Anal. Chem.* **1969**, *41*, 1219.

(12) Giddings, J. C. *Sep. Sci.* **1966**, *1*, 123.

(13) Giddings, J. C. *Science* **1993**, *260*, 1456.

(14) Giddings, J. C. *Anal. Chem.* **1995**, *67*, 592.

(15) Schimpf, M. E. *J. Liq. Chromatogr. Related Technol.* **2002**, *25*, 2101.

(16) Matyjaszewski, K.; Gaynor, S. G.; Kulfan, A.; Podwika, M. *Macromolecules* **1997**, *30*, 5192-5194.

(17) Mori, H.; Böker, A.; Krausch, G.; Müller, A. H. E. *Macromolecules* **2001**, *34*, 6871-6882.

(18) Neugebauer, D.; Zhang, Y.; Pakula, T.; Sheiko, S. S.; Matyjaszewski, K. *Macromolecules* **2003**, *36*, 6746-6755.

CHAPTER III

LONG BOTTLEBRUSHES AS SUPERSOFT ELASTOMERS

Preface

Molecular bottlebrushes discussed in this chapter are 'traditional' densely grafted macromolecules with varying lengths of poly(*n*-butyl acrylate) side chains, and a long backbone with a constant length (DP~2,000). Bottlebrush architecture allows for a natural disentanglement of polymer melts, which can be controlled by a structural manipulation of the grafts lengths. This work was is a continuation of study on viscoelastic behavior of bottlebrushes and their super-soft elastomeric properties.[1-3]

The research described in this chapter in a result of collaborative efforts between our group at CMU and prof. Sheiko's research teams from UNC Chapel Hill. I synthesized a series of bottlebrushes by combining RAFT and ATRP polymerization methods, preparing a series of samples with progressively increasing grafts length: 4, 10,

16, 24, 48 and 95. I also performed all GPC and ^{1}H NMR analyses to characterize the prepared series of bottlebrushes. Next, William Daniel, a graduate student at UNC, did further characterization of long brushes including imaging by atomic force microscopy (AFM), LB monolayers and rheological measurements of the storage and loss moduli. William extracted the data from all analyses and correlated it to the theoretical predictions. The results showed a good correlation of the plateau modulus with the theory, which was confirmed by scaling of $n_{sc}^{-1.38}$ which agreed with the theoretical one of $n_{sc}^{-1.5}$. In addition, the plateau moduli of bottlebrushes dropped linearly to as low as hundreds of Pascals, showing that bottlebrushes could be used as solvent-free supersoft elastomers with moduli much lower than traditional linear chain elastomers and gels.

III.I Introduction

Entanglements represent one of the most fundamental characteristics of polymer chains and play a dominating role in defining both structure and physical properties of polymeric materials, ranging from crystallization to flow.[4-7] Within a melt of polymer chains, due to restriction of chain motion, entanglements are responsible for strong viscoelastic behavior which is manifested in the development of the entanglement plateau of the dynamic storage modulus. For neat polymer, the lower limit of plateau modulus rests in the range of 10^5 Pa and is dictated by the inherent density of chain entanglements, which in turn depends on the chemical structure and architecture.[8] During crosslinking of a polymer melt into an elastomer, these entanglements become trapped permanently, and even at sufficiently low chemical crosslink density ($M_x >> M_e$), the shear modulus of an elastomer (G) becomes dominated by chain entanglements maintaining the modulus at the preordained lower limit as[4,9,10]

$$G \cong G_x + G_e \cong \rho RT\left(\frac{1}{M_x} + \frac{1}{M_e}\right) \cong \frac{\rho RT}{M_e} \qquad \text{(III. 1)}$$

where G_x and G_e - modulus contributions due to chemical cross-links and physical entanglements, respectively, ρ - mass density, M_x and M_e – number average molar masses of a network strand and an entanglement strand, respectively. Several strategies have been developed to disentangle polymer chains and thus reduce the lower limit for the shear modulus. One physical and laborious method is based on crosslinking of chains in a semidilute solution followed by solvent evaporation (Figure III.1a).[11,12] Synthetic methods are based on manipulation of molecular architecture. The possibilities of the

synthetic approach became clear from early studies of polyolefins with different branching densities[13,14] that were later extended to more complex architectures such as combs,[15-17] stars,[18-21] and dendrimers[22-25]. Figures III.1b-d display three prominent methods of creating low modulus elastomers utilizing control of molecular architecture: (b) The Olympic gel or interlinking ring gel first proposed by P. G. de Gennes,[26,27] (c) the crosslinking of non-interlinking polymer rings,[28,29] and finally (d) the architecture considered in this communication, self-disentanglement of densely grafted molecular bottlebrushes.[1-3,30,31]

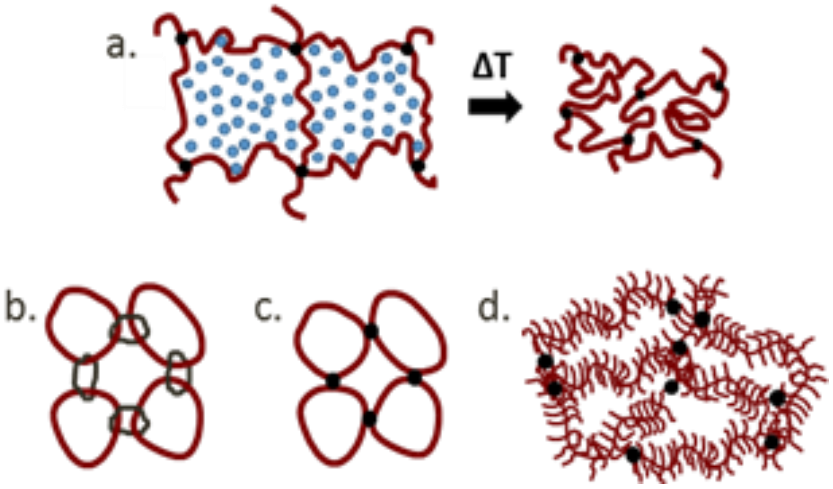

Figure III.1 Methodologies for reduction of entanglement density in elastomers. (a) semidilute crosslinking followed by solvent extraction (b) Olympic gel. (c) crosslinking of non-interlinking polymer rings. (d) crosslinking of cylindrical molecular brushes.

Bottlebrush macromolecules consist of a long polymer backbone with a distinctly high grafting density of side chains (Figure III.2a). From a range of synthetic methods, the so-called “grafting from” strategy offers a superior range of backbone degree of

polymerization (DP) ($n_{bb} \cong 10^2 - 10^4$) with controllable spacer grafting ($n_g = 1 - 10$) and side-chain DP ($n_{bb} \cong 1 - 200$).[32]

III.2 Experimental

Materials. *n*-Butyl acrylate (*n*BA, 99%, Acros) and (2-trimetylsiloxy)ethyl methacrylate (HEMA-TMS, Scientific Polymer Products) were purified by passing the monomer through a column filled with basic alumina to remove the inhibitor, 2,2′-azobis(2-methylpropionitrile) (AIBN, 98%, Aldrich) was recrystallized from methanol and dried under vacuum prior use. Sulfuric acid (20% fuming) was purchased from Alfa Aesar. All other reagents: 2-cyano-2-propyl 4-cyanobenzodithioate (98%), copper(I) bromide ($Cu^{I}Br$, 99.999%), copper(II) bromide ($Cu^{II}Br_2$, 99.999%), 4,4′-dinonyl-2,2′-dipyridyl (dNbpy, 97%), potassium fluoride (KF, 99%), tetrabutylammonium fluoride (TBAF, 1.0 M in THF), *α*-bromoisobutyryl bromide (98%), 2,5-di-*tert*-butylphenol (DTBP, 99%), triethylamine (TEA, ≤99%), 1-butanol (ACS reagent, ≥99.4%) and solvents were purchased from Aldrich and used as received without further purification.

Characterization. The conversion of *n*BA was determined from ^{1}H NMR spectra recorded in $CDCl_3$ as a solvent using Brüker 300 MHz spectrometer. Molecular weight distributions of the polymers were characterized by gel permeation chromatography (GPC) using Polymer Standards Services (PSS) columns (guard, 10^5, 10^3, and 10^2 Å), with THF eluent at 35 °C, flow rate 1.00 mL/min, and differential refractive index (RI) detector (Waters, 2410). The apparent number-average molecular weights (M_n) and

molecular weight dispersities (M_w/M_n) were determined with a calibration based on linear poly(methyl methacrylate) (PMMA) standards and diphenyl ether as an internal standard, using WinGPC 6.0 software from PSS. In addition, the number average molecular weight was measured by the AFM-LB method described elsewhere.[33] The samples for AFM measurement were prepared by Langmuir-Blodgett (LB) deposition. LB films were transferred onto freshly cleaved mica substrates at a constant surface pressure of 0.5 mN/m and a controlled transfer ratio. Imaging of individual molecules was performed in PeakForce QNM mode using a multimode AFM (Brüker) with a NanoScope V controller. We used silicon probes with a resonance frequency of 50-90 Hz and a spring constant of ~0.4 N/m. In-house developed computer software was used to analyze the AFM images. Typically, ensembles of XX molecules were analyzed to ensure standard deviation of the mean below 10%.

Synthesis of 1 P(HEMA-TMS)$_{2035}$ (2035-TMS). A 10 ml Schlenk flask was charged with 2-cyano-2-propyl 4-cyanobenzodithioate (0.0011 g, 0.0046 mmol), HEMA-TMS (10.0 mL, 45.9 mmol), AIBN (0.075 mg, 0.46 μmol, a stock solution) and toluene (0.5 mL). The solution was degassed by purging with nitrogen over 30 min. period. Afterwards, the sealed flask was immersed in an oil bath at 65 °C. Polymerization was terminated after 24 h and the polymer molecular weight was determined by THF GPC: $M_{n,GPC} = 3.26 \cdot 10^5$, and $M_w/M_n = 1.29$ (Figure III.2, gray). The degree of polymerization (DP) was calculated from the calibration curve ($M_{n,GPC}$=163.85·DP-7000) and determined to be 2035. The reaction mixture transferred to 100 mL pre-weighted, round-bottom

flask, then the remaining monomer was removed by flushing air overnight and the polymer was used for the next step without further purification.

Synthesis of 2 ($PBiBEM_{2035}$) (2035-Br). A 100 ml round-bottom flask was charged with **1** (4.40g, 21.8 mmol), KF (1.54 g, 26.1 mmol), DTBP (0.45 g, 2.18 mmol), and then dry THF (60 mL) was added under nitrogen. The reaction mixture was cooled down in an ice bath, followed by the injection of tetrabutylammonium fluoride (0.22 mL, 1.0 M in THF, 0.22 mmol) and subsequent dropwise addition of α-bromoisobutyryl bromide (6.01 g, 3.2 mL. 26.1 mmol) over the course of 20 min. Upon addition, the reaction mixture was allowed to reach room temperature and was stirred for another 16 h. Afterwards solids were filtered of and the mixture was precipitated into methanol/water (70/30), re-dissolved in chloroform (50 mL) and passed through the column filled with basic alumina. The product **2** was re-precipitated three times in hexanes and dried overnight under vacuum. Apparent molecular weight determined by THF GPC: $M_{n,GPC} = 6.94 \cdot 10^5$, and $M_w/M_n = 1.76$ (Figure III.2, black).

Synthesis of 3 ($PBiBEM_{2035}$-*g*-P*n*$BA_{3/4})_6$ (2035-*g*-3/4). A 10 mL Schlenk flask equipped with a stir bar was charged with macroinitiator **2** (0.1957 g, 0.7016 mmol of BiBEM groups), *n*BA (5.0 mL, 35.08 mmol), dNbpy (0.036 g, 0.088 mmol), $Cu^{II}Br_2$ (2.9 mg, 0.0130 mmol), and anisole (0.5 mL). The solution was degassed by three freeze-pump-thaw cycles. During the final cycle $Cu^{I}Br$ (4.4 mg, 0.0309 mmol) was quickly added to the frozen reaction mixture under nitrogen atmosphere. The flask was sealed, evacuated, back-filled with nitrogen five times, and then immersed in an oil bath thermostated at 70

°C. The polymerization was stopped after 20 h, and the monomer conversion was determined by ^{1}H NMR (6.7%), resulting in the brush polymer **3** with DP~3-4 of side chains. The polymer was purified by three precipitations from cold methanol, and dried under vacuum at room temperature, to a constant mass. Apparent molecular weight was determined using THF GPC: $M_{n,GPC} = 6.40 \cdot 10^5$, and $M_w/M_n = 1.76$ (Figure III.2, red).

Synthesis of 4 (PBiBEM$_{2035}$-*g*-P*n*BA$_{10}$) (2035-*g*-10). The reaction was set up and analyzed in the same way as **3**. The amounts of reagents used for the polymerization: macroinitiator **2** (0.1957 g, 0.7016 mmol of BiBEM groups), *n*BA (10.0 mL, 70.16 mmol), dNbpy (0.072 g, 0.175 mmol), $Cu^{II}Br_2$ (3.4 mg, 0.0153 mmol), anisole (1.0 mL) and $Cu^{I}Br$ (10.4 mg, 0.0724 mmol). The polymerization was stopped after 24 h at 10.0 % conversion, giving the brush polymer, **4**, with DP=10 of side chains. Apparent molecular weight determined by THF GPC: $M_{n,GPC} = 1.54 \cdot 10^6$, and $M_w/M_n = 1.19$ (Figure III.2, orange).

Synthesis of 5 (PBiBEM$_{2035}$-*g*-P*n*BA$_{16}$) (2035-*g*-16). The reaction was set up and analyzed in the same way as **3**. The amounts of reagents used for the polymerization: macroinitiator **2** (0.0979 g, 0.3508 mmol of BiBEM groups), *n*BA (10.0 mL, 70.16 mmol), dNbpy (0.072 g, 0.175 mmol), $Cu^{II}Br_2$ (1.9 mg, 0.0153 mmol), anisole (1.0 mL) and $Cu^{I}Br$ (11.3 mg, 0.0794 mmol). The polymerization was stopped after 18 h 30 min. at 8.0 % conversion, giving the brush polymer, **5**, with DP=16 of side chains. Apparent molecular weight determined by THF GPC: $M_{n,GPC} = 1.87 \cdot 10^6$, and $M_w/M_n = 1.19$ (Figure III.2, yellow).

Synthesis of 6 (PBiBEM$_{2035}$-*g*-P*n*BA$_{24}$) (2035-*g*-24). The reaction was set up and analyzed in the same way as **3**. The amounts of reagents used for the polymerization: macroinitiator **2** (0.0489 g, 0.1754 mmol of BiBEM groups), *n*BA (10.0 mL, 70.16 mmol), dNbpy (0.072 g, 0.175 mmol), $Cu^{II}Br_2$ (1.0 mg, 0.0153 mmol), anisole (1.0 mL) and $Cu^{I}Br$ (11.9 mg, 0.0833 mmol). The polymerization was stopped after 19 h at 6.0 % conversion, giving the brush polymer, **6**, with DP=24 of side chains. Apparent molecular weight determined by THF GPC: $M_{n,GPC} = 2.07 \cdot 10^6$, and $M_w/M_n = 1.20$ (Figure III.2, pale green).

Synthesis of 7 (PBiBEM$_{2035}$-*g*-P*n*BA$_{48}$) (2035-*g*-48). The reaction was set up and analyzed in the same way as **3**. The amounts of reagents used for the polymerization: macroinitiator **2** (0.0326 g, 0.1169 mmol of BiBEM groups), *n*BA (10.0 mL, 70.16 mmol), dNbpy (0.048 g, 0.117 mmol), $Cu^{II}Br_2$ (0.69 mg, 0.0031 mmol), anisole (1.1 mL) and $Cu^{I}Br$ (12.5 mg, 0.0877 mmol). The polymerization was stopped after 20 h 15 min. at 8.1 % conversion, giving the brush polymer, **7**, with DP=48 of side chains. Apparent molecular weight determined by THF GPC: $M_{n,GPC} = 3.38 \cdot 10^6$, and $M_w/M_n = 1.13$ (Figure III.2, dark green).

Synthesis of 8 (PBiBEM$_{2035}$-*g*-P*n*BA$_{95}$) (2035-*g*-95). The reaction was set up and analyzed in the same way as **3**. The amounts of reagents used for the polymerization: macroinitiator **2** (0.0245 g, 0.0877 mmol), *n*BA (10.0 mL, 70.16 mmol), dNbpy (0.144 g, 0.351 mmol), $Cu^{II}Br_2$ (2.0 mg, 0.0088 mmol), anisole and $Cu^{I}Br$ (23.8 mg, 0.1666 mmol). The polymerization was stopped after 30 h at 11.8 % conversion, giving the brush

polymer, **8**, with DP=95 of side chains. Apparent molecular weight determined by THF GPC: $M_{n,GPC} = 3.64 \cdot 10^6$, and $M_w/M_n = 1.12$ (Figure III.2, blue).

Typical procedure for side chains cleavage. A 20 mL glass vial equipped with a stir bar was charged with a bottlebrush (~50 mg) and dissolved in THF (~2 mL). Then 1-butanol (12 mL) was added followed by sulfuric acid (5 drops). The vial was closed, sealed and placed in an oil bath at 100°°C, for 7 days. Afterwards, the solvents were removed on the residues were dissolved in THF (~3 ml) and passed through basic alumina. The polymer was analyzed on THF GPC with PS standards to determine the number average molecular weight of the brush side chain ($M_{n,SC}$).

LB-AFM analysis of molecular weight distribution

A sample of each bottlebrush was taken as prepared and dissolved in chloroform. 30 mg of polymer was then deposited on a Langmuir Blodgett trough and compressed at a constant rate of 15 mm/min to a surface pressure of 0.5 mN/m. After compression a cleaned mica slip of known spatial dimensions was withdrawn from the water at a constant rate of 5 mm/min while the trough maintained a surface pressure of 0.5mN/m. The bottlebrush monolayer now deposited onto the mica surface was then taken for AFM analysis

III.3 Results and Discussion

III.3.1 Synthesis of Long Bottlebrushes

A series of long bottlebrushes was synthesized to study their viscoelastic behavior and correlate it with the length of incorporated grafts. Scheme III.1 depicts the approach applied in the preparation of long bottlebrushes. The synthesis was performed in three steps: i) the formation of a pre-backbone polymer with DP~2000 via RAFT polymerization, ii) a chemical modification of the pre-polymer into ATRP macroinitiator, and iii) the incorporation of side chains with varying lengths via the 'grafting from' approach under ATRP conditions.

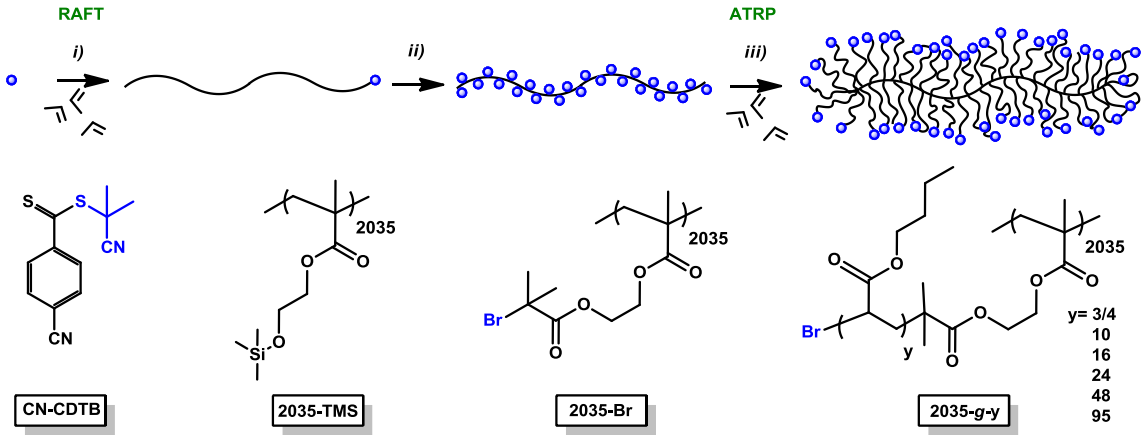

Scheme III.1 Synthetic approach used in the preparation of long bottlebrushes together with structures of prepared polymers.

RAFT polymerization was employed in the formation of poly(2-trimethyl-siloxyethyl) methacrylate (P(HEMA-TMS)) with a large degree of polymerization (DP) ~2000 (Scheme III.1). The following reaction conditions were used during the polymerization: [HEMA-TMS]:[CN-CDTB]:[AIBN] = [10,000]:[1.0]:[0.1], 5 vol. %

toluene, T = 65 ˚C. A high monomer to initiator ratio (10,000) was targeted, thus allowing for a high DP of the final polymer. In addition, the polymerization was terminated at a relatively low monomer conversion (22.4 %), hence decreasing the chance of broadening of the molecular weight distribution of the polymer. Yielded product (2035-TMS) was characterized via GPC analysis showing the formation of a high molecular weight polymer with a fairly narrow molecular weight distribution (Table III.1, 2035-TMS). The DP of 2035-TMS was determined as 2035, which was calculated from the calibration curve obtained from a series of P(HEMA-TMS) samples with varying degrees of polymerization using GPC characterization against PMMA standards. The GPC trace of 2035-TMS (Figure III.2, grey) showed a monomodal peak with a presence of a significant high molecular weight shoulder, which was attributed to an intermolecular coupling between growing polymer chains.

Next, crude **2035-TMS** was used in the synthesis of ATRP macroinitiator via one-pot in-situ deprotection and esterification reactions. The modification was accomplished by reacting **2035-TMS** with KF and catalytic amount of TBAF in dry THF, hence inducing a deprotection of TMS groups, followed by a slow addition of α-bromoisobutyryl bromide to incorporate ATRP-active ester functionalities. The macroinitiator, **2035-Br**, was isolated and purified via precipitations from MeOH/water (70/30, v/v) and hexanes, dried and analyzed via GPC. GPC results (Table III.1, **2035-Br**) showed a formation of a polymer with a higher molecular weight and broader molecular weight distribution as compared to initial **2035-TMS**. The broadening of $Đ$ was ascribed to the possibility of a physical aggregation, of **2035-Br** that might have

been caused by reduced solubility of the polymer in THF due to its high molecular weight (Figure III.2, black).

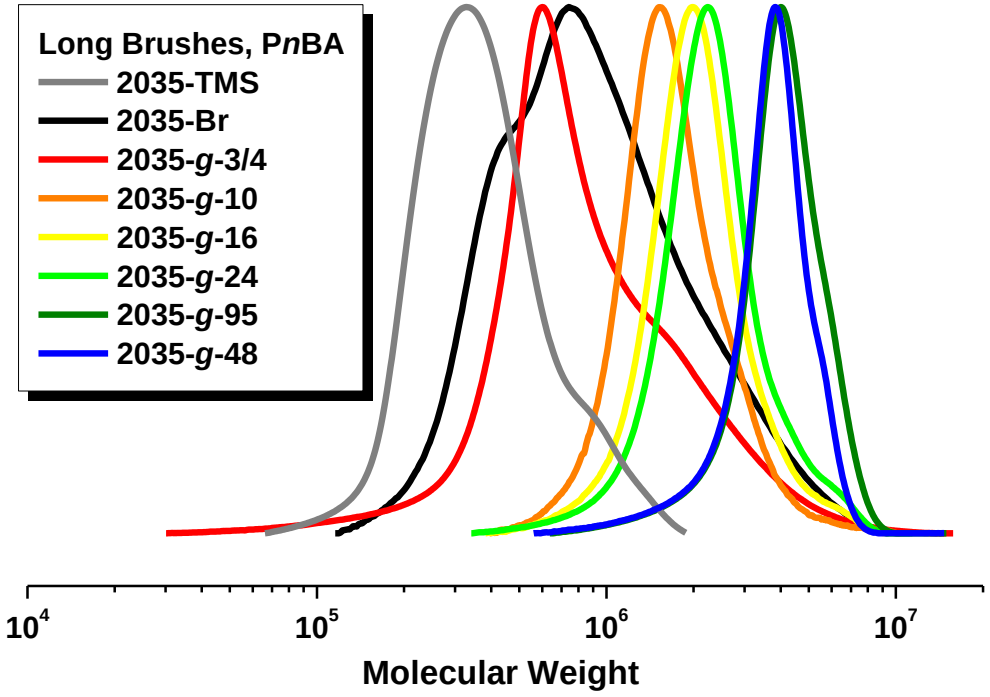

Figure III.2. GPC traces of (gray) $P(HEMA\text{-}TMS)_{2035,}$ (black) $PBiBEM_{2035}$, (red) $PBiBEM_{2035}$-*g*-P*n*$BA_{3/4}$, (orange) $PBiBEM_{2035}$-*g*-P*n*BA_{10}, (yellow) $PBiBEM_{2035}$-*g*-P*n*BA_{16}, , (pale green) $PBiBEM_{2035}$-*g*-P*n*BA_{24}, (dark green) $PBiBEM_{2035}$-*g*-P*n*BA_{48} and (blue) $PBiBEM_{2035}$-*g*-P*n*BA_{95}.

Table III.1 GPC and ^{1}H NMR characterization of prepared long bottlebrushes and their precursors.

Name	$DP_{SC,NMR}$ [a]	$M_n \cdot 10^{-5}$, [b]	$Đ$ [b]	$M_{n,SC} \cdot 10^{-3}$, [c]	$Đ_{,SC}$ [c]	DP_{SC} [d]	I_{eff} [e]
2035-TMS	N/A	3.26	1.29	N/A	N/A	N/A	N/A
2035-Br	N/A	6.94	1.76	N/A	N/A	N/A	N/A
2035-*g*-3/4	3/4	6.40	1.76	-	-	-	-
2035-*g*-10 BA-17	10	15.4	1.19	2.18	1.12	17	59
2035-*g*-16 BA-23	16	18.7	1.19	3.00	1.18	23	70
2035-*g*-24 BA-34	24	20.7	1.20	4.30	1.30	34	70
2035-*g*-48 BA-130	48	33.8	1.13	16.6	1.10	130	40
2035-*g*-95	95	36.4	1.14	14.4	1.13	112	85

[a] Degree of polymerization of side chance determined from the monomer conversion by ^{1}H NMR spectroscopy, $DP_{SC,NMR} = DP_{targeted} \cdot x_{nBA}$. [b] Determined by THF GPC using PMMA standards. [c] Determined by THF GPC using PSt standards. [d] Degree of the polymerization of side chains determined from the equation: $DP_{SC} = M_{n,SC} / MW_{nBA}$. [d] Initiation efficiency determined from the following equation: $I_{eff} = DP_{SC,NMR} / DP_{SC}$.

Table III.2 Reaction conditions used for the synthesis of long bottlebrushes: $PBiBEM_{2035}$-*g*-P*n*BA_y.

Ratios* / Name	$DP_{SC,NMR}$**	x_{nBA} / %	[*n*BA]	[$Cu^{I}Br$]	[$Cu^{II}Br_2$]	[dNbpy]
2035-*g*-3/4	3/4	11.8	800	1.9	0.10	4.0
2035-*g*-10	10	8.1	600	0.75	0.027	1.56
2035-*g*-16	16	6.0	400	0.475	0.025	1.0
2035-*g*-24	24	8.0	200	0.226	0.0238	0.5
2035-*g*-48	48	10.3	100	0.103	0.0217	0.25
2035-*g*-95	95	6.7	50	0.044	0.185	0.125

*Anisole 10 vol. %, T = 70˚C, [BiBEM] = [1]. **Degree of polymerization of side chance determined from the monomer conversion (x_{nBA}) by ^{1}H NMR spectroscopy, $DP_{SC,NMR} = DP_{targeted} \cdot x_{nBA}/100\%$.

In the last step, **2035-Br** was employed as a macroinitiator in the formation of a series of bottlebrushes with varying lengths of P*n*BA. All molecular bottlebrushes were synthesized via the 'grafting from' technique under normal ATRP conditions. In order to provide similar polymerization conditions for all brush syntheses, the following factors were kept constant: a) the temperature (70 ˚C), b) the monomer concentration ([*n*BA]) c) total copper content (1250 ppm vs. monomer) and d) the rate of polymerization

($R_p \sim \frac{[BiBEM]\cdot[CuBr]}{[CuBr_2]}$). Table III.2 summaries the ratios of reagents used in the generation of bottlebrush polymers with DPs of grafts: 3/4, 10, 16, 24, 48 and 95. The calculated degrees of polymerization of side chains ($DP_{SC,NMR}$) were obtained from the monomer conversion ($x_{n\mathrm{BA}}$)determined from ^{1}H NMR and the targeted DP. Therefore, the values obtained by this method provided the number average $DP_{SC,NMR}$ per bottlebrush molecule with an assumption of 100% grafting efficiency from **2035-Br**.

All bottlebrushes were subjected to side chains cleavage, thus allowing for determining the actual DP of grafts (DP_{SC}) as well as the initiation efficiencies of the grafting processes (I_{eff}). The side chains cleavage was performed via acid-catalyzed transesterification of the bottlebrushes, and then the GPC analysis was performed to assess the M_{n} values of detached grafts. Table III.1 summarizes the GPC results of cleaved grafts. In all cases DPs of cleaved side chains were larger than those obtained from the monomer conversion ($DP_{SC} > DP_{SC,NMR}$), which was ascribed to limited initiation efficiencies (I_{eff} ~ 40-70 %) from **2035-Br** macroinitiator.

III.3.2 Rheology of Long Bottlebrushes

In typical polymer melts, the molar mass of an entanglement strand is $M_e = 10^3 - 5 \cdot 10^4\ g/mol$ which prohibits synthesis of solvent-free elastomers with elasticity modulus below the entanglement limit $G_e \cong \rho RT/M_e \cong 10^5\ Pa$ (even if the molecular weight of the network strand M_x is larger than M_e).[34] On the contrary, bottlebrush

polymers are predicted to have G_e much lower (down to 100 Pa) and dependent on side-chain DP as

$$G_e \cong \frac{\rho RT}{M_e} \cong \frac{k_B T}{v_{K,br} N_e} \cong \frac{k_B T}{400 b^3 (\phi_g n_{sc})^{3/2}} \cong \frac{G_{e,linear}}{(\phi_g n_{sc})^{3/2}} \qquad \text{(III. 2)}$$

where $v_{K,br}$ – volume of a bottlebrush Kuhn-monomer, N_e – number of the Kuhn monomers per entanglement strand, b corresponds to a size of a chemical monomer, and $\phi_g \cong n_g^{-1}$ – grafting density of the side chains. This scaling prediction has been derived using the classical (Edwards) tube model[35] by considering the cylindrically-shaped bottlebrush macromolecules as a string of effective Kuhn monomers (Figure III.3a), having a volume of $v_{K,br} \cong b_K D^2$, where b_K and D are the Kuhn length and diameter of bottlebrush macromolecule, respectively.

The diameter of a P*n*BA bottlebrush depends on the degree of polymerization of the side chains (n_{sc}~) as $\cong b\sqrt{\phi_g n_{sc}}$, where $b \cong \sqrt{4v_0/(\pi l_0)}$ corresponds to the chemical monomer size. We have also calculated the bending constant of a bottlebrush macromolecule and shown that at moderately long side chains ($n_{sc} < 100$), the length of the bottlebrush Kuhn monomer is of the same order as the brush diameter, i.e. $b_K \cong D$. These relations give the following expression for the Kuhn monomer volume: $v_{K,br} \cong b^3(\phi_g n_{sc})^{3/2}$, which was used in equation III.2. The Kavassalis-Noolandi conjecture, which has previously been tested for numerous linear polymers, but not applied to mesoscopic cylindrically-shaped macromolecules, predicts a constant number $P_e \cong \sqrt{N_e}$ (≅20 for many classical linear polymers) of chains within an entanglement

volume.[36] This gives the number of the Kuhn monomers per entanglement segment as $N_e \cong P_e^2 = 400$. If the prediction by equation III.2 is valid, then bottlebrush melts can have a plateau modulus $(\phi_g n_{sc})^{3/2}$ times smaller than that of solvent free elastomer $G_e \cong 10^5\ Pa$. Thus, for melt of bottlebrush macromolecules having side chains with n_{sc}=50 and ϕ_g=0.6, the plateau modulus can be as low as $G_{e,br} \cong 600\ Pa$. This indicates that solvent-free elastomers can be synthesized with moduli <<10^5 Pa, matching that of polymeric gels.

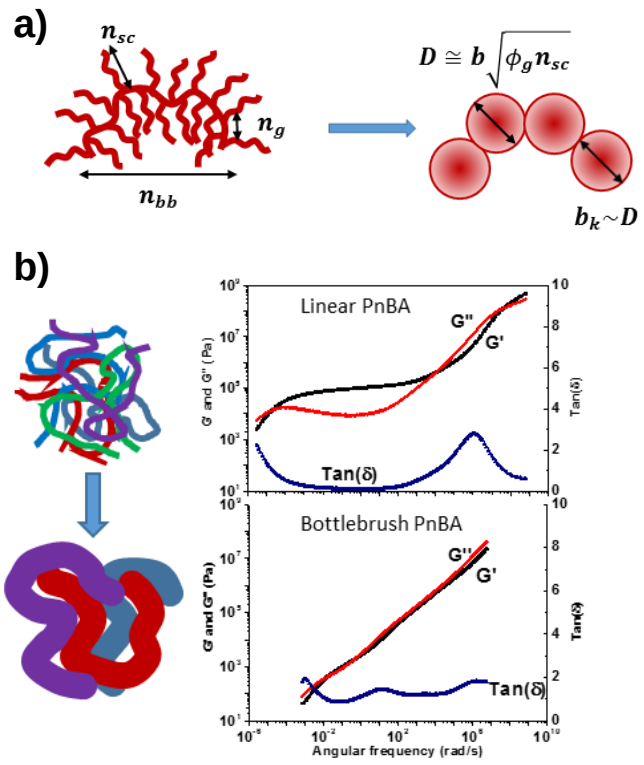

Figure III.3 a) Architecture of a bottlebrush macromolecule, and representaion of the effective Kuhn segment b_K and brush diameter D used in scaling analysis. n_{bb} and n_{sc} are the degrees of polymerization of the backbone and side chains, respectively, and $\boldsymbol{\phi_g} \cong$

n_g^{-1} is the grafting density, i.e. number of side-chains per backbone monomer. (b) Top, viscoelastic spectra of linear poly(*n*-butyl acrylate) polymer melt (M_n=1.1·10^6). Bottom, viscoelastic spectra of poly(*n*-butyl acrylate) bottlebrush melt with n_{sc}=8, ϕ_g=0.6, n_{bb}=2040, M_n=1.4·10^6. Spectra display strong retardation of elastic modulus in bottlebrush melt despite similar molar masses.

Table III.3 Characterization of long bottlebrush architectural parameter.

Sample	M_n, $10^{6,1}$	DP_{sc}[2]	$\phi_g \cdot n_{sc}$[3]	n_{sc}[4]	ϕ_g[5]	ϕ_t[6]	W, nm[7]	L, nm[8]	n_{bb}[9]	$Đ$[10]
2035-Br	0.69*	0	0	0	NA	NA	NA	NA	2035**	1.8
BA-6	NA***	6	3	NA	0.57	NA	NA	NA	NA	NA
BA-17	2.9	10	10	17	0.57	0.88	11	513	2052	1.5
BA-23	4.7	16	17	23	0.74	0.89	21	515	2060	1.6
BA-34	5.8	24	21	34	0.62	0.90	26	495	1980	1.6
BA-130	17.9	48	67	130	0.52	0.98	69	517	2068	1.5

[1]Number average molar mass determined from mass per unit area and molecular area using the LB-AFM method [2]Number average degree of polymerization (DP) of side-chains calculated from monomer conversion. [3]Number average DP of side-chains assuming 100% grafting efficiency (ϕ_g=1) as measured by LB-AFM. [4]Number average DP of side-chains determined by GPC of cleaved side-chains. [5]Grafting density

calculated from LB-AFM ϕ_g n_{sc} and cleavage n_{sc}. [6]Transfer ratio defined as ratio of change in LB trough area over area of transfer substrate. [7]Average width of the PBA bottlebrush samples from AFM. [8]Number average contour length of PBA bottlebrush samples measured using AFM. [9]Number average DP of the backbone determined from the AFM contour length as $n_{bb}=L/l_0$, where l_0=0.25 nm is the monomer length. [10]Dispersity of PBA bottlebrush contour length, PDI=L_w/L_n, where L_w and L_n are weight and number average lengths. [*]Number average molecular weight measured by THF GPC with RI detector using PMMA standards, [**]Number average DP of the backbone calculated from the calibration curve based on molecular weight of P(HEMA-TMS) by GPC. [***]Analysis was inaccurate due to poor AFM resolution of the closely spaced macromolecules having the shortest side chains.

The initial tests of bottlebrush melts exhibited a significantly different rheological behavior as compared to linear chains. upper graph in Figure III.3b displays classical entangled rheological behavior of a high-MW ($1.2\cdot10^6$ Da) linear poly(*n*-butyl acrylate) (PBA) with a plateau modulus of G_e =$1.1\cdot10^5$ Pa. In stark contrast, the lower graph in Figure III.3b demonstrates that bottlebrushes of the nearly same chemical composition and molecular weight as their linear counterparts have a Rouse-like relaxation of a weakly entangled melt over the incredibly broad range of seven decades of frequency. These data are in agreement with previous studies of similar systems and corroborate disentanglement of molecular bottlebrushes in the melt state.

Table III.4 P*n*BA bottlebrush polymer melt plateau modulus characterization**.**

Sample	G_e, Pa[1]	G_e, Pa[2]	tan(δ)[3]	n_e[4]	n_{bb}/n_e[5]
BA-6	11432 ± 331	7690±960	0.49 ± 0.020	461	4.4
BA-17	2421 ± 75	1588±301	0.71 ± 0.006	871	2.3
BA-23	1310 ± 54	831±138	0.72 ± 0.004	947	2.2
BA-34	938 ± 28	603±23	0.79 ± 0.005	1071	1.9
BA-130	178 ± 7	NA	0.86 ± 0.013	1768	1.2

[1]Plateau modulus determined by MIN method described above. [2]Plateau modulus determined by fitting the experimental data in Figure III.5 using the double reputation model. [3]Minimum in the ratio of loss and storage modulus used to determine value of plateau modulus. [4]Degree of polymerization (DP) of the entanglement strand calculated as $n_e \cong M_e n_{bb}/M$, where $M_e = \rho RT/G_e$ – molar mass of the entanglement strand, M - molar mass of bottlebrush (Table III.3), and n_{bb} – DP of the backbone (Table III.3) . [5]Entanglement ratio: ratio of the backbone DP and entanglement strand DP where n_{bb} = L/l_0 and l_0 =0.25 nm is the monomer length.

Below, the quantitative relation (equation III.2) between the entanglement modulus (G_e) of bottlebrush melts and the degree of polymerization of bottlebrush side chains (n_{sc}) was tested. Experimental verification of equation III.2 will also support the validity of extension of the Kavassalis-Noolandi conjecture to mesoscoic cylindrical molecules.

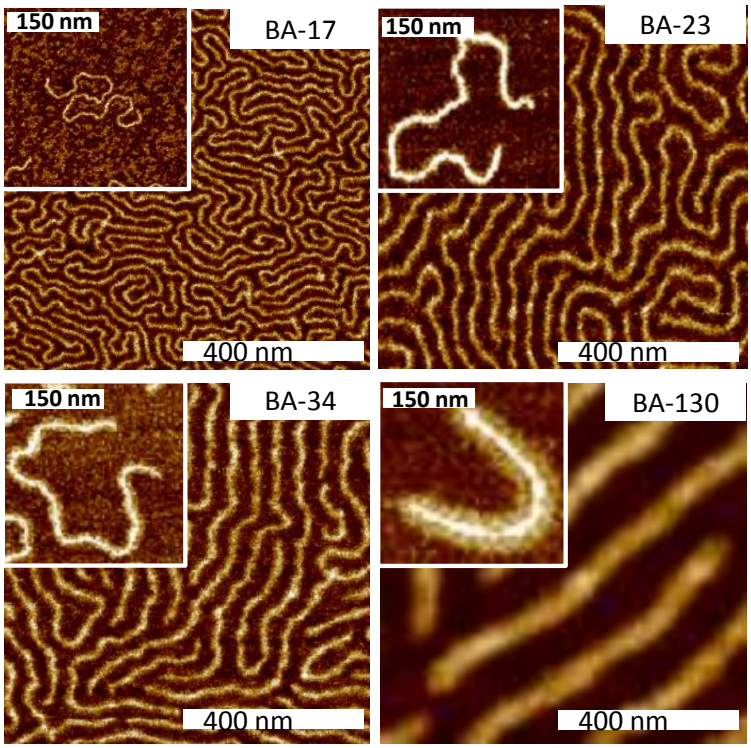

Figure III.4 AFM height images of the PBA bottlebrushes with different degrees of polymerization n_{sc} of PBA side chains. Large images generated from LB trough monolayer onto freshly cleaned mica substrates. Inset generated from dilute solution spin casting onto freshly cleaved mica substrates.

To minimize the number of variables, a systematic series of polymer bottlebrushes with an identical long backbone and different degrees of polymerization (DP) of the side chains were synthesized using the atom transfer radical polymerization technique.[36-38] To ensure the same backbone length, all bottlebrushes were synthesized by grafting *n*-butyl acrylate (*n*BA) from the same macroinitiator (2035-Br). Five bottlebrush samples were prepared with side-chain DP of 6, 17, 23, 34, and 130. The samples shall be referred to as (BA-n_{sc}) where n_{sc} denotes the number average side-chain DP.

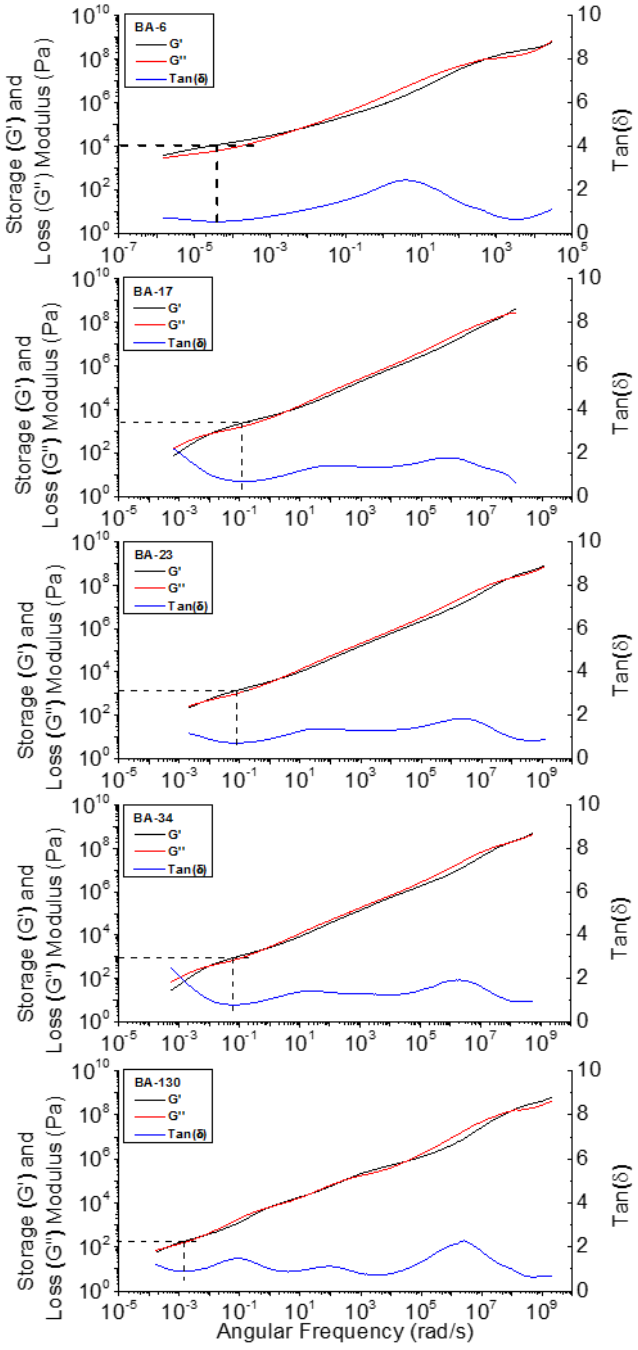

Figure III.5 Rheological spectra of PBA bottlebrush samples. In ascending order of n_{sc}. Dashed lines indicate the plateau modulus of the samples. Steady decrease in modulus as n_{sc} increases is apparent.

Given the architectural complexity and large size of molecular bottlebrushes, a combination of characterization techniques have been employed to measure independently the DP of the backbone (n_{bb}), the DP of side chains (n_{sc}), and the grafting density (ϕ_g). The results of molecular characterization are summarized in Table III.3. The backbone DP was measured by two methods: (i) GPC of the macroinitiator as n_{bb}=2035±100 (Table III.1) and (ii) AFM measurements of the bottlebrush contour length resulting in n_{bb}=2040±60 (Table III.3). All bottlebrush samples were analyzed by gel permeation chromatography (GPC) with light scattering detection to analyze molecular weight distribution. Since GPC analysis of large branched macromolecules is prone to errors, a molecular imaging of Langmuir-Blodget (LB) monolayers by AFM was employed to independently determine molecular weight (MW) distribution of the bottlebrushes.[39] Figure III.4 displays height micrographs of the polymer samples. The LB-AFM analysis gives the number average side-chain degree of polymerization per monomeric unit of the backbone as

$$\phi_g n_{sc} = \frac{M/n_{bb} - m_{bb}}{M_0} \qquad \text{(III. 3)}$$

where M is the number average molecular weight of the bottlebrush samples and n_{bb} is the number average DP of the backbone (Table III.3). To determine the grafting density ϕ_g we have conducted GPC analysis of cleaved side chains (Table III.1).[40,41] In addition, molecular imaging provided information about the width (W) of adsorbed bottlebrushes which is directly related to the molecular parameters as $W = \phi_g n_{sc} A_0 / l_0$, where l_0=0.25

nm is the monomer length of a fully extended backbone and A_0 is the monomer area of a LB film.

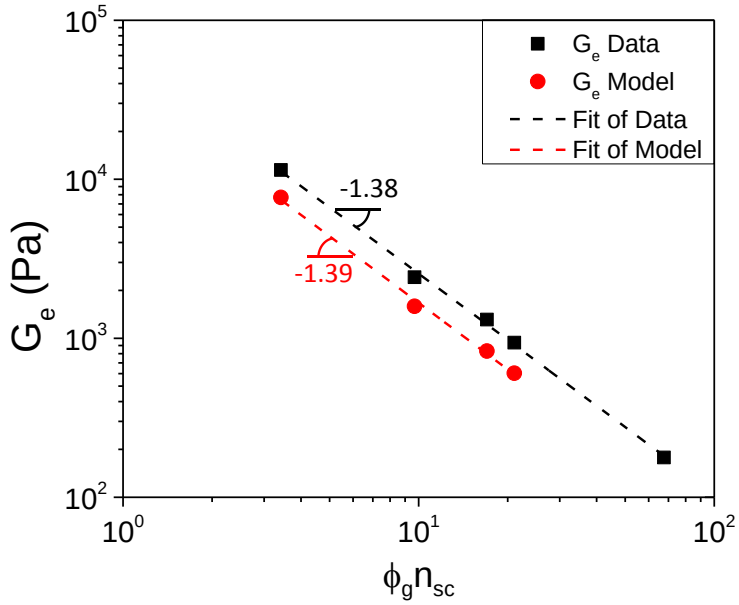

Figure III.6 Comparison of experimental data (■) with the theoretical fitting (●) of the plateau modulus as a function of degree of polymerization of poly(n-butyl acrylate) side chains (n_{sc}) corrected by the grafting density (ϕ_g). The trend in the theoretical fitting give excellent agreement with trend in experimental data both near -1.4, which is consistent with the scaling exponent -1.5 in equation V. 2.

To investigate the effect of n_{sc} on the plateau modulus of the polymer brushes, modulus versus frequency sweeps were performed in a window of 0.1 to 100 rad/s over a range of temperatures and strains on an AREA-G2 rheometer from TA Instruments. The frequency sweeps were used to generate master curves of modulus versus frequency using the WLF equation and TRIOS software from TA instruments. Figure III.5 shows

the relaxation spectra of the polymer samples extending between the high frequency glassy domain and the entanglement foot at low frequency. This extension is attributed to the increase in DP of the side chains as evidenced by Rouse-like relaxation and local minima in the tan(δ) at moduli corresponding to chain segments on the order of the side chain molecular weight. As the side-chain DP increases, an additional relaxation begins to distinguish itself from the side chain relaxation as evidenced by the formation of a second local minimum in tan(δ) between that of the side chain relaxation and the entanglement plateau foot. In BA-130, the two relaxations have fully separated and both manifest as a weak crossover of the storage modulus (G') over the loss modulus (G''). The nature of the second relaxation is tentatively ascribed to an overlap of the side-chains of neighboring bottlebrushes and will be investigated in future work.

In the low frequency regime, the entanglement plateau foot becomes less distinct as side-chain size increases with a shrinking frequency window displayed (Table III.4), which is attributed to elongation of the entanglement strand. As shown in Table III.4, the degree of polymerization (DP) of the entanglement strand for the studied bottlebrushes ranges from ca. 500 to 1800, which is significantly larger than the entanglement DP≅50 for conventional polymers. The terminal relaxation zone in the lowest frequencies beyond the entanglement plateau was not explored in detail due to extremely long relaxation times caused by large molecular weight and due to onset crosslinking at high temperature.

To analyze the relaxation spectra and determine the plateau modulus of the weakly-entangle bottlebrush melts we applied two methods. The first method was an empirical definition of the plateau modulus called the MIN method as described in detail by Lomellini.[42] In this method, the polymer melt entanglement modulus is taken as the value of the storage modulus at the frequency of the minimum in tan(δ) i.e. the maximum in stored stress within the entanglement regime. In the second method, the relaxation spectra in Figure III.5 were fit by the double reptation equation which accounted for molecular weight polydispersity. As expected for the weakly-entangled systems, the model resulted in lower absolute values of the entanglement plateau modulus than are found by the MIN method, but resulted in an identical relation between of plateau modulus and the n_{sc} of $G_e \propto {n_{sc}}^{-1.39}$. Full details of the modeling analysis can be found in the Supplemental Information. Figure III.6 displays the trend in plateau modulus with respect to n_{sc}; the results are summarized in Table III.4. The experimental data demonstrated good agreement with scaling analysis (eq. III.2). The modulus decreases with n_{sc} with an exponent of -1.38 which is close to the predicted -1.5 (eq. III.2). The bottlebrush melts display moduli on the order of hundreds of Pascals for n_{sc} = 130, which is a full three orders of magnitude lower than the plateau modulus of linear poly(*n*-butyl acrylate). By fitting the experimental data points ϕ_g=0.4 and $P_e = 17$ were obtained. The first number reasonably agrees with the experimentally determined grafting density ϕ_g=0.6±0.1, while the overlap parameter P_e is within the range of 16÷22 predicted by Kavassalis-Noolandi.

III.4 Conclusions

In conclusion, a series of polymer bottlebrushes was synthesized with a wide range of side-chain DP and carefully analyzed the molecular parameters of the materials using three different methods: Monomer conversion analysis, chemical cleavage with GPC, and LB AFM analysis. We measured the plateau modulus of these materials with excellent reproducibility and analyzed our data using known methods appropriate to the specifics of our system. The trend in plateau modulus closely matches that of scaling theory based on renormalizing a basic tube model to new chain thicknesses controlled by side-chain degree of polymerization. The bottlebrush melts show entanglement moduli in the range of hundreds of Pascals, three orders of magnitude below 10^5 Pa - the lower limit of typical linear polymers. Thus, self-disentanglement of bottlebrush macromolecules provides a new lower limit of modulus for solvent-free elastomers previously seen in swollen gel systems. In other words, these materials pushed the lower limit of modulus in dry neat polymer materials into ranges previously restricted to swollen gel materials. Such polymers may be useful for applications in the biomedical field where neat materials with moduli in the same range as human tissues are needed for reconstructive surgery or sound opaque biological implants.

III.5 References

(1) Neugebauer, D.; Zhang, Y.; Pakula, T.; Sheiko, S. S.; Matyjaszewski, K. *Macromolecules* **2003**, *36*, 6746-6755.

(2) Zhang, Y.; Constantini, N.; Mierzwa, M.; Pakula, T.; Neugebauer, D.; Matyjaszewski, K. *Polymer* **2004**, *45*, 6333-6339.

(3) Pakula, T.; Zhang, Y.; Matyjaszewski, K.; Lee, H.-i.; Boerner, H.; Qin, S.; Berry, G. C. *Polymer* **2006**, *47*, 7198-7206.

(4) Edwards, S. F.; Doi, M.; Oxford: Oxford University Pres: New York 1986.

(5) Rubinstein, M.; Colby, R. H.; Oxford University Press: New York, 2003.

(6) Larson, R. G.; Sridhar, T.; Leal, L. G.; McKinley, G. H.; Likhtman, A. E.; McLeish, T. C. B. *J. Rheol.* **2003**, *47*, 809.

(7) de Gennes, P. G. *J. Chem. Phys.* **1971**, *55*, 572.

(8) Fetters, L. J.; Lohse, D. J.; Richter, D.; Witten, T. A.; Zirkel, A. *Macromolecules* **1994**, *27*, 4639.

(9) Patel, S. K.; Malone, S.; Cohen, C.; Gillmor, J. R.; Colby, R. H. *Macromolecules* **1992**, *25*, 5241.

(10) Everaers, R., 1, 12.1. *New Journal of Physics* **1999**, *1*, 121.

(11) Urayama, K.; Kawamura, T.; Kohjiya, S. *J. Chem. Phys.* **1996**, *105*, 4833.

(12) Urayama, K.; Kawamura, T.; Kohjiya, S. *Polymer* **2009**, *50*, 347.

(13) Woods-Adams, P. M.; Dealy, J. M.; deGroot, A. W.; Redwine, O. D. *Macromolecules* **2000**, *33*, 7489.

(14) Yan, D.; Wang, W. J.; Zhu, S. *Polymer* **1999**, *40*, 1737.

(15) Inkson, N. J.; Graham, R. S.; McLeish, T. C. B.; Groves, D. J.; Fernyhough, C. M. *Macromolecules* **2006**, *39*, 4217.

(16) Kapnistos, M.; Vlassopoulos, D.; Roovers, J.; Leal, L. G. *Macromolecules* **2005**, *38*, 7852.

(17) Yurasova, T. A.; McLeish, T. C. B.; Semenov, A. N. *Macromolecules* **1994**, *27*, 7205.

(18) Pakula, T.; Vlassopoulos, D.; Fytas, G.; Roovers, J. *Macromolecules* **1998**, *31*, 8931.

(19) Milner, S. T.; McLeish, T. C. B. *Macromolecules* **1998**, *31*, 7479.

(20) Likos, C. N.; Lowen, H.; Watzlawek, M.; Abbas, B.; Jucknischke, O.; Allgaier, J.; Richter, D. *Phys. Rev. Lett.* **1998**, *80*, 4450.

(21) Roovers, J.; Zhou, L. I.; Toporowski, P. M.; Vanderzwan, M.; Iatrou, H.; Hadjichristidis, N. *Macromolecules* **1993**, *26*, 4324.

(22) Grayson, S. M.; Fréchet, J. M. *Chem. Rev.* **2001**, *101*, 3819.

(23) Uppuluri, S.; Keinath, S. E.; Tomalia, D. A.; Dvornic, P. R. *Macromolecules* **1998**, *31*, 4498.

(24) Zeng, F. W.; Zimmerman, S. C. *Chem. Rev.* **1997**, *97*, 1681.

(25) Bosman, A. W.; Janssen, H. M.; Meijer, E. W. *Chem. Rev.* **1999**, *99*, 1665.

(26) de Gennes, P. G.; Cornell University Press: Ithaca, 1979.

(27) Raphael, E.; Gay, C.; de Gennes, P. G. *J. Stat. Phys.* **1997**, *89*, 111.

(28) Zhang, K.; Lackey, M.; Cui, J.; Tew, G. N. *J. Am. Chem. Soc.* **2011**, *133*, 4140.

(29) Kricheldorf, H. R. *J. Polym. Sci. A Polym. Chem.* **2010**, *48*, 251.

(30) Hu, M.; Xia, Y.; McKenna, G. B.; Kornfield, J. A.; Grubbs, R. H. *Macromolecules* **2011**, *44*, 6935.

(31) Mpoukouvalas, A.; Li, W.; Graf, R.; Koynov, K.; Matyjaszewski, K. *ACS Macro Letters* **2013**, *2*, 23-26.

(32) Sheiko, S. S.; Sumerlin, B. S.; Matyjaszewski, K. *Prog. Polym. Sci.* **2008**, *33*, 759-785.

(33) Sheiko, S. S.; daSilva, M.; Shirvaniants, D. G.; LaRue, I.; Prokhorova, S. A.; Beers, K.; Matyjaszewski, K. *J. Am. Chem. Soc.* **2003**, *125*, 6725-6728.

(34) Fetters, L. J.; Lohse, D. J.; Colby, R. H.; Mark, J. E., Ed. New York, 1996.

(35) McLeish, T. B. C. *Advances in Physics* **2002**, *51*, 1379.

(36) Lee, H.-i.; Pietrasik, J.; Sheiko, S. S.; Matyjaszewski, K. *Prog. Polym. Sci.* **2010**, *35*, 24-44.

(37) Matyjaszewski, K. *Macromolecules* **2012**, *45*, 4015.

(38) Matyjaszewski, K.; Tsarevsky, N. V. *J. Am. Chem. Soc.* **2014**, *136*, 6513-6533.

(39) Borner, H. G.; Duran, D.; Matyjaszewski, K.; da Silva, M.; Sheiko, S. S. *Macromolecules* **2002**, *35*, 3387-3394.

(40) Sumerlin, B. S.; Neugebauer, D.; Matyjaszewski, K. *Macromolecules* **2005**, *38*, 702-708.

(41) Mukumoto, K.; Li, Y.; Nese, A.; Sheiko, S. S.; Matyjaszewski, K. *Macromolecules* **2012**, *45*, 9243.

(42) Lomellini, P. *Polymer* **1992**, *33*, 1255.

CHAPTER IV

MOLECULAR BOTTLEBRUSHES WITH BIMODAL SIDE CHAIN LENGTH

Preface

The following chapter describes the synthesis, characterization, and 2D organization of molecular bottlebrushes with a bimodal length of poly(*n*-butyl acrylate) (P*n*BA) side chains. Densely grafted copolymers were prepared via the "grafting from" approach using atom transfer radical polymerization (ATRP). A fraction of bromine chain ends was removed by selective capping with 4-butoxy-TEMPO, and subsequent chain extension of remaining active chains forming longer P*n*BA grafts. Brushes with the resulting bimodal side chains were characterized by Gel Permeation Chromatography (GPC) and Atomic Force Microscopy (AFM). AFM visualization of macromolecules confirmed the successful formation of architecture with a core-shell topology that corresponds to bottlebrushes with a bimodal length of P*n*BA grafts. Finally the 2D

polymer films were analyzed alongside monomodal bottlebrushes and equations were developed to correlate the effect of side chain DP (n_n) and side chain molecular weight distribution ($Đ$) on the average spacing between bottlebrushes in a monolayer. In addition, a screening of the efficiency of the capping process was done using a linear P*n*BA polymer as a model compound.

I designed and synthesized all linear and bottlebrush polymers, with the help of the former undergraduate student, Brittany Robertson, and analyzed the polymers through GPC and ^{1}H NMR characterizations. The LB-AFM analysis was performed by Dr. Yuanchao Li, and the equations were developed by William Daniel from prof. Sheiko's group at the University of North Carolina, Chapel Hill.

IV.1 Introduction

Molecular bottlebrushes are a distinct class of graft copolymers with side chains closely packed along a polymeric backbone.[1-5] A strong steric repulsion between grafts induces forces along the backbone of such macromolecules, compelling bottlebrushes to adapt an extended, cylindrical conformation.[6] These unique physical properties of bottlebrushes have drawn considerable attention directed towards exploring their potential applications. The intrinsic tension generated along the brush was exploited to induce a selective mechano-scission of chemical bonds, e.g.: disulfides or esters.[7-9] Additionally, the bulk properties resulting from the dense grafting were employed to prepare various materials suitable for use as bio-lubricants,[10] ionic conductors,[11] soft elastomers,[11-13] photonics,[5,14,15] stimuli responsive materials,[5] [16-18] large-pore membranes[19] or nano-networks[20]. In addition, the natural cylindrical shape of brush-polymers has been utilized in templating processes to form a variety of materials such as organic[21] and carbon[22] nanotubes, or metal[23] and inorganic[24] nanowires.

Densely grafted copolymers can be generated via three synthetic approaches: "grafting onto",[25] "grafting through"[26,27] and "grafting from".[1,28-30] Recent advances in ring opening metathesis polymerization (ROMP) have allowed for a broader use of the "grafting through" method, especially for the preparation of bottlebrushes with blocky backbones.[14,15] On the other hand, the "grafting from" procedure mainly relies on controlled radical polymerization techniques (CRP), in particular atom transfer radical (ATRP),[29,31-33] reversible addition-fragmentation chain transfer (RAFT)[21,34] and nitroxide

mediated (NMP)[35] polymerizations. This approach allows for the preparation of a vast number of brush-like architectures including gradient brushes,[36,37] brush-tail,[38] and brushes with blocky grafts,[19,24,39-41] while additionally providing great control over the grafting density and side chain length.

One of the benefits of ATRP is the possibility of post-polymerization modification, of the terminal polymeric halogens.[42,60] Methods for end group transformation include: a) nucleophilic substitution[43-45] with various agents such as azides, amines or phosphines, and b) atom transfer addition (ATRA): termination by combination of radicals[46] or reactions with species such as non-homopolymerizing comonomers,[43,47] addition-fragmentation transfer agents,[48,49] or stable radicals[50,51]. One of the most common and widely used classes of stable (persistent) radicals are nitroxides.[51] Nitroxides are secondary amine *N*-oxide radicals that are capable of quick, and under some conditions reversible, coupling with carbon centered radicals.[52]

2,2,6,6-Tetramethyl-1-piperidynyl-*N*-oxy (TEMPO), and its derivatives, have been used to mediate a stable free radical polymerization, called nitroxide mediated polymerization (NMP), of styrene.[31] Control in a NMP process is achieved through creation of a dynamic equilibrium between propagating radicals and dormant alkoxyamines, which occurs at elevated temperatures in the presence of an external radical source.[52-54] The covalent bond of alkoxyamine acrylates is much stronger than the one in styrene derivatives; therefore a traditional NMP is not suitable for polymerization of acrylic monomers.[31,54] The relatively high thermal stability of such covalent bonds

under mild conditions and fast capping of carbon centered radicals with TEMPO derivatives has been applied to determine rate constant values in ATRP processes. In this situation a halogen atom is abstracted in the presence of Cu (I) catalyst and subsequently trapped with nitroxide mediated radical via an ATRA process.[55,56]

With a growing number of methodologies for creating bottlebrush molecules it becomes increasingly problematic to properly characterize all of the structural details of these complicated and large molecules. Where a typical linear polymer has only its molecular weight distribution to consider, a polymer bottlebrush must be characterized by backbone, its molecular weight as well as its side chain molecular weight distribution, and grafting density. Such structural details directly relate to the physical properties of bottlebrush polymer materials which impact viscous properties and moduli. In order to develop a better means of characterizing the complicated structural details of molecular bottlebrushes we designed and synthesized two different series of such macromolecules. First series consisted of bottlebrushes with monomodal length distribution of side chains (monomodal bottlebrushes), whereas the second one had grafts with bimodal length distribution (bimodal bottlebrushes). Next, monomodal bottlebrushes were carefully analyzed using NMR, AFM, and LB techniques, thus allowing for determining the molecular weight distribution/dispersity ($Đ$) of the brush side chains as well as the grafting density of bottlebrushes (ϕ_g). Afterwards, the same analytical approach was then extended to a more complicated bottlebrush system, bimodal bottlebrushes.

The bimodal bottlebrush polymers were prepared using TEMPO-like persistent radicals in a selective end-group deactivation of polymers generated by ATRP. This is the first example and characterization of a bottlebrush with "core-shell" structure consisting of a densely grafted core and a shell with loosely packed side chains. Previous literature papers have described similar systems with bimodal brushes grafted from nanoparticles.[57,61] Such hybrids have shown enhanced particles dispersion abilities as well as improved thermal and mechanical properties in comparison to particles with monomodal grafts.[57,61] In the case of bottlebrushes, such bimodal grafts might be used to form new soft elastomers with interesting viscoelastic properties.[12,57,61]

IV.2 Experimental

Materials. 4-Butoxy-TEMPO (4-B-TEMPO) was donated by Nufarm. Tris(2-pyridylmethyl)amine (TPMA) and tris[2-(dimethylamino)ethyl]amine (Me_6TREN) were synthesized according to previously reported procedures.[58] *n*-Butyl acrylate (*n*BA, 99%, Acros) and (2-trimetylsiloxy)ethyl methacrylate (HEMA-TMS, Scientific Polymer Products) were purified by passing the monomer through a column filled with basic alumina to remove the inhibitor. All other reagents: ethyl α-bromoisobutyrate (EBiB, 98%), *p*-toluenesulfonyl chloride (TsCl, 98%), copper(I) bromide ($Cu^{I}Br$, 99.999%), copper(II) bromide ($Cu^{II}Br_2$, 99.999%), copper(I) chloride ($Cu^{I}Cl$, 99.995%), copper(II) chloride ($Cu^{II}Cl_2$, 99.999%), tin(II) 2-ethylhexanoate ($Sn(EH)_2$, 95%), 4,4′-dinonyl-2,2′-bipyridine (dNbpy, 97%) *N,N,N',N'',N''*-pentamethyldiethylenetriamine (PMDETA,

99%), potassium fluoride (KF, 99%), tetrabutylammonium fluoride (TBAF, 1.0 M in THF), α-bromoisobutyryl bromide (98%), 2,5-di-*tert*-butylphenol (DTBP, 99%), triethylamine (TEA, ≤99%), and solvents were purchased from Aldrich and used as received without further purification.

Characterization. The conversion of *n*BA was determined from ^{1}H NMR spectra recorded in $CDCl_3$ as a solvent using Brüker 300 MHz spectrometer. Molecular weight distributions of the polymers were characterized by gel permeation chromatography (GPC) using Polymer Standards Services (PSS) columns (guard, 10^5, 10^3, and 10^2 Å), with THF eluent at 35 °C, flow rate 1.00 mL/min, and differential refractive index (RI) detector (Waters, 2410). The apparent number-average molecular weights (M_n) and molecular weight dispersities ($Đ$) were determined with a calibration based on linear polystyrene (PSt) and poly(methyl methacrylate) (PMMA) standards and diphenyl ether as an internal standard, using WinGPC 6.0 software from PSS. The samples for AFM measurement were prepared by either Langmuir-Blodgett (LB) deposition or spin casting from dilute solutions in chloroform. LB films were transferred onto freshly cleaved mica substrates at a constant surface pressure of 0.5 mN/m. Imaging of indiIVdual molecules was performed in PeakForce QNM mode using a multimode AFM (Brüker) with a NanoScope V controller. Silicon probes with a resonance frequency of 50-90 Hz and a spring constant of ~0.4 N/m were used. In-house developed computer software was used to analyze the AFM images for 2D spatial dimensions.

Synthesis of P*n*BA macroinitiator with 100 % of Br chain ends (MI_{80}-Br). Purged *n*BA (50.0 mL, 350 mmol) was transferred via a purged syringe to a dry, 100-mL nitrogen-purged Schlenk flask. A solution of $Cu^{II}Br_2$ (7.8 mg, 0.035 mmol) and TPMA (61 mg, 0.21 mmol) in degassed anisole (3.0 mL) was added. The resulting mixture was stirred for 10 minutes, and then a purged solution of EBiB (514 μL, 3.5 mmol) in anisole (1.0 mL) was added. $Sn(EH)_2$ (113.5 μL, 0.35 mmol) in purged anisole (1 mL) was injected to begin the polymerization. An initial sample was taken via a purged syringe, and the sealed flask was placed in a thermostated oil bath at 60 °C. The polymerization was stopped after 16 hours reaching 80% monomer conversion as calculated by ^{1}H NMR spectroscopy. Number average molecular weight was determined by THF GPC using PSt standards: $M_{n,GPC}$ = 10,500 and $Đ$ = 1.15, which corresponded to DP of the macroinitiator 80. The polymer was next diluted with chloroform (100 mL) and passed through a column filled with natural alumina. The filtrate was concentrated on the rotary evaporator and then the remaining monomer was removed by blowing a gentle stream of air over the solution for the next 48 hrs.

Synthesis of P*n*BA macroinitiators with 100 % N_3 chain ends (P*n*BA_{80}-N_3). A 20 mL glass vial equipped with a stir bar was charged with P*n*BA_{80}-Br (0.50g, 0.048 mmol), excess of sodium azide (28.3 mg, 0.435 mmol) and DMF (10 mL). The vial was sealed and placed in an oil bath at 65 °C. The reaction was stopped after 48 hrs, the polymer was purified by three precipitations from cold methanol and dried overnight under vacuum. Number average molecular weight was determined by THF GPC using PSt standards: $M_{n,GPC}$ = 10,500 and M_w/M_n = 1.15.

Synthesis of P*n*BA macroinitiators with 50 % of N_3 chain ends (P*n*BA$_{80}$-N$_{3(0.5)}$). The syntheses and purifications were performed in the same way as for **P*n*BA$_{80}$-N$_3$**. The following ratios of reagents were used: [**P*n*BA$_{80}$-Br**]:[NaN_3] = [1]:[0.5] for 50 % of targeted capped chain ends.

Chain extension of P*n*BA$_{80}$-Br and P*n*BA$_{80}$-N$_3$ macroinitiators. A 10 mL Schlenk flask equipped with a stir bar was charged with **P*n*BA$_{80}$-Br/N$_3$** macroinitiator (0.20 g, 0.0174 mmol), *n*BA (2.0 mL, 14.0 mmol), PMDETA (6.2 μL, 0.030 mmol), $Cu^{II}Br_2$ (0.39 mg, 0.0017 mmol), and anisole (0.45 mL). The solution was degassed by three freeze-pump-thaw cycles. During the final cycle $Cu^{I}Br$ (4.0 mg, 0.0278 mmol) was quickly added to the frozen reaction mixture under nitrogen atmosphere. The flask was sealed, evacuated, back-filled with nitrogen five times, and then immersed in an oil bath thermostated at 60 °C. The polymerization was stopped after 40 h, and the progress of reaction was monitored by THF GPC analysis.

Chain extension of P*n*BA$_{80}$-N$_{3(0.5)}$ macroinitiators. The reaction was performed and characterized in the same way as the chain extension of **P*n*BA$_{80}$-Br**. The following ratio of regents was targeted: [**P*n*BA$_{80}$-Br**]:[*n*BA]=[800]:[1], assuming a quantitative nucleophilic substitution, and thus 50 mol. % content of **P*n*BA$_{80}$-Br** in **P*n*BA$_{80}$-N$_{3(0.5)}$**.

Chain extension of MI$_{80}$-Br. A 10 mL Schlenk flask equipped with a stir bar was charged with **MI$_{80}$-Br** macroinitiator (0.20 g, 0.0174 mmol), *n*BA (2.0 mL, 14.0 mmol), PMDETA (6.2 μL, 0.030 mmol), $Cu^{II}Br_2$ (0.39 mg, 0.0017 mmol), and anisole (0.45 mL). The solution was degassed by three freeze-pump-thaw cycles. During the final cycle

$Cu^{I}Br$ (4.0 mg, 0.0278 mmol) was quickly added to the frozen reaction mixture under nitrogen atmosphere. The flask was sealed, evacuated, back-filled with nitrogen five times, and then immersed in an oil bath thermostated at 60 °C. The polymerization was stopped after 40 h, and the progress of reaction was monitored by THF GPC analysis.

Synthesis of P*n*BA macroinitiators with 50 % 4-butoxy-TEMPO chain ends (MI_{80}-Br/$T_{0.5}$). A 10 mL Schlenk flask equipped with a stir bar was charged with **MI-Br** (0.50 g, 0.048 mmol), 4-butoxy-TEMPO (5.4 mg, 0.0238 mmol), Me_6TREN (5.5 mg, 0.0238 mmol), toluene (5 mL) and acetonitrile (1 mL). The flask was sealed and the solution was purged with nitrogen for 15 min. Next, $Cu^{I}Br$ (3.4 mg, 0.0238 mmol) was added to the frozen reaction mixture under nitrogen. The flask was sealed, evacuated, back-filled with nitrogen three times, and then the reaction mixture was stirred at room temperature for 30 min. The reaction was stopped by opening the flask to air. The polymer was purified by three precipitations from cold methanol, and dried overnight under vacuum. Number average molecular weight was determined by THF GPC using PSt standards: $M_{n,GPC}$ = 10,500 and $Đ$ = 1.15.

Chain extension of MI_{80}-Br/$T_{0.5}$ macroinitiator. The reactions was performed and characterized in the same way as the chain extension of **MI_{80}-Br**. The following ratio of regents was targeted: [P*n*BA_{80}-Br]:[*n*BA]=[800]:[1], assuming a quantitative capping with 4-butoxy-TEMPO, and thus 50 mol. % content of **MI_{80}-Br** in **MI_{80}-$T_{0.5}$**.

Synthesis of $P(HEMA\text{-}TMS)_{385}$. A 25 ml Schlenk flask was charged with TsCl (14.5 mg, 0.0766 mmol), HEMA-TMS (20.0 mL, 91.9 mmol), dNbpy (0.150 g, 0.368 mmol),

$Cu^{II}Br_2$ (6.1 mg, 0.0276 mmol), and anisole (2.2 mL). The solution was degassed by three freeze-pump-thaw cycles. During the final cycle, the flask was filled with nitrogen and $Cu^{I}Br$ (22.3 mg, 0.1562 mmol) was quickly added to the frozen reaction mixture. The flask was sealed, evacuated and back-filled with nitrogen five times and then immersed in an oil bath at 60 °C. Polymerization was stopped after 21 h 10 min. reaching 32.2 % conversion as determined by ^{1}H NMR, which corresponded to a DP of 385. Apparent molecular weight determined by THF GPC: $M_{n,GPC} = 6.83 \cdot 10^4$, and $Đ = 1.14$. The reaction mixture was diluted with chloroform, passed through neutral alumina to remove the catalyst, then concentrated and used for the next step without further purification.

Synthesis of PBiBEM$_{385}$ macroinitiator. A 50 ml round-bottom flask was charged with **P(HEMA-TMS)$_{385}$** (12.17 g, 60.3 mmol), KF (4.266 g, 72.3 mmol), DTBP (1.241 g, 6.025 mmol), and then dry THF (40 mL) was added under nitrogen. The reaction mixture was cooled down in an ice bath, followed by the injection of tetrabutylammonium fluoride (0.6 mL, 1.0 M in THF, 0.60 mmol) and subsequent dropwise addition of α-bromoisobutyryl bromide (15.2 g, 8.2 mL. 66.3 mmol) over the course of 30 min. Upon addition, the reaction mixture was allowed to reach room temperature and was stirred for another 16 h. Afterwards solids were filtered of and the mixture was precipitated into methanol/water (70/30), re-dissolved in chloroform (70 mL) and passed through the column filled with basic alumina. The product was re-precipitated three times in hexanes and dried overnight under vacuum. Molecular weight determined by THF GPC: $M_{n,GPC} = 6.85 \cdot 10^4$, and $Đ = 1.14$.

Synthesis of PBiBEM$_{365}$-*g*-P*n*BA$_{56}$ (0-100). A 25 mL Schlenk flask equipped with a stir bar was charged with **PBiBEM$_{385}$** (0.1957 g, 0.7016 mmol), *n*BA (20.0 mL, 140.3 mmol), dNbpy (0.144 g, 0.351 mmol), $Cu^{II}Br_2$ (2.0 mg, 0.0088 mmol), and anisole (2.2 mL). The solution was degassed by three freeze-pump-thaw cycles. During the final cycle $Cu^{I}Br$ (23.8 mg, 0.1666 mmol) was quickly added to the frozen reaction mixture under nitrogen atmosphere. The flask was sealed, evacuated, back-filled with nitrogen five times, and then immersed in an oil bath thermostated at 70 °C. The polymerization was stopped after 18 h at 28 % monomer conversion, as determined by ^{1}H NMR, resulting in the brush polymer **0-100** with DP~56 of side chains. The polymer was purified by three precipitations from cold methanol, and dried under vacuum at room temperature, to a constant mass. Apparent molecular weight was determined using THF GPC: $M_{n,GPC} = 7.6 \cdot 10^5$, and $Đ = 1.19$.

Synthesis of bottlebrushes with P*n*BA$_{56}$ side chains haIVng 50 and 20 % of 4-butoxy-TEMPO chain ends (SC$_{56}$-T$_{0.5}$ and SC$_{56}$-T$_{0.2}$). The syntheses and purifications were performed in the same way the extension of **MI$_{80}$-Br/T$_{0.5}$**. The following ratios of reagents were used: [**P*n*BA$_{56}$-Br**]:[4-butoxy-TEMPO] = [1]:[0.5] and [**P*n*BA$_{56}$-Br**]:[4-butoxy-TEMPO] = [1]:[0.2], obtaining **SC$_{56}$-T$_{0.5}$** and **SC$_{56}$-T$_{0.2}$** with 50 and 20 % of capped chain ends respectively.

Synthesis of bimodal P*n*BA bottlebrushes with 50 % of long grafts (50-50). A 10 mL Schlenk flask equipped with a stir bar was charged with **SC$_{56}$-T$_{0.5}$** (0.170 g of the brush, 0.085 g of P*n*BA$_{56}$-Br, 0.0126 mmol), *n*BA (2.52 mL, 17.7 mmol), PMDETA (1.4 μL,

0.0065 mmol), $Cu^{II}Br_2$ (70 μg, 0.0017 mmol), and anisole (0.28 mL). The solution was degassed by three freeze-pump-thaw cycles. During the final cycle $Cu^{I}Br$ (0.86 mg, 0.0060 mmol) was quickly added to the frozen reaction mixture under nitrogen atmosphere. The flask was sealed, evacuated, back-filled with nitrogen five times, and then immersed in an oil bath thermostated at 60 °C. The polymerization was stopped after 120 h, reaching 9.7% monomer conversion, which corresponds to DP~200 of extended SCs, i. e.: long grafts. **50-50** was purified via three precipitations into cold methanol. Apparent molecular weight was determined using THF GPC and PSt standards: $M_{n,GPC}$ = $1.01 \cdot 10^6$, and $Đ$ = 1.21. Linear P*n*BA side product was formed during the polymerization and it was removed via a selective precipitation of **50-50** from THF solution into methanol at room temperature (two times).

Synthesis of bimodal P*n*BA bottlebrushes 20 % of long grafts (20-80). The polymerization was set up in the same manner as for **50-50**, assuming 80 wt. % of **P*n*BA$_{56}$-Br** in **SC$_{56}$-T$_{0.2}$.** Apparent molecular weight was determined using THF GPC and PSt standards: $M_{n,GPC}$ = $9.1 \cdot 10^5$, and $Đ$ = 1.21. Linear P*n*BA side product was formed during the polymerization and it was removed via a selective precipitation of **20-80** from THF solution into methanol at room temperature (two times).

IV.3 Results and Discussion

IV.3.1 Synthetic Approach for the Preparation of Polymers with Bimodal Chain Length Distribution

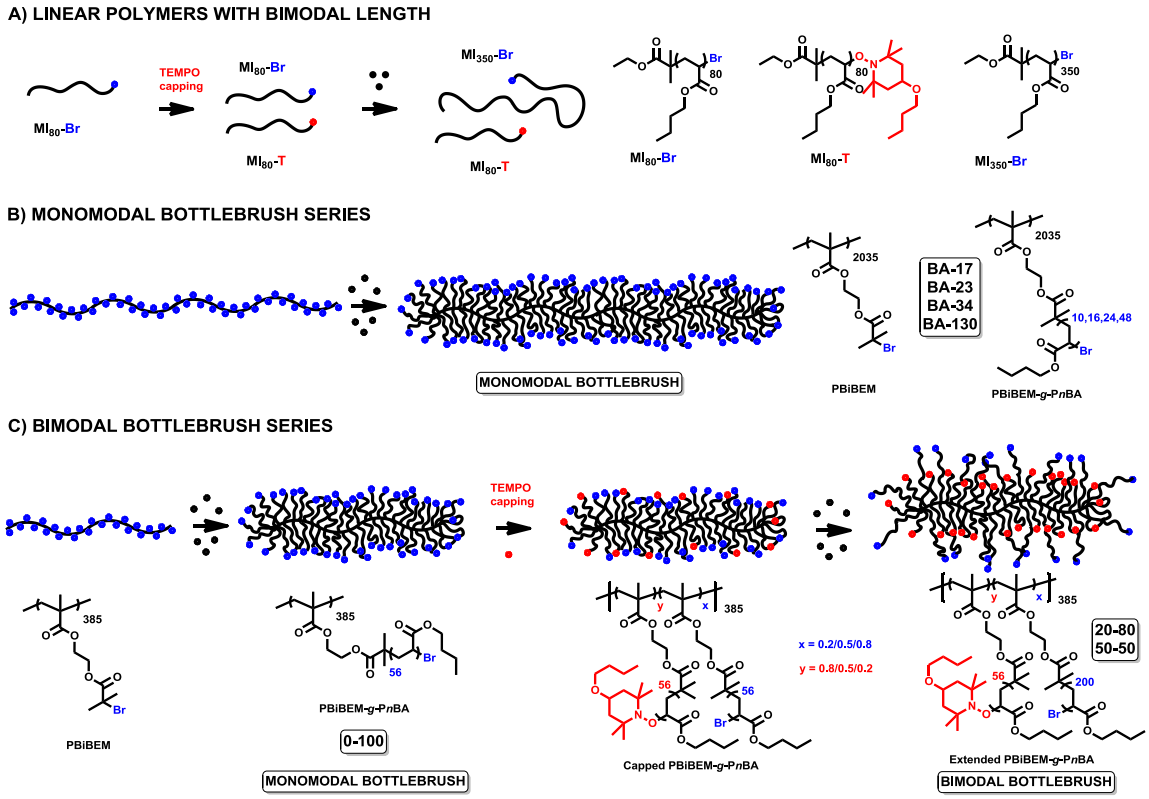

Scheme IV.1 The synthetic approach for the fabrication of (A) linear polymers with a bimodal length distribution and (B) monomodal, and (C) bimodal bottlebrushes.

In this work we describe a synthetic way of controlled incorporation of bimodality into the chain length, in polymers prepared via ATRP. Such approach required a selective and quantitative method of deactivation/removal of halogen atoms from polymer chain ends, which was accomplished through a biradical coupling reaction with a TEMPO-

based persistent radical. This synthetic method was applied to generate bimodal polymers with two architectures: (A) linear poly(*n*-butyl acrylate) (P*n*BA) and (B) bottlebrushes with P*n*BA grafts (Scheme IV.1). Both architectures were prepared in a three-step approach. First, the polymer synthesized by ATRP was reacted with 4-butoxy-TEMPO (4B-TEMPO) to cap a fraction of active end groups, followed by the chain extension of the remaining ATRP functionalities. 4B-TEMPO was used for a selective removal of halogen end groups, thus deactivating them for ATRP (Scheme IV.1).

IV.3.2 Synthesis of Linear Polymer with Bimodal Chain Length Distribution

Before attempting the synthesis of bimodal bottlebrushes, it was necessary to develop a method allowing a quantitative removal of ATRP-active chain ends. First, model studies with linear P*n*BA macroinitiator were performed, thus enabling a more feasible quantitative assessment of the end-capping process. Two types of reactions were tested: nucleophilic substitution with sodium azide and biradical coupling with a persistent radical, 4-butoxy-TEMPO (Scheme IV.2).

First a linear poly(*n*-butyl acrylate) macroinitiator was prepared via ARGET ATRP, using the following ratio of reagents: [*n*BA]:[EBiB]:[$Cu^{II}Br_2$]:[TPMA]:[Sn{EH}$_2$]= [100]:[1]:[0.01]:[0.06]:[0.1], 10 vol. % anisole, *T*=60 ˚C. The polymerization was stopped after 16 hrs resulting in ATRP macroinitiator with a degree of polymerization (DP) 80, MI_{80}-Br. The GPC

characterization of the polymer provided a monomodal signal with a number average molecular weight (M_n) and molecular weight distribution ($Đ$) of 10,500 and 1.15 (Figure IV.1, black).

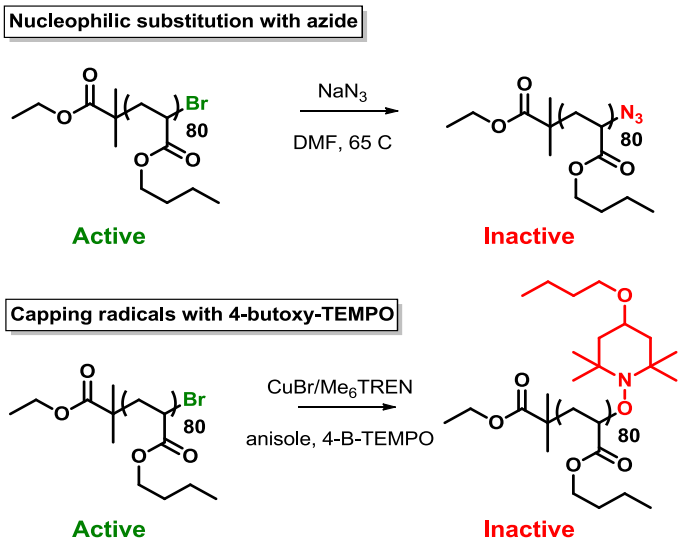

Scheme IV.2 Chain end substitution approaches used for linear P*n*BA macroinitiator.

In order to preserve high chain end functionality, the polymerization was stopped at ~80% monomer conversion. High chain end fidelity (>99%) was confirmed by extension of **MI_{80}-Br** with *n*-butyl acrylate. The polymerization was stopped after 40 hrs giving an extended polymer, P*n*BA_{170}-Br, with M_n = 22,100 and $Đ$ = 1.15 (Figure IV.1, blue). High chain end functionality (>99%) of **MI_{80}-Br** was confirmed by GPC results, which showed a clear shift of the initial signal towards higher MWs, without noticeable broadening of MWD and/or tailing towards lower MW values (Figure IV.1, blue).

The nucleophilic substitution with sodium azide was used as an approach to replace bromine chain ends as it is should provide a quantitative substitution of halogen atoms with groups that are inert towards ATRP. First, MI_{80}-Br was reacted with 10 and 0.5 equivalents of NaN_3 in DMF as a solvent, at 65 °C for 48h, thus targeting 100 % and 50 % of chain end replacement. The polymers were precipitated into cold methanol and dried under vacuum overnight, resulting in P*n*BA_{80}-N_3 and P*n*BA_{80}-$(N_3)_{0.5}$ polymers. Next, chain extensions of P*n*BA_{80}-N_3 and P*n*BA_{80}-$(N_3)_{0.5}$ were performed using the following conditions: [*n*BA]:[P*n*BA_{80}-Br]:[CuBr]:[$CuBr_2$]:[PMDETA] = [800]:[1.0]:[1.6]:[0.1]:[1.7], 10 vol. % anisole at 60 °C. The results of both polymerizations were determined by GPC analysis (Figure IV.2).

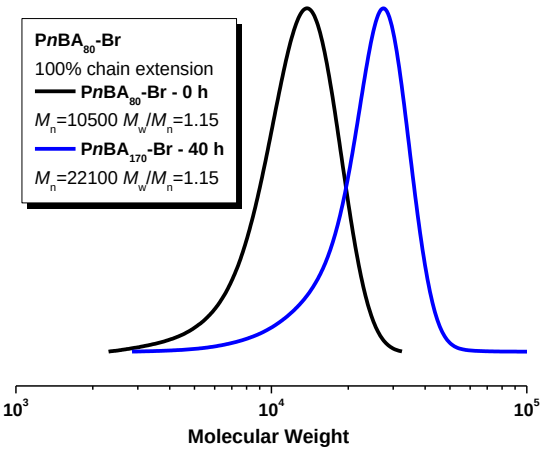

Figure IV.1 GPC traces of linear P*n*BA macroinitiator, **MI_{80}-Br**, (black) and the resulting polymer after chain-end extension, **P*n*BA_{170}-Br** (blue).

Figure IV.2a shows GPC traces of P*n*BA_{80}-N_3 before and after ATRP reaction. As expected, no shift of the initial P*n*BA_{80}-N_3 signal (Figure IV.2a) towards HMW values

was observed, which indicated that azide functionalized polymer did not undergo a chain-extension. However, GPC trace of the polymerization mixture after 44 hrs of the reaction time revealed the presence of oligomeric species, observed as a shoulder at LMW values (Figure IV.2a, blue). This observation suggested that even though azide end groups of P*n*BA$_{80}$-N$_3$ remained unreactive towards ATRP, the tested reaction conditions might induce a side process that resulted in the formation of new polymeric chains.

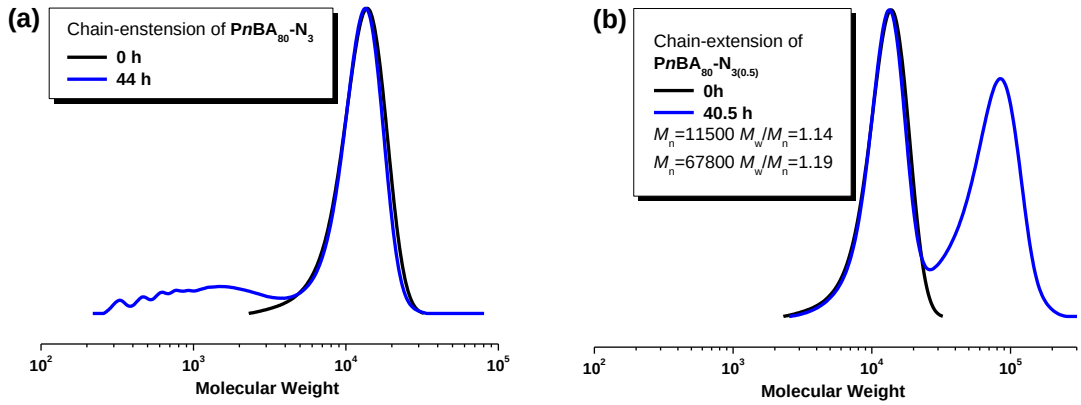

Figure IV.2 GPC traces of (a) **P*n*BA$_{80}$-N$_3$** and (b) **P*n*BA$_{80}$-(N$_3$)$_{0.5}$** before (black) and after (blue) a chain extension.

In order to test the quantitative results of the azide end group substitution, a chain extension of P*n*BA$_{80}$-(N$_3$)$_{0.5}$ was performed. Thus, P*n*BA$_{80}$-(N$_3$)$_{0.5}$ was chain extended under normal ATRP conditions, targeting [P*n*BA$_{80}$-Br]:[*n*BA] = [1]:[800] ratio (assuming quantitative capping). The polymerization was stopped at 13 % monomer conversion, as determined by ^{1}H NMR spectroscopy, which corresponded to DP$_{NMR,extended}$ ~105, if the capping with azide was quantitative (50 mol. %). Next, the theoretical DP values obtained from the monomer conversion were compared with the GPC results. The results

provided the bimodal distribution of the signal, with LMW values corresponding to unreacted P*n*BA$_{80}$-N$_3$ chains and extended polymer chains with Br end groups at higher MWs (Figure IV.2b, blue). M_n of HMW peak was 67,800, which corresponded to $DP_{GPC,total}$ = 530 of the extended polymer, and hence $DP_{GPC,extended} = DP_{GPC,total} - DP_{MI80-Br}$ = 530 - 80 = 450 of the extended block. The inconsistency of GPC and ^{1}H NMR results ($DP_{NMR,extended}$ = 105 vs. $DP_{GPC,extended}$ = 450) showed that the process of nucleophilic substitution did not provide a quantitative reaction. Around 90 % of polymer chains were inactive towards ATRP as opposed to targeted 50 mol %, meaning that there might be some side reaction occurring during azide substitution, leading to further deactivation of ATRP-functionalized polymers.

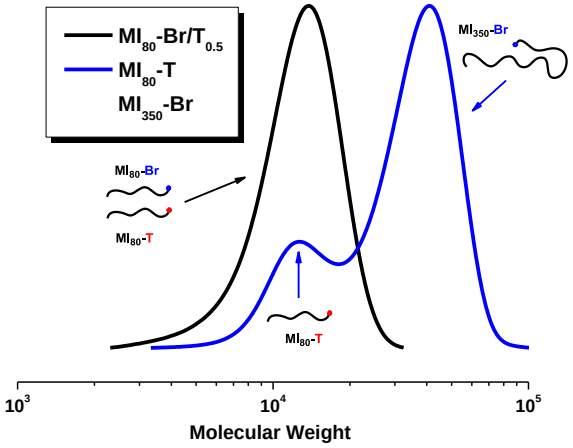

Figure IV.3 GPC traces of linear MI$_{80}$-Br macroinitiator capped with 0.5 eq. of 4-butoxy-TEMPO before (black) and after (blue) extension with *n*BA.

After the failure of azide substitution as a capping technique, a method of ATRP end group deactivation with TEMPO-like persistent radicals was applied. The efficiency

of end-group capping and the stability of the product under ATRP conditions were tested. Schemes IV.1A and IV.2 depict the approach used for the synthesis of linear polymer with bimodal distribution. The model studies were performed using a linear the same linear macroinitiator, MI_{80}-Br, as for the tests with sodium azide.

Afterwards, MI_{80}-Br was reacted with 0.5 eq. of 4B-TEMPO in the presence of $Cu^{I}Br/Me_6TREN$ catalyst, thus targeting deactivation of 50 mol. % of active end groups. The product, MI_{80}-Br/$T_{0.5}$, was purified and characterized by GPC showing no changes when compared to MI_{80}-Br (Figure IV.3A, black). Next, MI_{80}-Br/$T_{0.5}$ was chain extended under normal ATRP conditions, targeting the ratio of reagents: [P*n*BA_{80}-Br]:[*n*BA] = [1]:[800] (assuming quantitative capping). The polymerization was stopped at 33 % monomer conversion, which corresponds to theoretical DP of the extended block, $DP_{NMR,extended}$ = 265, and thus the total theoretical DP of the polymer, $DP_{NMR,total}$=$DP_{MI80-Br}$ + $DP_{NMR,extended}$ = 80+265 = 345. Next, the theoretical DP values obtained from the conversion were compared with the results of the GPC analysis. As expected, the chain extension provided a signal with bimodal distribution (Figure IV.3, blue), with the smaller, low molecular weight, peak corresponding to MI capped with 4B-TEMPO (MI_{80}-$T_{0.5}$) and a higher molecular weight (HMW) signal assigned to the extended polymer, MI_{350}-Br. M_n of HMW peak was 44,900 which corresponded to $DP_{GPC,total}$ = 350 of the extended polymer, and hence $DP_{GPC,extended}$ = $DP_{GPC,total}$ - $DP_{MI80-Br}$ = 350 – 80 = 270 of the extended block. The consistency of the results obtained from the monomer conversion and GPC analysis ($DP_{NMR,extended}$ = 265 vs. $DP_{GPC,extended}$ = 270) showed that the process of capping with 4-butoxy-TEMPO could be successfully applied to deactivate

end groups in polymers prepared by ATRP. In addition, 4-butoxy-TEMPO end functionalities did not show any reactivity under tested ATRP conditions.

IV.3.3 Synthesis of Monomodal Bottlebrushes

As already mentioned, one of the goals of this work was to design tools enabling more detailed structural characterization of densely grafted copolymers. For that purpose, we synthesized a series of well-defined monomodal bottlebrushes and subjected it to a thorough characterization using AFM, GPC and ^{1}H NMR methods. The results of these analyses were used to develop a series of equations, which were then applied in a structural characterization of bimodal bottlebrushes.

A series of monomodal bottlebrushes used in this study was based on a long backbone with a constant length (DP_{BB}=2035), and P*n*BA side chains with varying degrees of polymerization (DP_{SCs}=10, 16, 24 and 48) (Scheme IV.1B). All bottlebrushes were synthesized through the 'grafting from' approach by employing normal ATRP conditions. Poly(*n*-butyl acrylate) (P*n*BA) side chains were polymerized from ATRP macroinitiator, poly[2-(2-bromoisobutyryloxy)ethyl] methacrylate, thus obtaining a monomodal bottlebrush (Scheme 1B). Different graft lengths were attained by targeting different monomer to ATRP initiator ([*n*BA]:[I]) ratios, while keeping the monomer conversion ~10%.

Table IV.1 GPC characterization of monomodal and bimodal bottlebrush series.

Series	Sample	DP_{SC} [a]	n_n [b]	I_{eff} [c]	$M_n \cdot 10^{-5}$ [d]	$Đ$ [d]
Monomodal	**BA-17**	10	17	0.6	29	1.5
	BA-23	16	23	0.7	47	1.6
	BA-34	24	34	0.7	58	1.6
	BA-130	48	130	0.4	179	1.5
Bimodal	**0-100**	56	N/A	N/A	7.6	1.2
	20-80	(200-56)/85*	N/A	N/A	9.1	1.2
	20-80	(200-56)/128*	N/A	N/A	10.1	1.2

[a] Degree of polymerization of side chance calculated from the monomer conversion determined by ^{1}H NMR, using the equation: $DP_{SC} = \left(1 - \frac{A_{[M]} \times A_{[Anisole]_0}}{A_{[M]_0} \times A_{[Anisole]}}\right) \times DP_{target}$, where $A_{[M]_0}$ and $A_{[M]}$ are integrations for vinyl signals of the monomer at the beginning and end of the polymerization, and respective integrations of an internal standard, anisole, protons. [b] Degree of polymerization of side chains after cleaving from the brush backbone, measured using THF GPC with PS standards. [c] Initiation efficiency of the grafting process, $I_{eff} = \frac{DP_{SC}}{n_n}$. [d] Determined by THF GPC using PS standards. * Determined from the equation: $DP_{SC} = DP_{short} \times x_{short} + DP_{long} \times x_{long}$, where

DP_{short} and DP_{long} are degrees of polymerizations corresponding to short and long grafts of bimodal bottlebrushes, and x_{short} and x_{long} are their respective mole fractions.

Obtained monomodal bottlebrushes with DP_{SC}: 10, 16, 24 and 48, were then analyzed by THF GPC to obtain apparent number molecular weight (M_n) and the molecular weight distribution/dispersity ($Đ$) values (Table IV.1). DP_{SC} values were calculated from the monomer conversion and targeted DP values, assuming 100% initiation efficiency of the polymerization, or else 100% grafting density. However, in order to determine the actual length of side chains (n_n), monomodal bottlebrushes were subjected to an acidic hydrolysis, which cleaved grafts from the backbone (Table IV.1), and thus allowed for determination of initiation efficiencies (I_{eff}) of grafting processes. The preparation and characterization of monomodal bottlebrushes was not the main focus of this work; hence we do not discuss it here in details.

IV.3.4 Synthesis of Bimodal Bottlebrushes

After performing the synthesis of monomodal bottlebrushes and proving the efficiency of the TEMPO-capping approach in the incorporation of bimodality into the length distribution, we combined these two approaches to generate a new architecture, a bimodal bottlebrush (Scheme IV.1C).

First, a monomodal bottlebrush was prepared to serve as a platform for the synthesis of bimodal bottlebrushes. The approach analogous to that described above was

applied. The reaction was performed with the ratio of reagents: [*n*BA]:[I]=[400]:[1], in the presence of $Cu^{I}Br/Cu^{II}Br_2$/dNbpy as a catalytic system. A monomodal bottlebrush (**0-100**), with DP of the backbone 385 and DP of side chains 56, was obtained and then used in the formation of bimodal bottlebrushes (Scheme IV.1C).

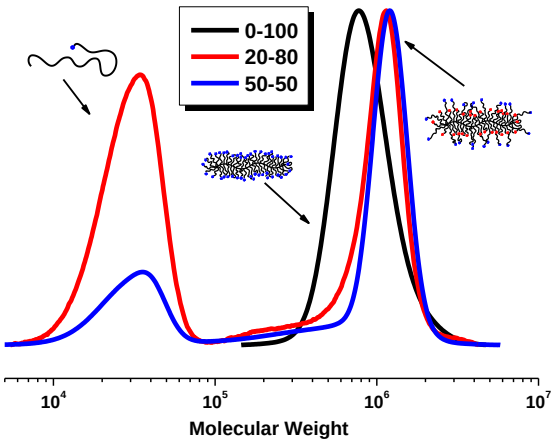

Figure IV.4 GPC traces of bottlebrush with P*n*BA grafts with the mole fraction of extended (long) side chains: 0 % (**0-100**, black), 20 % (**20-80**, red) and 50 % (**50-50**, blue) (low molecular weight peaks correspond to linear P*n*BA impurities formed during the extension process).

Next, two degrees of end-group substitution of **0-100** were targeted: 50% (**SC_{56}-$T_{0.5}$**) and 20% (**SC_{56}-$T_{0.2}$**). Respective reactions were performed with 0.5 and 0.2 equivalents of 4B-TEMPO per bromine end group, and equal amounts of CuBr(I)/Me_6TREN complex, in acetonitrile/toluene mixed solvents. The resulting brush polymers, **SC_{56}-$T_{0.5}$** and **SC_{56}-$T_{0.2}$**, were purified by three precipitations into cold methanol, and subsequently used in a chain extension process to achieve respective

bimodal brushes. This was accomplished through polymerizations analogous to that used in the synthesis of **0-100**. The grafting from $\mathbf{SC_{56}\text{-}T_{0.2}}$ and $\mathbf{SC_{56}\text{-}T_{0.5}}$ proceeded with the ratio of reagents [*n*BA]:[P*n*BA$_{56}$-Br]=[1400]:[1] and CuBr(I)/PMDETA as a catalyst. The extension of grafts yielded bimodal bottlebrushes with DP of side chains = 56 and 200, and respective grafting densities of the longer grafts, 20% (**20-80**) and 50% (**50-50**) (Table IV.1).

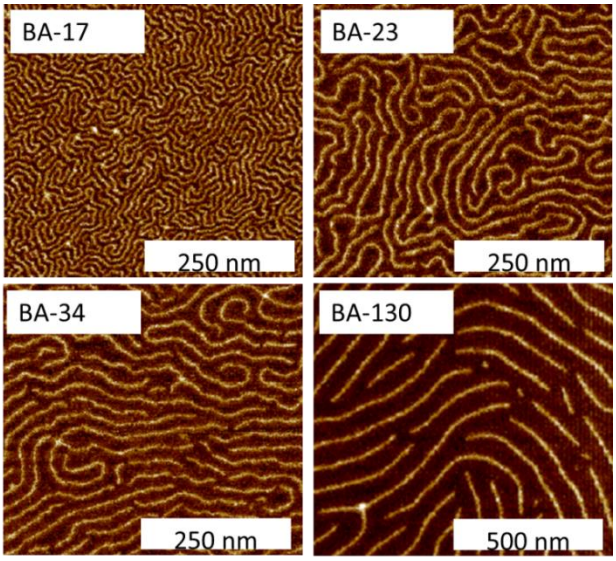

Figure IV.5 AFM height images of monomodal bottlebrushes with different degrees of polymerization (n_n) of side chains. Images were taken from LB trough monolayers transferred onto mica substrates.

The chain-extension in **20-80** and **50-50** was confirmed by the shift of GPC traces towards higher molecular weight values, as compared to **0-100** (Figure IV.4, blue and red). In all cases GPC signals were monomodal with narrow molecular weight distributions ($Đ$~1.2) demonstrating the formation of well-defined bottlebrushes (Table

IV.1). However, a more detailed analysis of GPC traces of **20-80** and **50-50** showed the appearance of low molecular weight peaks, which was ascribed to the formation of a linear P*n*BA with yet unknown mechanistic origin. The low molecular weight impurities in brushes **20-80** and **50-50** were removed via selective precipitation from THF solution into methanol at room temperature, hence providing pure bimodal bottlebrushes.

Table IV.2 Results of AFM analyses of monomodal and bimodal bottlebrush series

Series	Entry		<*d*> [a] / nm		<*L*> [a] / nm
			spin cast	LB	LB
Monomodal	**BA-17**		N/A	10±1	513±284
	BA-23		N/A	16±1	515±299
	BA-34		N/A	23±3	495±287
	BA-130		N/A	68±5	517±297
Bimodal	**0-100**		50±4	51±2	134±2
	20-80	**core**	50±7	78±4*	133±3
		shell	63±4		
	50-50	**core**	58±5	98±8*	130±2
		shell	82±4		

[a] Length <*L*> and width <*d*> of bottlebrushes obtained from AFM images of LB films or spin casted bottlebrushes on mica substrates. *Values measured for bimodal bottlebrushes before the removal of linear P*n*BA impurities.

Obtained results show that an addition of a non-stoichiometric amount of 4B-TEMPO allows for preservation of a fraction of bromine chain ends, whereas high

selectivity and yield of the process enables a good control over the fraction of chain extended polymers. This approach was successfully applied in the preparation of bimodal bottlebrushes with a controllable fraction of incorporated longer side chains.

IV.3.5 AFM Characterization of Monomodal and Bimodal Bottlebrushes

Atomic Force Microscopy (AFM) and the Langmuir Blodgett (LB) trough are powerful techniques for characterizing macromolecules in a two dimensional (2D) environment. AFM allows for measuring dimensions of a single bottlebrush molecule, whereas the LB trough provides a surface pressure of a known amount of material trapped at a water-air interface. When employed together, these two methods allow for determining the surface area per molecule as well as its contour length (<*L*>) and the two-dimensional width (<*d*>).

A thorough AFM characterization was performed to gain more insight into the structural properties and surface behaviors of the synthesized bottlebrushes. AFM visualization of LB monolayers of monomodal bottlebrushes (Figure IV.5) showed a typical semi-flexible for each sample, demonstrating a steady increment of the persistence length with the growth of the DP of the side chains. Additional evaluation of AFM images provided information about average lengths <*L*> and widths <*d*> of monomodal bottlebrushes (Table IV.2). As can be seen in Table IV.2, all <*L*> values were close to 500nm, thus proving that no carbon-carbon scission occurred within

bottlebrush backbones upon placing on substrate. In case of the brush widths, <*d*> values increased as the DP of grafts increased (Table IV.2).

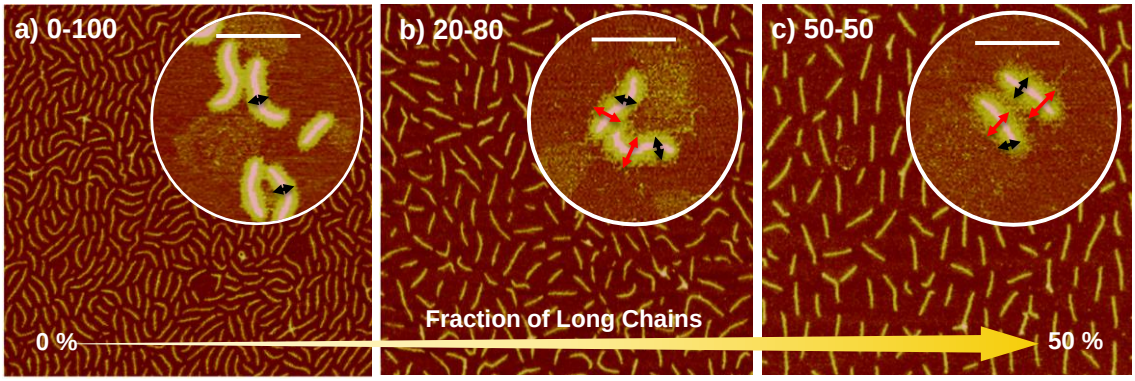

Figure IV.6 AFM images of LB films prepared from bottlebrushes with (a) monomodal, **0-100**, DP_{short}=56, and bimodal graft lengths (b) **20-80**, DP_{long}=200 (80%) and DP_{short}= 56 (20%), and (c) **50-50**, DP_{long}=200 (50%) and DP_{short}= 56 (50%), on mica surface, 2 μm area; Images of single brush molecules prepared by spin-casting methods are shown in circles. Black arrows correspond to the shorter side chains (core and red ones mark the longer grafts (shell); the scale bar is 200 nm.

AFM images of Langmuir-Blodgett (LB) monolayers of bimodal bottlebrush series are shown on Figure IV.6a-c. As expected, **0-100** displayed a semi-flexible of a typical monomodal brush. However, for **20-80** and **50-50** the macromolecular width was defined by DPs of both short and long side chains, as well as their relative molar ratio. The longer grafts of bimodal brushes were expected to adsorb on the surface stronger as compared to the shorter ones. In the case of **20-80** there were only 20% of chains with DP_{long}=200, meaning that the long side chains were not fully extended, as opposed to the ones in the **50-50** with 50 % of long grafts. As a result **50-50** showed a greater

intermolecular distance and higher backbone extension of macromolecules than **20-80** (Figure IV.6a-c).

A visualization of LB monolayer showed that an increment of the mole fraction of long chains led to the growth of the corresponding intermolecular molecular distance. In addition, an extension of macromolecules was also observed, which was observed as a gradual conformational change from worm- to rod-like topology. These observations are consistent with literature reports on surface properties of similar molecular bottlebrushes. Attractive forces between P*n*BA grafts and mica substrate lead to spreading of side chains on the surface, thus allowing for the visualizations of worm-like topologies with a single molecule resolution. In general, longer brush side chains occupy more space than their shorter equivalents, thus proving a greater brush width and consequently, the intermolecular distance (Figure IV.6a-c). Single molecule images of **0-100**, **20-80** and **50-50** are shown in circles on Figure IV.6a-c. In sample **0-100**, a clear boarder of the side chains edge could be resolved, which is consistent with the presence of a monomodal length of side chains with DP=56. In contrast, both **20-80** and **50-50** had a core-shell like topology, which corresponded to short and long grafts respectively (Figure IV.6a-c). The statistical analyses of AFM images of LB monolayer of **0-100**, **20-80** and **50-50** allowed for determination of the average lengths <*L*> and widths <*d*> of bottlebrushes (Table IV.2). In all cases, <*L*> was in the range of ~130 nm, which prove that the brushes were stable under tested experimental conditions and that no carbon-carbon scission occurred within the brush backbones upon placing on a water substrate.

Two methods were used to determine the widths <*d*> of bottlebrushes LB and spin-casing. In case of spin-cast films, high resolution images allowed for obtaining the breadths corresponding to both short (DP=56) and long (DP=200) side chains. For the shorter grafts, <*d*> values remained around 50 nm for all brushes, with only a slightly higher width for **50-50** (Table IV.2). As expected, the AFM data (LB and spin-casting) showed an increasing respective <*d*> values of total widths for **0-100**, **20-80** and **50-50** that was ascribed to the incorporation of a higher fraction (0, 20 and 50%) of long side chains, which on the other hand, was directly related to the brush widths (Table IV.2). Imagining of LB monolayer of **20-80** and **50-50** resulted in <*d*> values larger than the ones acquired by the spin-cast method. These results correlate with the linear P*n*BA impurities that were originally present in **20-80** and **50-50**, which caused an overestimation of the intermolecular distance obtained from the LB monolayer.

IV.3.6 Development of Equations for Structural Characterization of Bimodal Bottlebrushes

In this work we applied AFM and the LB trough to develop a simple methodology of measuring structural factors of bottlebrushes such as the grafting density (ϕ_g) and dispersities of side chains ($Đ$). The approach was then implemented and tested in two steps: (1) first, the developed characterization tool was validated by applying in the analysis of a series of well-defined monomodal bottlebrushes, and (2) second, the methodology was extended to new, more complex bimodal bottlebrushes.

The topology of a monomodal bottlebrush is relatively simple in comparison to that of a bimodal one. Because of that, we were able to perform a very thorough structural characterization of monomodal brushes by the combination of AFM-LB techniques, side chain cleavage (grafting efficiencies, I_{eff}) and GPC analyses (bottlebrushes and grafts molecular weight distributions, $Đ$).

Table IV.3 The results of AFM and LB analyses for monomodal and bimodal bottlebrushes.

Sample	A_{BR0}/nm^{2,a}	DP_{SC}	$n_n{}^b$	$\phi_g{}^c$	$Đ^d$	$n_a/n_n{}^e$	$n_a/n_n{}^f$	$n_{max}/n_n{}^g$
BA-17	0.28	10	17	0.51	1.12	1.14	1.16	1.65
BA-23	0.29	16	23	0.62	1.18	1.39	1.43	1.65
BA-34	0.29	24	34	0.63	1.30	1.38	1.43	1.71
BA-130	0.27	48	130	0.53	1.10	1.04	1.15	1.63
0-100	0.28	56[1]	N/A	0.50[2]	1.20[2]	N/A	1.12	1.68
20-80	0.37	85[1]	N/A	0.50[2]	1.45[3]	N/A	1.48	1.64
50-50	0.33	128[1]	N/A	0.50[2]	1.32[3]	N/A	1.32	1.69

[1] Estimated as $\phi_s n_s + \phi_l n_l$ where ϕ_s = (1-ϕ_l) = 0.2/0.5 and ϕ_l = 0.8/0.2 are respective mole fractions of long and short grafts, and n_s = 56 and n_l = 200 correspond to DPs of

long and short grafts respectively. [2] Estimated from typical values. [3] Calculated as $\frac{\phi_s {n_s}^2+\phi_l {n_l}^2}{{n_n}^2}$. [a] The area per *n*BA monomer on LB film at 0.5 mN/m. [b] Number average DP of side chains determined by THF GPC of cleaved side-chains, using PS standards [c] $\phi_g = \frac{\left(<d>+\frac{\pi*<d>^2}{4<L>}\right)*l_o}{A_{BR0}*n_n}$, where <*d*> and <*L*> are the width, and length of the bottlebrush, and l_0 is the length of *n*BA monomeric unit [d] Number average molecular weight distribution obtained from THF GPC measurements. [e] $n_{a=}\frac{W}{2*l_0}$, where n_a is the average DP of the adsorbed side chain and *w* is the weight fraction. [f] $\frac{n_a}{n_n} = \frac{\phi_g * A_{BR0}}{{l_0}^2 2}$. [g] n_{max}/n_n, where n_{max} is the average DP of adsorbed side chains assuming the longest ones adsorb first.

First, an LB trough was used to perform isothermal compression experiments and form LB monolayers of both monomodal (BA-17, BA-23, BA-34 and BA-130) and bimodal (**0-100**, **20-80** and **50-50**) bottlebrushes. Next, obtained isotherm data was used to extract the area per brush monomer (A_{BR0}) in each tested sample. In case of all monomodal brushes, obtained A_{BR0} values were practically the same, showing no dependency on the length of side chain (n_n). On the contrary, bimodal bottlebrushes displayed an increase of A_{BR0} values with increasing estimated dispersities of the side chains. The results of LB analysis can be found in Table IV.3.

The results of LB investigations of monomodal samples proved that the 2D area per monomer unit occupied by a brush (A_{BR0}) is largely independent of the DP of side chains; however, the bimodal bottlebrushes displayed a dependence on grafts weight distribution. In order to analyze that weight distribution dependence, a series of equations

(eq. IV.1-4) was developed to correlate the brush width (<*d*>) and the area per monomer unit (A_{BR0}), with the dispersity of the side chains (*Đ*) in tested brushes (Table IV.3).

An equation IV.1 is the result of the multiplication of the average DP of the side chains (n_n) and the grafting densities of bottlebrushes (Table IV.3).

$$n_n * \phi_g = \frac{\left(< d > + \frac{\pi * < d >^2}{4 < L >}\right) * l_o}{A_{BR0}} \qquad \text{(IV. 1)}$$

Where, <*d*> is the width and <*L*> the lengths of the bottlebrush obtained from AFM-LB analysis, and l_0 is the length of the *n*BA monomer unit. The results of the side chain cleavage of monomodal bottlebrushes provided the actual, average DPs of that grafts (n_n, Table IV.3). This, on the other hand, enabled extraction of the grafting density values of monomodal bottlebrushes (ϕ_g) from the equation IV.1.

Next, two alternate methods for determining the average DP of adsorbed side chains (n_a) were established (eq. IV.2-3). In the first method, AFM imaging was used to obtain the half width values of a bottlebrush macromolecule (<*d*>/2), which diIVded by the length of a single monomer unit (l_0) resulted in the average degrees of polymerization of grafts adsorbed on substrate (n_a) (eq. IV.2).

$$n_{a=} \frac{< d >}{2 * l_0} \qquad \text{(IV. 2)}$$

$$n_a = \frac{\phi_g * A_{BR0}}{{l_O}^2 2} * n_n \qquad \text{(IV. 3)}$$

The comparison of the average DP of adsorbed grafts (n_a), with the weight average DP of the side chains ($n_w = \frac{M_n * Đ}{MW_{nBA}}$) calculated from the GPC data of cleaved side chains in monomodal bottlebrushes, revealed that the average adsorbed side chain is nearly equal to the weight average side chain. Next, these values were compared with the size of the largest fraction of side chains (n_{max}) calculated from a normal distribution of side chains assuming that only the longest side chains make up the fraction of adsorbed grafts (ϕ), calculated as $\phi \cong \frac{{l_0}^2 2}{\phi_g * A_{L0}} = 0.51$, where l_0 = 0.25 nm, $\phi_g \approx 0.60$, and A_{BR0} = 0.41 nm^2/monomer. Then, from the empirical relation between n_a and n_w we obtained a relation of A_{BR0} and $Đ$, calculated as $A_{BR0} = \frac{{l_0}^2 2}{\phi_g}$. Based on this dependence a new equation (eq. IV.4) was derived, allowing for relating the brush width (<*d*>) with the $Đ$ of the side chains.

$$< d >= \left(-\frac{2 < L >}{\pi} + \sqrt{\frac{8 < L > * n_{n*} l_0 * Đ}{\pi} + \frac{4 < L >^2}{\pi^2}} \right) \qquad \text{(IV. 4)}$$

Afterwards, the developed equations were used to analyze more complex bimodal bottlebrushes. The equation IV.3 was applied to obtain the n_a values of the bimodal brushes (Table IV.3). The results showed that obtained values were nearly identical as the n_w calculated from NMR measurements of the bimodal brushes. In addition, the equation IV.2 failed to provide accurate data due to the relatively short backbones in bimodal bottlebrushes, which resulted in the bimodal bottlebrush conformation being in a transition zone between spherical and cylindrical one. Figure IV.7A and IV.7B display

the relation between n_a and n_w, and between a normalized universal coordinate and the n_n of the monomodal brushes.

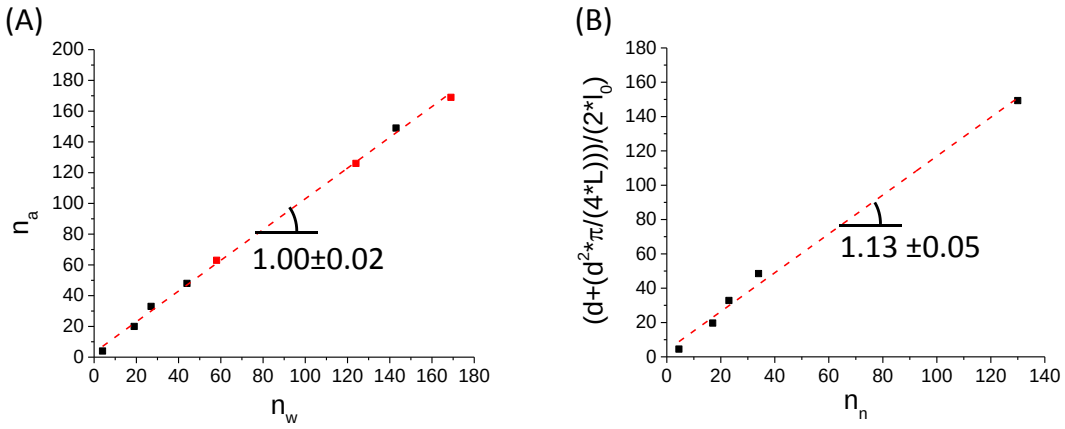

Figure IV.7 (A) The linear plot of n_a vs. n_w. The first data point represents theoretical M; the monomodal and bimodal bottlebrushes are marked as black and red squares respectively. (B) A universal coordinate derived from the equation IV.4 vs. n_n yielding the average dispersities of monomodal bottlebrushes.

IV.4 Conclusions

In summary, a method for the fabrication of molecular bottlebrushes with bimodal side chain length was developed. A selective and quantitative capping of carbon radicals with a persistent radical, 4-butoxy-TEMPO, was utilized to deactivate a fraction of bromine end groups in polymers prepared by ATRP. A consecutive extension of remaining active side chains resulted in well-defined molecular bottlebrushes with bimodal length of side chains with narrow molecular weight distributions (~1.2). A

detailed AFM analysis of bimodal bottlebrushes was performed, proving a core-shell topology resulting from the bimodality of grafts length.

In the second part, a series of equations was developed to allow a more in-depth structural characterization of bimodal bottlebrushes. For that purpose, a group of monomodal brushes was synthesized and analyzed via AFM LB comparing the data to the results of extensive characterization trough side chain cleavage and GPC analysis. The monomodal bottlebrushes proved the validity of the analytical relationships between n_a and n_w as well as between $<d>$ and $Đ$. This same analytical method was then applied to a more complex bimodal bottlebrush system. Although it was originally expected that the longer grafts preferably adsorbed on the mica surface while the short ones were stacked on top of macromolecules, a more random adsorption pattern, dominated by the weight average side chain DP was noticed. This observation was confirmed by the statistical analysis of n_a (obtained from equation IV.3) compared to the n_w determined from the monomer conversion.

The technique we described opens an opportunity to prepare a novel brush-like architecture with bimodal length distribution of grafts. Additionally, a group of described equation proves the validation of AFM LB as a technique for measuring the side chain $Đ$ and ϕ_g of numerous bottlebrush-like structures. Such architectures would potentially provide improved physical properties and characterization, such as viscoelastic behavior, that are quite different than those of 'regular' bottlebrushes and open access to a new class of soft elastomers.

IV.5. References

(1) Beers, K. L.; Gaynor, S. G.; Matyjaszewski, K.; Sheiko, S. S.; Moeller, M. *Macromolecules* **1998**, *31*, 9413-9415.

(2) Sheiko, S. S.; Prokhorova, S. A.; Beers, K. L.; Matyjaszewski, K.; Potemkin, I. I.; Khokhlov, A. R.; Moeller, M. *Macromolecules* **2001**, *34*, 8354-8360.

(3) Zhang, M.; Mueller, A. H. E. *Journal of Polymer Science, Part A: Polymer Chemistry* **2005**, *43*, 3461-3481.

(4) Sheiko, S. S.; Sumerlin, B. S.; Matyjaszewski, K. *Prog. Polym. Sci.* **2008**, *33*, 759-785.

(5) Lee, H.-i.; Pietrasik, J.; Sheiko, S. S.; Matyjaszewski, K. *Prog. Polym. Sci.* **2010**, *35*, 24-44.

(6) Lecommandoux, S.; Chécot, F.; Borsali, R.; Schappacher, M.; Deffieux, A.; Brulet, A.; Cotton, J. P. *Macromolecules* **2002**, *35*, 8878-8881.

(7) Li, Y.; Nese, A.; Matyjaszewski, K.; Sheiko, S. S. *Macromolecules* **2013**, *46*, 7196-7201.

(8) Li, Y.; Nese, A.; Lebedeva, N. V.; DaIVs, T.; Matyjaszewski, K.; Sheiko, S. S. *J. Am. Chem. Soc.* **2011**, *133*, 17479-17484.

(9) Burdyńska, J.; Li, Y.; Aggarwal, A. V.; Höger, S.; Sheiko, S. S.; Matyjaszewski, K. *J. Am. Chem. Soc.* **2014**, *136*, 12762-12770.

(10) Banquy, X.; Burdyńska, J.; Lee, D. W.; Matyjaszewski, K.; IsraelachIVli, J. *J. Am. Chem. Soc.* **2014**, *136* 6199-6202.

(11) Zhang, Y.; Constantini, N.; Mierzwa, M.; Pakula, T.; Neugebauer, D.; Matyjaszewski, K. *Polymer* **2004**, *45*, 6333-6339.

(12) Pakula, T.; Zhang, Y.; Matyjaszewski, K.; Lee, H.-i.; Boerner, H.; Qin, S.; Berry, G. C. *Polymer* **2006**, *47*, 7198-7206.

(13) Mpoukouvalas, A.; Li, W.; Graf, R.; Koynov, K.; Matyjaszewski, K. *ACS Macro Letters* **2013**, *2*, 23-26.

(14) Sveinbjörnsson, B. R.; Weitekamp, R. A.; Miyake, G. M.; Xia, Y.; Atwater, H. A.; Grubbs, R. H. *Proc. Natl. Acad. Sci* **2012**, *109*, 14332-14336.

(15) Miyake, G. M.; Weitekamp, R. A.; Piunova, V. A.; Grubbs, R. H. *J. Am. Chem. Soc.* **2012**, *134*, 14249-14254.

(16) Pietrasik, J.; Sumerlin, B. S.; Lee, R. Y.; Matyjaszewski, K. *Macromol. Chem. Phys.* **2007**, *208*, 30-36.

(17) Yamamoto, S.-i.; Pietrasik, J.; Matyjaszewski, K. *Macromolecules* **2007**, *40*, 9348-9353.

(18) Yamamoto, S.-i.; Pietrasik, J.; Matyjaszewski, K. *Macromolecules* **2008**, *41*, 7013-7020.

(19) Bolton, J.; Bailey, T. S.; Rzayev, J. *Nano Lett.* **2011**, *11*, 998-1001.

(20) Wu, D.; Nese, A.; Pietrasik, J.; Yeru Liang, M. K.; Huang, L.; Kowalewski, T.; Matyjaszewski, K. *ACS Nano* **2012**, *6*, 6208-6214.

(21) Huang, K.; Rzayev, J. *J. Am. Chem. Soc.* **2009**, *131*, 6880-6885.

(22) Tang, C.; Dufour, B.; Kowalewski, T.; Matyjaszewski, K. *Macromolecules* **2007**, *40*, 6199-6205.

(23) Yuan, J.; Schacher, F. H.; Drechsler, M.; Hanisch, A.; Lu, Y.; Ballauff, M.; Müller, A. H. E. *Chem. Mater.* **2010**, *22*, 2626-2634.

(24) Yuan, J.; Xu, Y.; Walther, A.; Bolisetty, S.; Schumacher, M.; Schmalz, H.; Ballauff, M.; Müller, A. H. E. *Nat. Mater.* **2008**, *7*, 718-722.

(25) Gao, H.; Matyjaszewski, K. *J. Am. Chem. Soc.* **2007**, *129*, 6633-6639.

(26) Jha, S.; Dutta, S.; Bowden, N. B. *Macromolecules* **2004**, *37*, 4365-4374.

(27) Neugebauer, D.; Zhang, Y.; Pakula, T.; Matyjaszewski, K. *Macromolecules* **2005**, *38*, 8687-8693.

(28) Cheng, G.; Boeker, A.; Zhang, M.; Krausch, G.; Mueller, A. H. E. *Macromolecules* **2001**, *34*, 6883-6888.

(29) Boerner, H. G.; Beers, K.; Matyjaszewski, K.; Sheiko, S. S.; Moeller, M. *Macromolecules* **2001**, *34*, 4375-4383.

(30) Sumerlin, B. S.; Neugebauer, D.; Matyjaszewski, K. *Macromolecules* **2005**, *38*, 702-708.

(31) Braunecker, W. A.; Matyjaszewski, K. *Progr. Polym. Sci.* **2007**, *32*, 93-146.

(32) Matyjaszewski, K.; Tsarevsky, N. V. *J. Am. Chem. Soc.* **2014**, *136*, 6513-6533.

(33) Matyjaszewski, K.; Tsarevsky, N. V. *Nat. Chem.* **2009**, *1*, 276-288.

(34) Li, Z.; Zhang, K.; Ma, J.; Cheng, C.; Wooley, K. L. *Journal of Polymer Science, Part A: Polymer Chemistry* **2009**, *47*, 5557-5563.

(35) Zehm, D.; Laschewsky, A.; Liang, H.; Rabe, J. P. *Macromolecules* **2011**, *44* 9635-9641.

(36) Lee, H.-i.; Matyjaszewski, K.; Yu, S.; Sheiko, S. S. *Macromolecules* **2005**, *38*, 8264-8271.

(37) Elsen, A. M.; Li, Y.; Li, Q.; Sheiko, S. S.; Matyjaszewski, K. *Macromol. Rapid Commun.* **2014**, *35*, 133-140.

(38) Stals, P. J. M.; Li, Y.; Burdyńska, J.; Nicolaÿ, R.; Nese, A.; A., A. R.; Palmans; Meijer, E. W.; Matyjaszewski, K.; Sheiko, S. S. *J. Am. Chem. Soc.* **2013**, *135*, 11421-11424.

(39) Yu-Su, S. Y.; Sheiko, S. S.; Lee, H.-i.; Jakubowski, W.; Nese, A.; Matyjaszewski, K.; Anokhin, D.; Ivanov, D. A. *Macromolecules* **2009**, *42* 9008-9017.

(40) Lee, H.-i.; Jakubowski, W.; Matyjaszewski, K.; Yu, S.; Sheiko, S. S. *Macromolecules* **2006**, *39*, 4983-4989.

(41) Lee, H.-i.; Matyjaszewski, K.; Yu-Su, S.; Sheiko, S. S. *Macromolecules* **2008**, *41*, 6073-6080.

(42) Snijder, A.; Klumperman, B.; Van der Linde, R. *Journal of Polymer Science, Part A: Polymer Chemistry* **2002**, *40*, 2350-2359.

(43) Coessens, V.; Matyjaszewski, K. *Macromol. Rapid Commun.* **1999**, *20*, 127-134.

(44) Matyjaszewski, K.; Nakagawa, Y.; Gaynor, S. G. *Macromol. Rapid Commun.* **1997**, *18*, 1057-1066.

(45) Li, L.; Wang, C.; Long, Z.; Fu, S. *Journal of Polymer Science, Part A: Polymer Chemistry* **2000**, *38*, 4519-4523.

(46) Asgarzadeh, F.; Ourdouillie, P.; Beyou, E.; Chaumont, P. *Macromolecules* **1999**, *32*, 6996-7002.

(47) Koulouri, E. G.; Kallitsis, J. K.; Hadziioannou, G. *Macromolecules* **1999**, *32*, 6242-6248.

(48) Bon, S. A. F.; Steward, A. G.; Haddleton, D. M. *Journal of Polymer Science, Part A: Polymer Chemistry* **2000**, *38*, 2678-2686.

(49) Tokuchi, K.; Ando, T.; Kamigaito, M.; Sawamoto, M. *Journal of Polymer Science, Part A: Polymer Chemistry* **2000**, *38*, 4735-4748.

(50) Beyou, E.; Jarroux, N.; Zydowicz, N.; Chaumont, P. *Macromol Chem Phys* **2001**, *202*, 974-979.

(51) Chambard, G.; Klumperman, B.; German, A. L. *Macromolecules* **2000**, *33*, 4417-4421.

(52) Braunecker, W. A.; Matyjaszewski, K. *Prog. Polym. Sci.* **2007**, *32* 93-146.

(53) Goto, A.; Fukuda, T. *Prog. Polym. Sci.* **2004**, *29*, 329-385.

(54) Georges, M. K.; Veregin, R. P. N.; Kazmaier, P. M.; Hamer, G. K. *Macromolecules* **1993**, *26*, 2987-2988.

(55) Solomon, D. H. *Journal of Polymer Science, Part A: Polymer Chemistry* **2005**, *43*, 5748-5764.

(56) Matyjaszewski, K.; Woodworth, B. E.; Zhang, X.; Gaynor, S. G.; Metzner, Z. *Macromolecules* **1998**, *31*, 5955-5957.

(57) Rungta, A.; Natarajan, B.; Neely, T.; Dukes, D.; Schadler, L. S.; Benicewicz, B. C. *Macromolecules* **2012**, *45*, 9303-9311.

(58) Britovsek, G. J. P.; England, J.; White, A. J. P. *Inorg. Chem.* **2005**, *44*, 8125-8134.

(59) Borner, H. G.; Duran, D.; Matyjaszewski, K.; da Silva, M.; Sheiko, S. S. *Macromolecules* **2002**, *35*, 3387-3394.

(60) Pintauer, T.; Coessens, V.; Matyjaszewski, K. *Progr. Polym. Sci.* **2001**, *26*, 337-377.

(61) Li, Y.; Tao, P.; Benicewicz, A. V. B. C.; Schadler, L. S. *Langmuir* **2013**, *29*, 1211-1220.

SECTION III

BOTTLEBRUSHES FROM FUNCTIONAL INITIATORS

CHAPTER V

MOLECULAR BOTTLEBRUSHES PREPARED FROM FUNCTIONAL ATRP DIINITIATORS

Preface

It was described in Chapter 1 that ATRP is a superior technique for the preparation of various bottlebrush architectures via the 'grafting from' approach. It was also shown that ATRP initiators can be prepared via straightforward esterification of alcohol groups, thus making a preparation of functional ATRP initiators a fairly simple process. The use of a difunctional ATRP initiator for the preparation of the bottlebrush backbone is a simple an approach to incorporate functionality into the backbone. This approach was utilized to generate a bottlebrush with a single S-S unit incorporated in its center. It allowed for a selective mechanoscission of such weaker bonds caused by the

tension intrinsically generated by bottlebrushes, and providing an access to a new class of materials, so called molecular tensile machines.

The following section describes four different di-functional ATRP initiators that were applied in the formation of molecular bottlebrushes with specific tags embedded in the center of the brush. A spiropyran-functionalized initiator was prepared by Dr. Zachary Kean and Diels-Alder adduct-based initiator was synthesized by Bobin Lee, a graduate student from Prof. Stephen Craig's group at Duke University. The initiator with embedded deuterium tag was synthesized by Brittany Robertson, an undergraduate student working under my supervision. Leah Heist, a graduate student from the group of Prof. Ed Samulski at UNC, Chapel Hill, performed analysis of d_4-tagged polymers via deuterium-NMR. I synthesized the triazole-based initiator and all polymeric materials, and performed their GPC and ^{1}H NMR characterization.

V.1 Introduction

Macromolecular bottlebrush polymers (BBPs) constitute a group of graft polymers having densely grafted side chains exhibiting gel-like properties in the melt.[1] These shape-persistent macromolecules have been targeted as materials for applications ranging from mechanosensors[2-4] and photonics[5-7] to bio-inspired lubricants[8] and super-soft elastomers[9,10]. In BBPs the resulting intra-macromolecular excluded volume interactions among the crowded graft side chains impacts the persistence length of the BBP backbone by restricting its ability to explore random-coil configurations on spatial scales characteristic of linear, non-grafted polymers.[1] In turn, the density of intermolecular entanglements in condensed neat phases of BBPs is reduced and as a result, networks comprised of covalently linked BBPs are anticipated to have very low moduli (~kPa) and are referred to as super-soft elastomers[11] or very soft networks[10]. In these stable supersoft elastomers the side chains in BBPs act as a pseudo-solvent that, unlike in hydrogels, are covalently attached to the polymer backbone.

The grafting density and side chain length can be tuned in BBPs in order to target applications requiring specific mechanical properties. In an earlier effort to quantify the effect of certain tunable features on the internal mobility of BBPs, poly((2-(2-bromopropionyloxy)ethyl methacrylate-***stat***-methyl methacrylate-g-butyl acrylate) (poly((BPEM-***stat***-MMA)-*g*-PBA)) was previously studied using proton NMR (^{1}H NMR) relaxation dynamics.[12] Pietrasik and coworkers measured the ^{1}H spin-spin relaxation time (T_2) and found that the proton T_2 of the BBP backbone decreased with increasing side

chain length and grafting density. Their observations indicated that molecular congestion on the interior of BBPs resulted in a significant decrease in molecular motion along the backbone. The T_2 relaxation times of protons on the PBA side chains showed a more complicated response.[12]

Herein we reexamined molecular bottlebrushes dynamics using deuterium NMR (^{2}H NMR) to monitor the local dynamics within the backbone and side chains of BBPs. Unlike ^{1}H relaxation, which is dominated by the dipole-dipole relaxation mechanisms among multiple protons at variable dynamical distances and chemical shift anisotropy relaxation mechanisms at high magnetic fields, ^{2}H relaxation is dominated by the well-defined quadrupolar interaction, i.e. an intra-carbon-deuterium bond interaction that is directly related to C—D bond reorientations.[13] For the purpose of this study we designed BBPs with a deuterium label covalently embedded in the center of the backbone chain.

BBPs can be synthesized via three methods: (i) 'grafting through',[11,14] (ii) 'grafting onto',[15] and (iii) 'grafting from'[1,16-18] strategies. The latter method is mainly performed via controlled radical polymerization (CRP) methods, in particular atom transfer radical polymerization (ATRP). The 'grafting from' via ATRP allows for a good control over the grafting density and lengths of the side chains and backbone. In addition, initiators utilized by ATRP can be easily obtained by simple organic reactions including esterification/amidation of hydroxyl/amine functionalities.

The structural simplicity of ATRP[19-21] initiating groups enables access to more complex functional ATRP initiators, which can be utilized to tune the topology and/or

properties of molecular bottlebrushes. Previous literature reports have described several examples of functional ATRP initiators used in the synthesis of bottlebrushes. For instance multifunctional initiators were applied to generate star-shaped bottlebrushes with three and four arms.[22] This concept was further expanded to a more complex hexa-functional initiator with a molecular spoked wheel (MSW) core.[4] This resulted in the formation of six-arm molecular stars that showed a selective mechano-scission of arms from the MSW core under selected conditions.[4] In another study, a difunctional ATRP initiator consisting of a disulfide (S-S) bond was used to incorporate a weak bond into the backbone of a bottlebrush, thus obtaining a molecular tensile machine.[2] The mechanical tension intrinsically generated by the brush enabled detailed kinetic studies of selective cleavage, of the S-S bond which could be controlled by tuning the length of the side chains or/and the properties of the selected substrate.[2,3] In this chapter, a similar approach was applied to design an ATRP di-initiator with a labeled quinone-d_4 ring and employ it for the formation of ^{2}H labeled BBP suitable for bottlebrush dynamics studies.

V.2 Experimental

Materials. *n*-Butyl acrylate (*n*BA, 99%, Acros) and (2-trimetylsiloxy)ethyl methacrylate (HEMA-TMS, Scientific Polymer Products) were purified by passing the monomer through a column filled with basic alumina to remove the inhibitor. All other reagents: terephthalic-d_4 acid (**TPA-d_4**, 98 atom % D), methanol (anhydrous, 99.8%), thionyl chloride ($SOCl_2$, >99%), lithium aluminum hydride (LAH, 95%), trimethylamine (TEA,

99%), copper(I) bromide ($Cu^{I}Br$, 99.999%), copper(II) bromide ($Cu^{II}Br_2$, 99.999%), copper(I) chloride ($Cu^{I}Cl$, 99.995%), copper(II) chloride ($Cu^{II}Cl_2$, 99.999%), 4,4′-dinonyl-2,2′-bipyridine (dNbpy, 97%), *N,N,N',N'',N''*-pentamethyldiethylenetriamine (PMDETA, 99%), potassium fluoride (KF, 99%), tetrabutylammonium fluoride (TBAF, 1.0 M in THF), *α*-bromoisobutyryl bromide (98%), 2,5-di-*tert*-butylphenol (DTBP, 99%), and solvents were purchased from Aldrich and used as received without further purification.

Characterization. The conversion of *n*BA was determined from ^{1}H NMR spectra recorded in $CDCl_3$ (unless stated otherwise) as a solvent using Brüker 300 MHz spectrometer. Molecular weight distributions of the polymers were characterized by gel permeation chromatography (GPC) using Polymer Standards Services (PSS) columns (guard, 10^5, 10^3, and 10^2 Å), with THF eluent at 35 °C, flow rate 1.00 mL/min, and differential refractive index (RI) detector (Waters, 2410). The apparent number-average molecular weights (M_n) and molecular weight dispersities ($Đ$) were determined with a calibration based on linear and poly(methyl methacrylate) (PMMA) standards and diphenyl ether as an internal standard, using WinGPC 6.0 software from PSS.

Synthesis of dimethyl terephthalate-d_4 (DMTP-d_4). A solution of terephthalic-d_4 acid (**TPA- d_4**) (0.50 g, 2.95 mmol) in anhydrous methanol (25 mL) was placed in a dry round bottom flask (100 mL) and was refluxed for 30 min. Next, thionyl chloride (9 mL) was added dropwise, and the mixture was maintained under reflux for 12 h. After being cooled to room temperature, the solvent was removed under reduced pressure. The

mixture was extracted twice with ethyl ether (30 mL) and washed with 0.1 M KOH solution. The combined organic layers were dried over $MgSO_4$ and the solvent was removed providing dimethyl terephthalate-d_4 (**DMTP- d_4**) as a white powder. The product was analyzed by ^{1}H NMR spectroscopy: (300 MHz, $CDCl_3$) δ: 3.95 (*s*, 6H, C*H*$_3$-O-COAr).

Synthesis 1,4-phenylenedimethanol-d_4 (PDM-d_4). A 50 mL two two-necked round-bottomed flask, fitted with a magnetic stirring bar inside, was dried in the oven and flushed with nitrogen. Next, $LiAlH_4$ (0.835 g, 22 mmol) was weighed into the flask under nitrogen atmosphere and the flask was equipped with a condenser and then immediately sealed. Dry ether (30 mL) was added to the flask maintaining a gentle reflux. The mixture was stirred for five minutes and then a solution of dimethyl terephthalate-d_4 (**DMTP-d_4**) (0.40 g, 2.0 mmol) in ether (20 mL) was added dropwise and allowed to stir for 1 h at room temperature. Afterwards, the flask was placed in an ice-water bath and water was slowly added to quench the reaction. After the evolution of hydrogen ceased, the reaction was stirred for another 5 min. and then 6 mL of 2 M NaOH was added to the flask. The reaction mixture was extracted with (25 mL x 2) and dried over $MgSO_4$. The solvent was removed and 1,4-phenylenedimethanol-d_4 (**PDM-d_4**) was obtained as a white powder and used for the next step without any further purification. ^{1}H NMR spectroscopy: (300 MHz, CD_3CN) δ: 4.58 (*d*, 4H, *J* = 5.9 Hz, HO-C*H*$_2$-Ar), 3.14 (*t*, 2H, *J* = 5.9 Hz, *H*O-CH_2-Ar).

Synthesis 1,4-phenylenebis(methylene) bis(2-bromo-isobutyrate)-d_4 (Br-d_4-Br). 1,4-Phenylenedimethanol-d_4 (**PDM-d_4**) (0.25 g, 1.76 mmol) and anhydrous THF (15 mL)

were added to a 25 mL flask. The flask was sealed and placed under nitrogen atmosphere. Next, TEA (0.6 mL, 4.3 mmol) was injected; then the 2-bromoisobutyryl bromide (0.48 ml, 3.9 mmol) was added dropwise and the resulting mixture was allowed to stir for 16 h. The solids were removed and the filtrate was diluted with DCM (50 mL). The solution was sequentially washed with 1 M HCl solution (25 mL), saturated sodium bicarbonate (25 mL) and brine (25 mL), and then dried over $MgSO_4$. The solution was passed through a short column filled with basic alumina and solvents were removed to obtain **Br-d$_4$-Br** as white powder. ^{1}H NMR spectroscopy: (300 MHz, $CDCl_3$) δ: 5.22 (*s*, 4H, O-CH_2-Ar), 1.96 (*s*, 12H, (CH_3)$_2$-CO-O-CH_2-Ar).

Synthesis of P(HEMA-TMS)$_{600}$-d$_4$ (TMS$_{600}$-d$_4$). A 25 ml Schlenk flask was charged with **Br-d$_4$-Br** (12.5 mg, 0.0287 mmol), HEMA-TMS (20.0 mL, 91.9 mmol), dNbpy (0.117 g, 0.287 mmol), $Cu^{II}Cl_2$ (3.1 mg, 0.0230 mmol), and anisole (2.2 mL). The solution was degassed by three freeze-pump-thaw cycles. During the final cycle, the flask was filled with nitrogen and $Cu^{I}Cl$ (11.4 mg, 0.1149 mmol) was quickly added to the frozen reaction mixture. The flask was sealed, evacuated and back-filled with nitrogen five times and then immersed in an oil bath at 65 C. Polymerization was stopped after 27 h reaching 18.7 % conversion as determined by ^{1}H NMR, which corresponded to a DP of 600. The apparent molecular weight determined for **TMS$_{600}$-d$_4$** by THF GPC was $M_{n,GPC} = 9.91 \cdot 10^4$, and $Đ = 1.13$ (Figure V.1, black). The reaction mixture was diluted with chloroform, passed through neutral alumina column to remove the catalyst, then concentrated and used for the next step without further purification.

Synthesis of d_4-PBiBEM$_{600}$ macroinitiator (Br_{600}-d_4). A 100 ml round-bottom flask was charged with **TMS_{600}-d_4** (11.5 g, 56.9 mmol), KF (3.695 g, 62.6 mmol), DTBP (1.173 g, 5.693 mmol), and then dry THF (60 mL) was added under nitrogen. The reaction mixture was cooled down in an ice bath, followed by the injection of tetrabutylammonium fluoride (0.57 mL, 1.0 M in THF, 0.57 mmol) and subsequent dropwise addition of α-bromoisobutyryl bromide (14.4 g, 7.7 mL. 62.6 mmol) over the course of 30 min. After the addition was complete the reaction mixture was allowed to reach room temperature and was stirred for another 16 h. Afterwards solids were filtered off and the mixture was precipitated into methanol/water (70/30), re-dissolved in chloroform (70 mL) and passed through a column filled with basic alumina. The product was re-precipitated three times in hexanes and dried overnight under vacuum. Molecular weight determined of **Br_{600}-d_4** by THF GPC: $M_{n,GPC} = 1.14 \cdot 10^5$, and $Đ = 1.13$, as shown in Figure V.1, blue curve.

Synthesis of P(BiBEM$_{600}$- *g*-*n*BA_5)-d_4 ((600-*g*-5)-d_4). A dry 10 ml Schlenk flask was charged with **Br_{600}-d_4** (0.3915 g, 1.403 mmol), *n*-butyl acrylate (10.0 mL, 70.2 mmol), 4,4′-dinonyl-2,2′-dipyridyl (0.144 g, 0.351 mmol), copper(II) bromide (11.0 mg, 0.0491 mmol), and anisole (1.0 mL). The solution was degassed by three freeze-pump-thaw cycles. During the final cycle, the flask was filled with nitrogen and copper(I) bromide (18.1 mg, 0.1263 mmol) was quickly added to the frozen reaction mixture. The flask was sealed, evacuated and back-filled with nitrogen five times and then immersed in an oil bath at 70 °C. The reaction was stopped after 65 h, by expositing the solution to air. The brush sample was purified by three precipitations of a solution of the polymer by addition

to cold methanol, and dried under vacuum at room temperature, to a constant mass. The monomer conversion (x_{nBA}) was calculated by ^{1}H NMR analysis, resulting in the brush polymer with the degree of polymerization of the side chains (DP_{SC}) 5. DP_{SC} was calculated using the following formula: $DP_{SC} = DP_{targeted} \cdot x_{nBA}/100\%$. Apparent molecular weight was determined using THF GPC (poly(methyl methacrylate) standards): $M_{n,GPC} = 3.24 \cdot 10^5$ and $Đ = 1.15$ (Figure V.1, red).

Synthesis of P(BiBEM$_{600}$- *g*-*n*BA$_{44}$)-d$_4$ ((600-*g*-44)-d$_4$). A dry 25 ml Schlenk flask was charged with **Br$_{600}$-d$_4$** (0.0979 g, 0.351 mmol), *n*-butyl acrylate (20.0 mL, 140 mmol), 4,4′-dinonyl-2,2′-dipyridyl (0.144 g, 0.351 mmol), copper(II) bromide (2.0 mg, 0.0088 mmol), and anisole (2.2 mL). The reaction was performed and the product was isolated in the same fashion as described for sample **(600-*g*-5)-d$_4$**. The reaction was stopped after 43 h giving a brush polymer with degree of polymerization of the side chains 44. Apparent molecular weight: Mn,GPC = 9.63·105 and Đ = 1.16, Figure V.1, green curve.

All brush syntheses from functional difunctional initiators were performed in analogous manner to that employed for sample **Br-d$_4$-Br**.

NMR Methods. All of the 1D spectra were taken on a Bruker B600 spectrometer operating at 92.12 MHz (2H frequency) using a liquid state cryoQNP probe with Z-gradients. All samples were dissolved in dichloromethane (DCM) and acquired in non-spinning sealed 5mm tubes at 298K. Before the ^{2}H acquisition, each sample was shimmed using the ^{1}H NMR free induction decay (FID). For the 1D experiments, a 90° pulse width of 139μs was used with a recycle delay of 1s. T_1 values were measured using

an inversion recovery pulse sequence. T_2 values were measured using a Car-Purcel-Meiboom-Gill (CPMG) pulse sequence, both included in the Bruker software. Peak intensities were recorded at different delay times. The peak intensities were fit to exponential functions; equations V.1 and V.2, where M is the measured peak intensity at time t and M_0 is the maximum peak intensity at t=0, in order to extract the relaxation times.[13]

$$\frac{M}{M_0} = 1 - 2e^{-t/T_1} \qquad \text{(V.1)}$$

$$\frac{M}{M_0} = e^{-t/T_2} \qquad \text{(V.2)}$$

V.3 Local Dynamics of Bottlebrush Polymers via ^{2}H NMR

V. 3.1 Results and Discussion

Molecular bottlebrushes dynamics were reexamined by using deuterium NMR (^{2}H NMR) to monitor the local dynamics within the backbone and side chains of BBPs. Unlike ^{1}H relaxation, which is dominated by the dipole-dipole relaxation mechanisms among multiple protons at variable dynamical distances and chemical shift anisotropy relaxation mechanisms at high magnetic fields, ^{2}H relaxation is dominated by the well-defined quadrupolar interaction, i.e. intra-carbon-deuterium bond interaction that is directly related to C—D bond reorientations.[13] For the purpose of this study we designed BBPs with a deuterium label covalently embedded in the center of the backbone chain.

V.3.1.1 Synthesis of Molecular Bottlebrushes-d_4

A deuterated ATRP di-initiator (**Br-d_4-Br**, Scheme V.1a) was employed to generate labeled molecular bottlebrushes (**BBP-d_4**) for the dynamics study via deuterium NMR (^{2}H NMR). The synthetic approach for the preparation of **BBP-d_4** involved two steps: 1) the formation of an ATRP di-initiator with a deuterium tag (**Br-d_4-Br**) (Scheme V.1a) and 2) the incorporation of **Br-d_4-Br** into the structure of a BBP (Scheme V.1b).

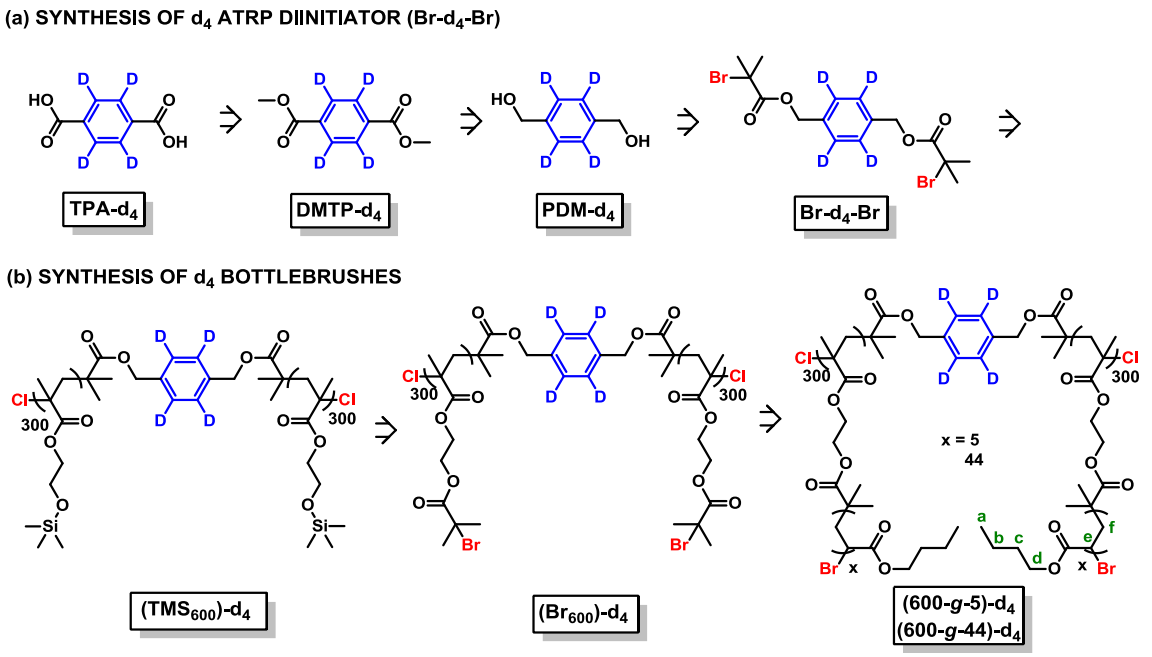

Scheme V.1 The synthetic pathway for the preparation of a) ATRP di-initiator-d_4 (**Br-d_4-Br**) and b) labeled BBPs with PnBA side chains ((**600-g-5/44)-d_4**).

Scheme V.1a shows the approach applied in the synthesis of the **Br-d_4-Br** difunctional initiator. In order to embed a deuterium label into **Br-d_4-Br**, a several chemical modifications were performed on a commercially available, deuterated

terephthalic acid (**TPA-d_4**, Scheme V.1a). The general methodology involved: i) an esterification of **TPA-d_4** to form its dimethyl ester (**DMTP-d_4**), ii) a reduction of **DMTP-d_4** to the corresponding diol (**PDM-d_4**), and iii) an esterification of **PDM-d_4** to form the ATRP di-initiator (**Br-d_4-Br**) (Scheme V.1a).

In the first step, **TPA-d_4** was transformed into its dimethyl ester, **DMTP-d_4** (Scheme V.1a). The modification of **TPA-d_4** was accomplished through reaction with an excess of thionyl chloride in anhydrous methanol. The esterification proceeded to completion within 12 h, as confirmed by ^{1}H NMR spectroscopy of the isolated product. ^{1}H NMR of **DMTP-d_4** showed a sole signal at 3.95 ppm, assigned to an incorporated methyl ester moieties, with no trace of the remaining acid. The second step involved a reduction of **DMTP-d_4** to the corresponding diol (**PDM-d_4**). The reaction was accomplished by applying an excess of lithium aluminum hydride ($LiAlH_4$) as a reducing agent in anhydrous ether under nitrogen atmosphere. **DMTP-d_4** was converted to **PDM-d_4** within 1h, which was confirmed via ^{1}H NMR analysis of the yielded product. The spectra of **PDM-d_4** showed a successful reduction, as proved by the disappearance of the methyl signal (3.95 ppm) of **DMT-d_4**, and the appearance of two new peaks, a triplet and a doublet (3.14 ppm and 4.58 ppm), which were ascribed to the respective hydroxyl and methylene groups of **PDM-d_4**. The final step allowed for incorporation of ATRP initiating functionalities into **PDM-d_4** through esterification with 2-bromoisobutyryl bromide in the presence of triethylamine. The final product, **Br-d_4-Br**, was characterized by ^{1}H NMR spectroscopy, confirming the quantitative esterification of **PDM-d_4**. The spectra of **Br-d_4-Br** showed two sets of singlet protons at 5.22 ppm and 1.96 ppm, which

corresponded to the methylene and methyl functionalities of **Br-d_4-Br**. In addition, the ^{1}H NMR analysis showed no evidence of any remaining **PDM-d_4** impurities.

The synthetic methodology applied in the preparation of **BBP-d_4** is shown on Scheme V.1b. BBPs were prepared via the "grafting-from" approach under normal ATRP conditions. First, (2-trimethylsiloxyethyl) methacrylate (HEMA-TMS) was polymerized from the labeled di-initiator, followed by esterification of the polymer with ATRP-active initiating moieties. The resulting ATRP macroinitiator was then used to graft poly(*n*-butyl acrylate) side chains forming the final labeled bottlebrushes (Scheme V.1b).

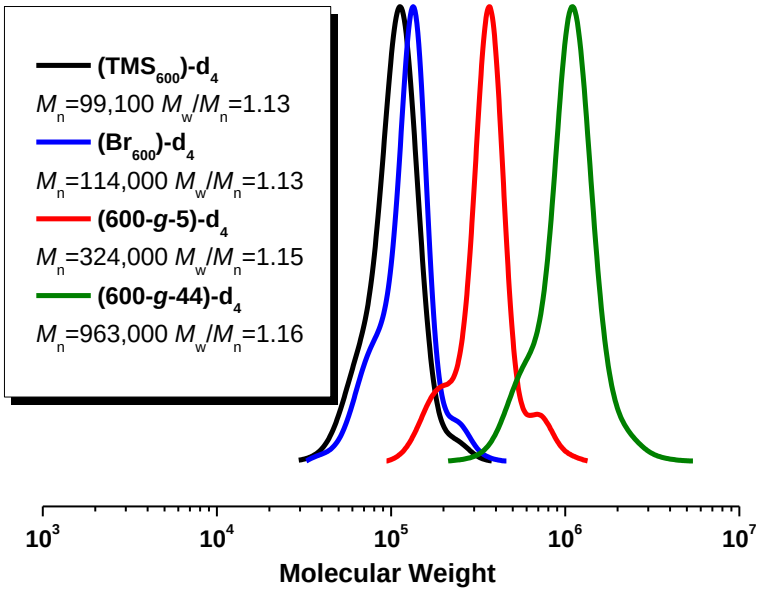

Figure V.1 GPC traces obtained for **(TMS_{600})-d_4** (black), **(Br_{600})-d_4** (blue), and bottlebrush polymers with side chains DP: 5, **(600-*g*-5)-d_4** (red) and 44, **(600-*g*-44)-d_4** (green).

HEMA-TMS was polymerized from **Br-d_4-Br** under normal ATRP conditions to form a linear polymer with a degree of polymerization DP = 600 and a d_4-tag incorporated in the chain center. The polymerization was conducted with the initial molar ratio of reagents [HEMA-TMS]:[**Br-d_4-Br**] = 3,200 and was stopped at a low monomer conversion (18.7 %) to avoid a significant intermolecular termination, and broadening of molecular weight distribution (*Đ*). In order to provide a high initiation efficiency from **Br-d_4-Br** initiator the reaction was performed under halogen exchange conditions, i.e. using $Cu^{I}Cl/Cu^{II}Cl_2$/dNbpy catalytic system instead of traditionally used copper (I/II) bromide complexes. The resulting [P(HEMA-TMS)$_{600}$]-d_4, **(TMS$_{600}$)-d_4**, was characterized by GPC showing the formation of a polymer (Figure V.1, black) with a narrow molecular weight distribution, *Đ* = 1.13, and the number average molecular weight, $M_n = 9.91 \cdot 10^4$.

Afterwards the sample labeled **(TMS$_{600}$)-d_4** was modified with ATRP reactive moieties to obtain an ATRP macroinitiator. The reaction was carried out under conditions previously described in literature reports. TMS protective groups on **(TMS$_{600}$)-d_4** were first removed in the presence of KF/TBAF, followed by the subsequent addition of *α*-bromoisobutyryl bromide, resulting in the formation of poly[2-(2-bromoisobutyryloxy)ethyl methacrylate]$_{600}$-d_4 macroinitiator (**(Br$_{600}$)-d_4**). **(Br$_{600}$)-d_4** was purified via precipitations from methanol/water mixture into hexanes, and then dried under vacuum. GPC analysis of a pure **(Br$_{600}$)-d_4** showed a monomodal signal with $M_n = 1.14 \cdot 10^5$ and *Đ* = 1.13, which is close to the values obtained for **(TMS$_{600}$)-d_4** (Figure V.1, blue).

In last step, poly(*n*-butyl acrylate) (P*n*BA) side chains were 'grafting from' **(Br$_{600}$)-d$_4$**, forming the bottlebrush by applying the normal ATRP conditions with $Cu^{I}Br/Cu^{II}Br_2$/dNbpy complex. The side chains were grafted from **(Br$_{600}$)-d$_4$** with two ratios of reagents, [*n*BA]:[BiBEM] = [400]:[1] and [50]:[1]. The polymerizations resulted in labeled bottlebrushes with respective DPs of side chains, 44 (**(600-*g*-44)-d$_4$**) and 5 (**(600-*g*-5)-d$_4$**). GPC analysis of **(600-*g*-5)-d$_4$** and **(600-*g*-44)-d$_4$** showed a clear shift of **Br$_{600}$-d$_4$** signal towards higher molecular weights (Figure V.1, red and green), giving polymers with $M_n = 3.24 \cdot 10^5$ and $9.63 \cdot 10^5$, and $Đ = 1.15$ and 1.16 respectively.

V.3.1.2 Dynamics in Bottlebrush Backbone (Br$_{600}$)-d$_4$

Our aim was to understand the local bottlebrush backbone dynamics by measuring NMR relaxation times (correlation times) as a function of BBP architecture. To that end, a well-defined ^{2}H label into **(Br$_{600}$)-d$_4$** was inserted into the macroinitiator and the relaxation behavior was measured with, and without grafted n-butyl acrylate side chains (**(600-*g*-5)-d$_4$** and **(600-*g*-44)-d$_4$**) (Scheme V.1b). Specifically labeling BBPs with deuterium enables one to probe the dynamics of local motion at the site of the C-D bond. NMR relaxation times T_1 and T_2 can be related to physically-relevant correlation times, τ_c, the time it takes the C—D bond to "forget" its original orientation (equations V.3-5).[23,24]

$$\frac{1}{T_1} = \frac{3\pi^2}{10}\left(\frac{e^2qQ}{h}\right)^2\left[\frac{\tau_c}{1+\omega^2\tau_c^2} + \frac{4\tau_c}{1+4\omega^2\tau_c^2}\right] \quad \text{(V.3)}$$

$$\frac{1}{T_2} = \frac{3\pi^2}{20}\left(\frac{e^2qQ}{h}\right)^2\left[3\tau_c + \frac{5\tau_c}{1+\omega^2\tau_c^2} + \frac{2\tau_c}{1+4\omega^2\tau_c^2}\right] \quad \text{(V.4)}$$

$$\text{fast motional limit } \left(\omega^2\tau_c^2 << 1\right): \frac{1}{T_1} = \frac{1}{T_2} = \frac{3\pi^2}{2}\left(\frac{e^2qQ}{h}\right)^2\tau_c \quad \text{(V.5)}$$

The particular label moiety, a quinone ring in the BBP backbone, was chosen so that all ^{2}H nuclei were magnetically equivalent and chemically shifted from the aliphatic hydrogens in the brush copolymer. The latter could interfere if natural abundance deuterium (0.015%) resonances from the side chains begin to dominate the spectrum. The ^{2}H NMR spectrum of the bottlebrush backbone (BBB) in Figure V.2 shows that the aromatic ^{2}H label has a chemical shift of 7.41 ppm, outside of the aliphatic region (1-4 ppm), and is sufficiently removed from the dichloromethane (DCM) solvent resonance (5.33 ppm). Initially our goal was to compare the backbone dynamics with and without grafted side chains. To this end we measured the relaxation times T_1 and T_2 for different concentrations of the labeled BBB in DCM. We estimated the overlap concentration as $\frac{1}{\sqrt{N}}$ of the BBB to be 0.04 g/mL and acquired relaxation measurements on three samples: 0.01 g/mL (c<c*), 0.04 g/mL (c~c*), and 0.09 g/mL (c>c*). For each concentration, T_1 and T_2 was determined (Table V.1) by exponential fits to equations V.1 and V.2 (Figure V.3). Within the experimental error, $T_1 = T_2$ in each sample implying that the fast motional limit applies, independent of BBB concentration. We also see that for

the range of concentrations measured, that the relaxation times are not particularly dependent on concentration suggesting that the relaxation is primarily caused by intra-backbone motions, rotations about and vibrations of the *para* axis of the labeled aromatic ring in BBB and not global reorientational motion of the whole polymer chain.[25]

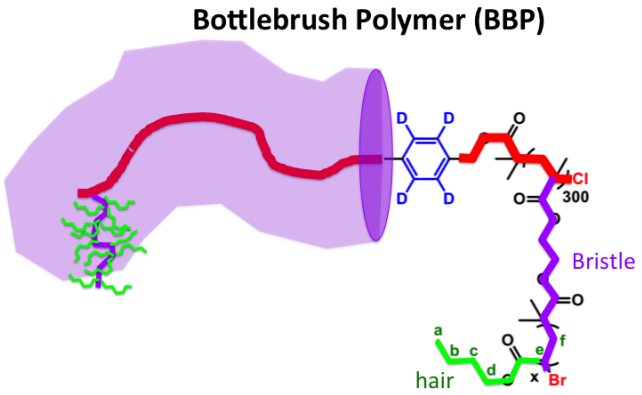

Figure V.2 Schematic diagram of bottlebrush polymer showing label in backbone, grafted "bristles" and "hair" on each of the bristles.

Table V.1 Relaxation data for decreasing concentrations of BBBs **(Br_{600})-d_4**.

	g·mL^{-1}	**T_1 (ms)**	**T_2 (ms)**
c > c*	0.089	43.7	40.0
c ~ c*	0.040	35.6	30.6
c < c*	0.014	41.0	23.5

In order to facilitate the discussion of the NMR data of the labeled BBB and BBP, we show a schematic of the polymer in Figure V.2.

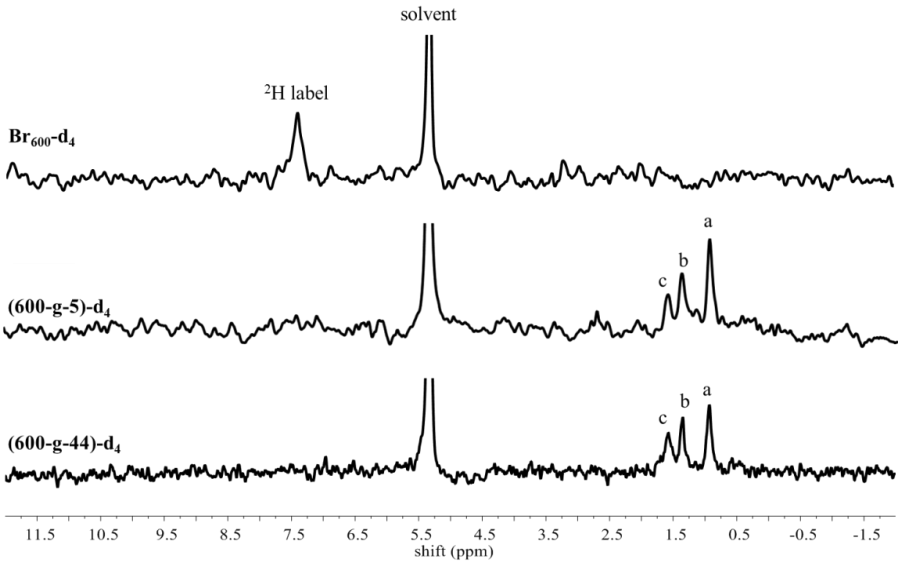

Figure V.3 ^{2}H 1D NMR spectra of **(Br_{600})-d_4** (0.09g/mL in DCM), **(600-*g*-5)-d_4** (10 wt% in DCM), and **(600-g-44)-d_4** (12 wt% in DCM).

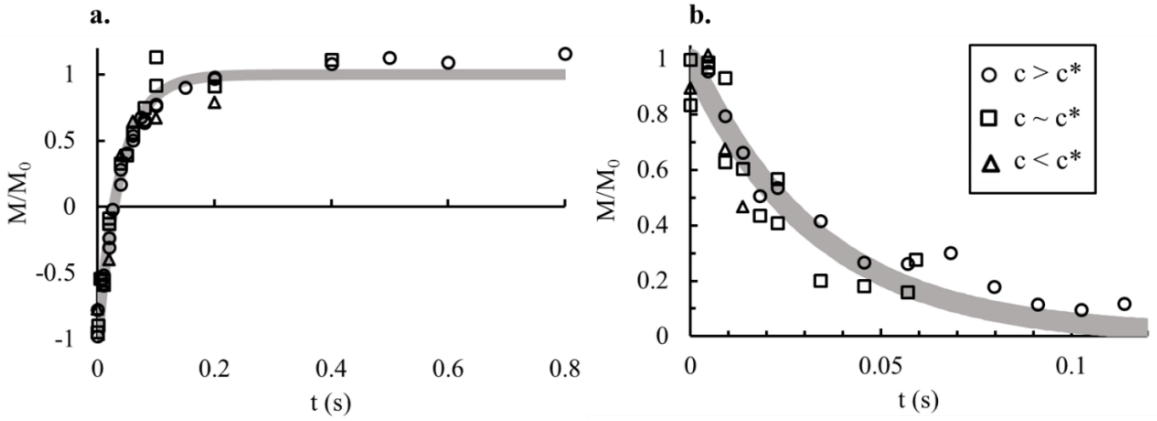

Figure V.4 Experimental data for determination of T_1 (a) and T_2 (b) for three concentrations of BB. Shaded line represents the estimated error in the exponential fit.

V.3.1.3 Dynamics in Bottlebrush Polymers, (600-*g*-5/44)-d_4

The NMR spectra and relaxation results of the simple bottle brush polymer backbone (BBB) change dramatically when the polymer backbone is grafted to make the BBP. For starters, the label resonance at 7.4 ppm in the linear BBB is not observable in the BBP spectrum (Figure V.3). The aromatic label's covalent linkage into the backbone insures that it reflects local reorientation of the backbone contour. But if the backbone correlation time becomes too long, i.e., if T_2 decreases and falls below the fast motion limit and loses its equivalence to T_1 (T_1 goes through a minimum and begins to increase), the backbone resonance linewidth increases. For very slow dynamics i.e. long correlation times, the linewidth of the resonance from the backbone label becomes very broad and cannot be detected with conventional high resolution NMR. Over the entire range of graft densities and graft side chain lengths we could access a degree of polymerization of the PBA unit (DP_{sc}) ranging from $DP_{sc} \sim 44$ to $DP_{sc} \sim 5$ with the ATRP chemistry, the label resonance was too broad to measure. Note that for short graft lengths (e.g., $DP_{sc} \sim 5$), the DP_{sc} is computed by the monomer conversion (x_{nBA}) (described in the synthetic section), which gives *on average* DPsc ~ 5.

In order to facilitate the discussion we will describe the bottlebrush structure as a backbone chain (stem) with grafted side chains ("bristles"). And, each bristle is comprised of a defined number of R (= PBA) units, and each PBA unit has a $CH_3CH_2CH_2CH_2$-O-CO- appendage, i.e., a butyl ester "hair" emanates from each segment of the bristle. In the BBP samples, the mobility within the bristle is sufficient to detect the natural abundance ^2H NMR resonances of the butyl ester extremity on the

bristle exterior. The PBA units in the graft sidechains exhibit resolved, natural abundance resonances in the bottlebrush **(600-*g*-5)-d_4** and **(600-*g*-44)-d_4** samples (Figure V.4). The differentiated natural abundance ^{2}H resonances of the butyl ester hairs on each bristle graft are labeled a-f in Scheme V.1b. The aliphatic units of the hair that are furthest from the grafted bristle's contour are the only peaks detected in the ^{2}H NMR spectra of the BBP. This suggests that the side chain dynamics within the dense grafted bristle environment surrounding the backbone stem are too slow (T_2 is too short) to detect natural abundance resonances for all of the protonated sites; only the positions a, b, and c at the extremity of the hair on each bristle have sufficient mobility to provide nicely resolved resonances. For these positions, the relaxation measurements fall within the fast motion limit with $T_1 = T_2$ within experimental error.

Table V.2 T_1 and T_2 data and calculated correlation times for **(600-*g*-44)-d_4**.

	g·mL^{-1}	***T*$_1$ (ms)**	**$\tau_{c,1}$(ps)**	***T*$_2$ (ms)**	**$\tau_{c,2}$ (ps)**
a	0.089	257	7.68	100	19.7
b	0.040	130	15.2	83.8	23.6
c	0.014	53.7	36.8	42.2	46.8

The relaxation data in Table V.2 reveals that as we move along the butyl ester hairs from the exterior methyl groups to the ester linkage to the bristle's contour, the dynamics slow down significantly. The resonance for the "d" methylene is already too

broad to show up in the spectrum. These findings support a picture of bottlebrush intra-macromolecular organization wherein significant steric repulsion among the crowded grafts result in dynamics too slow for the bristles and certainly for the constrained backbone to enable high resolution spectra.

V.4 Bottlebrushes with Mechanosensitive Tags

The following section was inspired by work on employing bottlebrushes as molecular tensile machines. A dense packing of side chains in bottlebrushes generates forces along the backbone that can range from the pico- to nano-Newtons. The tension can be large enough to induce scission of strong covalent bonds, such as carbon-carbon. The generated force is significant and can be adjusted by controlling factors such as the grafting density, side chains length and the properties of a substrate. In previous work, a weaker disulfide (S-S) bond was incorporated into the brush center to induce a selective scission of bonds, and thus allowing for testing the effect of mechanical force on the kinetics of disulfide reduction by dithiothreitol. Herein, other mechanosensitive molecules were incorporate into the brush structure and tested as potential mechanosensors.

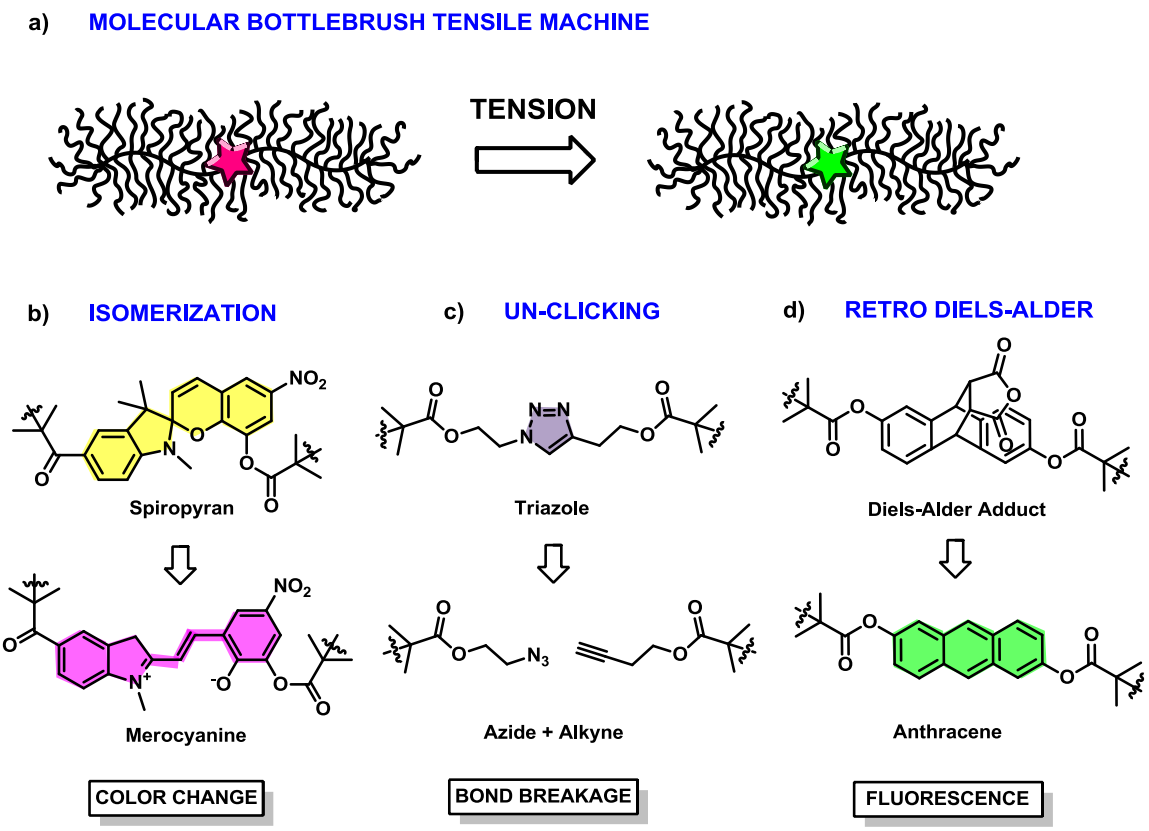

Figure V.5 a) A schematic representation of a molecular bottlebrush with a mechanoactive unit incorporated into center of the molecule. Examples of three mechansensitive units are: b) spiropyran, c) triazol ring and d) Diels-Alder adduct of anthracene and maleic anhydride.

V. 4.1 Results and Discussion

In this work three mechanosensitive di-initiators were employed in the synthesis of bottlebrushes as potential molecular tensile machines. Figure V.5a shows a schematic representation of a molecular bottlebrush with an incorporated mechanoactive tag.

Figure V.5b-d depicts structures of prepared di-initiators and their responses mechanical stimuli.

Figure V.5b shows the structure of spiropyran di-initiator (**Br-Sp-Br**) that was incorporated in P*n*BA bottlebrushes. Spiropyran is a very common mechanophore with the ability to response to different stimuli, including a UV-light, solvents as well as a mechanical stress. The ring in spiropyran opens in a response to stimulus, thus forming its conjugated form, merocyanine. The formation of merocyanine induces the change of color from pale yellow to deep purple, together with increased polarity caused by the presences of charged moieties (Figure V.5). The structure of the second diinitiator contained a triazole ring, and was prepared via the azide-alkyne 'click' reaction (**Br-Tri-Br**) using the previously reported procedure.[26] Bielawski *et al.* reported 1,2,3-triazole ring incorporated into poly(methyl acrylate) (PMA) can undergo a reversible 'click' reaction when the polymer solution is exposed to ultrasound.[26] Hence, it was proposed that the mechanical tension intrinsically generated by bottlebrushes can be utilized to reverse the 'click' process in bottlebrushes with an embedded triazole group (Figure V.5).[26] The last diinitiator's structure was based on a Diels-Alder (D.-A.) adduct of anthracene and maleic anhydride (**Br-Ant-Br**). The **Br-Ant-Br** unit is stable at room temperature; however it undergoes a retro-Diels-Alder reaction when exposed to elevated temperatures and/or mechanical force. This transformation results in generation of fluorescence due to the re-formation of anthracene and the restoration of conjugation to the three aromatic rings.

V.4.1.1 Synthesis of Mechanosensitive Bottlebrushes

The synthesis of mechanosensitive bottlebrushes was conducted in the same manner as that employed for the d_4-labelled bottlebrushes (**BBB-d_4**). First, 2-(trimethylsiloxy)ethyl methacrylate (HEMA-TMS) was polymerized from a functional di-initiator (**Br-I-Br**) via ATRP, followed by an esterification with *α*-bromoisobutyryl bromide to incorporate ATRP-active moieties, and then the 'grafting from' of P*n*BA side chains to form a bottlebrush.

In the first step, HEMA-TMS was polymerized from the three functionalized ATRP di-initiators, **Br-Sp-Br**, **Br-Tri-Br** and **Br-Ant-Br**, using normal ATRP conditions. Table V.3 summarizes the molar ratios of reagents used in the preparation of P(HEMA-TMS) polymers. Reactions were performed with high molar ratios of [HEMA-TMS]:[**Br-I-Br**], 3200 and 2000, while limiting monomer conversions (~ 30 %) (Table V.4). This allowed for suppressing the intermolecular coupling of growing polymer chains thereby keeping narrow molecular weight distributions. In addition, polymerizations of HEMA-TMS were performed under halogen exchange conditions, i.e. with CuCl/dNbpy complex as a catalytic system instead of CuBr-based catalyst, to ensure high initiation efficiencies from the ATRP di-initiators.[22,27]

Table V.3 ATRP reaction conditions used for the preparation of graft copolymers.

Name	Br-I-Br	$[HEMA\text{-}TMS]_0$	$[CuCl]_0$	$[CuCl_2]_0$	$[dNbpy]_0$
Sp-TMS$_{835}$	**Br-Sp-Br**[a]	3200	4.0	0.8	10
Tri-TMS$_{760}$	**Br-Tri-Br**[a]				
Ant-TMS$_{440}$	**Br-Ant-Br**[b]	2000	2.5	0.5	6.0

[a] Polymerization conducted in 20% (v/v) anisole at 60 °C. [b] Polymerization conducted in 10% (v/v) anisole at 70 °C. In each case the ratios of $[Br\text{-}I\text{-}Br]_0$ to other reagents was set as 1.0.

All polymerizations were stopped below 30 % monomer conversion forming polymers with DPs of 835 (**Sp-TMS$_{835}$**), 760 (**Tri-TMS$_{760}$**) and 440 (**Ant-TMS$_{835}$**), with respective spiropyrane, triazol and D-A tags. GPC analysis showed the formation of polymers with narrow MWDs, 1.1-1.2, thus proving good control over the polymerizations. Characterization data of **Sp-TMS$_{835}$**, **Tri-TMS$_{760}$** and **Ant-TMS$_{835}$** is collected in Table V.4. GPC traces, Figure V.6a,c,d, black curves show that the polymers displayed narrow monomodal signals, without significant tailing towards either low and high molecular weights.

Table V.4 Characterization of linear polymers prepared from spyropiran, triazole and Diels-Alder ATRP diinitiators.

Name	x_M / % [a]	$M_n \cdot 10^{-4}$, [b]	$Đ$ [b]	DP_{BB} [c]
Sp-TMS$_{835}$/Sp-MI$_{835}$	26.1	11.5/11.4	1.16/1.42	835
Tri-TMS$_{760}$/Tri-MI$_{760}$	23.1	27.0/89.2	1.22/1.39	760
Ant-TMS$_{440}$/Ant-MI$_{440}$	22.2	6.10/6.32	1.11/1.13	440

[a] Monomer conversion calculate from ^{1}H NMR, $x_M = \left(\frac{A_M \times A_{anisole,0}}{A_{M,0} \times A_{M\ anisole}}\right) \times 100\%$, A_M and $A_{anisole}$ are respective integrations for monomer and internal standard at the end of the reactions, and $A_{M,0}$ and $A_{ansiole,0}$ are the same signals at the beginning of the reaction. [b] Values obtained from THF GPC using linear PMMA standards. [c] Degree of the polymerization of the backbone calculated as $DP_{BB} = \frac{x_M \times DP_{target}}{100\%}$, where DP_{target} is a targeted DP.

Subsequently, P(HEMA-TMS) polymers were functionalized with ATRP reactive groups via a one pot, two-step process. The modification reactions were accomplished using the ratio of reagents: [HEMA-TMS]:[KF]:[TBAF]:[BiBBr]:[2,6-DTBP] = 1.0/1.2/0.01/1.2/0.01 in dry THF at 0 ºC to room temperature. The functionalization reaction provided ATRP macroinitiators: **Sp-MI$_{835}$**, **Tri-MI$_{760}$** and **Ant-MI$_{835}$**, with number average molecular weights and molecular weight distribution values similar to those of initial P(HEMA-TMS) polymers, as determined via GPC (Table V.4). GPC

eluograms of **Sp-MI$_{835}$**, **Tri-MI$_{760}$** and **Ant-MI$_{835}$** are shown as green traces on Figure V.6a, c and d respectively.

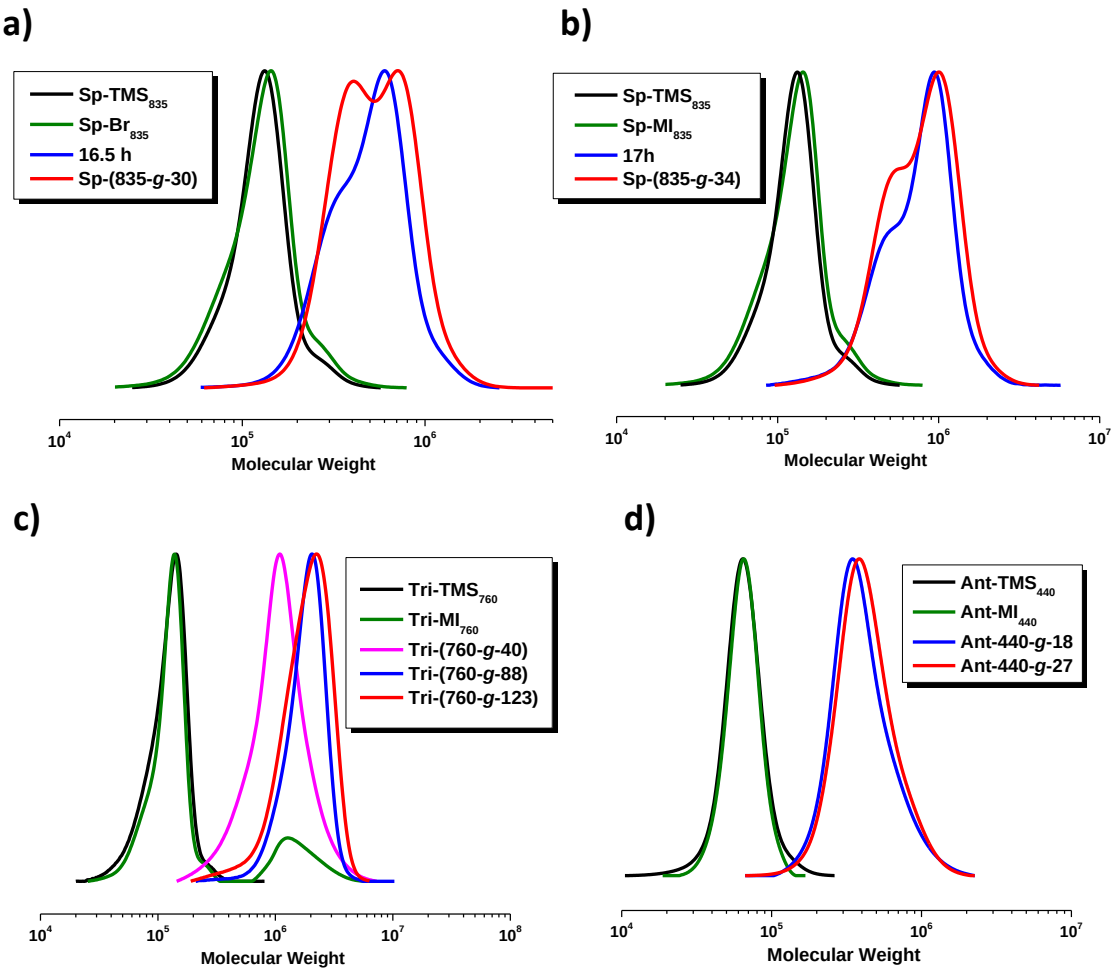

Figure V.6 GPC traces obtained during the polymerization of P*n*BA grafts from a) and b) **Sp-MI$_{835}$**, c) **Tri-MI$_{760}$**, and d) **Ant-MI$_{440}$**.

Next, normal ATRP was utilized for the 'grafting from' approach to polymerize P*n*BA grafts from the prepared macroinitiators, **Sp-MI$_{835}$**, **Tri-MI$_{760}$** and **Ant-MI$_{835}$**. The reaction conditions used for the synthesis of bottlebrushes are summarized in Table V.5.

In general, for targeted lower DP of the side chain a higher concentration of ATRP catalyst and less reactive complex, with dNbpy ligand was used. In contrast, longer grafts were synthesized with lower amounts of copper and more active copper complex formed with PMDETA ligands.

Two reaction conditions were tested for grafting from **Sp-MI$_{835}$**. First, a lower ratio of [*n*BA]:[BiBEM] = [400]:[1] with the less active catalytic complex of CuBr/dNbpy and higher temperature, 70 ˚C. GPC analysis of the reaction mixture revealed the formation of a polymer with bimodal weight distribution (Figure V.6a, blue).At the end of the reaction, the fraction of polymers forming the lower molecular weight signal in the final brush, **Sp-(835-*g*-30)**, increased, Figure V.6a, red curve. It was ascribed to the possible breaking of the brush backbone at the location of the incorporated spiropyrane. Therefore, the reaction was repeated at a higher ratio of [*n*BA]:[BiBEM] = [700]:[1], with a more active catalytic complex CuBr/PMDETA, at a lower temperature, 50 ˚C, hence reducing the possibility of degradation of the spiropyrane. However, GPC characterization of the formed brush, **Sp-(835-*g*-34)**, also revealed a bimodality of the GPC signal (Figure V.6b, red). The characterization of **Sp-(835-*g*-30)** and **Sp-(835-*g*-34)** is given in Table V.6. It was concluded that spiropyrane is unstable under tested ATRP conditions, which led to its degradation via scission of covalent bonds. Because of that, spiropyrane seems to be unsuitable for application as a mechanosensitive tag for the preparation of molecular tensile machines with bottlebrush topology.

Table V.5 ATRP reaction conditions used for the preparation of bottlebrushes.

Name*	PBiBEM	$[n\text{-BA}]_0$	$[CuBr]_0$	$[CuBr_2]_0$	$[dNbpy/PMDETA]_0$
Sp-(835-*g*-30)	**Sp-MI$_{835}$**	400	0.475	0.025	1.0/-
Sp-(835-*g*-34)**		700	0.475	0.025	-/0.5
Tri-(760-*g*-40)	**Tri-MI$_{760}$**	400	0.475	0.025	1.0/-
Tri-(760-*g*-88)		1400	0.475	0.025	-/0.5
Tri-(760-*g*-123)					
Ant-(440-*g*-17)	**Ant-MI$_{440}$**	150	0.36	0.045	0.81/-
Ant-(440-*g*-28)					

*All polymerizations were conducted in 10% (v/v) anisole at 70 °C. In each case the ratio of $[BiBEM]_0$ to other reagents was set as 1.0. ** The polymerization was conducted at 50 ˚C.

In the case of the **Tri-MI$_{760}$**, three lengths of side chains, 40, 88 and 123, were grafted from the macroinitiator by applying conditions summarized in Table V.5. GPC analyses of the resulting brushes, **Tri-(760-*g*-40)**, **Tri-(760-*g*-88)** and **Tri-(760-*g*-123)**, provided polymers with *Đ* values larger (1.3-1.6) than that of **Tri-TMS$_{760}$** (1.22), which might have been caused by the possibility of triazole degradation leading to broadening

of molecular weight distributions (Figure V.6c). GPC characterization of **Tri-(760-*g*-40)**, **Tri-(760-*g*-88)** and **Tri-(760-*g*-123)** is given in Table V.6.

Table V.6 Summary of characterization, of bottlebrushes with functional diinitiators.

Name	x_M / % [a]	M_n [b]	$Đ$ [b]	DP_{SC} [c]
Sp-(835-*g*-30)	7.6	567,000	1.29	30
Sp-(835-*g*-34)	4.9	669,000	1.30	34
Tri-(760-*g*-40)	10.0	892,000	1.37	40
Tri-(760-*g*-88)	6.3	1,760,000	1.30	88
Tri-(760-*g*-123)	8.8	1,480,000	1.58	123
Ant-(440-*g*-17)	11.8	355,000	1.23	17
Ant-(440-*g*-28)	18.7	358,000	1.21	28

[a] Monomer conversion determined by ^{1}H NMR using: $x_M = \left(\frac{A_{[M]} \times A_{[Anisole]_0}}{A_{[M]_0} \times A_{[Anisole]}}\right) \times 100\%$, where $A_{[M]_0}$ and $A_{[M]}$ are integrations of the monomer vinyl signals of at the beginning and end of the reaction, and corresponding internal standard values. [b] Determined by THF GPC with PMMA standards. [c] $DP_{SC} = DP_{targeted} \cdot x_M/100\%$.

Afterwards, the ability of **Tri-(760-*g*-40)** to undergo 'unclicking' was tested by LB AFM analysis. **Tri-(760-*g*-40)** was placed on water surface, thus exposing brushes to intrinsic tension. The sample was visualized after exposure to tension for 0 h and 20 h.

The statistical analysis was performed to determine the number average brush length (L), and thus assess of the retro-click occurred. The results showed that no detectable chain scission occurred for **Tri-(760-*g*-40)** within 20 hours, as the L values were 193±4 nm and 198±4 nm at 0 h and 20 h respectively. It is conclued that the force required to 'unclick' the trazole ring was not sufficient. The force was calculated as 40 nm × 24 mN/m=0.96 nN, using the values of the brush width and surface energy.

Finally, the **Ant-MI$_{440}$** macroinitiator was used to graft side chains with DPs 17 and 28 by employing the reaction conditions summarized in Table V.5. GPC traces showed bottlebrushes with monomodal signals (Figure V.6d, blue and red) and narrow molecular weight distribution values (Table V.6), proving that these conditions provided good control over the grafting process and no degradation of the final brushes, **Ant-(440-*g*-17)** and **Ant-(440-*g*-28)**.

V.5 Conclusions

Labeled linear and bottlebrush polymers were synthesized via ATRP from a tagged ATRP di-initiator. The design of the di-initiator allowed for embedding of quinone-d_4 ring in the polymer center, thus enabling a study of the brush dynamics via ^{2}H NMR. The dynamics of the backbone "stem" of bottlebrush polymers are severely limited by the densely crowded array of grafted side chain "bristles." Slow dynamics dominate even when the average bristle length is very short (e.g., $DP_{sc} \sim 5$) preventing the observation of a high resolution ^{2}H NMR spectrum of deuterium labeled backbone.

Efforts to detect the latter resulted in NMR resonances from natural abundance deuterium in the mobile butyl ester sheath on the exterior of the bristle grafts rather than the backbone incorporated quinone-d_4 ring. But even in that relatively mobile sheath, a gradient of molecular dynamics was evident as one approaches the bristle graft. In summary there is a hierarchy of dynamics in bottle brush polymers; an essentially static arrangement of backbone segments within the core of the bottlebrush with mobility governed by overall rotational diffusion of the entire macromolecule and similar dynamically-constrained grafted bristle contours with only rapid dynamics on the NMR time scale apparent in the aliphatic bristle sheath.

In addition, three stimuli-responsive ATRP diinitiators were employed in the synthesis of mechanosensitive bottlebrushes. Spiropyrane, 1,2,3-triazole and anthracene-maleic anhydride D-A adduct were incorporated in the brush center to study their mechanical response to tension generated intrinsically by brushes. Bottlebrushes were prepared by the 'grafting from' approach under ATRP conditions. It was observed that spiropyrane undergoes degradation during the grafting of side chains, leading to the brush scission at spiropyrane location. In case of a triazole ring, the stability of the brush was much higher; however, broadening of molecular weight distribution in the forced bottlebrushes might suggest a small fraction of degraded product. On the other hand, D-A adduct provided molecular bottlebrushes with narrow MWD, showing no evidence of instability of the mechanosensitive tag. The results show that ATRP is a powerful technique for generation of functional initiators, however one needs to carefully consider the stability of the functionality under ATRP conditions.

V.6 References

(1) Sheiko, S. S.; Sumerlin, B. S.; Matyjaszewski, K. *Prog. Polym. Sci.* **2008**, *33*, 759-785.

(2) Li, Y.; Nese, A.; Lebedeva, N. V.; Davis, T.; Matyjaszewski, K.; Sheiko, S. S. *J. Am. Chem. Soc.* **2011**, *133*, 17479-17484.

(3) Li, Y.; Nese, A.; Matyjaszewski, K.; Sheiko, S. S. *Macromolecules* **2013**, *46*, 7196-7201.

(4) Burdyńska, J.; Li, Y.; Aggarwal, A. V.; Höger, S.; Sheiko, S. S.; Matyjaszewski, K. *J. Am. Chem. Soc.* **2014**, *136*, 12762-12770.

(5) Lee, H.-i.; Matyjaszewski, K.; Yu-Su, S.; Sheiko, S. S. *Macromolecules* **2008**, *41*, 6073-6080.

(6) Miyake, G. M.; Piunova, V. A.; Weitekamp, R. A.; Grubbs, R. H. *Angew. Chem. Int. Ed.* **2012**, *51*, 11246-11248.

(7) Sveinbjörnsson, B. R.; Weitekamp, R. A.; Miyake, G. M.; Xia, Y.; Atwater, H. A.; Grubbs, R. H. *Proc. Natl. Acad. Sci* **2012**, *109*, 14332-14336.

(8) Banquy, X.; Burdyńska, J.; Lee, D. W.; Matyjaszewski, K.; Israelachvili, J. *J. Am. Chem. Soc.* **2014**, *136* 6199-6202.

(9) Zhang, Y.; Constantini, N.; Mierzwa, M.; Pakula, T.; Neugebauer, D.; Matyjaszewski, K. *Polymer* **2004**, *45*, 6333-6339.

(10) Pakula, T.; Zhang, Y.; Matyjaszewski, K.; Lee, H.-i.; Boerner, H.; Qin, S.; Berry, G. C. *Polymer* **2006**, *47*, 7198-7206.

(11) Neugebauer, D.; Zhang, Y.; Pakula, T.; Matyjaszewski, K. *Macromolecules* **2003**, 6746-6755.

(12) Pietrasik, J.; Sumerlin, B. S.; Lee, H.-i.; Gil, R. R.; Matyjaszewski, K. *Polymer* **2007**, *48*, 496-501.

(13) Levitt, M. H.; Wiley, Ed. 2008.

(14) Neugebauer, D.; Zhang, Y.; Pakula, T.; Matyjaszewski, K. *Macromolecules* **2005**, *38*, 8687-8693.

(15) Gao, H.; Matyjaszewski, K. *J. Am. Chem. Soc.* **2007**, *129*, 6633-6639.

(16) Beers, K. L.; Gaynor, S. G.; Matyjaszewski, K.; Sheiko, S. S.; Moeller, M. *Macromolecules* **1998**, *31*, 9413-9415.

(17) Boerner, H. G.; Beers, K.; Matyjaszewski, K.; Sheiko, S. S.; Moeller, M. *Macromolecules* **2001**, *34*, 4375-4383.

(18) Cheng, G.; Boeker, A.; Zhang, M.; Krausch, G.; Mueller, A. H. E. *Macromolecules* **2001**, *34*, 6883-6888.

(19) Matyjaszewski, K.; Xia, J. H. *Chem. Rev.* **2001**, *101*, 2921-2990.

(20) Matyjaszewski, K. *Macromolecules* **2012**, *45*, 4015-4039.

(21) Matyjaszewski, K.; Tsarevsky, N. V. *J. Am. Chem. Soc.* **2014**, *136*, 6513-6533.

(22) Matyjaszewski, K.; Qin, S.; Boyce, J. R.; Shirvanyants, D.; Sheiko, S. S. *Macromolecules* **2003**, *36*, 1843-1849.

(23) Abragam, A.; Clarendon Press: 1961.

(24) Bovey, F. A.; Mirau, P. A.; Elsevier Science: 1996.

(25) Mirau, P. A.; Wiley-Interscience: 2005.

(26) Brantley, J. N.; Wiggins, K. M.; Bielawski, C. W. *Science* **2011**, *333*, 1606-1609.

(27) Matyjaszewski, K.; Shipp, D. A.; Wang, J.-L.; Grimaud, T.; Patten, T. E. *Macromolecules* **1998**, *31*, 6836-6840.

CHAPTER VI

MOLECULAR STARS FROM SPOKED WHEEL HEXA-INITIATOR

Preface

In Chapter 1 it was described that the ‘grafting from’ approach can be applied in the preparation of molecular bottlebrushes with variety of different topologies. ATRP was proved to be a superior technique for the ‘grafting from’ method, as it allows for a great control over lengths of both side chains and backbones with the use of a wide diversity of monomers. In addition, it was also shown that the topology and properties of molecular bottlebrushes can be further modified by applying a functional ATRP initiator. Such approach was utilized to generate a bottlebrush with a single S-S unit incorporated in its center, which allowed for a selective mechanoscission of such a bond resulted from the tension generated intrinsically by bottlebrushes. Moreover, the design of tri- and tetra-

functional ATRP initiators enabled the synthesis of so called “molecular stars”, which resembled polymeric stars with three and four brush arms respectively.

This section describes the synthesis of molecular stars with six brush arms that were generated from ATRP with molecular spoked wheel (MSW) skeleton. MSW initiator was designed and synthesized by Dr. Vikas A. Aggarwal from Prof. Sigurd Höger’s group at University of Bonn in Germany. All AFM characterizations were performed by Dr. Yuanchao Li from the group of Prof. Sergei S. Sheiko, at University of North Carolina, Chapel Hill. All molecular stars were prepared and characterized by me under supervision of Prof. Kris Matyjaszewski.

This novel MSW initiator was utilized to prepare a series of star-shaped bottlebrushes having six arms, and with varying lengths of arms, and side chains, i. e. **(450-*g*-20)$_6$**, **(450-*g*-40)$_6$**, **(300-*g*-60)$_6$** and **(300-*g*-150)$_6$**. GPC analysis and molecular imaging by AFM confirmed the formation of well-defined macromolecules with narrow molecular weight distributions. Upon adsorption to an aqueous substrate, the bottlebrush arms underwent prompt dissociation from the MSW core, followed by scission of covalent bonds in the bottlebrush backbones. The preferential cleavage of the arms is attributed to strong steric repulsion between bottlebrushes at the MSW branching center. Star-shaped macroinitiators may undergo aggregation which can be prevented by sonication.

VI.1 Introduction

The continuous development in the areas of a controlled radical polymerization (CRP) and organic synthesis has enabled an access to a variety of complex macromolecules with vast number of well-defined topologies.[1-3] In particular, molecular bottlebrushes, a unique type of graft copolymers with side chains densely packed along a linear polymer chain, have garnered a great deal of attention.[4-11] The high grafting density generates strong steric repulsion between the tethered side chains resulting in the corresponding increase in the persistence length and disentanglement of bottlebrushes. A distinct worm-like conformation of molecular bottlebrushes along with their exceptional length[12] (up to several micrometers), affords the ability to image individual molecules using Atomic Force Microscopy (AFM). Therefore, molecular bottlebrushes have been widely used as model systems for experimental studies of a single molecule ordering, motion, and reactivity at interfaces surface.[8]

In synthetic chemistry, dense grafting has been explored as a versatile platform for the design of complex molecular and supramolecular systems with bottlebrushes as shape-persistent mesoblocks. Bottlebrushes can be prepared via three different approaches: "grafting through",[13] "grafting onto",[14] and "grafting from" [4,8,15-17]. CRP techniques, in particular atom transfer radical (ATRP),[3,18-20] reversible addition−fragmentation chain-transfer (RAFT)[21,22] and nitroxide mediated (NMP)[23] polymerizations, have granted a convenient route for the preparation of well-defined molecular brushes. Both the grafts and backbones may have different branching

topologies and chemical compositions that can be altered separately, which exceedingly expands the range and sophistication of molecular architectures, and thus materials' properties as compared to those of linear polymers.

Up to now, a variety of densely grafted copolymers with different architectures were prepared including brush–coil,[24] diblock (both within the backbone and side chains),[21,25-30] gradient[31,32] and multi-arm star-like brushes.[33] Such unique macromolecules have also been extensively investigated in areas of supersoft elastomers,[34,35] photonics,[10,28,29,36], organic nanotubes,[11,21] biomimetic materials,[37-39] networks and porous materials[27,40] or lithography/nanofabrication[41,42].

The design of ATRP initiator can also be employed to modify the architecture of densely grafted copolymers. Previously, the multifunctional ATRP initiators were used to prepare three- and four-armed architectures, which combined the properties of both polymeric stars and molecular bottlebrushes.[33] AFM imaging of individual molecules provided a visual confirmation of star-shaped bottlebrushes, also allowing for the correlation of the type of a catalytic system with the structural quality of obtained polymers. Star-like bottlebrushes displayed a distinct ordering of monolayers, showing transition under compression, from a dendritic- to a disk-like conformation.[43]

In this work, we have designed a novel type of molecular spoked wheel (MSW) ATRP initiator, which allows for the synthesis of molecular star bottlebrushes with a higher number of arms than reported previously, and a planar topology that is forced by the disk-like structure of the initiator. MSWs form a new class of conjugated macrocycles

with multiple aromatic rings and alkyne groups covalently linked together[44-48] to form an exceptionally rigid and highly fluorescent structures.[49-53] These unique molecules can be potentially utilized as optically active materials,[54] molecular wires[55] or environmentally confined reaction containers[56]. It was also shown previously that they are useful tools for fundamental studies of the understanding of the microscopic electronic structure of conjugated polymers.[50] For the purpose of this study, we have synthesized a sixfold, hydroxy-functionalized MSW (**$MSW_{6\text{-}OH}$**) and converted it to a well-defined ATRP initiator (**$MSW_{6\text{-}Br}$**). The ATRP functionalized MSW allowed for the preparation of star-like bottlebrushes with a distinct hexa-arm topology. Star-shaped bottlebrushes with varying lengths of arms and side chains were generated by grafting poly(*n*-butyl acrylate) from star-like backbones under normal ATRP conditions. Polymers were characterized by Gel Permeation Chromatography (GPC) and Atomic Force Microscopy (AFM), proving the formation of star-shaped polymers. AFM analysis allowed for the direct visualization of star-shaped bottlebrushes with distinctive topological differences resulting from varied lengths of both grafts and arms.

VI.2 Experimental

Materials. *n*-Butyl acrylate (*n*BA, 99%, Acros) and (2-trimetylsiloxy)ethyl methacrylate (HEMA-TMS, Scientific Polymer Products) were purified by passing the monomer through a column filled with basic alumina to remove the inhibitor. All other reagents: copper(I) bromide ($Cu^{I}Br$, 99.999%), copper(II) bromide ($Cu^{II}Br_2$, 99.999%), copper(I)

chloride ($Cu^{I}Cl$, 99.995%), copper(II) chloride ($Cu^{II}Cl_2$, 99.999%), 4,4′-dinonyl-2,2′-dipyridyl (dNbpy, 97%) *N,N,N',N'',N''*-pentamethyldiethylenetriamine (PMDETA, 99%), potassium fluoride (KF, 99%), tetrabutylammonium fluoride (TBAF, 1.0 M in THF), *α*-bromoisobutyryl bromide (98%), 2,5-di-*tert*-butylphenol (DTBP, 99%), triethylamine (TEA, ≤99%) and solvents were purchased from Aldrich and used as received without further purification.

Characterization. The conversion of *n*BA was determined from ^{1}H NMR spectra recorded in $CDCl_3$ as a solvent using Brüker 300 MHz spectrometer. The particle size was measured using a Zetasizer Nano from Malvern Instruments. The sonication was performed using Ultrasonic cleaner model FS20 from Fisher Scientific with a sweep frequency of 40 kHz. Molecular weight distributions of the polymers were characterized by gel permeation chromatography (GPC) using Polymer Standards Services (PSS) columns (guard, 10^5, 10^3, and 10^2 Å), with THF eluent at 35 °C, flow rate 1.00 mL/min, and differential refractive index (RI) detector (Waters, 2410). The apparent number-average molecular weights (M_n) and molecular weight dispersities (M_w/M_n) were determined with a calibration based on linear poly(methyl methacrylate) (PMMA) standards and diphenyl ether as an internal standard, using WinGPC 6.0 software from PSS. In addition, the number average molecular weight was measured by the AFM-LB method described elsewhere.[73] The samples for AFM measurement were prepared by either Langmuir-Blodgett (LB) deposition or spin casting from dilute solutions. LB films were transferred onto freshly cleaved mica substrates at a constant surface pressure of 0.5 mN/m and a controlled transfer ratio. Imaging of individual molecules was performed in

PeakForce QNM mode using a multimode AFM (Brüker) with a NanoScope V controller. We used silicon probes with a resonance frequency of 50-90 Hz and a spring constant of ~0.4 N/m. In-house developed computer software was used to analyze the AFM images with respect to arm size and molecular weight distribution of star-like bottlebrushes. Typically, ensembles of 200-300 molecules were analyzed to ensure standard deviation of the mean below 10%.

Synthesis of 1 $[P(HEMA\text{-}TMS)_{450}]_6$ $(450\text{-}TMS)_6$. A 10 ml Schlenk flask was charged with **$MSW_{6\text{-}Br}$** (0.0137 g, 0.0019 mmol), HEMA-TMS (4.0 mL, 18.4 mmol), dNbpy (0.023 g, 0.056 mmol), $Cu^{II}Cl_2$ (0.62 mg, 0.0046 mmol), and anisole (1.0 mL). The solution was degassed by three freeze-pump-thaw cycles. During the final cycle, the flask was filled with nitrogen and $Cu^{I}Cl$ (22.6 mg, 0.0230 mmol) was quickly added to the frozen reaction mixture. The flask was sealed, evacuated and back-filled with nitrogen five times and then immersed in an oil bath at 60 °C. Polymerization was terminated after 69 h reaching 26.1% conversion as determined by ^{1}H NMR, which corresponded to a DP of ~450 per arm. Apparent molecular weight determined by THF GPC: $M_{n,GPC}$ = $2.70 \cdot 10^5$, and M_w/M_n = 1.22. The reaction mixture was diluted with chloroform, passed through neutral alumina to remove the catalyst, then concentrated and used for the next step without further purification.

Synthesis of 2 $(PBiBEM_{450})_6$ $(450\text{-}Br)_6$. A 50 ml round-bottom flask was charged with **1** (1.711 g, 5.80 mmol), KF (0.513 g, 8.70 mmol), DTBP (0.120 g, 0.580 mmol), and then dry THF (15 mL) was added under nitrogen. The reaction mixture was cooled down in an

ice bath, followed by the injection of tetrabutylammonium fluoride (0.12 mL, 1.0 M in THF, 0.120 mmol) and subsequent dropwise addition of α-bromoisobutyryl bromide (2.67 g, 1.43 mL. 11.6 mmol) over the course of 10 min. Upon addition, the reaction mixture was allowed to reach room temperature and was stirred for another 16 h. Afterwards solids were filtered of and the mixture was precipitated into methanol/water (70/30), re-dissolved in chloroform (30 mL) and passed through the column filled with basic alumina. The product **2** was re-precipitated three times in hexanes and dried overnight under vacuum. Apparent molecular weight determined by THF GPC: $M_{n,GPC}$ = $2.80 \cdot 10^5$, and M_w/M_n = 1.39.

Synthesis of 3a (PBiBEM$_{450}$-*g*-P*n*BA$_{20}$)$_6$ (450-*g*-20)$_6$. A 25 mL Schlenk flask equipped with a stir bar was charged with macroinitiator **2** (0.0870 g, 0.3086 mmol of BiBEM groups), *n*BA (17.6 mL, 123.4 mmol), dNbpy (0.126 g, 0.309 mmol), $Cu^{II}Br_2$ (1.7 mg, 0.0077 mmol), and anisole (2.5 mL). The solution was degassed by three freeze-pump-thaw cycles. During the final cycle $Cu^{I}Br$ (21.0 mg, 0.1466 mmol) was quickly added to the frozen reaction mixture under nitrogen atmosphere. The flask was sealed, evacuated, back-filled with nitrogen five times, and then immersed in an oil bath thermostated at 60 °C. The polymerization was stopped after 20 h, and the monomer conversion was determined by both gravimetry and ^{1}H NMR, resulting in the brush polymer **3a** with DP~20 of side chains. The polymer was purified by three precipitations from cold methanol, and dried under vacuum at room temperature, to a constant mass. Apparent molecular weight was determined using THF GPC: $M_{n,GPC} = 1.24 \cdot 10^6$, and M_w/M_n = 1.48.

Synthesis of 3b (PBiBEM$_{450}$-*g*-P*n*BA$_{40}$)$_6$ (450-*g*-40)$_6$. The reaction was set up and analyzed in the same way as **3a** except the reaction temperature was 70 °C. The amounts of reagents used for the polymerization: macroinitiator **2** (0.0554 g, 0.1964 mmol of BiBEM groups), *n*BA (11.2 mL, 78.6 mmol), dNbpy (0.080 g, 0.196 mmol), $Cu^{II}Br_2$ (1.1 mg, 0.0049 mmol), anisole (1.25 mL) and $Cu^{I}Br$ (13.3 mg, 0.0933mmol). The polymerization was stopped after 23 h 20 min. giving the brush polymer, **3b**, with DP 40 of side chains. Apparent molecular weight determined by THF GPC: $M_{n,GPC} = 1.06 \cdot 10^6$, and $M_w/M_n = 1.61$.

Synthesis of 4 [P(HEMA-TMS)$_{300}$]$_6$ (300-TMS)$_6$. The reaction was set up and analyzed in the same way as **1**. The amounts of reagents used for the polymerization: **MSW$_{6\text{-}Br}$** ATRP initiator (0.0164 g, 0.0023 mmol), HEMA-TMS (3.0 mL, 17.2 mmol), dNbpy (0.017 g, 0.041 mmol), $Cu^{II}Cl_2$ (0.46 mg, 0.0034mmol), anisole (0.75 mL) and $Cu^{I}Cl$ (1.7 mg, 0.0172 mmol). The polymerization was stopped after 39 h 10 min. reaching 30.1% conversion, which corresponded to DP~300 per arm giving the polymer, **4**, with DP~300 per arms. Apparent molecular weight determined by THF GPC: $M_{n,GPC} = 1.64 \cdot 10^5$, and $M_w/M_n = 1.12$.

Synthesis of 5 (PBiBEM$_{300}$)$_6$ (300-Br)$_6$. The reaction was set up and analyzed in the same way as **2**. The amounts of reagents used for the functionalization: the polymer **4** (0.50 g, 2.5 mmol), KF (0.161 g, 2.72 mmol), DTBP (0.051 g, 0.248 mmol), dry THF (15 mL), TBAF (0.013 mL, 1.0 M in THF, 0. 013 mmol), and α-bromoisobutyryl bromide (0.626 g, 0.37 mL. 2.72 mmol) over the course of 10 min. The reaction was performed

twice to ensure quantitative functionalization of the macroinitiator **5**. The polymer was purified by dialysis against THF using 50kDA MWCO membranes. The polymer was stored as a solution in anisole to avoid aggregation. Apparent molecular weight determined by THF GPC: $M_{n,GPC} = 2.23 \cdot 10^5$, and $M_w/M_n = 1.20$.

Synthesis of 6a (PBiBEM$_{300}$-*g*-P*n*BA$_{60}$)$_6$ (300-*g*-60)$_6$. The reaction was set up and analyzed in the same way as **3a**. The amounts of reagents used for the polymerization: macroinitiator **5** (0.0283 g, 0.0993 mmol of BiBEM groups), *n*BA (19.8 mL, 139.0 mmol), PMDETA (0.0086g, 10.4 μL, 0.0496 mmol), $Cu^{II}Br_2$ (0.55 mg, 0.0025 mmol), anisole (2.2 mL) and $Cu^{I}Br$ (6.7 mg, 0.0472 mmol). The polymerization was stopped after 15 h 30 min. giving the brush polymer, **6a**, with DP 60 of side chains. Apparent molecular weight determined by THF GPC: $M_{n,GPC} = 1.11 \cdot 10^6$, and $M_w/M_n = 1.20$.

Synthesis of 6b (PBiBEM$_{300}$-*g*-P*n*BA$_{150}$)$_6$ (300-*g*-150)$_6$. The reaction was set up and analyzed in the same way as **6a**. The polymerization was stopped after 49 h 30 min. giving the brush polymer, **6b**, with DP 150 of side chains. Apparent molecular weight determined by THF GPC: $M_{n,GPC} = 1.93 \cdot 10^5$, and $M_w/M_n = 10.2$.

VI.3 Results and Discussion

VI.3.1 Synthesis and Characterization of the Molecular Stars Based Six-fold ATRP-Initiator $MSW_{6\text{-}Br}$

The synthetic approach used for the preparation of sixfold $\mathbf{MSW_{6\text{-}Br}}$ ATRP initiator was based on the previous reports on analogous molecular spoked wheels.[50,57] In this paper we introduced synthetic adjustments (modifications) that allowed for the synthesis of $\mathbf{MSW_{6\text{-}Br}}$. A complete description of synthetic procedures including all organic precursors and sample characterization is described in the literature.

The synthesis of $\mathbf{MSW_{6\text{-}Br}}$ relied on the preparation of its hexa-hydroxy precursor, $\mathbf{MSW_{6\text{-}OH}}$. The incorporated hydroxyl functionalities allow post-cyclization modification of the MSW providing access to new, more complex MSWs which can be potentially used in the generation of novel, advanced materials. Furthermore, due to the strong propensity of previously prepared MSWs analogues towards the aggregation, we also aimed to eliminate such tendency in $\mathbf{MSW_{6\text{-}Br}}$, thus ensuring the polymerization exclusively from unimolecular initiator species.[50] This was accomplished through the groups (Figure VI.1a). As proved by DLS results in chloroform and toluene (Figure VI.2), the incorporation of the branching in MSWs resulted in the successful suppression of their aggregation. It was ascribed to the reduced ability of MSWs to interact via π-π stacking as well as their improved solubility as compared to structures with linear hexadecyl groups.

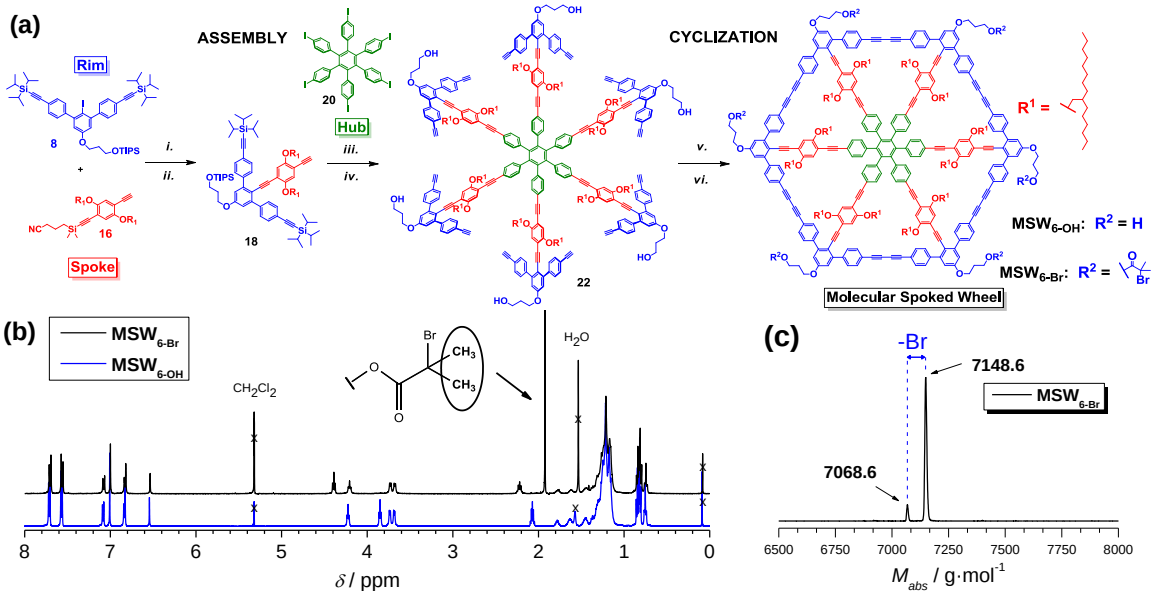

Figure VI.1 (a) The synthetic approach and chemical structures of the rim (blue), spoke (red), hub (green) and molecular spoked wheel (MSW) derivatives. *i.* $Pd(PPh_3)_2Cl_2$, CuI, PPh_3, THF, piperidine, µw (microwave), 120 °C, 12 min, 92 %; *ii.* K_2CO_3, THF, methanol, r.t., 2 h, 100 %. *iii.* Pd_2dba_3, CuI, dppf, THF, piperidine, 80 °C, 17 h, 81 %; *iv.* TBAF, THF, 0 °C – r.t., 3 h, 74 %; *v.* α-bromoisobutyryl bromide, pyridine, CH_2Cl_2, 0 °C, 2 h. (b) NMR spectra of **$MSW_{6\text{-}OH}$** and **$MSW_{6\text{-}Br}$** in CD_2Cl_2. The spectra show the methyl groups in **$MSW_{6\text{-}Br}$** as sharp singlet signal at 1.92 ppm. (c) MALDI-TOF of **$MSW_{6\text{-}Br}$** showing the high purity of the sixfold initiator.

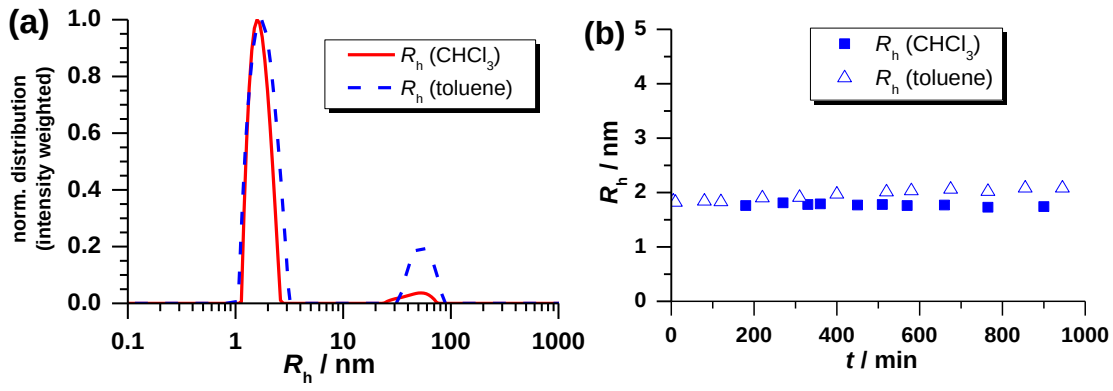

Figure VI.2 DLS measurements of two samples of **MSW$_{6\text{-OtBDMS}}$** (6 mg/mL in toluene and chloroform) (a) CONTIN-analysis, recorded 765 min and 945 min after dissolving the sample, respectively. In toluene, 85 % of the scattered light is attributed to the monomer whereas in $CHCl_3$ it is 95 %. (b) Cumulant-analysis of the autocorrelation curves at 30°. The evolution of the first cumulant over time is displayed: for the toluene solution a very slight increase of the first cumulant can be observed, while it is constant for the $CHCl_3$ solution.

MSW$_{6\text{-OH}}$ was obtained via a convex modular approach, based on the design of individual modules: the **rim** (blue), **spoke** (red) and **hub** (green). All the building blocks were linked together prior the cyclization (Figure VI.1a). The most crucial step was the design of the functional **rim** (Figure VI.1a, blue) with incorporated hydroxyl functionality. The structure of the **rim** was based on *m*-terphenyl-scaffold modified with 3-[(triisopropylsilyl)oxy]propyl linker (TIPSO-), which allowed for the incorporation of a protected hydroxyl group into the molecule (Figure VI.1a). Next, the **rim** was attached to the **spoke** (Figure VI.1a) to form a spoke-rim module (Figure VI.1a), which was later selectively deprotected and then linked to the **hub** (Figure VI.1a, green). A subsequent

deprotection of the assembled product yielded a MSW precursor with free six hydroxyl (Figure VI.1a) groups, which was directly cyclized under pseudo high-dilution conditions to form the desired **MSW$_{6\text{-}OH}$** (Figure VI.1a). Then, **MSW$_{6\text{-}OH}$** was converted into a well-defined ATRP initiator, **MSW$_{6\text{-}Br}$** through a sixfold esterification reaction with α-bromoisobutyryl bromide and pyridine (Figure VI.1a). The esterification of **MWS$_{6\text{-}OH}$** proceeded with high yields (89%) and efficiency, as confirmed by the appearance of the signal at 1.94 ppm corresponding to CH_3- protons of ATRP moieties in the ^{1}H NMR spectra of **MSW$_{6\text{-}Br}$** (Figure VI.1b). MALDI-TOF analysis of **MWS$_{6\text{-}Br}$** showed the presence of two peaks corresponding to pure molecules, and molecules that lost one bromine atom upon ionization (molar mass 7148.6 Da and 7068.6 Da respectively), thus confirming a very high purity of the final ATRP hexa-initiator.

VI.3.2 Synthesis and Characterization of Hexa-arm Macroinitiators

The synthetic pathway for the synthesis of star-shaped brushes is shown in scheme VI.1. Molecular bottlebrush arms were prepared via double "grafting-from" approach under normal ATRP conditions. First, (2-trimethylsiloxyethyl) methacrylate (HEMA-TMS) was polymerized from multi-functional ATRP initiator (**MSW$_{6\text{-}Br}$**), followed by a subsequent esterification with ATRP-active moieties. Finally, poly(*n*-butyl acrylate) side chains were grafted from six-arm ATRP macroinitiators, resulting in star-shaped molecular bottlebrushes (Scheme VI.1).[33] P(HEMA-TMS) was grafted from **MSW$_{6\text{-}Br}$** under normal ATRP conditions to form arms of stars with degrees of

polymerization (DPs) 450 (**(450-TMS)$_6$**) and 300 (**(300-TMS)$_6$**). Reactions were performed with high molar ratios of [M]:[I] (9600 and 6000 respectively) while keeping polymerizations at limited monomer conversions (~ 30 %), thereby suppressing the intermolecular termination between growing arms, and subsequent star-star coupling. To ensure high initiation efficiencies from the multi-functional initiator, **MSW$_{6\text{-Br}}$**, the polymerizations of HEMA-TMS were performed with Cu^{I}Cl/dNbpy complex as a catalytic system.[33,60] Earlier results revealed ATRP reactions under halogen exchange conditions produce well-defined stars with narrow arm length distributions and improved grafting efficiency, as compared to traditionally used Cu^{I}Br-based catalyst.

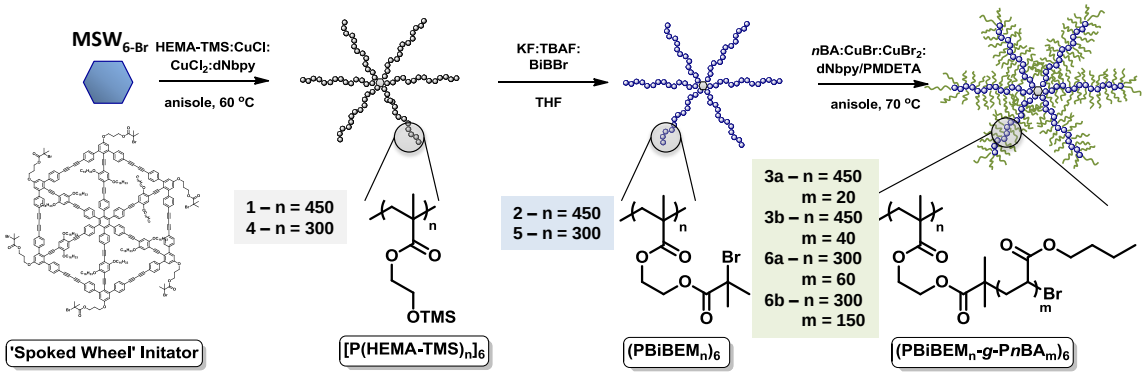

Scheme VI.1 The synthesis of star-like bottlebrushes with hexa- ATRP initiator (**MSW$_{6\text{-Br}}$**) via double "grafting-from" approach.

[P(HEMA-TMS)$_{450}$]$_6$ (**(450-TMS)$_6$**) and [P(HEMA-TMS)$_{300}$]$_6$ (**(300-TMS)$_6$**) were characterized by GPC confirming the formation of star-polymers (Figure VI.3, black) with narrow MWDs, M_w/M_n = 1.22 and 1.12 respectively (Table VI.1, samples 1 and 4). The number average MWs (M_n) for the macroinitiators **(450-TMS)$_6$** and **(300-TMS)$_6$**, were lower than the corresponding theoretical values ($M_{n,th}$). This was attributed to a

compact structure of star-shaped P(HEMA-TMS) polymers, which resulted in hydrodynamic volumes smaller than the dimensions of linear PMMA standards.

The functionalization of **(450-TMS)$_6$** and **(300-TMS)$_6$** with ATRP reactive groups was performed via one pot, two-step process, following a previously reported procedure.[4] First, TMS-blocked hydroxyl groups were deprotected in a presence of KF/TBAF, followed by the subsequent addition of α-bromoisobutyryl bromide, resulting in the formation of respective PBiBEM macroinitiators **(450-Br)$_6$** and **(300-Br)$_6$**. ^{1}H NMR spectroscopy of polymers confirmed the full deprotection of –OTMS together with the quantitative incorporation of ATRP functionalities, as indicated by the disappearance of TMS signals and the downfield shift of both adjacent CH_2 peaks of P(HEMA-TMS).[61] GPC characterization of **(450-Br)$_6$** and **(300-Br)$_6$** gave respective M_w/M_n = 1.39 and 1.20 (Table VI.1, samples 2 and 5), showing no significant shift of signals as compared to the corresponding P(HEMA-TMS) materials (Figure VI.3, red). Broadening of the molecular weight distribution of **(450-Br)$_6$** (Table VI.1, sample 2) was related to the presence of a high molecular weight signal in the GPC trace (Figure VI.3a, red), which was ascribed to a small fraction of polymeric aggregates present in the sample.

During the preparation of **(450-Br)$_6$** it was noticed that the macroinitiator could undergo aggregation in THF. The following section is focused on discussing the process of the formation of physical aggregates.

Table VI. 1 The characterization of backbones and star-like bottlebrush polymers prepared from **MSW$_{6\text{-Br}}$**.

Sample	Polymer structure	Name/DP$_{arm\text{-}g\text{-}SC}$[a]	$M_{n,th}\cdot10^{-6}$[b]	$M_{n,GPC}\cdot10^{-6}$[c]	M_w/M_n[c]	$M_{n,AFM}\cdot10^{-6}$[d]	M_w/M_n[e]
1	[P(HEMA-TMS$_{450}$)]$_6$	**(450-TMS)$_6$**	0.55	0.27	1.22	N/A	N/A
2	(PBiBEM$_{450}$)$_6$	**(450-Br)$_6$**	0.76	0.28[f]	1.39[f]	N/A	N/A
3a	(PBiBEM$_{450}$-*g*-P*n*BA$_{20}$)$_6$	**(450-*g*-20)$_6$**	7.67	1.24	1.48	3.7	1.27
3b	(PBiBEM$_{450}$-*g*-P*n*BA$_{40}$)$_6$	**(450-*g*-40)$_6$**	14.6	1.06	1.61	5.3	1.30
4	[P(HEMA-TMS$_{300}$)]$_6$	**(300-TMS)$_6$**	0.37	0.16	1.12	N/A	N/A
5	(PBiBEM$_{300}$)$_6$	**(300-Br)$_6$**	0.51	0.22	1.20	N/A	N/A
6a	(PBiBEM$_{300}$-*g*-P*n*BA$_{60}$)$_6$	**(300-*g*-60)$_6$**	14.3	1.11	1.20	6.4	1.26
6b	(PBiBEM$_{300}$-*g*-P*n*BA$_{150}$)$_6$	**(300-*g*-150)$_6$**	35.1	0.19	10.2	10.3	1.28

[a] Calculated from the monomer conversion obtained by ^{1}H NMR. $DP_{arm} = [A_{CH_2(polymer)}/A_{CH_2(monomer+polymer)}] \times [DP_{target}/6]$; where $A_{CH_2(monomer+polymer)}$ and $A_{CH_2(polymer)}$ are the respective areas under the curve corresponding to -CH_2- protons of the polymer only and the monomer and the polymer total, and DP_{target} is a targeted DP of HEMA-TMS vs. **MSW$_{6\text{-Br}}$**; $DP_{SC} = [1 - (A_{[nBA]}/A_{[nBA]_0})] \times DP_{target}$; where $A_{[nBA]}$ and $A_{[nBA]_0}$ are the integrations of vinyl protons of *n*BA vs. anisole as an internal standard. [b] $M_{n,th} = 6 \times DP_{arm} \times (MW_{arm,monomer} + DP_{SCs} \times MW_{nBA}) + MW_{MSW}$. [c] Determined by THF GPC using linear PMMA standards. [d] Number average molecular weight determined as a ratio of mass per unit area from LB film transfer and number of molecules per unit area from molecular imaging by AFM. [e] Molecular weight distributions calculated by assuming a constant molecular weight per unit arm length for each sample. [f] Analyzed by DMF GPC using linear PMMA standard.

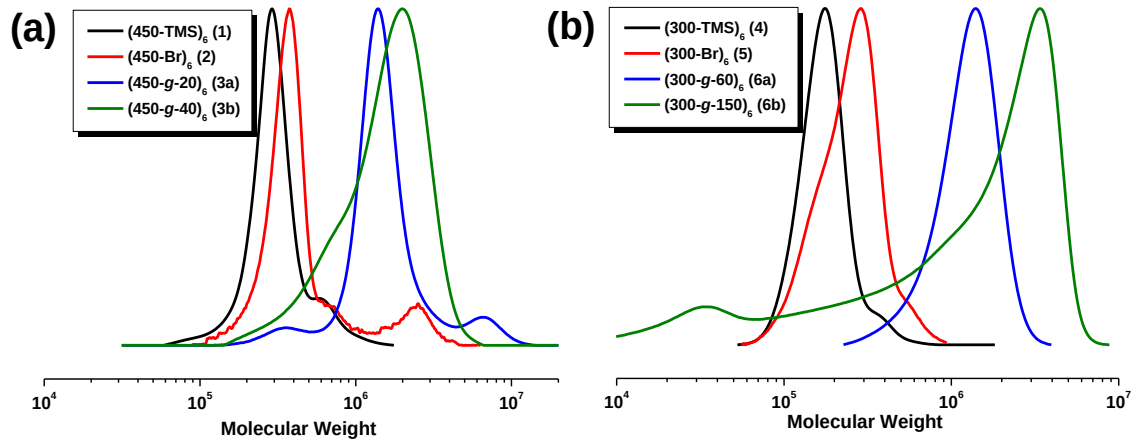

Figure VI.3 GPC traces of (a) $[P(HEMA\text{-}TMS_{450})]_6$ **((450-TMS)$_6$**, black), $(PBiBEM_{450})_6$ **((450-Br)$_6$**, red), $(PBiBEM_{450}$-*g*-$(PnBA_{20})_6$ (**(450-*g*-20)$_6$**, blue) and $(PBiBEM_{450}$-*g*-$(PnBA_{40})_6$ (**(450-*g*-40)$_6$**, green), (b) $[P(HEMA\text{-}TMS_{300})]_6$ **((300-TMS)$_6$**, black), $(PBiBEM_{300})_6$ (**(300-Br)$_6$**, red), $(PBiBEM_{300}$-*g*-$(PnBA_{60})_6$ (**(300-*g*-60)$_6$**, blue) and (PBiBEM300-*g*-$(PnBA_{150})_6$ (**(300-*g*-150)$_6$**, green).

VI.3.3 Aggregation of $(PBiBEM_{450})_6$ Macroinitiator

Copolymers consisting of both rigid and flexible segments have gained a great deal of attention due to their unique solution and bulk properties.[62] They self-assemble into morphologies with different degrees of complexity at hydrodynamic volumes much lower than those of coil-coil block copolymers. Aggregation of block copolymers with various topologies, including rod-coil,[63,64] coil-ring-coil[65] or rod-coil star,[62] have been studied, showing their ability to form unique supramolecular assemblies, such as micelles, hollow spheres,[62] hollow cylindrical brushes,[65] or mushroom-like morphologies.[64] Thus, they are excellent candidates as potential building blocks for the

preparation of highly regular nanostructures with controllable size and shape, and novel properties.[64]

Similar behavior was observed during the synthesis of **(450-Br)$_6$**, a structure with a rigid disc-shaped core and flexible polymeric arms. When the polymer was characterized via THF GPC, a molecular weight (HMW) peak was observed on the eluogram (Figure VI.4a), which was ascribed to the formation of physical aggregates. In order to exclude the possibility of contamination-induced aggregation, a series of additional precipitations of **(450-Br)$_6$** were performed to further purify the material. However, only stronger aggregation of the polymer was observed showing practically no signal corresponding to the single polymer species, while revealing a HMW peak (Figure VI.4a, blue-dashed) confirming the aggregation of the polymer.

However, as mentioned in the synthetic section for **MSW$_{6\text{-Br}}$**, its derivatives proved to be non-aggregating in good solvents such as chloroform and toluene as confirmed by DLS data (Figure VI.2).[50] Therefore, more detailed studies were performed to explain the formation of aggregates by **(450-Br)$_6$**. Two main reasons were proposed: (1) THF might act as a good solvent for polymeric arms slightly worse for the MSW core, (2) the difference in polarities/solubility between the core and arms might induce the phase segregation during the purification, thus favoring the formation of stable aggregates in THF.

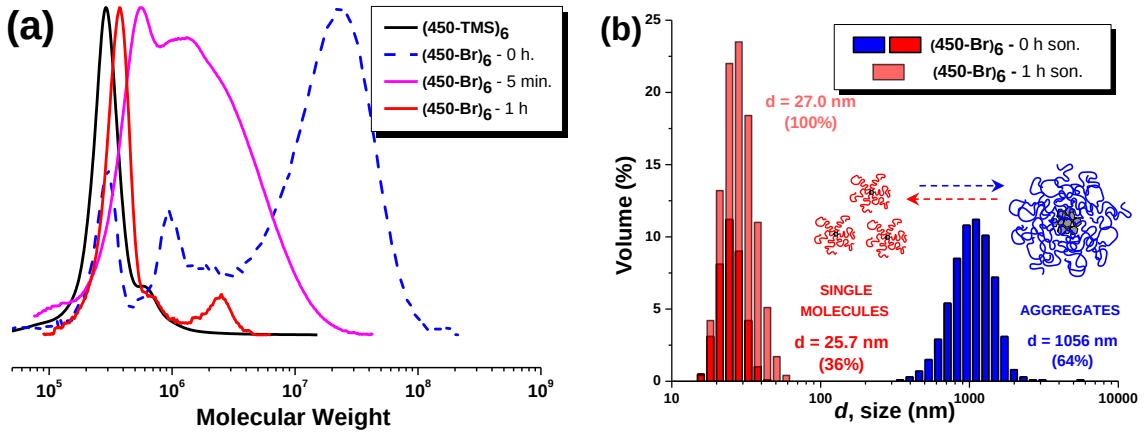

Figure VI.4 GPC traces (a) of $[P(HEMA\text{-}TMS\neg450)]_6$ (**(450-TMS)$_6$**, black), $(PBiBEM_{450})_6$ **(450-Br)$_6$**,) after drying (blue-dashed), sonication in THF for 5 min. (magenta line) and 1 h (red line). DLS analysis of b) $(PBiBEM_{450})_6$ sonicated in THF for 1 h (**(450-Br)$_6$**, pale red) and dry (**(450-Br)$_6$**, blue and red) performed in THF solutions at C = 10 mg/mL.

First, the effect of THF as a solvent on the solubility of **MSW$_{6\text{-Br}}$** was tested. THF GPC data showed an exclusive presence of single molecule species (not shown), suggesting that THF is a fairly good solvent for the core, and most likely was not the main driving force for the aggregation of **(450-Br)$_6$**. It suggested that it is the incompatibility between the hydrophobic, rigid core and flexible, more polar polymeric arms that could lead to the phase segregation and the formation of physical assemblies with the MSWs located in their centers.

In order to study the stability of **(450-Br)$_6$** aggregates, we prepared THF solutions directly from a pure, dried sample, then subjected to sonication for various periods of time, and analyzed via GPC (Figure VI.4a). As shown in Figure VI.4a (orange line), 5 min of sonication resulted in a significant shift of the HMW aggregate peak towards

lower molecular weights. A nearly complete dissociation of **(450-Br)$_6$** was obtained within 1 h of sonication (Figure VI.4a, red line). Note that no low molecular weight degradation product was detected on any of GPC traces. This behavior proved that the nature of aggregates was purely physical, and the process could be reversed by sonication without a degradation of **(450-Br)$_6$** star-shaped macroinitiators.

Additionally, dynamic light scattering (DLS) analysis of the polymer solutions in THF was performed to confirm the presence of both single molecules and physical aggregates, based on the different treatment of the solution of **(450-Br)$_6$**. Two solutions of **(450-Br)$_6$**, before (0 h) and after 1 h of sonication, were simultaneously characterized via GPC and DLS. GPC eluogram of the solution of **(450-Br)$_6$** before sonication showed only a small fraction of individual macromolecules, whereas the remaining majority stayed in the aggregated state (Figure VI,4a, blue-dashed). Such co-existence of two fractions was reflected in the bimodal size distribution observed by DLS. The analysis of the hydrodynamic radius showed two types of species, with particle sizes of 25.7 nm and 1056 nm corresponding to single molecules and polymeric aggregates respectively (Figure VI.4b, red and blue respectively). GPC trace of **(450-Br)$_6$** sonicated for 1 h (Figure VI.4a, red line) showed mainly single macromolecules, which was confirmed by the presence of a monomodal peak at Rh=27.0 nm in DLS spectra (Figure VI.4b, pale red). Additionally, a negligible change in the size distribution of single species before and after sonication (Rh=25.7 nm and 27.0 nm respectively) further proved that no detectable degradation of **(450-Br)$_6$** occurred.

The aggregation behavior of the **(450-Br)$_6$** macroinitiator was further studied by AFM and compared with the star-shaped P(HEMA-TMS) precursor (**(450-TMS)$_6$**). The images of **(450-TMS)$_6$** and **(450-Br)$_6$** were obtained from thin films on mica substrates prepared by spin-casting method (Figure VI.5). In order to determine the solvent effect on the behavior, the polymers were prepared in chloroform and in THF, and then characterized by AFM. Molecular imaging of **(450-Br)$_6$** and **(450-TMS)$_6$** samples prepared from chloroform solutions showed uniformly dispersed objects that were ascribed to single molecules (Figure VI.5a,c). On the contrary, the solutions in THF demonstrated strong molecular aggregation. As can be seen in Figure VI.5b, the **(450-Br)$_6$** sample in THF demonstrated co-existence of individual molecules, with a distinct hexa-arm shaped topology, and their aggregates as outlined in red and blue circles respectively. Association of the spoked-wheel macroinitiators in THF was even more pronounced for **(450-TMS)$_6$** resulting in the formation of large aggregates, with distinct micellar-like topology (Figure VI.5d).

The ability of **(450-Br)$_6$** to form weak, yet stable, aggregates in THF was clearly confirmed via different analyses, showing that the process can be fully reverted through sonication (Figure VI.4). AFM characterization proved the aggregation could also be disrupted when a more effective solvent, such as chloroform, was used to solubilize **(450-Br)$_6$** (Figure VI.5a,b). On the other hand, more contradictory results were obtained for **(450-TMS)$_6$**. AFM imaging indicated on a very strong tendency to of the polymer to aggregate in THF (Figure VI.5d), whereas GPC data showed only well-defined, single

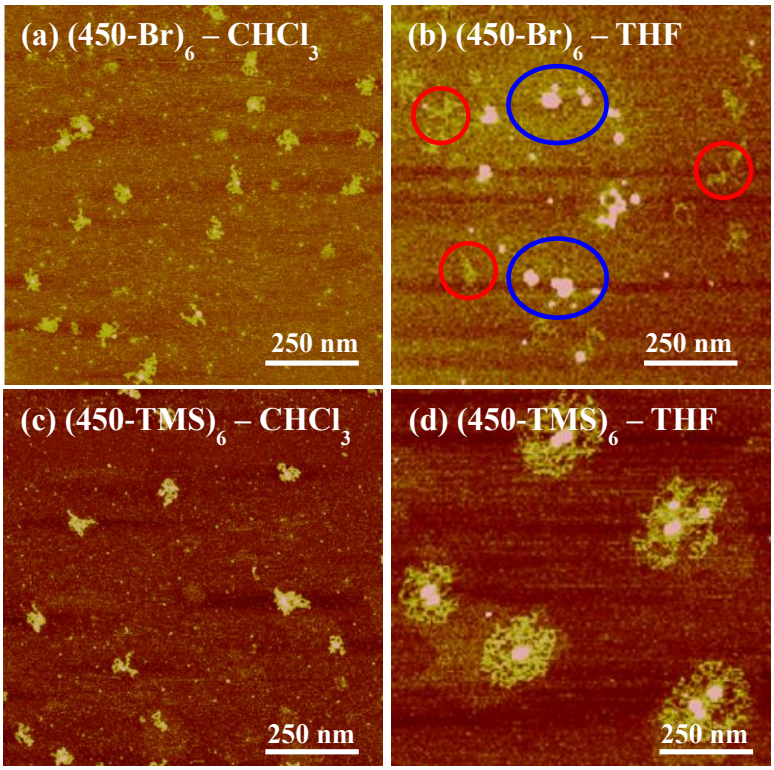

Figure VI.5 AFM height micrographs of thin films prepared by spin-casting of (450-Br)6 solutions in a) chloroform and b) THF and **(450-TMS)$_6$** solutions in c) chloroform and d) THF using mica as the substrates. The concentration of the solutions used for spin casting was ~ 0.001 mg/ml.

molecule species (Figure VI.4a, black). This could be explained by different treatments of **(450-TMS)$_6$** samples used for both analyses. The functionalization of **(450-TMS)$_6$** was performed directly from the reaction mixture without any isolating the polymer, hence the sample for GPC was withdrawn directly from the polymerization solution. On the contrary, **(450-TMS)$_6$** specimen used for AFM was purified and fully dried prior the analysis to minimize the amount of impurities on mica surface during imaging. The results for both **(450-Br)$_6$** and **(450-TMS)$_6$** indicated that the aggregation occurred during

the isolation of polymers from the solution caused by the phase-separation of polymeric arms and MSW core into micelle-like aggregates. The solvent effect determined by AFM showed that such aggregates could be disrupted in chloroform, however were fairly stable in THF and needed the additional stimuli, sonication, to reverse the process. This suggested that the later of two solvents was slightly worse for solubilizing stars with MSW core.

In order to avoid the aggregation observed during the synthesis of **(450-Br)$_6$**, the next macroinitiator, **(300-Br)$_6$**, was prepared in a slightly different manner. The polymer was purified via dialysis against THF and then stored as a solution in anisole, thus allowing for the purification of **(300-Br)$_6$** without its direct isolation. GPC analysis of the polymer showed the presence of single species without any indication of the aggregation (Figure VI.3b, red), which was maintained over the period time the solution of **(300-Br)$_6$** was used for side chain grafting,

The results of GPC, DLS and AFM analyses showed that star-shaped polymers with MSW core could form fairly weak, though stable, aggregates in THF solution due to the incompatibility between arms and the core. More importantly, the process of self-assembly was proved to be fully reversible when **(450-Br)$_6$** solution was exposed to sonication. Such properties of star-shaped polymers with MSW core might open new opportunities for their application as a new class of building blocks for the preparation of mechano-responsive, supramolecular assemblies.[66]

VI.3.4 Synthesis and Characterization of Star-shaped Bottlebrushes

Due to the tendency of **(450-Br)$_6$** to form aggregates, the solution of the polymer was sonicated prior to attempting the SCs grafting step, thus allowing for the restoration of individual macroinitiator species. Poly(*n*-butyl acrylate) (P*n*BA) side chains were grafted from **(450-Br)$_6$** using the "grafting from" approach. Two polymerizations from the **(450-Br)$_6$** were performed under normal ATRP conditions utilizing $Cu^{I}Br$/dNbpy catalyst with the ratio of [*n*BA]:[BiBEM]=[400]:[1]. The polymerizations were stopped at different monomer conversions, generating star-like bottlebrush polymers with DPs of P*n*BA grafts = 20 (**(450-*g*-20)$_6$**) and 40 (**(450-*g*-40)$_6$**). GPC analysis of **(450-*g*-20)$_6$** and **(450-*g*-40)$_6$** showed the shift of **(450-Br)$_6$** peak signal towards higher MWs (Figure VI.3a, blue and green); however some broadening of MWDs was also observed (Table VI.1, samples 3a and 3b). The higher M_w/M_n values of **(450-*g*-20)$_6$** and **(450-*g*-40)$_6$** were related to the presence of small fractions of high and/or low molecular shoulders in both GPC traces (Figure VI.3a, blue and green). The formation of high molecular weight (HMW) GPC peaks was likely due to small amounts of the residual macroinitiator aggregates that persisted during the side chains grafting as well as the possibility of the intermolecular coupling between growing macromolecules. On the other hand, the origin of the low MW (LMW) peak was not fully understood. It has been tentatively ascribed to single arms, i. e. the linear bottlebrush. It was suspected that the highly congested structure of a star-shaped bottlebrush might be inducing a spontaneous cleavage of arms from the core. The loss of an arm would lead to relaxation of the highly strained architecture of the hexa-armed bottlebrush through the reduction of the steric hindrance between their bulky arms. GPC traces of **(450-*g*-20)$_6$** and **(450-*g*-40)$_6$** showed in both

cases a presence of LMW polymers, which might indicate that the scission of arms from the highly congested core could occur in a solution for brush-stars arms with relatively short side chains.

In order to prepare a smaller star-shaped macroinitiator, shorter arms with DP=300 (**(300-TMS)$_6$**) were polymerized from **MSW$_{6\text{-}Br}$**. The reduction of the arm length should suppress the tendency of the polymer to form aggregates. The "grafting from" **(300-Br)$_6$** was performed with a higher ratio of [*n*BA]:[BiBEM]=[1400]:[1], enabling longer side chains at lower monomer conversions and diminishing an intermolecular termination. Also, dNbpy was replaced with more active ligand, PMDETA, to avoid a significant drop in the polymerization rate caused by dilution of the catalytic system. The reaction was stopped at 4.5% monomer conversion, giving P*n*BA molecular bottlebrush with average DP_{SC}=60 of side chains (**(300-*g*-60)$_6$**). The GPC characterization showed a clear shift of **(300-Br)$_6$** signal towards higher molecular weights (Figure VI.3b, blue), while keeping a low value of M_w/M_n = 1.20 (Table VI.1, sample 5). Neither low nor high molecular weight impurities were observed for **(300-g-60)$_6$**, which suggests that shorter arms (300 vs. 450) result in less steric hindrance and provide enough space for the accommodation of brushes with longer side chains. The same polymerization conditions were used to graft longer side chains, reaching 11.1% monomer conversion and thus obtaining DP_{SC}=150 of grafts (**(300-*g*-150)$_6$**).

Interestingly, when compared to **(300-*g*-60)$_6$**, the star-brush with longer side chains displayed a much broader MWD, M_w/M_n ~ 10 (Table VI.1, sample 6b) and a significant tailing towards LMWs in the GPC trace (Figure VI.3b, green). This indicated that a noticeable degradation of the material occurred during the polymerization,

suggesting that both grafts and the arm lengths contribute to the steric crowding in star-bottlebrushes, and most likely inducing a scission of arms from the MSW core.

More accurate MWD data for star-shaped bottlebrushes were obtained by using a combination of molecular imaging by AFM and the Langmuir-Blodget (LB) technique, which was shown to be particularly suitable for large branched macromolecules.[45]

VI.3.5 AFM Characterization of Star-shaped Bottlebrushes

AFM was employed to image both single molecules prepared by spin-casting and individual stars within dense monolayer prepared by the LB technique. The imaging process is greatly favored by spreading of the side chains, which increases both the persistence length of adsorbed bottlebrushes and the distance between the neighboring molecules.[5,33,67,68] Figure 3d,e depicts high resolution images of single molecules that demonstrate distinct "octopus"- and "starfish"-like (although with 6/5 arms, not 8) topologies for **(450-*g*-20)$_6$** and **(300-*g*-60)$_6$** respectively. AFM micrographs of LB monolayers of respective bottlebrushes **(450-*g*-20)$_6$**, **(450-*g*-40)$_6$**, **(300-*g*-60)$_6$,** and **(300-*g*-150)** are depicted in Figure VI.6b,c,e,f. Similar to the single molecules, star-bottlebrushes exhibit a gradual change of the conformation from a worm-like shape to a rigid rod-like shape with increasing length of the grafts. This behavior is in agreement with literature reports on an extension of the polymer backbone and the corresponding increase of the persistence length of bottlebrush macromolecules upon synthetic elongation of the side chains.[7,69]

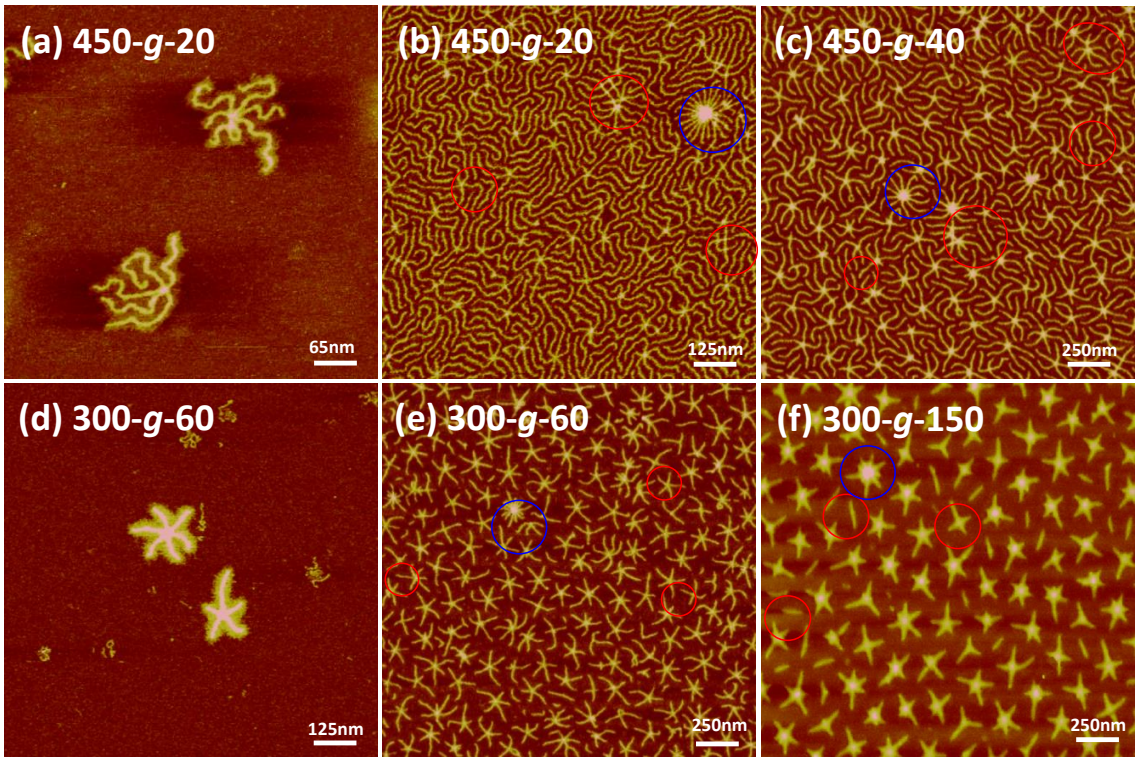

Figure VI.6 AFM height micrographs of (a) $(PBiBEM_{450}\text{-}g\text{-}PnBA_{20})_6$ (**$(450\text{-}g\text{-}20)_6$**), and (d) $(PBiBEM_{300}\text{-}g\text{-}PnBA_{60})_6$ (**$(300\text{-}g\text{-}60)_6$**) spin-cast from dilute chloroform solutions onto mica, and (b) $(PBiBEM_{450}\text{-}g\text{-}PnBA_{20})_6$ (**$(450\text{-}g\text{-}20)_6$**), (c) $(PBiBEM_{450}\text{-}g\text{-}PnBA_{40})_6$ (**$(450\text{-}g\text{-}40)_6$**), (e) $(PBiBEM_{300}\text{-}g\text{-}PnBA_{60})_6$ (**$(300\text{-}g\text{-}60)_6$**), and (f) $(PBiBEM_{300}\text{-}g\text{-}PnBA_{150})_6$ (**$(300\text{-}g\text{-}150)_6$**) prepared by Langmuir-Blodgett deposition using mica as the substrate. Blue circles indicate aggregated or/and cross-linked molecular stars, and red circles highlight structures with imperfections/missing arms/cross-links.

High resolution imaging of individual molecules by AFM was employed to characterize both molecular weight distribution (MWD) and length distribution of individual arms. Table VI.1 outlines the MWD data obtained by measuring mass per unit area from LB and number of molecules per unit area by AFM. The AFM-LB combination was shown to be particularly suitable for large branched macromolecules.[45]

As expected, the AFM-LB numbers for M_n are higher than the corresponding numbers obtained by GPC that are usually underestimated for large and branched macromolecules. Clear resolution of the individual arms enabled accurate statistical analysis of the number arm length $<L_n>$ as well as the arm length distribution $<L_w>/<L_n>$ as summarized in Table VI.2. The narrow length distributions ($<L_w>/<L_n>$~1.1) of arms in all star-shaped bottlebrushes proved the uniformity of structures, thus confirming well-controlled polymerization processes at each synthetic step (Table VI.2). In every case, arms in star-shaped bottlebrushes were extended, which was reflected in lengths of repeating units falling in the range of 0.23-0.25 nm. The values were close to the monomeric unit length in a fully extended zig-zag chain (0.25 nm) and showed and an excellent agreement of AFM results with the DPs of arms obtained from the monomer conversion by ^{1}H NMR spectroscopy (Table VI.2). However, the monomeric length of the arm in **(300-*g*-150)$_6$** is noticeably larger than 0.25 nm, which could be due to overestimation of the arm length in bottlebrushes with short arms and relatively long side chains.

AFM images also allowed clear visualization of several types of structural imperfections in the obtained star-shaped bottlebrushes (Figure VI.6). First, we observed single molecules with more than six arms (blue circles), which could be ascribed to physical aggregation of **(450-Br)$_6$** macroinitiators during the side chain grafting. Second, a few irregular structures with interconnected arms linking several star-like brushes were also noticed (blue circles). This was attributed to the coupling between growing arms of P(HEMA-TMS) stars (**(450-TMS)$_6$** and **(300-TMS)$_6$**) during ATRP processes. Third, a significant fraction of macromolecules with the number of arms lower than six (red circles) was observed which might have two origins: (i) synthetic and (ii) physical. The

less than six number of arms could be related to the limited initiation efficiency from **MSW$_{6\text{-Br}}$** initiator as reported previously for the fabrication of three- and four-armed brush polymers.[33] The second cause is mechanical cleavage of the arms due to the strong tension enhancement at the branching core of the bottlebrush stars.

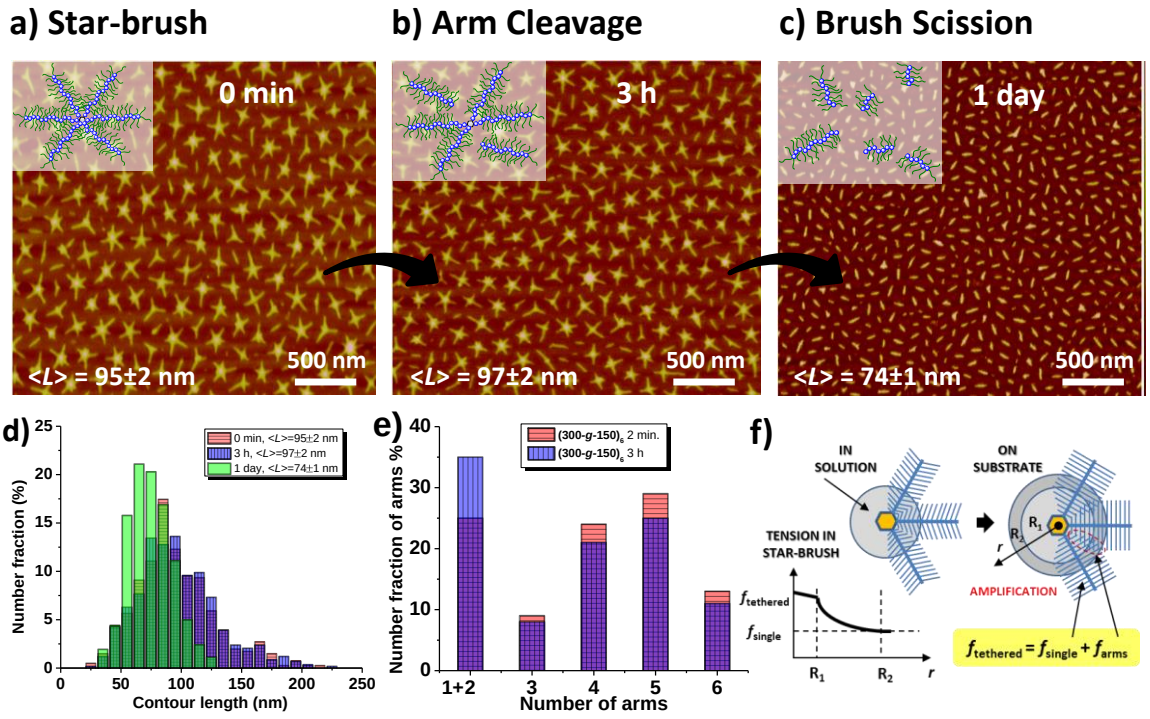

Figure VI.7 AFM height micrographs of LB films of **(300-*g*-150)$_6$** transferred from water/2-propanol (99.5/0.5 wt/wt%) surface onto mica substrates after (a) 2 min. (b), 3 h and (c) 1 day. (d) The number distribution of contour length of **(300-*g*-150)$_6$** after 2 min. (red), 3 h (blue) and 1 day (green) (More than 400 molecules counted). (e) The number fraction of objects with different number of arms. (f) A schematic representation of the side chains tapering near the core in solution and the amplification of force on the substrate.

As reported previously, bottlebrush structures are able to generate significant tension in their backbone due to steric repulsion between densely grafted side chains.[70] Depending on the side-chain length and grafting density, and the interaction with the surrounding environment (solvent, substrate, neighboring macromolecules), the backbone tension, can be amplified from the pico-Newton to nano-Newton range. Mechanical forces of this magnitude are sufficient to break covalent bonds.[7,71]

Table VI.2 AFM characterization star-bottlebrushes.

Sample	Name	$\langle L_n \rangle$ /nm[a]	$\langle L_w \rangle / \langle L_n \rangle$[b]	$DP_{arm,NMR}$	$\langle L_{mon} \rangle$/nm[c]
3a	**(450-*g*-20)$_6$**	105±3	1.09	450	0.23±0.01
3b	**(450-*g*-40)$_6$**	112±3	1.07	450	0.25±0.01
6a	**(300-*g*-60)$_6$**	69±2	1.09	300	0.23±0.01
6b	**(300-*g*-150)$_6$**	95±2	1.12	300	0.32±0.01

[a] Number average contour length of the individual arms of star-like bottlebrushes imaged by AFM. [b] Length dispersity: the ratio of weight average ($\langle L_w \rangle$) and number average ($\langle L_n \rangle$) arm lengths, determined as $\langle L_w \rangle / \langle L_n \rangle = \langle L_n^2 \rangle / \langle L_n \rangle^2$. [c] $\langle L_{mon} \rangle = \langle L_n \rangle / DP_{arm,NMR}$.

Additional amplification of bond tension occurs in tethered bottlebrushes that also exhibit gradient of tension due to steric repulsion between the neighboring bottlebrushes.[72] As shown in Figure VI.7, for the star-brush **(300-*g*-150)$_6$**, after adsorption on water/2-propanol (99.5/0.5 wt/wt%) mica surface for three hours, the number fraction of molecules with one and two arms increased from ~25% to 35%,

accompanied by the corresponding decrease in the number fractions of molecules with three, four, five and six arms, while the average length of arms hardly changed. This indicates that bottlebrush stars undergo preferential cleavage of the arms from the MSW core. After 24 hours, there were almost no molecules with multiple arms remained. In addition, the average arm length decreased by ~20 nm, suggesting scission of covalent bonds in the backbone of individual bottlebrush arms, which occurred at a slower rate than the arm cleavage process.

The preferential cleavage of the arms was ascribed to stronger steric repulsion of neighboring arms at the MSW core (Figure VI.7f). In addition, the ester bond connecting the core and the arm could be more vulnerable than C-C bonds under aqueous conditions,[70] which might also favor the cleavage of the arms. In contrast, neither the cleavage of the arms nor the backbone scission within the arms was observed for the star-brushes with shorter side chains within 24 hours, i.e., **(450-*g*-20)$_6$**, **(450-*g*-40)$_6$** and **(300-*g*-60)$_6$** (Figure VI.8). This was due to the short grafts that were not able to generate large enough tension along the backbone to break a covalent bond. Figure VI.8 shows the number fraction distribution of molecules with different number of arms after adsorption on water/2-propanol (99.5/0.5 wt/wt%) mica surface for 2 min. and 21, 20 and 12 hours, for **(450-*g*-20)$_6$**, **(450-*g*-40)**$_6$ and **(300-*g*-60)$_6$** respectively. No cleavage of the arms or the backbone scission was observed for those star-brushes.

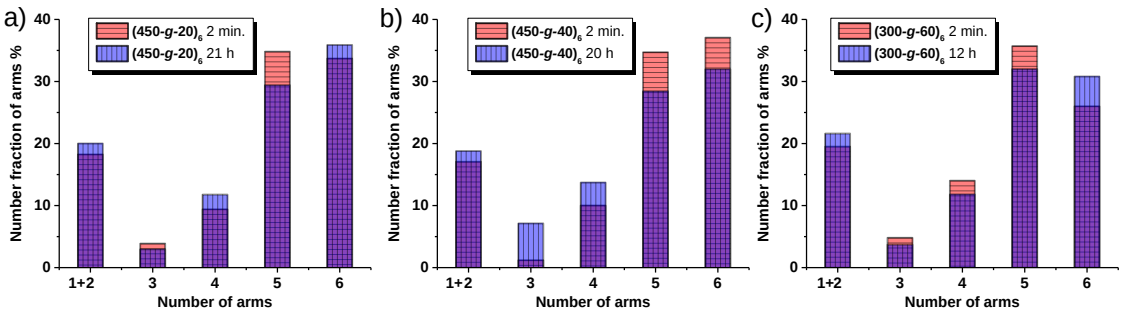

Figure VI.8 The number fraction of objects with different number of arms in star-brushes: (a) **(450-*g*-20)$_6$**, (b) **(450-*g*-40)$_6$** and (c) **(300-*g*-60)$_6$**.

VI.4 Conclusions

In conclusion, a rational design of a rigid, well-defined MSW hexa-ATRP initiator allowed for the preparation of polymeric materials with novel properties, allowing for focusing tension to specific bonds and potentially selective bond activation/scission. Star-shaped bottlebrushes were synthesized via the combination of advanced synthetic methods and ATRP. Side chains were grafted from star-shaped macroinitiators yielding the following polymers: **(450-*g*-20)$_6$**, **(450-*g*-40)$_6$**, **(300-*g*-60)$_6$** and **(300-*g*-150)$_6$**.

AFM imaging of such architectures confirmed the unusual ‘starfish’ and ‘octopus’-like topologies of star-brush polymers, proving the successful synthesis of these complex polymeric architectures. During the synthesis, it was discovered that PBiBEM macroinitiators **(450-Br)$_6$** demonstrate a strong tendency to form physical aggregates through the hydrophobic interactions of MSW cores. The association process was prevented by sonication of polymer solutions prior to the analysis and brush synthesis. Reported star-like brush polymers represent a new class of polymers that integrate the

properties of both bottlebrushes and molecular spoked wheels. The cleavage of the arms from the MSW core occurred preferentially, which may shed light on the design of molecular tensile machines that can focus mechanical tension on specific bonds.

VI.5 References

(1) Webster, O. W. *Science* **1991**, *251*, 887-893.

(2) Hawker, C. J.; Wooley, K. L. *Science* **2005**, *309*, 1200-1205.

(3) Braunecker, W. A.; Matyjaszewski, K. *Progr. Polym. Sci.* **2007**, *32*, 93-146.

(4) Beers, K. L.; Gaynor, S. G.; Matyjaszewski, K.; Sheiko, S. S.; Moeller, M. *Macromolecules* **1998**, *31*, 9413-9415.

(5) Sheiko, S. S.; Prokhorova, S. A.; Beers, K. L.; Matyjaszewski, K.; Potemkin, I. I.; Khokhlov, A. R.; Moeller, M. *Macromolecules* **2001**, *34*, 8354-8360.

(6) Zhang, M.; Mueller, A. H. E. *Journal of Polymer Science, Part A: Polymer Chemistry* **2005**, *43*, 3461-3481.

(7) Sheiko, S. S.; Sun, F. C.; Randall, A.; Shirvanyants, D.; Rubinstein, M.; Lee, H.-i.; Matyjaszewski, K. *Nature* **2006**, *440*, 191-194.

(8) Sheiko, S. S.; Sumerlin, B. S.; Matyjaszewski, K. *Prog. Polym. Sci.* **2008**, *33*, 759-785.

(9) Gao, H.; Matyjaszewski, K. *Prog. Polym. Sci.* **2009**, *34*, 317-350.

(10) Lee, H.-i.; Pietrasik, J.; Sheiko, S. S.; Matyjaszewski, K. *Prog. Polym. Sci.* **2010**, *35*, 24-44.

(11) Tang, C.; Dufour, B.; Kowalewski, T.; Matyjaszewski, K. *Macromolecules* **2007**, *40*, 6199-6205.

(12) Lecommandoux, S.; Chécot, F.; Borsali, R.; Schappacher, M.; Deffieux, A.; Brulet, A.; Cotton, J. P. *Macromolecules* **2002**, *35*, 8878-8881.

(13) Neugebauer, D.; Zhang, Y.; Pakula, T.; Matyjaszewski, K. *Macromolecules* **2005**, *38*, 8687-8693.

(14) Gao, H.; Matyjaszewski, K. *Journal of the American Chemical Society* **2007**, *129*, 6633-6639.

(15) Cheng, G.; Boeker, A.; Zhang, M.; Krausch, G.; Mueller, A. H. E. *Macromolecules* **2001**, *34*, 6883-6888.

(16) Boerner, H. G.; Beers, K.; Matyjaszewski, K.; Sheiko, S. S.; Moeller, M. *Macromolecules* **2001**, *34*, 4375-4383.

(17) Sumerlin, B. S.; Neugebauer, D.; Matyjaszewski, K. *Macromolecules* **2005**, *38*, 702-708.

(18) Matyjaszewski, K.; Tsarevsky, N. V. *Journal of the American Chemical Society* **2014**, *136*, 6513-6533.

(19) Matyjaszewski, K.; Xia, J. *Chem. Rev.* **2001**, *101*, 2921-2990.

(20) Matyjaszewski, K.; Tsarevsky, N. V. *Nat. Chem.* **2009**, *1*, 276-288.

(21) Huang, K.; Rzayev, J. *Journal of the American Chemical Society* **2009**, *131*, 6880-6885.

(22) Li, Z.; Zhang, K.; Ma, J.; Cheng, C.; Wooley, K. L. *Journal of Polymer Science, Part A: Polymer Chemistry* **2009**, *47*, 5557-5563.

(23) Zehm, D.; Laschewsky, A.; Liang, H.; Rabe, J. P. *Macromolecules* **2011**, *44* 9635-9641.

(24) Stals, P. J. M.; Li, Y.; Burdyńska, J.; Nicolaÿ, R.; Nese, A.; A., A. R.; Palmans; Meijer, E. W.; Matyjaszewski, K.; Sheiko, S. S. *Journal of the American Chemical Society* **2013**, *135*, 11421-11424.

(25) Lee, H.-i.; Jakubowski, W.; Matyjaszewski, K.; Yu, S.; Sheiko, S. S. *Macromolecules* **2006**, *39*, 4983-4989.

(26) Rzayev, J. *Macromolecules* **2009**, *42*, 2135-2141.

(27) Bolton, J.; Bailey, T. S.; Rzayev, J. *Nano Lett.* **2011**, *11*, 998-1001.

(28) Miyake, G. M.; Piunova, V. A.; Weitekamp, R. A.; Grubbs, R. H. *Angew. Chem. Int. Ed.* **2012**, *51*, 11246-11248.

(29) Sveinbjörnsson, B. R.; Weitekamp, R. A.; Miyake, G. M.; Xia, Y.; Atwater, H. A.; Grubbs, R. H. *Proc. Natl. Acad. Sci* **2012**, *109*, 14332-14336.

(30) Yu-Su, S. Y.; Sheiko, S. S.; Lee, H.-i.; Jakubowski, W.; Nese, A.; Matyjaszewski, K.; Anokhin, D.; Ivanov, D. A. *Macromolecules* **2009**, *42* 9008-9017.

(31) Lee, H.-i.; Matyjaszewski, K.; Yu, S.; Sheiko, S. S. *Macromolecules* **2005**, *38*, 8264-8271.

(32) Elsen, A. M.; Li, Y.; Li, Q.; Sheiko, S. S.; Matyjaszewski, K. *Macromol. Rapid Commun.* **2014**, *35*, 133-140.

(33) Matyjaszewski, K.; Qin, S.; Boyce, J. R.; Shirvanyants, D.; Sheiko, S. S. *Macromolecules* **2003**, *36*, 1843-1849.

(34) Zhang, Y.; Constantini, N.; Mierzwa, M.; Pakula, T.; Neugebauer, D.; Matyjaszewski, K. *Polymer* **2004**, *45*, 6333-6339.

(35) Pakula, T.; Zhang, Y.; Matyjaszewski, K.; Lee, H.-i.; Boerner, H.; Qin, S.; Berry, G. C. *Polymer* **2006**, *47*, 7198-7206.

(36) Miyake, G. M.; Weitekamp, R. A.; Piunova, V. A.; Grubbs, R. H. *Journal of the American Chemical Society* **2012**, *134*, 14249-14254.

(37) Chen, P.; Li, C.; Liu, D.; Li, Z. *Macromolecules* **2012**, *45*, 9579-9584.

(38) Ding, J.; Xiao, C.; Tang, Z.; Zhuang, X.; Chen, X. *Macromol. Biosci.* **2011**, *11*, 192-198.

(39) Ding, J.; Xiao, C.; Zhao, L.; Cheng, Y.; Ma, L.; Tang, Z.; Zhuang, X.; Chen, X. *Journal of Polymer Science, Part A: Polymer Chemistry* **2012**, *49*, 2665-2676.

(40) Wu, D.; Nese, A.; Pietrasik, J.; Yeru Liang, M. K.; Huang, L.; Kowalewski, T.; Matyjaszewski, K. *ACS Nano* **2012**, *6*, 6208-6214.

(41) Sun, G.; Cho, S.; Clark, C.; Verkhoturov, S. V.; Eller, M. J.; Li, A.; Pavía-Jiménez, A.; Schweikert, E. A.; Thackeray, J. W.; Trefonas, P.; Wooley, K. L. *Journal of the American Chemical Society* **2013**, *135*, 4203–4206.

(42) Hong, S. W.; Gu, W.; Huh, J.; Sveinbjornsson, B. R.; Jeong, G.; Grubbs, R. H.; Russell, T. P. *ACS Nano* **2013**, *7*, 9684–9692.

(43) Boyce, J. R.; Shirvanyants, D.; Sheiko, S. S.; Ivanov, D. A.; Qin, S.; Börner, H.; Matyjaszewski, K. *Langmuir* **2004**, *20*, 6005-6011.

(44) Iyoda, M.; Yamakawa, J.; Rahman, M. J. *Angew. Chem. Int. Ed.* **2011**, *50*, 10522.

(45) Höger, S. *Pure Appl. Chem.* **2010**, *82*, 821.

(46) Haley, M. *Pure Appl. Chem.* **2008**, *80*, 519.

(47) Zhang, W.; Moore, J. S. *Angew. Chem. Int. Ed.* **2006**, *45*, 4416.

(48) Bunz, U. H. F.; Rubin, Y.; Tobe, Y. *Chem Soc. Rev.* **1999**, *28*, 107.

(49) Mössinger, D.; Hornung, J.; Lei, S.; De Feyter, S.; Höger, S. *Angew. Chem. Int. Ed.* **2007**, *46*, 6802-6806.

(50) Aggarwal, V.; Thiessen, A.; Idelson, A.; Kalle, D.; Würsch, D.; Stangl, T.; Steiner, F.; Jester, S.-S.; Vogelsang, J.; Höger, S.; Lupton, J. M. *Nat. Chem.* **2013**, *5*, 964-970.

(51) Mössinger, D.; Chaudhuri, D.; Kudernac, T.; Lei, S.; De Feyter, S.; Lupton, J. M.; Höger, S. *Journal of the American Chemical Society* **2010**, *132*, 1410-1423.

(52) Lei, S.; Ver Heyen, A.; De Feyter, S.; Surin, M.; Lazzaroni, R.; Rosenfeldt, S.; Ballauff, M.; Lindner, P.; Mössinger, D.; Höger, S. *Chem. Eur. J.* **2009**, *15*, 2518-2535.

(53) Höger, S.; Tahara, K.; Lei, S.; Mössinger, D.; Kozuma, H.; Inukai, K.; Van der Auweraer, M.; De Schryver, F. C.; Tobe, Y.; De Feyter, S. *Chem. Commun.* **2008**, 3897-3899.

(54) Schwartz, B. J. *Nat. Mater.* **2008**, *7*, 427-428.

(55) Schwartz, B. J. *Annu. Rev. Phys. Chem.* **2003**, *54*, 141-172.

(56) Dawn, S.; Dewal, M. B.; Sobransingh, D.; Paderes, M. C.; Wibowo, A. C.; Smith, M. D.; Krause, J. A.; Pellechia, P. J.; Shimizu, L. S. *Journal of the American Chemical Society* **2011**, *133*, 7025.

(57) Aggarwal, A. V.; Jester, S.-S.; Taheri, S. M.; Förster, S.; Höger, S. *Chem. Eur. J.* **2013**, *19*, 4480-4495.

(58) Mössinger, D.; Chaudhuri, D.; Kudernac, T.; Lei, S. D. F., S.; Lupton, J. M.; Höger, S. *Journal of the American Chemical Society* **2010**, *132*, 1410-1423.

(59) Li, Y.; Nese, A.; Hu, X.; Lebedeva, N. V.; LaJoie, T. W.; Burdyńska, J.; Stefan, M. C.; You, W.; Yang, W.; Matyjaszewski, K.; Sheiko, S. S. *ACS Macro Lett.* **2014**, *3*, 738-742.

(60) Matyjaszewski, K.; Shipp, D. A.; Wang, J.-L.; Grimaud, T.; Patten, T. E. *Macromolecules* **1998**, *31*, 6836-6840.

(61) Neugebauer, D.; Zhang, Y.; Pakula, T.; Sheiko, S. S.; Matyjaszewski, K. *Macromolecules* **2003**, *36*, 6746-6755.

(62) Gohy, J.-F.; Chiper, M.; Guillet, P.; Fustin, C.-A.; Hoeppener, S.; Winter, A.; Hoogenboom, R.; Schubert, U. S. *Soft Matter* **2009**, *5*, 2954-2961.

(63) Radzilowski, L. H.; Stupp, S. I. *Macromolecules* **1994**, *27*, 7747-7753.

(64) Stupp, S. I.; LeBonheur, V.; Walker, K.; Li, L. S.; Huggins, K. E.; Keser, M.; Amstutz, A. *Science* **1997**, *276*, 384-389.

(65) Rosselli, S.; Ramminger, A.-D.; Wagner, T.; Lieser, G.; Höger, S. *Chem. Eur. J.* **2003**, *9*, 3481-3491.

(66) Zhao, J.; Pispas, S.; Zhang, G. *Macromol. Chem. Phys.* **2009**, *210*, 1026-1032.

(67) Borner, H. G.; Duran, D.; Matyjaszewski, K.; da Silva, M.; Sheiko, S. S. *Macromolecules* **2002**, *35*, 3387-3394.

(68) Pietrasik, J.; Sumerlin, B. S.; Lee, H.-i.; Gil, R. R.; Matyjaszewski, K. *Polymer* **2007**, *48*, 496-501.

(69) Elli, S.; Ganazzoli, F.; Timoshenko, E. G.; Kuznetsov, Y. A.; Connolly, R. *J. Chem. Phys.* **2004**, *120*, 6257-6267.

(70) Schmidt, S. W.; Kersch, A.; Beyer, M. K.; Clausen-Schaumann, H. *Phys. Chem. Chem. Phys.* **2011**, *13*, 5994-5999.

(71) Lebedeva, N. V.; Nese, A.; Sun, F. C.; Matyjaszewski, K.; Sheiko, S. S. *Proc. Natl. Acad. Sci* **2012**, *109*, 9276-9280.

(72) Sheiko, S. S.; Panyukov, S.; Rubinstein, M. *Macromolecules* **2011**, *44* 4520-4529.

(73) Sheiko, S. S.; daSilva, M.; Shirvaniants, D. G.; LaRue, I.; Prokhorova, S. A.; Beers, K.; Matyjaszewski, K. *J. Am. Chem. Soc.* **2003**, *125*, 6725-6728.

SECTION IV

BIO-INSPRED GRAFT COPOLYMERS

CHAPTER VII

BIO-INSPIRED ARTIFICIAL LUBRICANTS

Preface

For many years biological macromolecules have been an inspiration to scientists. Among various biomacromolecules present in nature there is a group known as proteoglycans. Proteoglycans have a graft-like topology and comprise of a linear protein-based core with glycosaminoglycan chains loosely attached to it. Those brush-like biomolecules are abundant in human body and perform a variety of crucial roles, such as cell signaling and surface protection, lung clearance as well as the lubrication of joints. Recent work done by our collaborator, prof. Jacob Israelachvili from UCSB, has shown that another brush-like protein, Lubricin, is abundant in synovial liquid and is a crucial component allowing for a successful joint lubrication.

After the discussion with prof. Israelachvili, we decided to design of a bottlebrush polymer, whose architecture closely mimics that of Lubricin. I designed and synthesized of polymeric materials, and characterized them via GPC and ^{1}H NMR analyses. Dr. Xavier Banquy performed all surface forces apparatus (SFA) measurements, as well as

AFM characterization of the hydrophilic bottlebrush. Dr. Yuanchao Li from UNC did AFM imaging of the hydrophobic bottlebrush. Combined efforts provided us with very exciting results, showing that synthetic bottlebrushes could not only successfully mimic the lubrication behavior of Lubricin, but also outperform it by showing lower frictions at much higher loads. In addition, we were able to extend the idea to organic solvent-based systems, which exhibited even lower friction coefficients at the same pressure as the water-soluble bottlebrush.

VII.1 Introduction

This report describes the development of a multi-block polymer whose architecture was inspired from a protein known as lubricin (LUB), a major component of mammalian synovial fluids.[1] Studies have shown that LUB is a key element for providing excellent lubrication, anti-adhesion and wear protection to articular cartilage surfaces.[2-4] These unique properties arise from the highly complex architecture of the protein, known as "bottle-brush". As for many other mucins, lubricin can self-associate to form a highly interconnected network. It can also form dimers or multimers whose conformation on a surface can be described as a loop.[3,5] It is this particular conformation in combination with its bottlebrush architecture that is believed to provide the excellent tribological properties to this protein.

A key requirement for a good lubricant is to reduce the friction force or friction coefficient between shearing surfaces independently over a wide range of shearing speeds, applied loads and contact areas. Such a combination of properties is often called Amontons-like behavior and is often observed in solid contacts but rarely in lubricated ones. The lubrication effect in many systems, such as LUB[3] or synthetic polymer/molecular brushes[6,7] has been shown to operate independently of the contact area and/or the shearing speed, but only in a narrow range of applied loads/pressures and shear rates.

On the other hand, lubricating systems, such as linear polymer loops, which is also the conformation adopted by LUB, are poor lubricants, or at least not better than polymer brushes, especially under high (MPa) loads.[8,9] The main reason for this poor

behavior is the ability of polymer loops to easily bridge surfaces and to increase the adhesion between them as well as the much slower dynamics of the loop segments which tends to increase frictional dissipation under high sliding speeds.

In an effort to fill this technological gap, a polymer mimic of LUB was designed. The polymer architecture was based on a triblock polymer with a bottlebrush central block (Figure VII.1) and two lateral linear blocks designed to provide strong adhesion to the surfaces it adsorbs to. The arrangement of the three different blocks was expected to promote the formation of polymer loops when adsorbed on surfaces.

VII.2 Experimental

Materials. Methyl methacrylate (MMA, 99%, Aldrich), 2-(trimethylsilyloxy)ethyl methacrylate (HEMA-TMS, Scientific Polymer Products, Inc.) and 2-(dimethylamino)ethyl methacrylate (DMAEMA, 98%, Aldrich) were passed through a column filled with basic alumina prior to use. 2-Methacryloyloxyethyl phosphorylcholine (MPC, 97%, Aldrich) was recrystallized from acetonitrile and dried under vacuum overnight at room temperature before polymerization. Copper(I) bromide ($Cu^{I}Br$, 99.999%, Aldrich), copper(II) bromide ($Cu^{II}Br_2$, 99.999%, Aldrich), copper(I) chloride ($Cu^{I}Cl$, ≥99.995% trace metals basis, Aldrich), copper(II) chloride ($Cu^{II}Cl_2$, ≥99.995% trace metals basis, anhydrous, Aldrich), 2,2′-bipyridyl (bpy, 99%, Aldrich), 4,4′-Dinonyl-2,2′-dipyridyl (dNbpy, 97%, Aldrich), potassium fluoride (KF, 99%, spray-dried, Aldrich), tetrabutylammonium fluoride (TBAF, 1M solution in THF, Aldrich), α-bromoisobutyryl bromide (98%, Aldrich), bromoethane (98%, Aldrich), and tributyltin

hydride (97%, Aldrich) were used without any additional purification. Tris(2-pyridylmethyl)amine (TPMA)[10] and ethylene bis(2-bromoisobutyrate) (diBr)[11] were synthesized according to previously published procedures. THF was tapped off a solvent purification column, and all other solvents were used as received.

Equipment and Analysis. Proton nuclear magnetic resonance (^{1}H NMR) spectroscopy was performed using Bruker 300 MHz spectrometer. In all cases deuterated chloroform ($CDCl_3$) was used as a solvent, except for **pMPC ABA** where deuterated methanol (CD_3OD) was used instead. ^{1}H chemical shifts are reported in ppm downfield from tetramethylsilane (TMS). Apparent molecular weights and molecular weight distributions measurements of polymers were measured by size exclusion chromatography (SEC) using Polymer Standards Services (PSS) columns (guard, 10^5, 10^3, and 10^2 Å), with THF or DMF as eluent at 35 °C at a constant flow rate of 1.00 mL/min, and differential refractive index (RI) detector (Waters, 2410). The apparent number-average molecular weights (M_n) and molecular weight distribution ($Đ$) were determined with a calibration based on linear poly(methyl methacrylate) (PMMA) standards and diphenyl ether as an internal standard.

Synthesis of poly[(HEMA-TMS)$_{400}$-*stat*-PMMA$_{400}$) (B).[11-13] A dry 25 mL Schlenk flask was charged with diBr (0.0083 g, 0.023 mmol), $Cu^{II}Br_2$ (0.0061 g, 0.028 mmol), dNbpy (0.1127 g, 0.276 mmol), HEMA-TMS (9.28g, 10.0 mL, 45.9 mmol), MMA (4.59 g, 4.9 mL, 45.9 mmol) and anisole (3.0 mL). The solution was degassed by three freeze-pump-thaw cycles. During the final cycle, the flask was filled with nitrogen and $Cu^{I}Br$ (0.0158 g, 0.110 mmol) was quickly added to the frozen reaction mixture. The flask was sealed, evacuated and back-filled with nitrogen five times, and then immersed in an oil bath at 40

°C. Reaction was stopped after 12 h 30 min. via exposure to air, reaching the degree of polymerization of the product 800. The monomers consumption was calculated by the integration of MMA and HEMA-TMS vinyl groups signal (C*H*H=C-CH_3, 6.11 ppm or 5.56 ppm) against the internal standard (anisole, *o*,*p*-Ar-H, 6.91 ppm). The product **B** was purified by three precipitations from methanol, dried under vacuum for 16 h at room temperature, and analyzed by ^{1}H NMR spectroscopy. The ratio of PMMA (*s*, broad, CO-O-CH_3, 3.54-3.68 ppm) to P(HEMA-TMS) (*s*, broad, O-Si(CH_3)$_3$, 0.11-0.21 ppm) peaks resulted in the polymer composition, P(HEMA-TMS)$_{400}$-co-PMMA$_{400}$. Apparent molecular weights were determined using THF SEC: M_n = 88,700; $Đ$ = 1.19.

Synthesis of poly[(DMAEMA$_{95}$-*stat*-MMA$_{90}$)-*b*-(HEMA-TMS$_{400}$-*stat*-MMA$_{400}$)-*b*-(DMAEMA$_{95}$-*stat*-MMA$_{90}$)] (ABA).[14,15] A dry 10 mL Schlenk flask was charged with **B** (1.05 g, 0.0088 mmol), $Cu^{II}Cl_2$ (as a stock solution, 0.59 mg, 4.4 μmol), dNbpy (0.0358 g, 0.0875 mmol), DMAEMA (2.20 g, 2.4 mL, 14.0 mmol), MMA (1.40 g, 1.5 mL, 14.0 mmol) and anisole (3.9 mL). The solution was degassed by three freeze-pump-thaw cycles. During the final cycle, the flask was filled with nitrogen and $Cu^{I}Cl$ (0.0037 g, 0.0376 mmol) was quickly added to the frozen reaction mixture. The flask was sealed, evacuated and back-filled with nitrogen five times, and then immersed in an oil bath at 60 °C. Reaction was stopped after 46 h 45 min. via exposure to air. The product was precipitated from hexanes (twice) and water, re-dissolved in chloroform and passed through neutral alumina. The solvent was removed and the purified product was dried overnight under vacuum at room temperature. The ^{1}H NMR spectra of a pure **ABA** was used to evaluate its final composition, giving poly[(DMAEMA$_{95}$-*stat*-MMA$_{90}$)-*b*-(HEMA-TMS$_{400}$-*stat*-MMA$_{400}$)-*b*-(DMAEMA$_{95}$-*stat*-MMA$_{90}$). The structure of the

polymer was determined from the ratio of selected polymer signals: PMMA (*s*, broad, CO-O-CH_3, 3.54-3.68 ppm), P(HEMA-TMS) (*s*, broad, O-Si(CH_3)$_3$, 0.11-0.21 ppm) and PDMAEMA (*m*, CH_2-NMe_2, 2.55-2.65 ppm). Apparent molecular weights were obtained using DMF SEC: M_n=99,500 and $Đ$=1.56.

Chain-end removal from poly[(DMAEMA$_{95}$-*stat*-MMA$_{90}$)-*b*-(HEMA-TMS$_{400}$-*stat*-MMA$_{400}$)-*b*-(DMAEMA$_{95}$-*stat*-MMA$_{90}$)] (ABA-H).[16] ABA polymer (2.00 g, 0.012 mmol), tributyltin hydride (0.364 g, 0.34 mL, 0.196 mmol), tris(2-pyridylmethyl)amine (0.0073 g, 0.025 mmol), and anisole (12.0 mL) were placed in a 10 ml Schlenk flask. The reaction mixture was deoxygenated by two freeze–pump–thaw cycles. During the last cycle CuBr (0.0018 g, 0.0125 mmol) was added to the frozen mixture. The flask was sealed, evacuated and back-filled with nitrogen four times. The reaction mixture was thawed and stirred at room temperature for 24 h. The polymer, **ABA-H**, was purified by dialysis against THF:MeOH (2:1) for 48 h using tubes with a pore size molar mass cut off 50,000 kDa. Molecular weights were determined by using DMF SEC: M_n=186,000 and $Đ$=1.23.

Synthesis of poly[(qDMAEMA$_{95}$-*stat*-MMA$_{90}$)-*b*-(HEMA-TMS$_{400}$-*stat*-MMA$_{400}$)-*b*-(DMAEMA$_{95}$-*stat*-MMA$_{90}$)] (qABA).[17] ABA-H (0.4300 g, 0.0026 mmol) was placed in 20 mL vial and dissolved in acetone (15 mL). The solution was cooled in an ice bath to 0 °C, followed by a slow addition of bromoethane (0.47 g, 0.32mL, 4.3 mmol). The reaction was stirred at room temperature for the next 48 h. The solvent was removed and the product was dried under vacuum at room temperature. ^{1}H NMR spectra of the product, **qABA**, showed the quantitative quaternization of -NMe_2 groups, as confirmed by the disappearance of signals corresponding to methylene (CH_2-NMe_2, 2.55-2.65 ppm)

and methyl groups (*m*, CH_2-N(CH_3)$_2$, 2.27-2.35) of PDMAEMA. Apparent molecular weights were determined using DMF SEC: M_n=105,000 and $Đ$=1.36.

Synthesis of poly[(qDMAEMA$_{95}$-*stat*-MMA$_{90}$)-*b*-(BiBEM$_{400}$-*stat*-MMA$_{400}$)-*b*-(DMAEMA$_{95}$-*stat*-MMA$_{90}$)] (qABA MI).[11-13] The polymer, **qABA** (0.1840 g, 0.98 μmol of polymer; 0.0754 g, 0.3773 mmol of HEMA-TMS units), potassium fluoride (0.031 g, 0.526 mmol) and 2,6-di-*tert*-butylphenol (0.0090 g, 0.0439 mmol) were placed in a 20 ml round bottom flask. The flask was sealed, flushed with nitrogen, and dry THF (7 mL) was added. The mixture was cooled in an ice bath to 0 °C, tetrabutylammonium fluoride solution in THF (1M, 0.44 mL, 0.44 mmol) was injected to the flask, followed by the drop-wise addition of 2-bromoisobutyryl bromide (0.121 g, 65 μL, 0.526 mmol). After the addition the reaction mixture was allowed to reach room temperature and stirring was continued for 24 h. The solids were filtered off, and the solution was precipitated into methanol:water (70:30, v/v%). The precipitate was re-dissolved in chloroform and passed through a short column filled with basic alumina. The filtrate was re-precipitated three times from chloroform into hexanes and dried under vacuum overnight at room temperature. Apparent molecular weights were determined using THF SEC: M_n=198,000 and $Đ$=1.24.

Synthesis of poly{(qDMAEMA$_{95}$-*stat*-MMA$_{90}$)-*b*-[(BiBEM$_{400}$-*g*-MPC$_{45}$)-*stat*-MMA$_{400}$]-*b*-(DMAEMA$_{95}$-*stat*-MMA$_{90}$)] (pMPC ABA).[18] A dry 5 mL Schlenk flask was charged with polymer **qABA MI** (1.6 mg, 0.0074 μmol of polymer; 0.8 mg, 2.8 μmol of BiBEM), 2-methacryloyloxyethyl phosphorylcholine (0.254 g, 0.860 mmol), 2,2'-bipyridyl (1.5 mg, 0.97 μmol), copper (II) chloride (as a stock solution, 0.077 mg, 0.57 μmol), and methanol (1.0mL). The solution was degassed by three freeze-pump-

thaw cycles. After the final cycle copper (I) chloride (43.4 μmol/mL stock solution, 0.1 mL, 0.43 mg, 4.3 μmol) was added to the thawed reaction mixture under nitrogen atmosphere, and the flask was immersed in an oil bath thermostated at 50 °C. The reaction was stopped after 5 h 30 min. by expositing the solution to air, achieving the **PMPC ABA** brush. The resulting brush was purified by dialysis against MeOH for 48 h using tubes with a pore size molar mass cut off 50,000 kDa. The Monomer conversion was calculated by ^{1}H NMR analysis, resulting in the average degree of polymerization of the side chains, DP~45. Apparent molecular weights were not determined as polymer was soluble neither in THF nor in DMF.

Synthesis of poly{(qDMAEMA$_{95}$-*stat*-MMA$_{90}$)-*b*-[(BiBEM$_{400}$-*g*-*t*BA$_{30}$)-*stat*-MMA$_{400}$]-*b*-(DMAEMA$_{95}$-*stat*-MMA$_{90}$)] (p*t*PA ABA). A dry 25 mL Schlenk flask was charged with polymer **qABA MI** (0.26 g of the polymer; 0.13 g, 0.34 mmol of BiBEM), *tert*-butyl acrylate (17.5 g, 136 mmol), dNbpy (0.14 g, 0.34 mmol), copper (II) bromide (1.9 mg, 8.5 μmol), and anisole (2.2 mL). The solution was degassed by three freeze-pump-thaw cycles. After the final cycle copper (I) bromide (23.2 mg, 162 μmol) was added to the frozen reaction mixture under nitrogen atmosphere. The flask was sealed, evacuated and back-filled with nitrogen five times, and then immersed in an oil bath at 60 °C. Reaction was stopped after 17 h via exposure to air, reaching 7.4% monomer conversion, which corresponded to DP of SCs 30. The polymer was purified via three precipitations from methanol:water mixture (70:30 v/v) and dried under vacuum overnight. Apparent molecular weights were determined using THF SEC: $M_n = 2.94 \cdot 10^5$; $Đ = 1.19$.

AFM imaging

AFM imaging was performed on a MFP 3D from Asylum in standard tapping mode in air. Silicon tips (on nitride cantilever) with a resonance frequency of 50-90 kHz and a spring constant of ~0.4 N/m were used. The samples were prepared by depositing a droplet of polymer on a mica substrate. After one hour of adsorbtion, the remnant polymer solution was gently removed and the surface was carefully rinsed with water.

SFA experiments

Materials. Ruby mica sheets were purchased from S& J Trading Inc. (Glen Oaks, NY, USA). MilliQ quality water. Milli-Q quality water was obtained from a Millipore Gradient A 10 purification system (resistance 18.2 MΩ.cm, TOC: 4 ppb). Phosphate buffer saline was purchased from Sigma Aldrich.

Surface Forces Measurements: Normal Interaction Forces. Measurements of the normal interaction forces $F_{\perp}$ between two opposing surfaces as a function of the separation distance were carried out using a Surface Forces Apparatus SFA 2000.[19] The normal interaction force $F_{\perp}$ is determined by measuring the deflection of the spring cantilever (spring constant of 1000 N/m) that supports the lower surface. The distance between the surfaces is measured using Multiple Beam Interferometry (MBI).[20]

A white light beam is shined through the surfaces and the interference fringes generated from the reflections of the light beam between the two back-silvered mica sheets are analyzed in a spectrometer equipped with a digital camera (Hamamatsu Orca® 03G, USA). The separation distance *D* between the surfaces is calculated (to ±1 Å) from the

wavelength of the interference fringes (also called fringes of equal chromatic order, FECO).

Back-silvered mica surfaces were glued silver side down on glass cylindrical disks (curvature of 1 cm) using thermoset glue (Epon® 1004F). The two disks were mounted in the SFA chamber in a cross cylinder geometry and brought into mica-mica adhesive contact in dry air in order to determine the reference position using MBI (mica-mica contact). Afterward, the cylindrical disks were separated by roughly 1 mm and 20 μL of polymer solution was injected between the surfaces using a glass syringe (Hamilton®). Immediately after injection, the bottom of the SFA chamber was filled with water in order to saturate the surrounding vapors and to limit evaporation of the injected liquid. The normal interaction forces $F_{\perp}$ between the two polymer coated surfaces as a function of surface separation were determined on approaching (compression) and separating (decompression) the surfaces using the recently developed 3D sensor-actuator.[19,21] The approach and separation velocities of the upper surface were controlled via a function generator. Experiments were reproduced at least twice with two different sets of mica surfaces. Force profiles and friction measurements were performed on an average of three contact positions on each pair of surfaces.

Friction Force Measurements. The friction force $F_{\parallel}$ was measured by moving the upper surface horizontally using the 3D sensor actuator. The sliding velocity was controlled using a function generator and calibrated before the experiments using a laser displacement detection device (Keyence® LKG10 laser head). Friction forces were determined by measuring the deflection of wire springs holding the upper surface using semi-conductive strain gauges. The detection limit of the friction force was 3×10^{-3} mN,

and the signal noise rms was 1×10^{-3} mN. Using this device, the lateral sliding speed could be varied from 0.01 to 100 μm/s. Before measuring the friction forces, three cycles of normal compression/decompression were performed on the same contact position. All friction measurements were made by sliding back and forth the upper surface at a given normal force and sliding velocity and over a traveled distance of 15 μm. Simultaneously to the friction force measurements, FECO fringes were recorded to determine the separation distance between the surfaces, the contact area and any possible deformations of the contact.

VII.3 Results and Discussion

VII.3.1 Synthetic Strategy

Lubricin (LUB) is a protein composed of a polypeptide backbone with highly glycosylated mucinous domain intercalated between globular subdomains (one hemopexin- (PEX) and two somatomedin-like (SMB) segments) (Figure VII.1A).[3] Due to the presence of the brush-like middle block, LUB adopts cylindrical conformation with a contour length of 200±50 nm and diameter of several nanometers.[22,23] The middle block is decorated with short carbohydrates capped with sialic acid, which incorporate a significant negative charge to the segment, whereas the end domains carry the majority of the positive charge (Figure VII.1A).[22-25]

To closely resemble the LUB structure the synthetic polymer was designed to comprise of two main topological features of the protein: 1) the central bottlebrush

domain (B), with water soluble and biocompatible grafts, to ensure good lubrication behavior, and 2) the outer linear segments (A), bearing positively charged moieties, as anchoring blocks for adsorption on mica surface (Figure VII.1B).

The mimic of LUB was obtained in six synthetic steps via the combination of Atom Transfer Radical Polymerization (ATRP) and post-modification techniques (Figure VII.1C), The B segment was synthesized through the copolymerization of (2-trimethylsiloxy)ethyl methacrylate (HEMA-TMS) and methyl methacrylate (MMA), yielding a flexible, yet densely grafted (~50%), precursor of the brush segment. The targeted degree of polymerization (DP) of the polymer was ~800, which corresponds to a fully extended chain with *l*~200 nm, a value closely matching that of LUB (Scheme VII.1).[22] In the next step, the di-initiator was chain extended with copolymers of (2-dimethylamino)ethyl methacrylate (DMAEMA) and MMA, form ing the ABA triblock copolymer, with average DP of ~ 185 per each A block. The quaternization of DMAEMA with ethyl bromide generated a positive charge on domains A, for a strong adsorption on negatively charged mica surfaces in aqueous solution (Scheme VII.1). Next, OTMS moieties were replaced with ATRP initiating functional groups, thus enabling the attachment of polyzwitterionic branches (DP~45) in the brush segment through the 'grafting from' approach (Scheme VII.1). Poly(2-methacryl-oyloxyethyl phosphorylcholine)] (pMPC) was chosen for side chains due to the excellent biocompatibility of this polymer as well as recent reports showing that surface grafted brushes of pMPC exhibit extremely good lubrication under physiological pressure (between 2-7.5 MPa). The application of ATRP and the 'grafting from' method resulted in a multifunctional ABA bottle-brush triblock copolymer. Noteworthy, such synthetic

pathway offers access to broad spectra of ABA bottlebrush analogues as it allows for an excellent control over topological factors, such as the domain size, or the composition, length or packing density of grafts, which may be crucial for the design of efficient artificial lubricants.

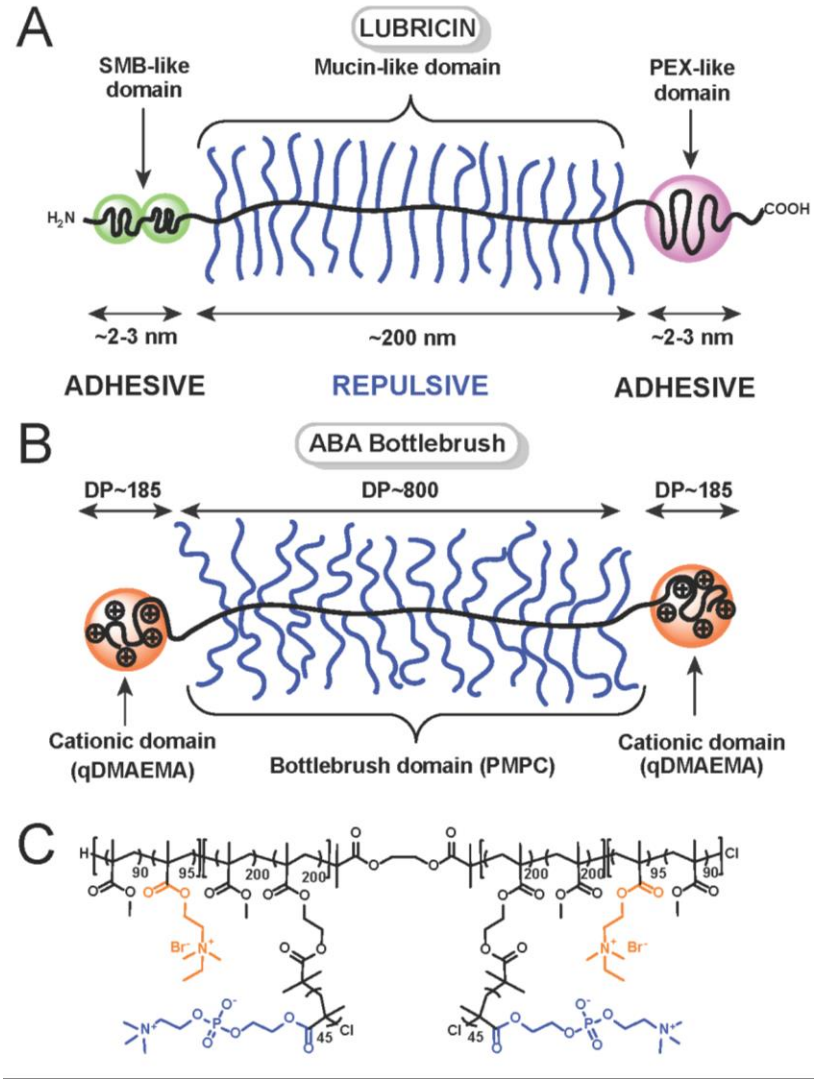

Figure VII.1 Schematic representations of the protein LUB found in mammalian synovial fluids (A) and the bottle-brush polymer mimicking LUB (B-C).

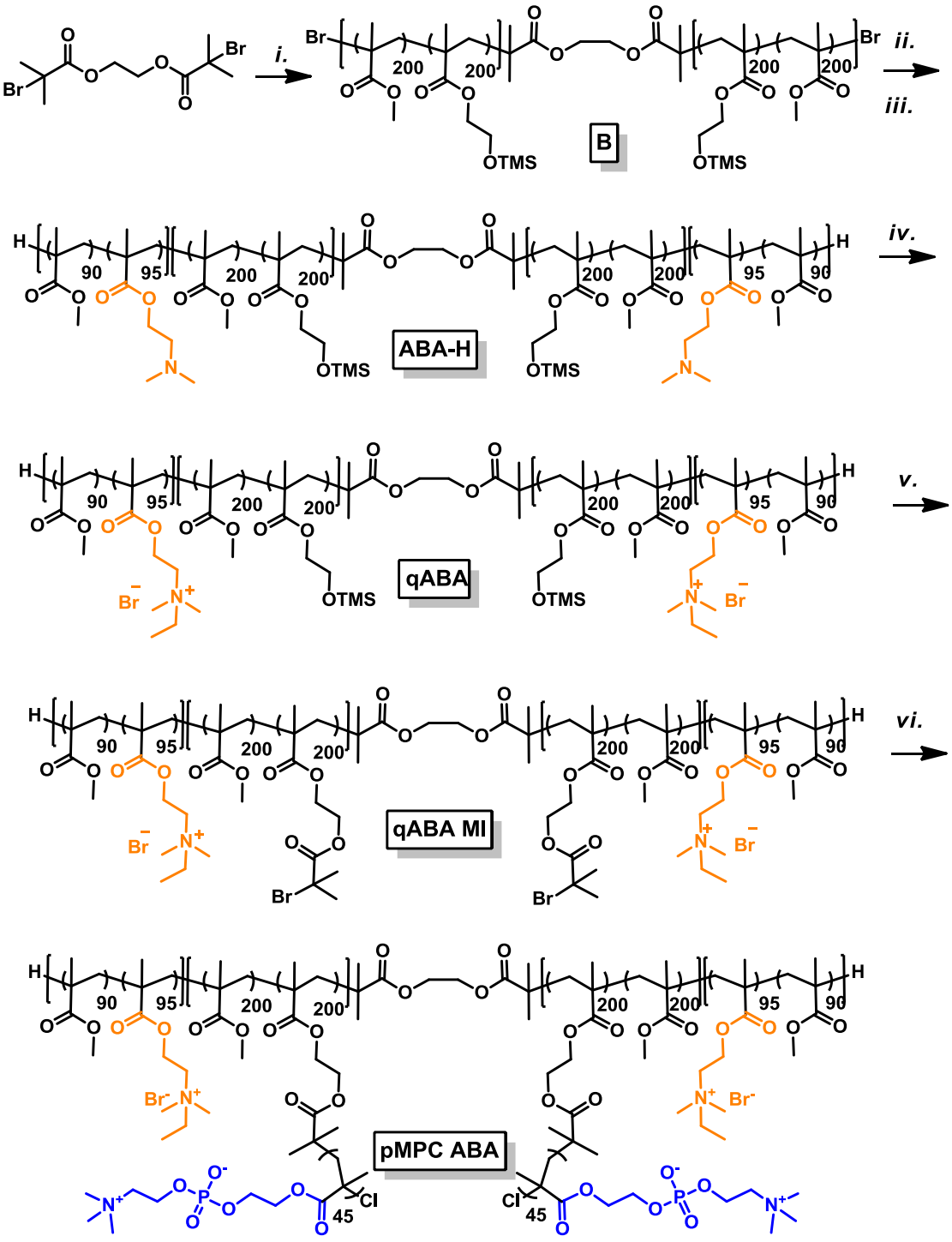

Scheme VII.1 Synthetic pathway for the preparation of the hydrophilic ABA bottlebrush copolymer (**pMPC ABA**).

VII.3.1.1 Synthesis of Hydrophilic ABA Bottlebrush

The synthetic design for the bio-inspired lubricant was described in the previous section. First, the block B was synthesized from ATRP diinitiator, 1,2-bis(2-bromo-isobutyryloxy)ethane (2-Br), by copolymerization of methyl methacrylate (MMA) and 2-trimethylsiloxyethyl methacrylate (HEMA-TMS) at the molar ratio [MMA]:[HEMA-TMS]:[2-Br]:[CuBr]:[$CuBr_2$]: [dNbpy] = [2000]:[2000]:[1.0]:[4.8]:[1.2]:[12] at 40 ˚C in 20 vol. % of anisole (scheme VII.1). The polymerization was stopped at 12.5h, at 20.0% of the monomers conversion, which corresponded to the total DP of 800, of the copolymer (B). The GPC analysis of **B** gave a signal with M_n=8.87·10^4 and low molecular weight distribution, $Đ$=1.19 (Figure VII.2, black). The polymerization was well controlled; however, a small low molecular shoulder was observed on the GPC trace of **B**. This phenomenon was ascribed to the issues with the initiation efficiency related to the use of ATRP diinitiator.

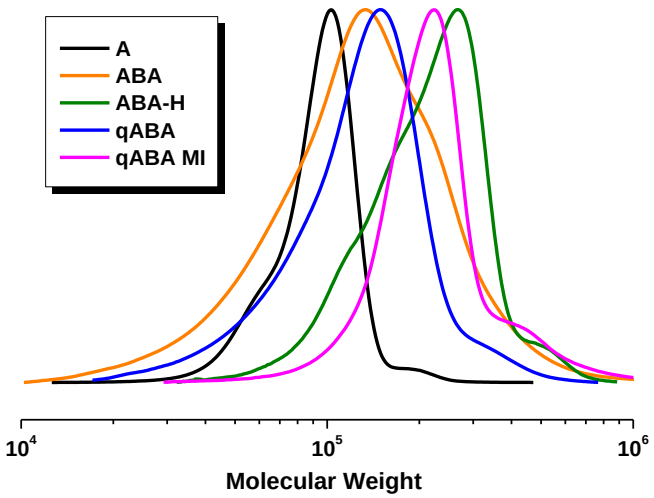

Figure VII.2 GPC traces recorded for polymers (black) **B**, (orange) **ABA**, (green) **ABA-H**, (blue), **qABA** and (pink) **qABA MI**.

Next, ^{1}H NMR spectroscopy of the purified **B** was performed to determine the composition of the copolymer (Figure VII.3, blue). The molar ratio of PMMA to P(HEMA-TMS) was calculated by comparing the areas under peaks of two sets of protons: a signal at 3.5-3.7 ppm corresponding to the methoxy (CO-O-CH_3) groups of PMMA, and methylene protons (-CH_2CH$_2$-OTMS) at 3.9-4.2 ppm of P(HEMA-TMS). The ratio of PMMA to P(HEMA-TMS) was 1:1 corresponding to the final composition of **B**: P(HEMA-TMS)$_{400}$-*co*-PMMA$_{400}$.

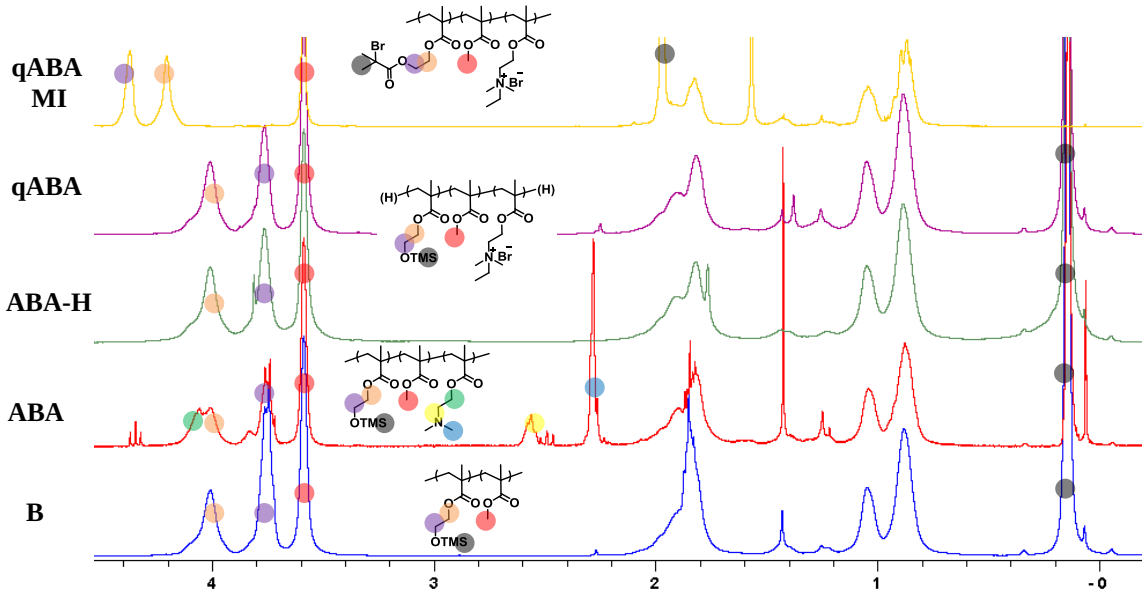

Figure VII.3 ^{1}H NMR spectra recorded for polymers (blue) **B**, (red) **ABA**, (green) **ABA-H**, (purple), **qABA** and (yellow) **qABA MI**.

The second synthetic step involved blocking of **B** to form a triblock copolymer, (**ABA**). For that purpose, **B** was utilized as a macrodiinitiator in a chain-extension reaction with MMA and 2-(*N*,*N*-dimethylaminoethyl)methacrylate (DMAEMA), thus achieving **ABA** triblock (Scheme VII.1). The polymerization was performed at 60 ˚C, targeting the molar ratio of reagents: [MMA]:[DMAEMA]:[B]:[CuCl]:[CuCl$_2$]:[dNbpy]

= [1600]:[1600]:[1.0]:[4.3]:[0.5]:[10] with 10 vol.% anisole. $CuCl/CuCl_2$/dNbpy was used as a catalyst to perform ATRP under halogen exchange conditions, hence allowing for an improved initiation efficiency of the process as compared to traditional ATRP with CuBr-based complexes.[26] The reaction was stopped at 10.1% conversion of monomers, which corresponded to DP=160 per each **A** block. GPC characterization of **ABA** showed the formation of a product with a higher molecular weight (M_n=9.95·10^4) and broader molecular weight distribution (*Đ*=1.56) (Figure VII.2, orange) than the starting polymer **B** (*Đ*=1.12). Afterwards, purified **ABA** was analyzed via ^{1}H NMR spectroscopy to evaluate its final composition: poly[(DMAEMA$_{95}$-*co*-MMA$_{90}$)-*b*-(HEMA-TMS$_{400}$-*co*-MMA$_{400}$)-*b*-(DMAEMA$_{95}$-*co*-MMA$_{90}$). The structure of the polymer was assessed from the relative intensities of selected sets of protons in PMMA, P(HEMA-TMS) and PDMAEMA. The following signals and functionalities were used: 3.5-3.7 ppm from the methoxy- (CO-O-C*H*$_3$) of PMMA, 3.9-4.2 ppm from methylene- (-C*H*$_2$CH$_2$-OTMS) of P(HEMA-TMS), and 2.6-2.7 ppm from methylene- (C*H*$_2$-NMe$_2$) in PDMAEMA (Figure VII.3, red).

After accomplishing the synthesis of **ABA** triblock copolymers, several chemical transformations were performed to obtain the required macroinitiator for the brush formation. The first modification involved a removal of halogen end groups from **ABA**. This was done to avoid any possibility of a chain extension of **ABA** from the end groups during the final, 'grafting from' step. The removal of halogen functionalities was done with a 50-fold excess of $SnBu_3H$ agent in the presence of CuBr/TPMA complex (Scheme VII.1). The GPC characterization of **ABA-H** showed a signal with M_n= 1.86·10^5 and *Đ*=1.23 (Figure VII.2, green). The second chemical modification allowed for an

incorporation of a positive charge into the structure of **ABA-H** through a quaternization of tertiary amine groups, of PDMAEMA component. The reaction was done in acetone with a 10-fold excess of bromoethane alkylating agent per amino group (Scheme VII.1). GPC analysis of **qABA** gave the signal with M_n= $1.05 \cdot 10^5$ and $Đ$ = 1.36 (Figure VII.2, blue). The completion of the process was confirmed by ^{1}H NMR spectroscopy (Figure VII.3, purple) of **qABA**. The evaluation of the spectra before (Figure VII.3, red) and after (Figure VII.3, purple) the quaternization allowed for detecting the shift of the signals characteristic for PDMAEMA. The disappearance of selected PDMAEMA protons: methyl- (2.3 ppm, N(CH_3)$_2$) and methylene- (2.5-2.7 ppm, CH_2N), was indicative of the consumption of PDMAEMA, and thus a successful quaternization with ethyl bromide. The final step involved the incorporation of ATRP active functionalities through *in situ* deprotection and esterification of –OTMS groups in **qABA**. The reaction was performed under standard reaction conditions, [HEMA-TMS]:[KF]:[TBAF]:[BiBBr] = [1.0]:[1.1]:[1.0]:[1.2], in THF. A small modification was done to ensure a quantitative functionalization of P(HEMA-TMS), which involved using the ratio of TBAF:HEMA-TMS = 1:1 instead of typically used catalytic amounts of TBAF. GPC analysis of the product (**qABA MI**) gave M_n = $1.98 \cdot 10^5$ and $Đ$ = 1.24 (Figure VII.2, magenta). ^{1}H NMR spectroscopy of pure **qABA MI** was used to confirm the efficiency of the functionalization reaction (Figure VII.3, yellow). The disappearance of the TMS signal together with the shift of two methylene peaks towards higher values were indicative of the successful incorporation of 2-bromoisobutyryloxy- groups into **qABA MI**.

After synthesizing **qABA MI** it was used as a macroinitiator to prepare a hydrophilic bottlebrush by grafting 2-methacryloyloxyethyl phosphorylcholine (MPC)

side chains. The following conditions were applied: [MPC]:[BiBEM]:[CuCl]:[$CuCl_2$]:[bpy] = [300]:[1.0]:[1.5]:[0.2]:[3.4], [MPC]=1M in methanol at 50 °C (Scheme VII.1). The reaction was stopped after 5.5h reaching 16% monomer conversion, as determined by ^{1}H NMR spectroscopy. Due to the lack of the solubility of the product in DMF or THF it was not analyzed by GPC chromatography. The product, **pMPC ABA**, was purified and used for further characterization via AFM and SFA measurements.

VII.3.1.2 Synthesis of Hydrophobic ABA Bottlebrush

Synthesized **qABA MI** is a versatile platform for the generation of bottlebrushes with properties controlled by the choice of the monomer used in the side chain grafting process. The previous section discussed the synthesis of pMPC bottlebrush exhibiting high water-solubility and biocompatibility, which was further studied as bio-inspired lubricant. In this section, the same synthetic approach was used to prepare a polymeric lubricant that would display good solubility in solvents with lower polarity then that of water and methanol. A bottlebrush with a structure analogous to that of **pMPC ABA**, but more hydrophobic grafts, could be used as a lubricant in organic media to decrease friction coefficient and preserve surfaces from a potential damage.

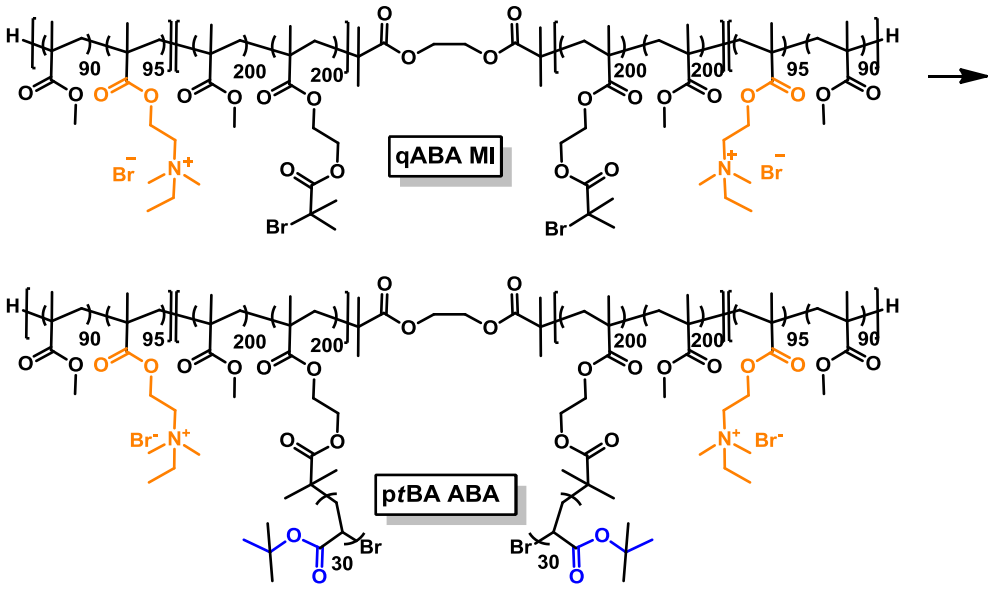

Scheme VII.2 Synthetic pathway for the preparation of the hydrophobic ABA bottlebrush copolymer (**p*t*BA ABA**).

In order to synthesize a hydrophobic bottlebrush, *tert*-butyl acrylate (*t*BA) was used as a monomer in the process of grafting from **qABA MI**. The same macroinitiator was applied as in case of **pMPC ABA**, hence the preparation required only one synthetic step. P*t*BA side chains were grafted from the backbone under ATRP reaction conditions with the molar ratio of reagents [*t*BA]:[BiBEM]:[CuBr]:[$CuBr_2$]:[dNbpy] = [400]:[1.0]:[0.475]:[0.025]:[1.0] with 10 vol. % anisole at 60 °C. Reaction was stopped after 17h reaching 7.4 % monomer conversion equivalent to DP=30 of P*t*BA side chains. GPC analysis resulted in the polymer with M_n= 2.94·10^5 and $Đ$=1.84 (Figure VII.4, blue)

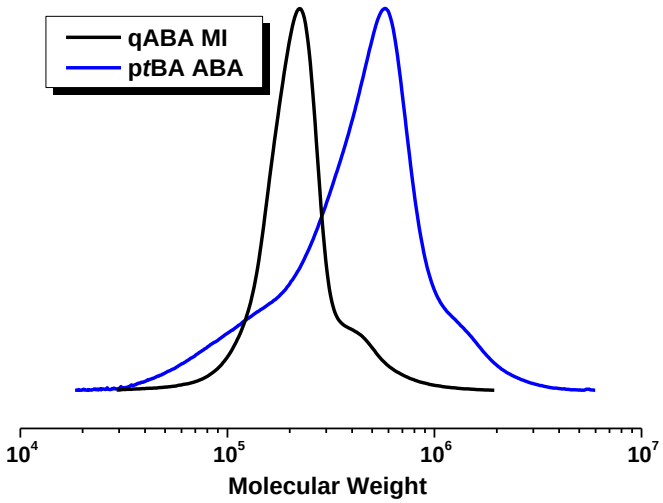

Figure VII.4 GPC traces recorded for (black) **qABA MI** and (blue) **p*t*BA ABA.**

VII.3.2 Lubrication Studies via AFM and SFA Measurements

VII.3.2.1 Hydrophilic ABA Bottlebrush

The ABA bottle-brush polymer[27-29] was prepared via the combination of Atom Transfer Radical Polymerization (ATRP)[30,31] and different post-modification techniques (Scheme VII.1) using the 'grafting from' approach. Since the surfaces of study are made of atomically flat mica, the adhesive (A) blocks of the polymer were composed of a positively charged amine monomer (quaternized 2-(dimethylaminoethyl) methacrylate, qDMAEMA), and a hydrophobic (methyl methacrylate, MMA) monomer. These two components strongly adsorb on negatively charged mica surfaces in aqueous solution via electrostatic and hydrophobic interactions. The bottlebrush block was composed of a flexible MMA backbone with attached polyzwitterionic branches of poly(2-methacryloyl-oxyethyl phosphorylcholine)] (pMPC) (Scheme VII.1). The use of pMPC as side

branches was motivated by the excellent biocompatibility of this polymer[32,33] as well as recent reports showing that surface grafted brushes of pMPC exhibit extremely good lubrication under physiological pressure (between 2-7.5 MPa).[6,33]

When adsorbed on a mica surface from a diluted solution (Figure VII.5A), individual polymer chains could be resolved by atomic force microscopy (AFM). Figure VII.5 shows a significant difference in organization of the polymer chains when adsorbed from solutions at 37 and 370 μg/mL (Figure VII.5A and B, respectively). At 37 μg/mL, isolated chains were rarely observed. Most of the chains tend form small aggregates of two to five molecules. At 370 μg/mL, the surface was almost fully covered by a monolayer of polymer chains (Figure VII.6B). In the monolayer, the polymer chains tend to maximize possible contacts with their neighboring molecules by adopting an extended conformation.

The results show that as the concentration in polymer increased from 0.37 mg/mL to 370 mg/mL, the interaction forces become more repulsive. At low polymer concentration, the interaction force present an instability (jump in to contact) due to the expulsion (squeeze out) of one to two layers of polymer upon compression. Presence of such instability was directly correlated to the coverage of the polymer on the surface, purely repulsive forces corresponding to an almost fully covered surface.

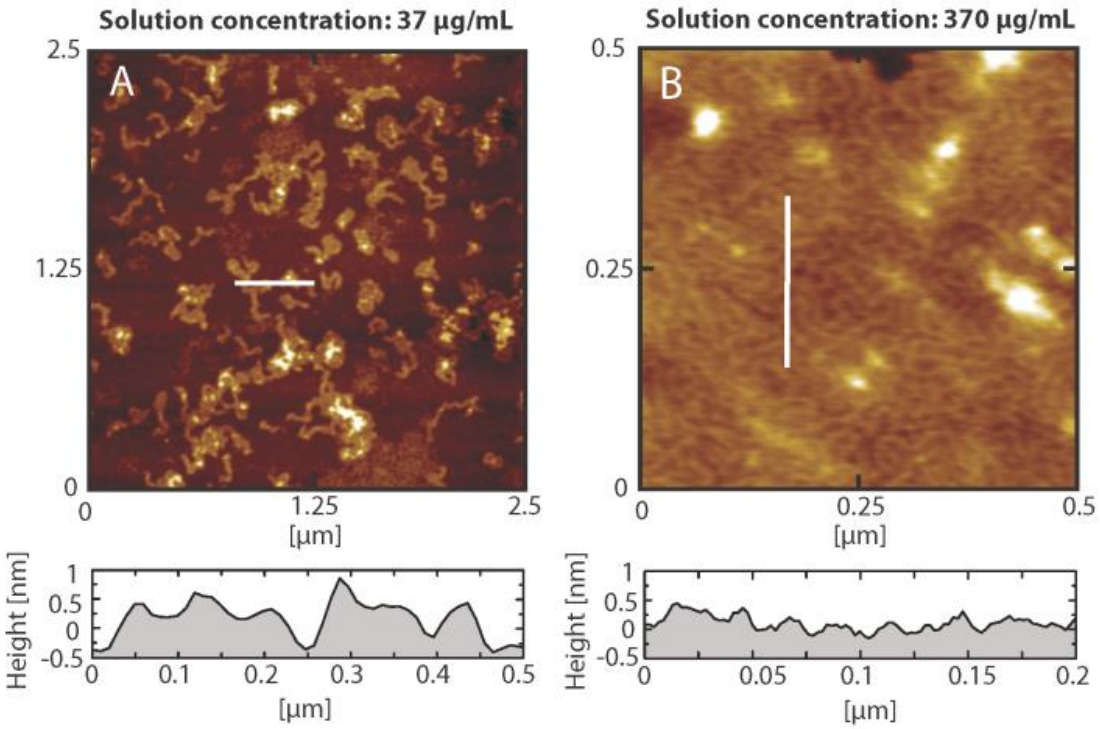

Figure VII.5 Atomic Force Microscopy imaging in air of the polymer chains adsorbed on a freshly cleaved mica surface from a solution at (A) 37 µg/mL, and (B) 370 µg/mL.

Figure VII.7 shows the interaction forces, reported as $F_{\perp}/R$, $F_{\perp}$ being the normal interaction force and R the surface curvature, between mica surfaces immersed in a solution of polymer at 370 µg/mL in phosphate buffer saline (PBS) or pure water were measured at 25°C using the SFA. In both media, the interaction forces presented a strong dependence on the approach speed, $v_{\perp}$. Long range interaction forces, starting from 60 nm in PBS and 100 nm in pure water, were systematically detected at $v_{\perp}$ = 4 nm/s. The final polymer film thickness, measured at the highest compression force (pressure 1.5 MPa), was found to be independent of $v_{\perp}$ and equal to approximately 5 nm.

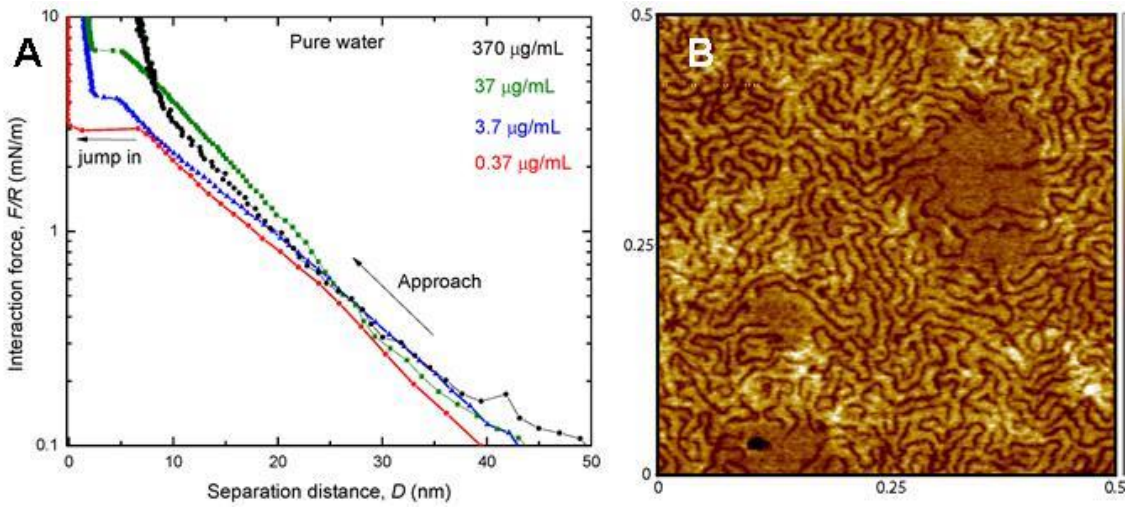

Figure VII.6 (A) Evolution of the interaction forces between two mica surfaces immersed in pure water in presence of the triblock polymer brush. (B) AFM phase image (in air) of a polymer monolayer deposited from water at 370 μg/mL on mica. The image clearly shows the existence of a polymer monolayer on mica. This monolayer does not fully cover the surface but still can hold normal pressure as high 2.5 MPa which could not be achieved at lower polymer concentrations.

Interestingly, the interaction forces measured upon compression of the surfaces at the highest confinement speed ($v_{\perp}$ = 4 nm/s) exhibited quasi periodic instabilities (Figure VII.7A and B) on the first approach. These instabilities correspond to transient accelerations of the surfaces (jumps in) over separation distances ΔD of 3-5 nm due to the squeeze out of 1 to 2 molecular layers of polymer chains. Such instabilities systematically disappeared during the separation of the surfaces as well as in subsequent approaches performed immediately after separation of the polymer film. Such phenomena are re markably similar to previously reported experiments on molecular fluids such as linear alkanes[34] where the confinement speed was also found to affect the number of molecular layers trapped between the surfaces as well as their fluidity. Independently of the confinement speed, the measured interaction forces were found to

be repulsive and reversible although a small hysteresis was systematically found during the first approach-separation cycle in PBS.

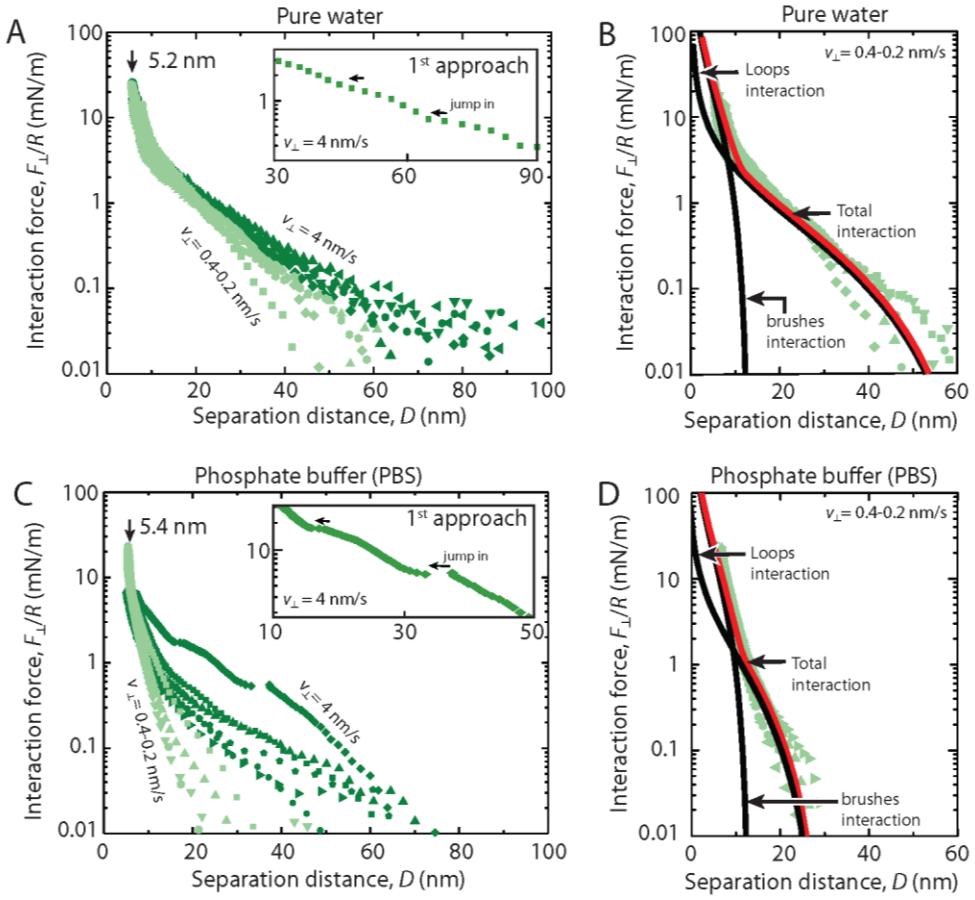

Figure VII.7. Normal interaction forces between two mica surfaces immersed in a polymer solution in pure water (A and B) and in PBS (C and D). A and C show the effect of the confinement speed on the range of the interaction forces and the structuring of the polymer solution at the interfaces. High confinement speed generates longer range repulsive interaction forces mostly due to the extra contribution of the viscous forces (compared to low approach speed). B and D show the good agreement between the loop and brush models (Eq. VII.1 and VII.2) and the experimental data obtained at low $v_\perp$.

The force curves shown in Figure VII.7B and D were measured at a confinement speed of $v_{\perp}$ = 0.2 nm/s, which corresponds to quasi-equilibrium conditions. The forces present a long range exponential interaction component with a decay length of approximately 2 nm in PBS and 9 nm in pure water. If the long range component of the interaction was of electrostatic origin, the decay length should be the Debye length, λ_D, which in the present case was estimated to be less than 1 nm in PBS and 60 nm in pure water (taking into account the electrostatic charges and counter ions coming from the polymer free in solution[35]). The difference between the calculated Debye length, λ_D, and the measured decay length in PBS and pure water are sufficiently large to confirm that the long range repulsive forces are not electrostatic but of steric origin.

Table VII.1 Unperturbed brush and loop heights and characteristic pressures obtained from fitting equation VII.1 to the experimental data shown in figure VII.7B and D.

Polymer solution	**Short range (SR) interaction (brushes interaction)**		**Long range (LR) interaction (loops interaction)**	
	L_{SR} [nm]	$p_{0\text{-}SR}$	L_{LR} [nm]	$p_{0\text{-}LR}$
In water	6.5±1	2.5×10^5	33±1	1.5×10^3
PBS	6.5±1	2.5×10^5	15±2	7×10^3

Given the architecture of the polymer and its expected loop conformation on the surfaces, an effective brush interaction model was used to describe the long range component of the interaction forces.[36] In this model, the polymer loop is assumed to be

equivalent to two diblock polymers of half the bottle-brush domain molecular weight. The short range interaction forces were assumed to be dominated by the direct interaction between the bottle-brush domains and were modeled by a brush-brush interaction model. The general expression of the model is:[37]

$$\frac{F_{\perp}(D)}{R} = 2\pi W = 2\pi(W_{LR} + W_{SR}) \qquad \text{(VII. 1)}$$

where W is the interaction energy between flat surfaces and LR and SR stand for Long Range and Short Range, respectively. The expression of the LR and SR components can be written as:[38,39]

$$W_i = p_{0i} L_i \left[\frac{1}{u} + u^2 - \frac{u^5}{5} - \frac{9}{5}\right] \qquad \text{(VII. 2)}$$

where p_0 is the intrinsic scale for the pressure and L is the unperturbed brush height, u=D/2L and i = LR or SR.

Figures VII.7 B and D showed the agreement between the proposed model and the experimental data. The fitted values of L_{SR} (Table VII.1) are independent of the media (pure water or PBS) which suggested that the conformation of the pMPC brushes was insensitive to the salt concentration. This observation are consistent with recent reports showing that the conformation of pMPC grafted brushes or pMPC chains free in solution are almost insensitive to salt concentration.[6,40] The value of the unperturbed length of the brush L_{SR} was found to be 6.5 nm (Table VII.1) which was close to the expected theoretical value of 6 nm and about one third of the contour length L_c=2nl=18 nm, n being the number of monomer units in one side chain (n=45) and l the characteristic

segment length (estimated to be ~ 0.2 nm).[40-42] The unperturbed height of the loops, L_{LR}, obtained from the long range component of the interaction forces was found to be 15 nm in PBS and 33 nm in pure water which correspond respectively to approximately 30% and 65% of the fully extended loop height (based on a contour length of 200 nm estimated by AFM imaging).

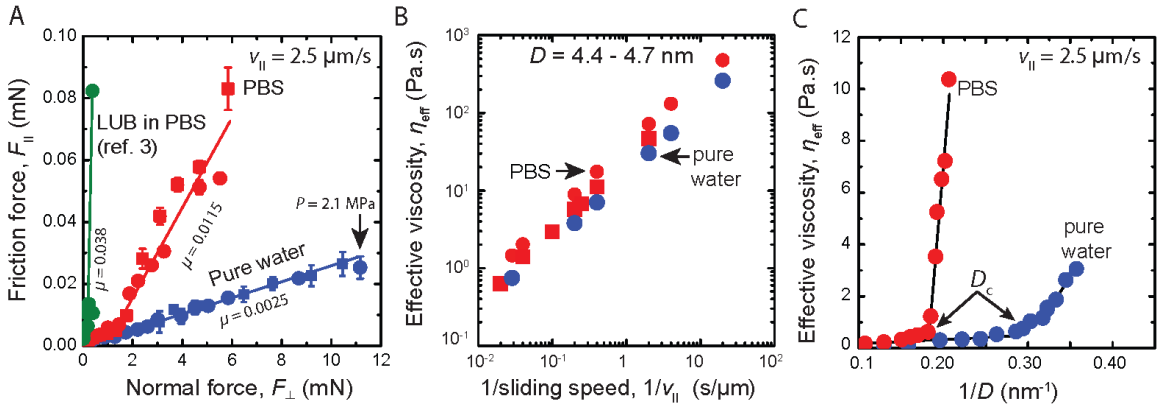

Figure VII.8 Experimental observation of Amontons-like behavior of the molecular brushes thin film in pure water and PBS. (A) Experimental data showing that the friction coefficient μ is independent of the applied load; (B) Results showing that the viscosity of the confined film is inversely proportional to sliding speed at constant separation distance; (C) Results showing that the viscosity is inversely proportional to the separation distance above and below a critical separation distance D_c.

The conformational change in the distal part of the adsorbed polymer from the increase in salt concentration can be ascribed to two main factors, namely, the increased affinity of the bottle-brush domain to the surface, and the screening of the electrostatic interaction between the lateral blocks of the polymer and the surface. From these observations we expect the conformation of a polymer chain at the surface in pure water

to be a single loop while in PBS it is expected to adopt multiple loops and train conformations.

The lubrication properties of the polymer were also found to be sensitive to the surrounding media (Figure VII.8A). When the surfaces were sheared in pure water, the measured friction force, $\boldsymbol{F}_{\parallel}$, was found to depend linearly on the applied normal load, $F_{\perp}$, and to vanish at $F_{\perp} = 0$, which is consistent with the previous observation that no adhesion forces were measured in this system.

The measured friction coefficient, μ, defined as $\mathrm{d}\boldsymbol{F}_{\parallel} / \mathrm{d}F_{\perp}$, was equal to 0.0025±0.0001 in pure water solution and 0.0115±0.0003 in PBS solution at a normal pressure of 2.1 MPa, well into the physiological range. These values are well below the friction coefficient of 0.038 reported for lubricin under similar conditions of sliding speed and concentration (Figure VII.8A).[3] Interestingly, above a normal force of 0.4 mN (P = 0.4 MPa), the friction coefficient of lubricin was reported to increase sharply which was also accompanied by the triggering of surface wear. Such drastic changes in lubrication properties were similarly observed in the present system in PBS only for $\boldsymbol{F}_{\perp} > \mathbf{1.5}\ \boldsymbol{mN}$(or D < 5 nm). Below this value, the friction coefficients of the mimetic polymer measured in PBS and pure water were found to be nearly identical.

The separation distance D at which the sudden increase in friction force occurs in PBS corresponds to the transition from a two layers film to a single monolayer film. The increase in friction force in the monolayer film is firstly due to the increase of the attractive interaction between the bottlebrush domains and the mica surfaces which, as mentioned earlier, causes a partial collapse of the loop conformation, and secondly to the

partial screening of the attractive electrostatic interaction between the lateral blocks of the polymer chains and the surface. The screening of the electrostatic attraction enhances the mobility of the lateral blocks allowing transient (weak) adhesive bridges to form during shear via the still remaining hydrophobic forces.

The observed linear relationship between $\boldsymbol{F}_{\parallel}$ and $\boldsymbol{F}_{\perp}$ already suggested that the system exhibits Amontons-like behavior. Such behavior, most commonly observed for non-lubricated "solid" contacts, is essentially due to the peculiar rheological properties of the confined fluid. Thus, Figure VII.8B and C show that the effective viscosity of the confined thin film, $\boldsymbol{\eta_{eff}}$, is inversely proportional to the sliding speed and to the separation distance, and can therefore be written as $\eta_{\mathbf{eff}} = \boldsymbol{B/v_{\parallel}D}$, where B is a constant. In addition, in the purely osmotic compression regime (very small D), the normal pressure between the surfaces can be written as $\boldsymbol{P_{\perp} = -\partial W_{SR}/\partial D = +C/D^2}$. Thus assuming Couette flow between the surfaces, the expression of the friction coefficient, $\boldsymbol{\mu}$, becomes:

$$\mu = \frac{F_{\parallel}}{F_{\perp}} = \left(\frac{\eta_{\mathrm{eff}} A v_{\parallel}}{D}\right)/F_{\perp} \qquad \text{(VII. 3)}$$

where A is the contact area. Substituting for the expressions for $\eta_{\mathbf{eff}}$ and $\boldsymbol{P_{\perp} = F_{\perp}/A}$, the friction coefficient can be written as:

$$\mu = \frac{B}{C} \qquad \text{(VII. 4)}$$

which is independent of A, $\boldsymbol{v}_{\parallel}$ and $\boldsymbol{F}_{\perp}$ and therefore follows all three Amontons' laws.

Amontons-like behavior has been reported for single components fluids such linear alkanes or polymer melts. The results suggested that such behavior could be obtained, or even designed, in polymer solutions as well. Key properties leading to such behavior are the shear thinning of the confined fluid, the increase of $\eta_{\mathbf{eff}}$ with confinement, and a repulsive, roughly $1/D^{n}$, force-distance or pressure-distance dependence.

VII.3.2.2 Hydrophobic ABA Bottlebrush

In addition to the detailed AFM and SFA analysis of the hydrophilic bottlebrush, initial studies on the hydrophobic bottlebrush, **P*t*BA ABA**, were also performed. The AFM imaging of **P*t*BA ABA** spin-casted on mica surface showed the presence of molecules characteristic to bottlebrush topology (Figure VII.9). The brush section (block B) was determined by AFM and calculated as ~200nm, which agreed with the DP=800 estimated for the monomers conversion. Moreover, **P*t*BA ABA** molecules on surface adapted a peculiar folded conformation which could be ascribed to a fairly low grafting density of the brush as well as its composition. In addition, the AFM of Langmuir-Blodgett monolayer of the brush showed a relatively small intermolecular distance, which was correlated with the low grating density estimated as ~40% (Figure VII.9B).

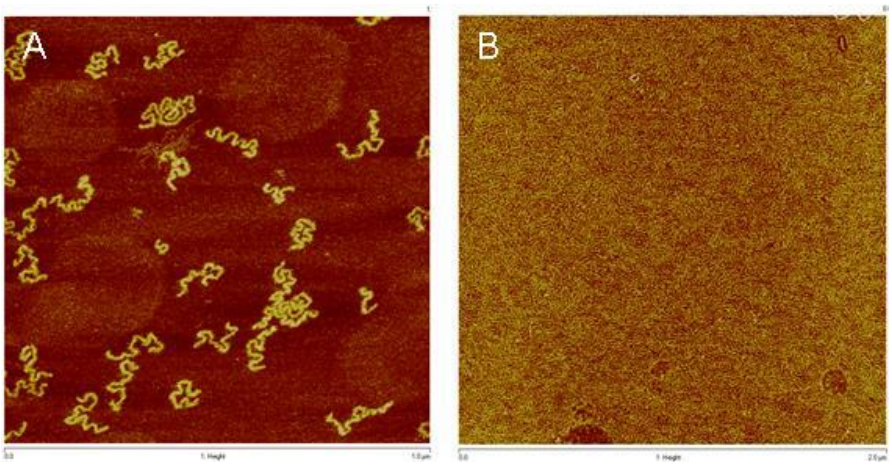

Figure VII.9 AFM images of **p*t*BA ABA** prepared by A) spin-casting and B) LB deposition of monolayer on mica surface.

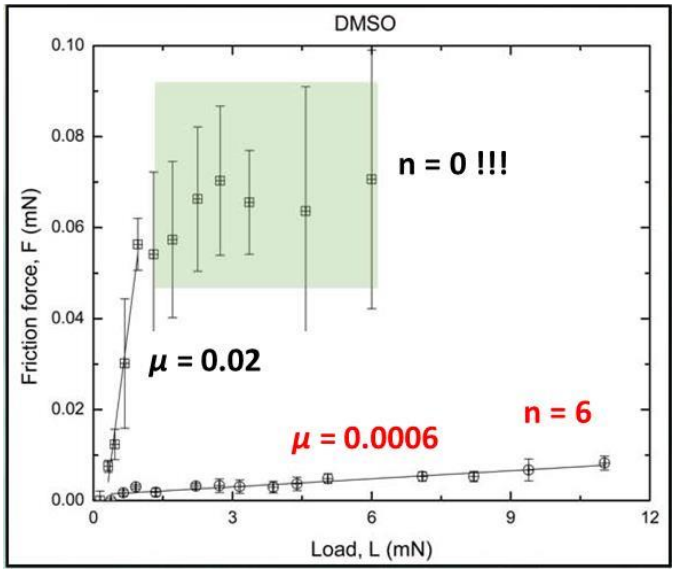

Figure VII.10 Experimental data of SFA measurement of p*t*BA ABA in DMSO, showing that the friction coefficient μ is independent of the applied load.

Further characterization involved SFA studies of p*t*BA ABA, which allowed for assessing the lubrication properties of the brush in organic media. DMSO was chosen as an organic solvent due to a good solubilization of the material as well as its high boiling

point preventing the solution from a rapid evaporation. Therefore, time-consuming measurements could be performed without a risk of any significant loss of a solvent, and hence concentration changes of tested solutions.

The studies were performed at 370 μL/mL concentration. Friction forces were measured at different loads, which resulted in the measured friction coefficient, μ, equal to 0.0006 (Figure VII.10). More importantly, the frictions coefficient was independent of the applied loads, sustaining as much as ~12 MPa, which is way above a normal force of 0.4 mN (P = 0.4 MPa). Interestingly, during the first in-run measurements the detected friction coefficient was in range of 0.02, showing much poorer lubrication behavior than the later results (Figure VII.10). The phenomenon was explained by the equilibration of brush molecules on surfaces that occurred during the first in-run. This, on the other hand, led to the formation of a brush monolayer, which is responsible for the protection and lubrication of the surface. Later in-runs provided a much lower friction coefficient, showing a good repeatability for up to six tests.

These results show that p*t*BA ABA exhibits excellent lubrication properties while protecting surfaces from damage at very high loads. This preliminary results show that bio-inspired artificial lubricant can also be applied to organic media, hence having a possible future in applications such as lubricants for car engines or piping requiring a friction reduction during the transportation of fluids.

VII.4 Conclusions

The results show that excellent lubricating properties and Amontons-like behavior can be obtained simultaneously for the first time from adsorbed polymer brushes, which expands drastically the arsenal of strategies for the development of efficient artificial synovial fluids.

In this study it was shown that molecular brushes having triblock architecture can form polymer loops when strongly adsorb on a surface. The excellent lubricating properties of these polymers even when confined to a monolayer arise from the strong osmotic repulsion between the side chains of the molecular brushes and the surfaces, which favor the flow of water molecules during shear and thereby improve lubrication. The results show that the excellent lubricating properties of the polymer are maintained independently of the shearing speed or applied load even under molecular confinement. The work was also expanded to more hydrophobic system by means of tuning the composition of bottlebrush side chains. That change improved solubility in organic media, thus allowing for testing friction in DMS. The results showed even lower friction coefficient then that of a hydrophilic brush, which was independent on applied loads up to 120 atms. This approach suggests new ways to design polymeric lubricants custom designed to work on specific surfaces or solvent conditions.

VII.5 References

(1) Swann, D. A.; Sotman, S.; Dixon, M.; Brooks, C. *Biochem J* **1977**, *161*, 473-85.

(2) Swann, D. A.; Hendren, R. B.; Radin, E. L.; Sotman, S. L.; Duda, E. A. *Arthritis Rheum* **1981**, *24*, 22-30.

(3) Zappone, B.; Ruths, M.; Greene, G. W.; Jay, G. D.; Israelachvili, J. N. *Biophys J* **2007**, *92*, 1693-1708.

(4) Waller, K. A.; Zhang, L. X.; Elsaid, K. A.; Fleming, B. C.; Warman, M. L.; Jay, G. D. *P Natl Acad Sci USA* **2013**, *110*, 5852-5857.

(5) Zappone, B.; Greene, G. W.; Oroudjev, E.; Jay, G. D.; Israelachvili, J. N. *Langmuir* **2008**, *24*, 1495-1508.

(6) Chen, M.; Briscoe, W. H.; Armes, S. P.; Klein, J. *Science* **2009**, *323*, 1698-1701.

(7) Drobek, T.; Spencer, N. D. *Langmuir* **2008**, *24*, 1484-1488.

(8) Yin, F.; Bedrov, D.; Smith, G. D.; Kilbey, S. M. *The Journal of chemical physics* **2007**, *127*, 084910.

(9) Eiser, E.; Klein, J.; Witten, T. A.; Fetters, L. J. *Phys Rev Lett* **1999**, *82*, 5076-5079.

(10) Britovsek, G. J. P.; England, J.; White, A. J. P. *Inorg. Chem.* **2005**, *44*, 8125-8134.

(11) Boerner, H. G.; Beers, K.; Matyjaszewski, K.; Sheiko, S. S.; Moeller, M. *Macromolecules* **2001**, *34*, 4375-4383.

(12) Beers, K. L.; Gaynor, S. G.; Matyjaszewski, K.; Sheiko, S. S.; Moeller, M. *Macromolecules* **1998**, *31*, 9413-9415.

(13) Neugebauer, D.; Zhang, Y.; Pakula, T.; Sheiko, S. S.; Matyjaszewski, K. *Macromolecules* **2003**, *36*, 6746-6755.

(14) Zhang, X.; Matyjaszewski, K. *Macromolecules* **1999**, *32*, 1763-1766.

(15) Shipp, D. A.; Wang, J.-L.; Matyjaszewski, K. *Macromolecules* **1998**, *31*, 8005-8008.

(16) Coessens, V.; Matyjaszewski, K. *Macromolecular Rapid Communications* **1999**, *20*, 66-70.

(17) Cho, H. Y.; Srinivasan, A.; Hong, J.; Eric Hsu, D. K.; Bohaty, A. K.; Paik, H.-j.; Hollinger, J. O.; Matyjaszewski, K. *Biomacromolecules* **2011**, *12*, 3478-3486.

(18) Kobayashi, M.; Masami, T.; Takahara, A. *Faraday Discuss.* **2012**, *156*, 403-412.

(19) Israelachvili, J.; Min, Y.; Akbulut, M.; Alig, A.; Carver, G.; Greene, W.; Kristiansen, K.; Meyer, E.; Pesika, N.; Rosenberg, K.; Zeng, H. *Rep Prog Phys* **2010**, *73*, 036601.

(20) Israelachvili, J. *J Colloid Interf Sci* **1973**, *44*, 259-272.

(21) Kristiansen, K.; Banquy, X.; Zeng, H.; Charrault, E.; Giasson, S.; Israelachvili, J. *Advanced Materials* **2012**, *24*, 5236-41.

(22) Jay, G. D. *Curr. Opin. Orthop.* **2004**, *15*, 355-359.

(23) Swann, D. A.; Slayter, H. S.; Silver, F. H. *J. Biol. Chem.* **1981**, *256*, 5921-5925.

(24) Jay, G. D.; Britt, D. E.; Cha, C. J. *J. Rheumatol.* **2000**, *27*, 594-600.

(25) Jay, G. D.; Harris, D. A.; Cha, C. J. *Glycoconj. J.* **2001**, *18*, 807-815.

(26) Matyjaszewski, K.; Qin, S.; Boyce, J. R.; Shirvanyants, D.; Sheiko, S. S. *Macromolecules* **2003**, *36*, 1843-1849.

(27) Matyjaszewski, K.; Tsarevsky, N. V. *Nat. Chem.* **2009**, *1*, 276-288.

(28) Lee, H.-i.; Pietrasik, J.; Sheiko, S. S.; Matyjaszewski, K. *Prog. Polym. Sci.* **2010**, *35*, 24-44.

(29) Sheiko, S. S.; Sumerlin, B. S.; Matyjaszewski, K. *Prog. Polym. Sci.* **2008**, *33*, 759-785.

(30) Matyjaszewski, K. *Macromolecules* **2012**, *45*, 4015-4039.

(31) Matyjaszewski, K.; Xia, J. *Chem. Rev.* **2001**, *101*, 2921-2990.

(32) Ishihara, K.; Ueda, T.; Nakabayashi, N. *Polym J* **1990**, *22*, 355-360.

(33) Moro, T.; Takatori, Y.; Ishihara, K.; Konno, T.; Takigawa, Y.; Matsushita, T.; Chung, U. I.; Nakamura, K.; Kawaguchi, H. *Nat Mater* **2004**, *3*, 829-836.

(34) Bureau, L. *Phys Rev Lett* **2007**, *99*, 225503.

(35) Tadmor, R.; Hernandez-Zapata, E.; Chen, N. H.; Pincus, P.; Israelachvili, J. N. *Macromolecules* **2002**, *35*, 2380-2388.

(36) Alonzo, J.; Mays, J. W.; Kilbey, S. M. *Soft Matter* **2009**, *5*, 1897-1904.

(37) Israelachvili, J. *Intermolcular and Surface Forces*; 3rd ed.; Academic Press: San Diego, 2011.

(38) Milner, S. T.

(41) Matsuda, Y.; Koba; Witten, T. A.; Cates, M. E. *Macromolecules* **1988**, *21*, 2610-2619.

(39) Milner, S. T.; Witten, T. A.; Cates, M. E. *Europhys Lett* **1988**, *5*, 413-418.

(40) Kobayashi, M.; Terayama, Y.; Kikuchi, M.; Takahara, A. *Soft Matter* **2013**, *9*, 5138-5148.

yashi, M.; Annaka, M.; Ishihara, K.; Takahara, A. *Langmuir* **2008**, *24*, 8772-8778.

(42) Kikuchi, M.; Terayama, Y.; Ishikawa, T.; Hoshino, T.; Kobayashi, M.; Ogawa, H.; Masunaga, H.; Koike, J.; Horigome, M.; Ishihara, K.; Takahara, A. *Polym J* **2012**, *44*, 121-130.

CHAPTER VIII

SUMMARY AND OUTLOOK

The focus of this thesis was on the synthesis of molecular bottlebrushes with complex architectures and their applications in different areas of material science. The thesis was divided into four sections which allowed for putting a broader perspective on the discussed projects.

In the first section I reviewed the recent progress in the bottlebrush field, focusing on advances made in the field in the past five years. The overview concentrated on several crucial areas of the brush field. The introduction covered the current status in the approaches for the bottlebrushes synthesis, followed by selected studies on their physical properties, self-assembly in bulk, solution and on surfaces, and concluded with using them as templating agents. The recent reports on molecular bottlebrushes show a continuous interest in developing new synthetic tools, which would provide access to more complex architectures with even better control over their structural factors. In addition, a lot of attention has been put on studying the physical properties of

bottlebrushes, which is crucial from the point of view of their prospective applications in various areas of material science.

The second section combined three different projects (Chapters II-IV) that focused on the structure-property relationships of one-component molecular bottlebrushes. Essentially, the main purpose was to present how varying structural details in bottlebrushes, without modifying their chemical composition, influences their physical properties. Chapter II summarized the synthesis of graft copolymers through the 'grafting from' approach under ATRP, and correlated their thermal diffusion behavior with the topological features, such as the grafting density, and lengths of both the side chains and backbone. The preliminary results showed that such polymeric libraries are excellent platforms for a more systematic physical behavior of graft copolymers. It could be employed in establishing a better understanding of transitions between different topologies, for instance a star-brush or comb-brush. In Chapter III, the same synthetic approach was used to form a series of bottlebrushes with a long, constant backbone and a varying length of the side chains. The results showed that the plateau modulus of bottlebrushes changed linearly with the graft length, providing values as low as few hundreds Pa. The results show a great promise of the use of long molecular brushes as physical supersoft elastomers. As compared to previous brush-based soft elastomers, this approach does not require intermolecular cross-linking, also allowing for a fine tuning of the materials softness via the control of the graft length. Chapter IV discussed a synthetic method for incorporation of bimodality into the length distribution of side chains in brush polymers. The use of TEMPO allowed for a selective deactivation of end groups in brushes prepared via ATRP without affecting ATRP process itself. The results describe a

new architecture of molecular bottlebrush, which may have interesting viscoelastic properties, and hence potential interest in new elastomeric materials. In addition, the concept of capping with TEMPO provides access to thermosensitive brushes, which can applied in the formation of soft elastomers with tunable cross-linking density. Moreover, new small molecules may be tested as capping agents as a way of tuning the end-group brush functionalities, which can also be used to prevent unintended brush. cross-linking. The bimodal structure can be further expanded to bi-component systems with long glassy blocks, thus forming thermoplastic bottlebrushes elastomers.

The third section focused on the use of functional ATRP multiinitiators as a way of tuning the brush properties. Chapter V covered four examples of ATRP diinitiators that were incorporated into the brush center. That method enabled for embedding small molecules in bottlebrushes, for the purpose of acting a label tag or mechanosensitive functionality. Chapter VI described a more complex ATRP hexainitiator with the core composed of a molecular spoked wheel. The structure of the initiator provided the formation of complex molecular stars combining characteristics of both the star and brush polymers. In addition, the rigidity of the core was found to induce a selective mechanical cleavage of brush arms from the core. The results show that a smart design of ATRP initiators is an excellent way of fine tuning of molecular bottlebrushes that enables for site-specific location of the functional group. This approach can be exploited in the formation of new mechanosensitive materials or used a way of modifying the topology of molecular brushes.

The final section focused on designing a synthetic bio-mimic of the natural lubricant via combination of ATRP and synthetic techniques. In this project a complex,

multistep synthesis was applied to generate hydrophilic and hydrophobic ABA triblock brushes with structures inspired by that of Lubricin. The results of lubrication tests indicated a superior lubrication of properties of the bio-mimic in water, showing lower frictions under much higher pressures than possible for the natural protein. In addition, the preliminary results suggested that the concept can be extended to hydrophobic lubricants, as was displayed by excellent lubrication of the other brush in organic media. The remarkable results show that there is a huge potential in the use of bottlebrushes as lubricants in different media. The idea can be easily expanded to other monomers that would allow for tuning the solubility of the brush. For instance the use of hydrocarbons can be exploited in the generation of a new class of lubricants for oil engines, or additives for reducing friction in piping transportation of liquids.

The current trend in the field of molecular bottlebrushes shows a continuously increasing interest in synthesizing new and more complex molecular bottlebrushes, with their used as foundational building block for next generation materials. Even though much progress has been recently done in this area of cylindrical brushes, there is even more that needs to be done to enable a better understanding and a full appreciation of those unique polymeric architectures.